

The Impact of Bacteria on the Biophysics of Water Retention and Flow in Soil

Patrica Dello Sterpaio

A thesis for the degree of Doctor of Philosophy at



2012

This item is protected by original copyright.



The impact of bacteria on the biophysics of water retention and flow in soil

**A thesis submitted in partial fulfilment of the requirements of the
University of Abertay, Dundee
for the degree of Doctor of Philosophy**

Patricia Dello Sterpaio MSc BSc (Hons)

University of Abertay, Dundee

May 2012

DECLARATION

Personal declaration of work

I, Patricia Dello Sterpaio, confirm that the original research work presented in this thesis is my own. Where information has been derived from other sources, I can confirm that this has been acknowledged. No part of this thesis has been submitted in any form elsewhere for any award.

Signed Date

Chair of Examination Committee declaration

I certify that this thesis is the true and accurate version of the thesis approved by the examiners.

Signed Date

(Dr Scott Hardie)

(Chair of Examination Committee)

ABSTRACT

Understanding soil structure, in particular the void spaces through which water, gases and solutes flow and in which organisms exist, is vital to a sustainable future on earth. The investigation of the structural behaviour of soil under different influences is fundamental to understanding and protecting the soil.

This study has investigated the impact of bacteria on the biophysics of water retention and flow, aiming to elucidate the effect of three key components produced by the model organism, *Pseudomonas fluorescens* SBW25. Cellulose is an extracellular polysaccharide involved in the formation of the matrix of the bacterial biofilm, lipopolysaccharide is a cell membrane component required for bacterial attachment, and viscosin is a biosurfactant released from the bacteria. Four isogenic strains mutated so as to heighten or suppress production of one of these key components were used in addition to the wild-type strain.

Labfield sandy loam soil was sieved and packed into replicate experimental cores which were incubated with different bacterial treatments. Following sterilisation, the gravimetric water content ($u \text{ g g}^{-1}$) of the soil was determined at equilibrated matric potentials from -1 cm to -100 cm during two wet-dry cycles. Sorptivity ($S, \text{mm s}^{-1/2}$) of the soil, indicative of water repellency, was determined using a mini-infiltrometer setup and has been reported as the rate of infiltration of water into the soil. Bacteria have been shown to increase water repellency of soil, decrease the total water content at saturation and increase the water retaining ability of the soil as it drains ($p < 0.05$). Three-dimensional analysis of core scale structure was carried out using micro X-ray computed tomography (μXCT) and of aggregate scale structure using synchrotron- μXCT . Volumetric analyses of the 3D structures has shown decreased pore connectivity and destabilisation of aggregates in soil systems treated with bacteria deficient in the production of a key extracellular component, cellulose, LPS or viscosin ($p < 0.05$).

Analyses of cracking patterns in two types of sandy loam soil, Labfield and Bullionfield has highlighted the importance of taking into account the soil type and its composition when studying soils, as even within soil classification groups different behaviours are observed.

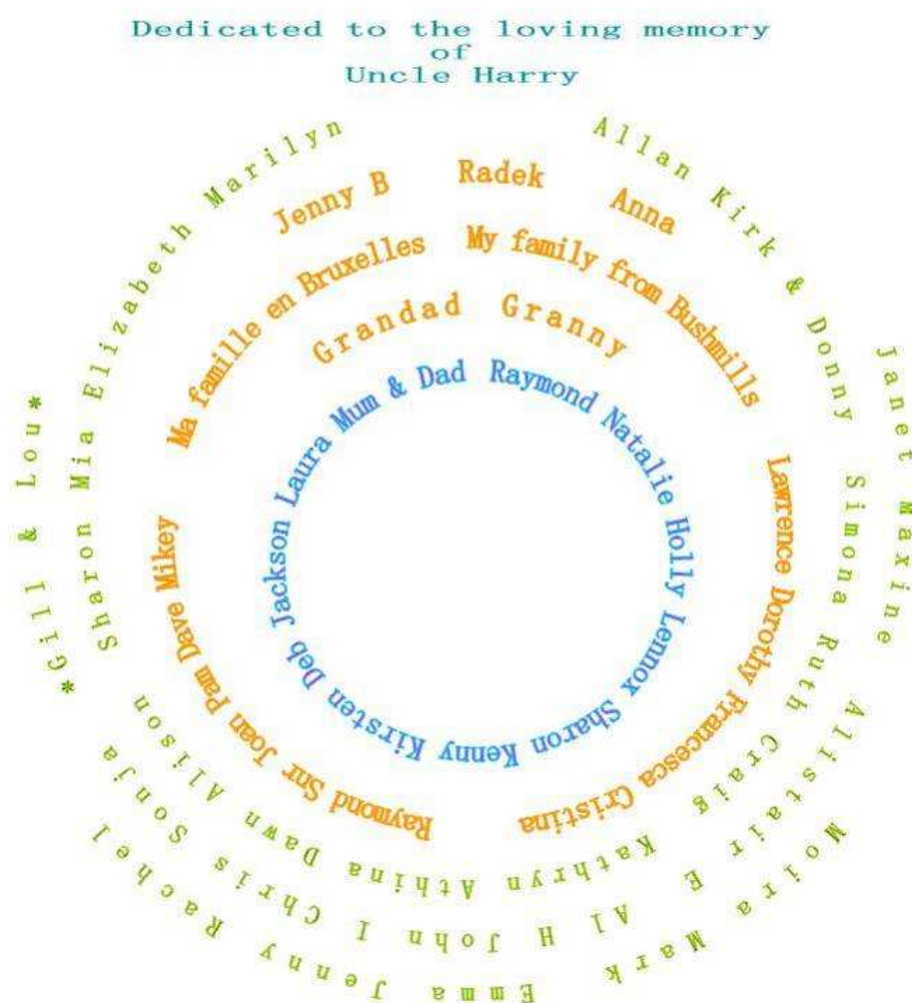
This study has provided clear evidence of the ability of bacteria and their extracellular components to impact upon (i) the hydrodynamics of water retention and flow in soil and (ii) the structural organisation, aggregation and stabilisation of soil.

ACKNOWLEDGEMENTS

I would like to thank Dr Andrew Spiers for taking over as my primary supervisor after $\frac{2}{3}$ of my original supervisory team, Professors Iain Young and John Crawford whom I found entertaining, educational, motivational and incredibly supportive, emigrated to Australia at the same time. My sincerest gratitude goes to the consistent $\frac{1}{3}$ of my original team, Dr Phil Collier, without whose guidance, philosophy and kind support I would not have reached the final goal.

Thanks also to Wilfred and Philippe for their input.

Rather than list all the people who have loved and supported me in many different ways over the years I have created a "Circle of Thanks" to my wonderful family and fabulous friends.



I would also like to dedicate this to the memory of a wonderful member of staff who was a very supportive secretary of the Research Degrees Committee, *Dawn Keen*.

Sadly, just the month before my viva my wonderful Grandad passed away - he was so pleased I had finished, I just wish he could have seen what I had written. Probably the most intelligent, true gentleman I ever met, he would have probably read this thesis and understood much, though not even written in his native French.

Tu me manques toujours, Grandad.

CONTENTS

Title	i
Declaration	ii
Abstract	iii
Acknowledgements	iv
Contents	v
List of figures	xi
List of tables	xxv
List of equations	xxviii
References	240

1	Introduction.....	1
1.1	Soil.....	1
1.2	Structural measurements of soil pores	3
1.2.1	Porosity	4
1.2.2	Fractal dimension.....	5
1.2.3	Pore size distribution.....	7
1.2.4	Pore connectivity.....	8
1.2.5	Cracking analysis	8
1.3	Soil hydrodynamics	9
1.3.1	The water retention curve.....	10
1.3.2	Sorptivity	14
1.3.3	Water repellency	16
1.4	Bacteria in soil.....	17
1.4.1	Key bacterial components of interest in this study.....	19
1.4.1.1	Lipopolysaccharide	19

1.4.1.2	The surfactant viscosin	21
1.4.1.3	Exopolysaccharides	22
1.4.2	Model organism – <i>Pseudomonas fluorescens</i> SBW25	28
1.5	X-ray computed tomography	33
1.5.1	X-ray physics	33
1.5.2	The CT scanner	33
1.5.3	Applications of XCT in soil analyses.....	41
1.5.4	Thresholding	42
1.6	Aims of study	44
2	Methodological approaches used in this thesis	46
2.1	Introduction	46
2.2	The experimental cores.....	47
2.3	The soil	48
2.4	The bacteria	50
2.5	Sterilisation	51
2.6	Statistical analyses.....	53
2.7	Experimental design.....	55
3	Materials and Methods	57
3.1	Chemicals, reagents and buffers.....	57
3.2	Bacterial strains and growth media	57
3.3	Bacterial culture conditions	58
3.4	Sampling and preparation of soil	59
3.4.1	Soil cores	60
3.4.2	Soil slurries for cracking plates.....	62
3.4.3	Preparation of aggregates.....	62
3.5	Hydrodynamic analyses	63

3.5.1	Water retention	63
3.5.1.1	Calculation of gravimetric water content.....	66
3.5.1.2	Calculation of absolute drainage	67
3.5.1.3	Calculation of percentage drainage.....	68
3.5.2	Sorptivity	68
3.5.2.1	Calculation of sorptivity	70
3.6	Imaging for structural analyses.....	71
3.6.1	Computed tomography (CT).....	71
3.6.2	Photographing of cracked plates	72
3.7	Image processing.....	72
3.7.1	3D-image reconstruction	72
3.7.2	ImageJ despeckling and thresholding	74
3.7.3	2D Image processing	77
3.8	3D and 2D physical measurements using SCAMP v1.1	80
3.8.1	Porosity.....	81
3.8.2	Fractal dimension.....	81
3.8.3	Pore-size distribution.....	83
3.8.4	Pore connectivity.....	84
3.9	Statistical analyses.....	85
4	Studies on the effects of <i>Pseudomonas fluorescens</i> SBW25 and key mutants on selected soil hydrodynamics	88
4.1	Introduction	88
4.2	Chapter aims and research objectives	88
4.3	Results.....	90
4.3.1	Water retention curves	90
4.3.1.1	Introduction	90

4.3.1.2	Investigation of the impact of bacteria on GWC.....	93
4.3.1.3	Investigation of the impact of bacteria on absolute water drainage.....	98
4.3.1.4	Investigation of impact of bacteria on percentage water drainage	103
4.3.1.5	Summary of the observed impact of bacteria on water retention curves.	107
4.3.2	Sorptivity	108
4.3.2.1	Introduction	108
4.3.2.2	Investigation of the impact of bacteria on sorptivity	109
4.3.2.3	Summary of observed impact of bacteria on sorptivity	110
4.4	Summary of studies on the effects of bacteria on soil hydrodynamics	110
4.5	Chapter discussion.....	115
4.5.1	Discussion	115
4.5.2	The impact of bacteria on the hydrodynamics of cycle A.....	119
4.5.3	The impact of bacteria on the hydrodynamics of cycle B.....	126
4.5.4	This research in context	132
4.5.5	Summary statement	133
4.6	Future work.....	134
5	The use of microtomography in the investigation of the effects of <i>Pseudomonas fluorescens</i> SBW25 and key mutants on Labfield soil .	
	138
5.1	Introduction	138
5.2	Chapter aims and research objectives	140
5.3	Results.....	141
5.3.1	Resolution variability in acquired data	142
5.3.1.1	The expected effect of different resolutions on porosity measurements .	143
5.3.1.2	The expected effect of different resolutions on fractal dimension measurements.....	146

5.3.1.3	The expected effect of different resolutions on pore-size distribution measurements.....	146
5.3.2	Core scale soil structure.....	147
5.3.2.1	Introduction	147
5.3.2.2	Investigation of the impact of bacteria on core porosity	147
5.3.2.3	Investigation of the impact of bacteria on core fractal dimension.....	149
5.3.2.4	Summary of observed impact of bacteria on core scale soil structure	153
5.3.3	Aggregate scale soil structure	154
5.3.3.1	Introduction	154
5.3.3.2	Investigation of the impact of bacteria on aggregate porosity	155
5.3.3.3	Investigation of the impact of bacteria on aggregate fractal dimension...	157
5.3.3.4	Investigation of the impact of bacteria on aggregate pore-size distribution...	159
5.3.3.5	Investigation of the impact of bacteria on aggregate pore connectivity ...	165
5.3.3.6	Summary of the observed impact of bacteria on aggregate scale soil structure	171
5.4	Chapter discussion.....	172
5.4.1	Introduction	172
5.4.2	Core scale soil structure.....	174
5.4.3	Aggregate scale soil structure	190
5.4.4	This research in context.....	192
5.4.5	Summary statement.....	193
5.5	Future work.....	195
6	Study on the effects of <i>Pseudomonas fluorescens</i> SBW25 and selected mutants on cracking structure in two sandy loam soils	198
6.1	Introduction	198

6.2	Chapter aims and research objectives	199
6.3	Results.....	200
6.3.1	Soil cracking structure.....	201
6.3.1.1	Introduction	201
6.3.1.2	Investigation of the impact of bacteria on crack density.....	204
6.3.1.3	Investigation of the impact of bacteria on crack heterogeneity	208
6.3.1.4	Investigation of the impact of bacteria on crack connectivity	212
6.3.1.5	Summary of the impact of bacteria on soil cracking structure.....	216
6.4	Chapter discussion.....	218
6.4.1	Introduction	218
6.4.2	Discussion	219
6.5	Future work.....	223
7	Discussion and conclusions	224
7.1	The behaviour of bacteria in soil.....	224
7.2	The applicability of laboratory investigations to the field	233
7.3	Future work.....	236
7.3.1	Adding the 4 th dimension, the time scale	237
7.4	Conclusions	238

LIST OF FIGURES, TABLES AND EQUATIONS

LIST OF FIGURES

- Figure 1.1 Factors affecting soil aggregation. Pedogenic = formation of soil, anthropogenic = influences of humans. Figure 2 in Bronick (2005). 3
- Figure 1.2 Soil texture classification triangles from the US (left) and the UK (right). The US has 12 soil classes, whereas the UK has 11. USDA (United States Department of Agriculture) triangle from <http://www.stevenswater.com/articles/images/soiltexturetriangle.jpg>, UK triangle from <http://www.scotland.gov.uk/Resource/Img/47121/0020508.gif>. 4
- Figure 1.3 Illustration of a regular and evenly distributed structural arrangement (a and b) and a clumped and irregular distribution (c and d) and the respective fractal dimension values as drawn in Li (2000). 7
- Figure 1.4 Capillarity in soil is due to adhesive and cohesive forces of between the water molecules and the soil particles. 10
- Figure 1.5 Typical water retention curves for sand, silt loam and clay soils from Fredlund and Xing (1994). Saturated water content is indicative of porosity, and the slopes of the curves are representative of variable pore size distributions. 11
- Figure 1.6 Schematic of water retention curve of soil. The drying curve at 0 Ψ_M (matric potential) is equivalent to a saturated sample (blue area), where all connected pores are full of water (θ_s). As Ψ_M increases the larger pores start to empty and the curve becomes negative (yellow). As the slope of the curve decreases this is indicative of the reflection curve where most of the larger pores are now empty and the smaller pores start to empty (green). θ is soil water content. 12
- Figure 1.7 Menisci and films of fluid in a drained porous structure. Menisci of water are held in pores by capillarity, whereas the film of wetting fluid on the surfaces of the solid material is held by adhesion. Brown areas represent soil aggregates, blue areas represent water and black dotted areas represent air-filled pore space. 13

Figure 1.8 Illustration of water infiltration curve highlighting the rapid infiltration rate and linear relationship of the curve in the first 1 to 3 minutes which defines the soil sorptivity. Adapted from Hallett (2007).	15
Figure 1.9 Illustration of outer cell envelope of gram-positive and gram-negative bacteria (Figure 1 in Vollmer, 2012). LPS = lipopolysaccharide, OMP = outer membrane protein.....	18
Figure 1.10 General schematic structure of bacterial lipopolysaccharide. Smooth type (S) LPS possess a hydrophilic polysaccharide specific O-chain of 2 or more repetitive units. Semi-rough (SR) type LPS contain a single repetitive unit of specific O-chain. Rough type (R) LPS do not have any specific O-chain units. The hydrophobic Lipid A head is anchored in the bacterial cell membrane. Image adapted from Pupo and Hardy (2009).	20
Figure 1.11 Chemical structure of viscosin, a cyclic lipopeptide surfactant. The polar cyclic oligopeptide region is hydrophilic and the non-polar fatty acid (lipid) tail is hydrophobic. Image adapted from Saini <i>et al.</i> (2008).	21
Figure 1.12 The basic chemical structure of alginate (C ₆ H ₈ O ₆) _n . Image from Chaplin (2012).	23
Figure 1.13 The basic chemical structure of cellulose (C ₆ H ₁₀ O ₅) _n . Image from Chaplin (2012).	24
Figure 1.14 The inter- and intra-chain hydrogen bonding in cellulose I. Dashed lines: inter-chain hydrogen bonding. Solid lines: intra-chain hydrogen bonding. Image from Festucci-Buselli <i>et al.</i> (2007).	25
Figure 1.15 Hydrogen-bonding patterns in cellulose I α (A) and I β (B) based on the crystal structures of Nishiyama <i>et al.</i> (2002; 2003) adapted from Festucci-Buselli (2007). Differences in hydrogen bonds are represented by coloured lines. (C) is an overlay of I α (A, black) and I β (B, grey).	25
Figure 1.16 Illustration of fluorescent labelling of bioaggregate of <i>Bacteroides</i> sp. to visualise exopolymeric substances. (a) Phase contrast image; (b) green (FITC) proteins; (c) yellow (Nile red) lipids; (d) cyan blue (ConA) α -d-glucopyranose polysaccharides; (e) red (SYTO 63) nucleic acids; (f) pink (SYTOX Blue) dead cells; (g) blue (Calcofluor white) β -d-glucopyranose polysaccharides; (h) purple blue	

(Calcium Green) calcium. Bar = 300 μm . Image from Adav *et al.* (2010). The reader is directed to image (g) staining of β -d-glucopyranose polysaccharides by Calcofluor white. 27

Figure 1.17 Microphotographs for *Pseudomonas fluorescens* SBW25 Wrinkly-spreader (WS) cellulose-overexpressing mutant. The air-liquid interface biofilm samples are stained with Calcofluor highlighting cellulose fibres. A. A large clump of material viewed at low magnification (10x); and B, viewed at medium magnification (40x) showing the variations in structure, including net-like regions, pore and fibres. C. Bacterial cells associated closely with cellulose fibres seen at high magnification (100x). D. Enlargements of the central portion of C showing a single cellulose fibre with a width of approximately the same as that of a cells ($<0.02 \mu\text{m}$). Note that *P. fluorescens* cells show a high level of autofluorescence. Images and description reused with kind permission from Dr A.J. Spiers (Spiers *et al.*, 2003). 28

Figure 1.18 Foaming behaviour of wild-type SBW25 in KB cultures. The expression of the surfactant viscosin by wild-type SBW25 is readily demonstrated by the foaming of cultures in comparison with *ViscA* cultures. King's B microcosms were inoculated with wild-type SBW25 ('SM') and the viscosin-deficient mutant *ViscA* and incubated statically or with shaking for 24 hours at 28°C. The microcosms were then briefly shaken together and allowed to settle; the purple arrow highlighting the foaming produced by wild-type SBW25 expressing viscosin. Expression is delayed in shaken microcosms, perhaps because under better aeration conditions the culture has yet to reach stationary phase growth. The *ViscA* mutant shows no sign of foaming in either static or shaken microcosms. 31

Figure 1.19 Illustration of emission and continuous spectrum of X-rays. K-shell characteristic radiation emission spectrum spikes at single energies and Bremsstrahlung continuous spectrum of photons at a range of energies given off as electrons lose energy upon encountering the target atoms. Maximum photon energy is at the energy of the electron beam. Image courtesy of Andrew Ramsey, Nikon-Metrology, Tring, UK. 35

Figure 1.20 From X-ray source to 3D reconstructed dataset. X-rays produced by the X-ray source (gun) pass through the sample which is rotated through 360° and at each rotational angle the detector panel receives X-ray of different intensities

(levels of attenuation). The data from each position and rotation of the sample is sent to a high-performance PC which uses computational algorithms to create 2D slice images and the reconstructed 3D datasets. 37

Figure 1.21 Aerial view of the Advanced Photon Source at Argonne National Laboratory, Argonne, Illinois. Image credit Argonne National Laboratories. 38

Figure 1.22 Illustration of the 35 beamline sectors around the Advanced Photon Source ring. The studies carried out in this work were undertaken at Beamline Station 13-BM-D. BM = bending magnet. D denotes the end station out of 4 stations at this sector. Image credit Argonne National Laboratories. 38

Figure 1.23 Schematics of the beamline sector at the Advanced Photon Source. Image credit Argonne National Laboratories. 39

Figure 1.24 Schematic of magnets which bend the photon beam along the beamline of the Advanced Photon Source. Image credit Argonne National Laboratories. 40

Figure 1.25 Schematic of data acquisition from the monochromatic beam through the sample to the detector. Image credit Argonne National Laboratories. 41

Figure 1.26 Thresholding of a greyscale image to a segmented black and white image. A is an 8-bit greyscale image of a soil matrix and B is the segmented image following thresholding. C is a magnified image of a region of a soil matrix, notice the individual pixels visible, and D is the resultant thresholded and segmented image. 43

Figure 2.1 Sagittal radiographic image of an experimental soil core. An experimental core packed with Labfield soil has been imaged using The SIMBIOS Centre CT HMX scanner and processed by CTPro software. A sagittal section is shown. The darker vertical lines visible on the outer edges of this image are the plastic ring used to hold the core. The red crosshairs represent the rotational axes used in the 3D reconstruction process by the CTPro software. 50

Figure 2.2 Simplified schematic of statistical analysis of interactive effects of factors in the experimental system leading to pairwise comparison of treatment types. 54

Figure 2.3 Schematic overview of experimental design process and associated Results chapters. Soil preparation involved initial sterilisation steps to eradicate

native soil biota so as to start experimental processes with a control soil free from influences extraneous to those being investigated.	56
Figure 3.1 Schematic representation of moisture content of soil cores for inoculation with bacteria.	61
Figure 3.2 Mounted ~ 2 mm sieved aggregate. Close-up of mounted aggregate from sieved Labfield soil (~ 2 mm)	63
Figure 3.3 Water retention apparatus schematic and photograph	64
Figure 3.4 Schematic of water retention curve. At each matric potential the water content was plotted giving the characteristic water retention curve.	65
Figure 3.5 Schematic illustration of the pore, aggregate and core scale relationships. Water flow would be expected to be unhindered by bacterial presence in the pores between the aggregates. Macropores are defined in this study as being >300 μm and mesopores as being 30 – 300 μm	67
Figure 3.6 Schematic of miniaturised infiltrometer to measure sorptivity. Mass loss from the water reservoir on the balance due to water uptake by the soil core through the conductance tube was recorded at 2 second intervals using Ohaus® BalanceTalk software	69
Figure 3.7 Illustration of axial image stack creation from a soil core by VGStudio Max. The 3D volume was sliced on the axial plane by VGSM to create individual sequential tiff files for import into ImageJ.	74
Figure 3.8 Schematic of soil core analysis cuboid. The central cuboid was selected to reduce processing time and RAM requirements.....	75
Figure 3.9 Illustration of analysis cuboid from soil aggregate	76
Figure 3.10 Despeckled and thresholded image in ImageJ.....	77
Figure 3.11 Labfield soil; cracking plate thresholding. A. Original photograph; B. ImageJ-suggested threshold value of 128; C. Amended threshold value of 118. ...	78
Figure 3.12 Labfield soil; cracking plate despeckling. A. Original photograph; B. Despeckling stage 1 – selection of cracks using wand (tracing) tool in ImageJ	

(screenshot); C. Despeckling stage 2 – clear outside function applied to the wand-selected image; D. Despeckling stage 3 – eraser tool used to remove final noise interference..... 78

Figure 3.13 Bullionfield soil; cracking plate image thresholding. A. Original photograph; B. ImageJ-suggested threshold value of 146; C. Labfield-threshold value of 118; D. Amended threshold value of 136 (uncleaned). 79

Figure 3.14 Determination of resolution of cracking plate images using ImageJ and ruler image. By drawing a straight line of known length (1 cm) in ImageJ (yellow line indicated by lower arrow); pixel length (113.33) is presented in the information bar of the ImageJ interface (indicated by upper arrow). 80

Figure 3.15 Schematic illustration of box counting method for fractal dimension on representative images of A. homo- and B. heterogeneity. Box size (r) = 1 is the smallest box that will cover the whole image. The image is then magnified to its maximum resolution (= pixel size) so that the box size is now $1/\text{pixel size}$ ($1/10$) and the number of $1/10$ boxes containing pore pixels is counted ($N(r)$). The magnification is then reduced until the next box size that covers the image evenly is reached (here $1/5$) and the $N(r)$ is counted again. This process is repeated with the final $N(r)$ count being for the maximum box size, which will be the total number of pixels of shortest side of the image divided by 2 (here 5 pixels wide) and therefore $r = 1/2$ 82

Figure 3.16 Illustration of calculation of fractal dimension for representative homo- and heterogeneous images. The linear regression equation for the line of log-log plot of box count against box size [$\log(N(r)) / -\log(1/r)$] is determined and fractal dimension is the slope of the line. Here the graph demonstrates the heterogeneous image of clustered pores has a higher fractal dimension (1.35) than the homogeneous image of uniformly distributed pores (1.18)..... 83

Figure 3.17 Schematic representation of calculation of pore-size distribution in SCAMP V1.1. The user selects the pore colour, enters sample resolution (28.4 μm in this example) and minimum sphere size to include. SCAMP V1.1 puts down spheres inside each pore space and “inflates” the sphere in integer multiples until soil is encountered on the opposite side. This is then recorded as percentage coverage of total pore space at sphere radius e.g. “3x”. This continues throughout

the segmented volume until all pore spaces have been counted. A table of pore size percentage coverage is generated and the “mean pore size” is calculated..... 84

Figure 3.18 Typical output from pore connectivity analysis in SCAMP v1.1. Each connected pore is reported in terms of volume, surface area and connectivity. The connectivity is representative of “percentage of total sample pore volume in the associated pore”. 85

Figure 3.19 Diagrammatic representation of statistical hierarchy 86

Figure 4.1 Schematic of experimental design highlighting moisture retention assay used to produce data for the water retention curves. 90

Figure 4.2 Water retention curve of wet/dry cycle A for sandy loam (Labfield) soil with different bacterial legacies. Mean gravimetric water content of the soil cores plotted against the equilibrated matric head level shows the characteristic water retention curve. dH₂O = bacteria-free control soil, SM = wild-type bacteria-control soil, *ViscA*, WS, WS-4 and WS-5 = bacteria treatments. Error bars were calculated as the standard error of the means of each treatment type (n = 10)..... 91

Figure 4.3 Water retention curve of wet/dry cycle B for sandy loam (Labfield) soil with different bacterial legacies. Mean gravimetric water content of the soil cores plotted against the equilibrated matric head level shows the characteristic water retention curve. dH₂O = bacteria-free control soil, SM = wild-type bacteria-control soil, *ViscA*, WS, WS-4 and WS-5 = bacteria treatments. Error bars were calculated as the standard error of the means of treatment types (n = 10)..... 92

Figure 4.4 Mean GWC at key matric head levels for soils under different treatment types in cycle A. Error bars were calculated as the standard error of the means of treatment types (n = 10)..... 94

Figure 4.5 Mean GWC at key matric head levels for soils under different treatment types in cycle B. Bacterial legacy of the mutant strains considerably reduced the GWC of the soil at saturation level (0 cm). Macropore (-10 cm) and mesopore (-80 cm) GWCs were increased by SM-treatment, but reduced by some of the mutant-strain treatments. Error bars were calculated as the standard error of the means of each treatment type (n = 10)..... 97

Figure 4.6 Overview of drainage from macropores and mesopores for soil cores under different treatment types. Blue bars represent mean macropore drainage (g/g) and green bars represent mean mesopore drainage (g/g) for each treatment type-soil, in cycle A and cycle B. Error bars were calculated as the standard error of the means of each treatment type (n = 10). 99

Figure 4.7 Macropore drainage for soil cores under different treatments. Significantly different ($p < 0.05$) treatments are indicated by lettering within each cycle. No statistical comparison has been made between cycles and as such no inference is intended between cycle A and cycle B. Error bars were calculated as the standard error of the means of each treatment type (n = 10)..... 100

Figure 4.8 Mesopore drainage for soils under different treatments. Significantly different ($p < 0.05$) treatments are indicated by lettering within each cycle. No comparison has been made between cycles at this stage and as such no inference is intended between cycle A and cycle B. Error bars were calculated as the standard error of the means of each treatment type (n = 10). 101

Figure 4.9 Percentage drainage from pores of soil with different bacterial legacies 104

Figure 4.10 Sorptivity of sandy loam soil with different bacterial legacies. Mean sorptivity is shown for each experimental core under different bacterial treatments. Statistical differences between measured sorptivities are indicated by the different letters ($p < 0.05$). Error bars were calculated as the standard error of the means of each treatment type (n = 10)..... 109

Figure 4.11 Schematic illustration of the key bacterial components under investigation. LPS (lipopolysaccharide) is composed of hydrophilic polysaccharide tail and hydrophobic lipo-head unit making the compound amphiphilic overall; cellulose is amphiphilic with both polar and non-polar side chains; and viscosin comprises a cyclic peptide head unit with a non-polar fatty acid tail resulting in an overall hydrophobic compound. Moieties are not scaled..... 112

Figure 4.12 Schematic representation of the chemical and conformational structures of viscosin (top), lipopolysaccharide (middle) and cellulose (bottom). Figure drawn by PDSterpaio. Viscosin (Saini *et al.*, 2008) and LPS are amphiphilic overall due to

their hydrophobic and hydrophilic component parts, and cellulose is highly insoluble and inelastic (Ross <i>et al.</i> , 1991).....	117
Figure 5.1 Schematic of experimental design highlighting CT imaging and 3D structural analyses.....	142
Figure 5.2 Schematic overview of resolution impact on reported porosity in thresholded images. The higher resolution of 15.3 μm gives a more accurate report of porosity than the 28.4 μm report; however, in a complete soil sample, the balance of under- and over-reporting of porosity in a 28.4 μm -scanned dataset could reasonably be accepted as true at the range of resolutions used.....	145
Figure 5.3 Mean porosity of cores under different treatment types. Mean porosity of Labfield soil cores under different treatment types measured using 3D volumetric data generated by μXCT scanning is shown. Significantly different ($p < 0.05$) treatments are indicated by lettering. No comparison has been made between cycles at this stage and as such no inference is intended between Cycle A and Cycle B. Error bars were calculated as the standard error of the means of each treatment type ($n = 10$).	148
Figure 5.4 Mean fractal dimension of cores under different treatment legacies in cycle A. Mean fractal dimension of Labfield soil cores in Cycle A under different treatment types measured using 3D volumetric data generated by μXCT scanning is shown. Significantly different ($p < 0.05$) treatments are indicated by lettering. Error bars were calculated as the standard error of the means of each treatment type ($n = 10$).	150
Figure 5.5 Mean fractal dimension of cores under different treatment legacies in cycle B. Mean fractal dimension of Labfield soil cores in Cycle B under different treatment types measured using 3D volumetric data generated by μXCT scanning is shown. Significantly different ($p < 0.05$) treatments are indicated by lettering. No comparison has been made between sterilisation methods at this stage and as such no inference is intended between antibiotic and autoclave methods. Error bars were calculated as the standard error of the means of each treatment type ($n = 5$).	151
Figure 5.6 Mean porosity of aggregates under different treatment legacies. Mean porosity of 2 mm aggregates from Labfield soils under different treatment types	

measured using 3D volumetric data generated by synchrotron μ XCT scanning is shown. Significantly different ($p < 0.05$) treatments are indicated by lettering. Error bars were calculated as the standard error of the means of each treatment type ($n = 13$). 156

Figure 5.7 Mean fractal dimension of aggregates under different treatment legacies. Mean fractal dimension of 2 mm aggregates from Labfield soils under different treatment types measured using 3D volumetric data generated by synchrotron μ XCT scanning is shown. Significantly different ($p < 0.05$) treatments are indicated by lettering. Error bars were calculated as the standard error of the means of each treatment type ($n = 13$). 158

Figure 5.8 Overview of observed porosity across different pore size classes and relationship between maximum and mean pore sizes in aggregates under different treatment legacies. The pore-size distribution curve (A) for 2 mm Labfield aggregates from Labfield soils under different treatment types measure using 3D volumetric data generated by synchrotron μ XCT scanning is shown along with the maximum and mean pore size class relationship (B). Error bars were calculated as the standard error of the means of each treatment type ($n = 13$)..... 160

Figure 5.9 Maximum pore size of aggregates from Labfield soils under different treatment types. Pore size distribution was measured using 3D volumetric data generated by synchrotron μ XCT scanning. Significantly different ($p < 0.05$) treatments are indicated by lettering. Error bars were calculated as the standard error of the means of each treatment type ($n = 13$). 161

Figure 5.10 Reported mean pore size of aggregates from Labfield soils under different treatment types. Pore size distribution was measured using 3D volumetric data generated by synchrotron μ XCT scanning. No comparison has been made between sterilisation methods at this stage and as such no inference is intended between antibiotic and autoclave methods. Error bars were calculated as the standard error of the means of each treatment type ($n = 7$). 162

Figure 5.11 Mean percentage of total observed porosity present in the smallest pore class ($5.54 \mu\text{m}$) of aggregates from Labfield soils under different treatment types. Pore size distribution was measured using 3D volumetric data generated by synchrotron μ XCT scanning. Significantly different ($p < 0.05$) treatments are

indicated by lettering. Error bars were calculated as the standard error of the means of each treatment type (n = 13). 164

Figure 5.12 Overview of pore connectivity of 20 largest pores in Labfield aggregates under different treatment types measured using 3D volumetric data generated by synchrotron μ XCT scanning Error bars were calculated as the standard error of the means of each treatment type (n = 13). 165

Figure 5.13 Mean pore connectivity in largest 20 pores (top; pore 1, maximum 80% connected; middle pores 2 to 9, maximum 7% connected; bottom: pores 10 to 20, maximum 0.5% connected) of aggregates under different treatment legacies. Pore connectivity was measured using 3D volumetric data generated by synchrotron μ XCT scanning. Significantly different ($p < 0.05$) treatments within pore number are indicated by lettering. No comparison between pore numbers is inferred. Error bars were calculated as the standard error of the means of each treatment type (n = 13). 167

Figure 5.14 Proportion of total observed porosity present in largest 20 connected pores for Labfield aggregates under different treatment types. Mean percentage of total aggregate porosity connected in the 20 largest pores were measured using 3D volumetric data generated by synchrotron μ XCT scanning is shown. Significantly different ($p < 0.05$) treatments are indicated by lettering. Error bars were calculated as the standard error of the means of each treatment type (n = 13). 170

Figure 5.15 Hierarchical categorisation of pores as described by Elliott and Coleman (1988). Vertical cross section of highly structured soil showing macroaggregates (>250 μ m) and microaggregates (20 - 250 μ m). Pores are categorised into: (1) macropores, (2) intermacroaggregate, (3) intramicroaggregate including (4) intermicroaggregate space. Illustration by S.L. Rose (Figure 3 in Elliott and Coleman (1988) Let the soil work for us, p26). 174

Figure 5.16 Schematic 2D representation of change in porosity due to disintegration of soil particles following a wet/dry (WD) cycle. On the left (1) a 20 μ m soil particle occupies one 15 μ m pixel entirely, which, on segmentation of the image will be reported as solid (S), the remainder of the particle occupies $\frac{1}{3}$ each of two further pixels, and $\frac{1}{9}$ of the 4th pixel. These three pixels will be reported as void (V) upon segmentation. Thus, the whole volume of 4 pixels will have a porosity of 75%. On

the right (2), the 20 μm particle has been swollen upon wetting and disintegrated upon drying leaving 4 new particles each $< 20 \mu\text{m}$. Due to the configuration of the smaller particles within the pixels, reported porosity has been decreased to 50% as measured by image analysis following segmentation..... 177

Figure 5.17 Component-soil grain interactions for cellulose, lipopolysaccharide and viscosin. The gel-like mesh provided by cellulose would provide support for the aggregates during hydrated and desiccated stages leading to a physically stable environment. Both LPS and viscosin would provide interaggregate binding during periods of desiccation, but on hydration of the environment, inversion of the amphiphilic moieties would allow movement of grains and restructuring of the soil. 180

Figure 6.1 Schematic of experimental design highlighting 2D analysis 201

Figure 6.2 Typical cracking patterns for Labfield and Bullionfield soils under different treatment types. dH_2O no inc = unincubated control soil, dH_2O inc = incubated control soil. No data is available for Labfield- dH_2O inc as the slurry bag burst during the homogenisation process. 203

Figure 6.3 Comparison of different bacterial treatments on the crack density of two sandy loam soils. Mean crack density is shown for experimental cracking plates of two different soil types under different bacterial treatments. Statistical differences between the measured crack density for the treatment types within each soil type are shown ($p < 0.05$). No analysis between soil types is shown in this figure. ABCD refer to Bullionfield soil only; ABCDE refer to Labfield soil only. No data is available for Labfield dH_2O incubated (dH_2O inc) treatment. dH_2O no inc = not incubated soil control. Error bars were calculated as the standard error of the means of each treatment type ($n = 7$). 205

Figure 6.4 Comparison of crack density in two sandy loam soils with different bacterial legacies. Mean crack density is shown for experimental cracking plates of two different soil types under different bacterial treatments. Statistical differences between the measured crack density for the soil types within each treatment type are shown ($p < 0.05$). No analysis between treatment types is shown in this figure. AB, CD, EF, GH, IJ and KL refer to statistically significant difference in disparate analyses. No data is available for Labfield dH_2O incubated (dH_2O inc) treatment.

dH₂O no inc = unincubated soil control. Error bars were calculated as the standard error of the means of each treatment type (n = 7). 207

Figure 6.5 Comparison of different bacterial treatments on the fractal dimension of cracking patterns in two sandy loam soils. Mean fractal dimension is shown for experimental cracking plates under different bacterial treatments. Statistical differences between the fractal dimensions for the treatment types within each soil type are shown (p < 0.05) No analysis between soil types is shown in this figure. ABCD refer to Bullionfield soil only. ABCDE refer to Labfield soil only. No data is available for Labfield dH₂O incubated (dH₂O inc) treatment. dH₂O no inc = not incubated soil control. Error bars were calculated as the standard error of the means of each treatment type (n = 7). 209

Figure 6.6 Comparison of the fractal dimension of cracks in two sandy loam soils with different bacterial legacies. Mean fractal dimension is shown for experimental cracking plates of two different soil types under different bacterial treatments. Statistical differences between the measured fractal dimensions for the soil types within each treatment type are shown (p < 0.05). No analysis between treatment types is shown in this figure. AB, CD, EF, GH, IJ and KL refer to statistically significant difference in disparate analyses. No data is available for Labfield dH₂O incubated (dH₂O inc) treatment. dH₂O no inc = unincubated soil control. Error bars were calculated as the standard error of the means of each treatment type (n = 7). 211

Figure 6.7 Comparison of different bacterial treatments on the connectivity of cracking in two sandy loam soils. Mean percentage of total crack density in the largest 20 cracks is shown for experimental cracking plates under different bacterial treatments. Statistical differences between the connectivity for the treatment types within each soil type are shown (p < 0.05) No analysis between soil types is shown in this figure. ABCDEF refer to Bullionfield soil only. ABC refer to Labfield soil only. No data is available for Labfield dH₂O incubated (dH₂O inc) treatment. dH₂O no inc = not incubated soil control. Error bars were calculated as the standard error of the means of each treatment type (n = 7). 213

Figure 6.8 Comparison of the connectivity of cracks in two sandy loam soils with different bacterial legacies. Mean percentage of total crack density in the largest 20 cracks is shown for experimental cracking plates of two different soil types under

different bacterial treatments. Statistical differences between the measured connectivity of the soil types within each treatment type are shown ($p < 0.05$). No analysis between treatment types is shown in this figure. A, BC, DE, FG, H and I refer to statistically significant difference in disparate analyses. No data is available for Labfield dH₂O incubated (dH₂O inc) treatment. dH₂O no inc = unincubated soil control. Error bars were calculated as the standard error of the means of each treatment type ($n = 7$). 215

Figure 6.9 Typical cracking patterns generated under different carbon additions: (a) 0 control, (b) 0.1, (c) 0.5, (d) 1.0, (e) 5.0 and (f) 10 mg C g⁻¹ soil, and the accompanying graph of crack heterogeneity (+1 SEM is indicated). Different letters denote significant differences ($p < 0.05$). From Fig.1 and Fig.2 Preston *et al.* (2001). 220

Figure 7.1 Back-scattered scanning electron micrographs of particle and pore size in sand (left) and silt+clay (right). Large sand-sized quartz particles (sp) are visible in both environments, while smaller ground quartz particles (*) are only present in the resin (r)-infiltrated pore space in the silt+clay environment. Scale bars = 100 μ m. These images would be the expected before and after destabilisation (left and right respectively) observations following a wet-dry cycle of soil incubated with the mutant bacterial strains. Image from Carson *et al.* (2010). 227

Figure 7.2 Illustration of the determination of heterogeneity and homogeneity in soil using the fractal dimension obtained from the box-counting method. 232

Figure 7.3 Elemental map of soil thin section showing heterogeneity of distribution of copper (Cu = red), manganese (Mn = blue) and calcium (Ca = green). Hotspots of copper have been analysed by μ -SXRF and the multichannel analyser (MCA) spectra are shown in the inset graphs. In each inset graph, the blue curve shows the summed MCA spectra of the high-Cu region and the red curve shows the individual MCA spectrum of the highest-Cu pixel in the region. Pixel size is 5 μ m. The total map area is 0.870 \times 0.875 mm. Image from Strawn and Baker (2008). 235

LIST OF TABLES

Table 1.1 Bacterial cellulose producers and their respective cellulose structures. From Bielecki <i>et al.</i> (2002) adapted from Jonas and Farrah (1998).....	26
Table 1.2 Overview of selected studies using CT to investigate soil structural properties pertinent to this work.	42
Table 2.1 Composition of the Labfield and Bullionfield soils.....	49
Table 3.1 <i>P. fluorescens</i> SBW25 strains used in this work detailing designation, genotype and reference.	57
Table 4.1 Pairwise comparison of the effect of bacterial treatment type on gravimetric water content of Labfield soil in cycle A	95
Table 4.2 Pairwise comparison of the effect of bacterial treatment type on gravimetric water content of Labfield soil in cycle B	97
Table 4.3 Pairwise comparison of the effect of bacterial treatment type on absolute drainage of Labfield soil in cycle A.....	102
Table 4.4 Pairwise comparison of the effect of bacterial treatment type on absolute drainage of Labfield soil in cycle B.....	102
Table 4.5 Pairwise comparison of the effect of bacterial treatment type on % total drainage of Labfield soil for cycles A and B.....	105
Table 4.6 Pairwise comparison of the effect of bacterial treatment type on % macropore drainage of Labfield soil for cycles A and B.....	106
Table 4.7 Pairwise comparison of the effect of bacterial treatment type on % mesopore drainage of Labfield soil for cycles A and B.....	106
Table 4.8 Pairwise comparison of the effect of bacterial treatment type on sorptivity of Labfield soil.....	109
Table 4.9 Legacy property of interest for each bacterial strain used in this study. All bacteria are strains of <i>Pseudomonas fluorescens</i> SBW25, with SM being the wildtype control capable of producing all properties listed depending on growth	

conditions. Each of the other strains are isogenic mutants of the SM strain. Detailed genotypic information is presented in Table 3.1	111
Table 4.10 Summary of water, bacteria and legacy compound states at key stages in the setup of the inoculated soil cores and subsequent cycles of the water retention experiment	113
Table 4.11 Impact of bacteria on soil hydrodynamic responses. SM response is compared with that of bacteria-free dH ₂ O control response. For the response of mutant bacteria treatments compared against SM control response, except where stated. • indicates no effect observed; ↓ indicates reduced response observed; ↑ indicates heightened response observed by the removal of one of the key exopolymers from the soil treatment.	114
Table 4.12 Summary and description of hydrodynamic measurements and calculations	115
Table 5.1 Pairwise comparison of the effect of bacterial treatment type on core scale porosity of Labfield soil	148
Table 5.2 Pairwise comparison of the effect of bacterial treatment type on core scale fractal dimension of Labfield soil	152
Table 5.3 Pairwise comparison of the effect of bacterial treatment type on aggregate mean pore size in Labfield soil	163
Table 5.4 Pairwise comparisons in 20 largest connected pores of the effect of bacterial treatment type on aggregate scale pore connectivity of Labfield soil	168
Table 5.5 Pairwise comparison of the effect of bacterial treatment type on aggregate proportion of total porosity in 20 largest connected pores in Labfield soil	170
Table 6.1 Pairwise comparison of the effect of bacterial treatment type on crack density for Bullionfield and Labfield soils	206
Table 6.2 Pairwise comparison of the effect of soil type on the crack density of soils under different bacterial treatments	208
Table 6.3 Pairwise comparison of the effect of bacterial treatment type on crack heterogeneity for Bullionfield and Labfield soils	210

Table 6.4 Pairwise comparison of the effect of soil type on the heterogeneity of soils under different bacterial treatments	212
Table 6.5 Pairwise comparison of the effect of bacterial treatment type on crack connectivity for Bullionfield and Labfield soils	214
Table 6.6 Pairwise comparison of the effect of soil type on the connectivity of soils under different bacterial treatments	215
Table 6.7 Summary overview of changes in soil crack structure in the presence of different bacterial treatment types.	217

LIST OF EQUATIONS

Equation 1.1 Representation of Infiltration	15
Equation 3.1 Bulk density	60
Equation 3.2 Gravimetric water content of soil	66
Equation 3.3 Calculation of Δm_{ac}	67
Equation 3.4 Calculation of Δm_{es}	67
Equation 3.5 Percentage macropore drainage	68
Equation 3.6 Percentage mesopore drainage	68
Equation 3.7 Percentage total drainage	68
Equation 3.8 S, Sorptivity	70
Equation 3.9 f, fillable porosity	70
Equation 3.10 S, Sorptivity in this study	71
Equation 3.11 Q, rate of infiltration	71

CHAPTER 1

1 Introduction**1.1 Soil**

Soil is the basic substrate for plant and animal life and is a major part of the water, nitrogen and carbon cycles. The many functions of soil include the provision of food, storage of water and prevention of flooding, cleansing of water and air from pollution, and, after the oceans, soil is the largest store of carbon on the planet. The sustainability of food production and the well-being of society is vitally linked to understanding soil structure and behaviour (Nunan *et al.*, 2002; Nunan *et al.*, 2003; Bronick, 2005; Ruamps *et al.*, 2011). In a recent press release by the British Society of Soil Science titled “Planet Under Pressure 2012” the need to address the capacity of the world’s soils to produce food, whilst maintaining the contribution of the same to climate change mitigation, global water supply and biodiversity conservation is becoming increasingly urgent (Allton, 2012). The carbon, nitrogen and water cycles are all linked with both climate control and the growth of plants for nutrition. As carbon is released from the soil into the atmosphere in the form of carbon dioxide (CO₂) it, along with the other main greenhouse gases (methane, CH₄; water vapour, H₂O; ozone, O₃; and nitrous oxide, N₂O) traps solar radiation in the atmosphere resulting in a warmer climate. As the temperature of the climate rises, carbon stored in the oceans is released leading to more CO₂ in the atmosphere, and so the incremental warming is perpetuated. Whilst we are unable to actively cool the oceans to keep the carbon in the water we can act to minimise the carbon released from the soil

through better soil management practices, and through maintaining or increasing areas of vegetation which absorb CO₂ from the atmosphere, thus preventing further rise in the temperature of the atmosphere.

Soil is composed of minerals derived from the parent material (clay, silt, sand), organic materials from the decomposition of plants and animals and open spaces or voids that may be air or water-filled. It is the variability in these components that make soil such a complicated medium to study. Not only does the soil itself vary greatly from one area to the next, but the additional elements present in soil such as plant material, animals and microorganisms further add to the complexity of soil. All of these properties have individual and combined effects on the structure and hydrodynamics (the flow and retention of water) of the soil. Add to that the different practices in tillage and fertilisation, drought and wildfires, flooding, deforestation, crop/planting regimens etc. and the picture of the study of soil grows increasingly complex.

In its widest sense, soil structure is defined as *“the size, shape and arrangement of solids and voids, continuity of pores and voids, their capacity to retain and transmit fluids and organic and inorganic substances. and ability to support vigorous root growth and development”* (Lal, 1991). The basic unit of the soil is the aggregate, which is composed of mineral particles, organic matter, water, air, and additional binding agents. Aggregates occur in a range of sizes, usually being categorised into macroaggregates (>250 µm) and microaggregates (<250 µm) with further size categories being defined (Tisdall and Oades, 1982). The mechanism of

soil aggregation is just as complex as the soil itself, with many factors influencing the formation and stabilisation of soil aggregates. For an excellent review of soil solid phase structure and aggregate formation and turnover, the reader is directed to Bronick (2005) (Figure 1.1 summarises these factors).

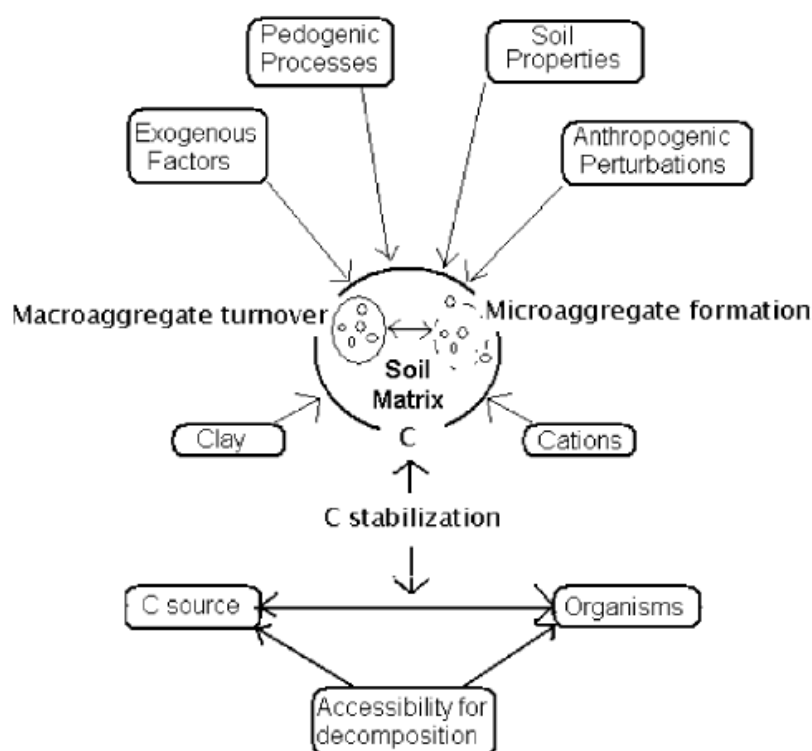


Figure 1.1 Factors affecting soil aggregation. Pedogenic = formation of soil, anthropogenic = influences of humans. Figure 2 in Bronick (2005).

1.2 Structural measurements of soil pores

Understanding the pore space in soil is the key to understanding water flow, which in turn governs the movement of solutes, nutrients, microbes and gases through the soil profile (Young *et al.*, 2001). With each different measurement of the properties of pore space, a more complete picture of the structure of the soil in question is attained.

1.2.1 Porosity

The soil pore space is the fraction of soil not occupied by solid material which can be air-filled or water-filled. Porosity is a fraction of the total volume therefore has a value between 0 and 1. Factors affecting soil porosity include soil texture, which is the proportions of clay, sand and silt (Figure 1.2), soil structure in terms of how the particles are bound together, compaction due to rainfall events or anthropogenic processes, and levels and types of organic matter present.

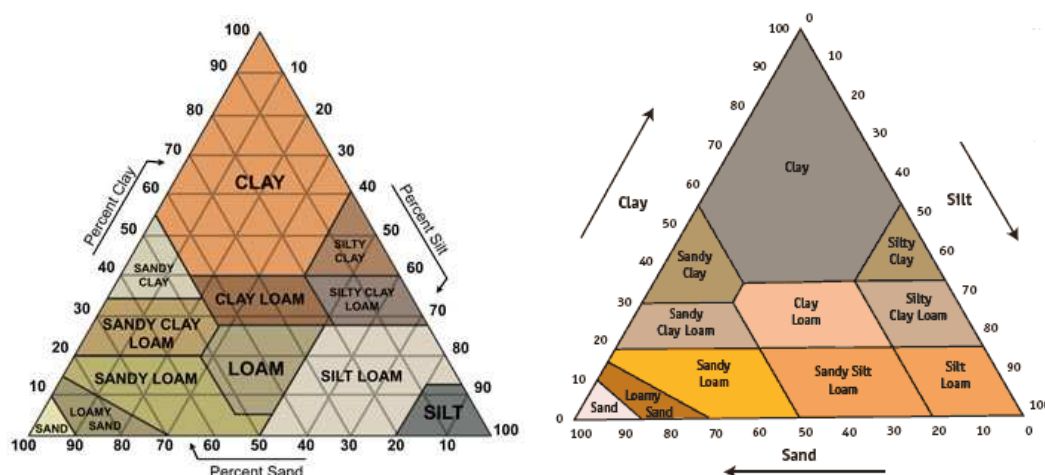


Figure 1.2 Soil texture classification triangles from the US (left) and the UK (right). The US has 12 soil classes, whereas the UK has 11. USDA (United States Department of Agriculture) triangle from <http://www.stevenswater.com/articles/images/soiltexturetriangle.jpg>, UK triangle from <http://www.scotland.gov.uk/Resource/Img/47121/0020508.gif>.

Nimmo (2004) discusses the different methods of measuring porosity. Whilst measuring water, gas or mercury-filled porosity have been the methods of choice until the advent of thin-sectioning or 3D tomographic image analyses, these former methods were limited in that only accessible

pore space was measured. Vesicles of pore space that are not connected to the soil boundary were not included in the calculation of porosity in these studies. On the other hand, image analysis methods do include these unreachable vesicles in their calculations, but are limited by their image resolution, so in these cases the porosity calculated is that of observed porosity. Depending on the purpose of the investigations, each of the methods has their merits and limitations (Nimmo, 2004).

Whilst porosity is a useful measurement in understanding the proportion of soil available for water flow and gas transport processes, the temporal location and spatial distribution of these void areas is crucial to developing a fuller picture of the soil structure.

1.2.2 Fractal dimension

Fractal dimension is a measure of how the complexity of a pattern changes as the scale at which it is measured changes (Falconer, 2003). In a Euclidean space objects have dimensions of integer values, 1 for a line, 2 for a plane and 3 for a volume. Fractal dimension, on the other hand, is a measure of the complexity of an object and has values in the ranges $[1, 2]$ in 2-dimensions, and $[2, 3]$ in 3-dimensions. The key to understanding fractal dimension is to consider the topological dimension in question. If the object is volume-filling (pore volume in soil), then it is 3 dimensional, a surface filling object (pore surface area) is 2 dimensional and if it is a line filling object then it is 1 dimensional. The further away the fractal dimension is from the

topological dimension, the more irregular the structure of the object. So a surface ($D=2$) that is close to a dimension of 3 is a very irregular surface and is nearly volume-filling, for example a piece of paper crushed into a ball is a very irregular surface, but an almost smooth solid sphere.

Many studies use fractal dimension as a measure of the structure of pore space in the soil volume (Figure 1.3) (Gibson *et al.*, 2006; Papadopoulos *et al.*, 2008; Luo and Lin, 2009; Tarquis *et al.*, 2009; Kumar *et al.*, 2010; Kravchenko *et al.*, 2011). As with porosity measurements, fractal parameters can be deduced from indirect measurements e.g. water retention curves (Crawford *et al.*, 1995) or directly using image analysis (Preston *et al.*, 2001; Young and Crawford, 2001; Tarquis *et al.*, 2009).

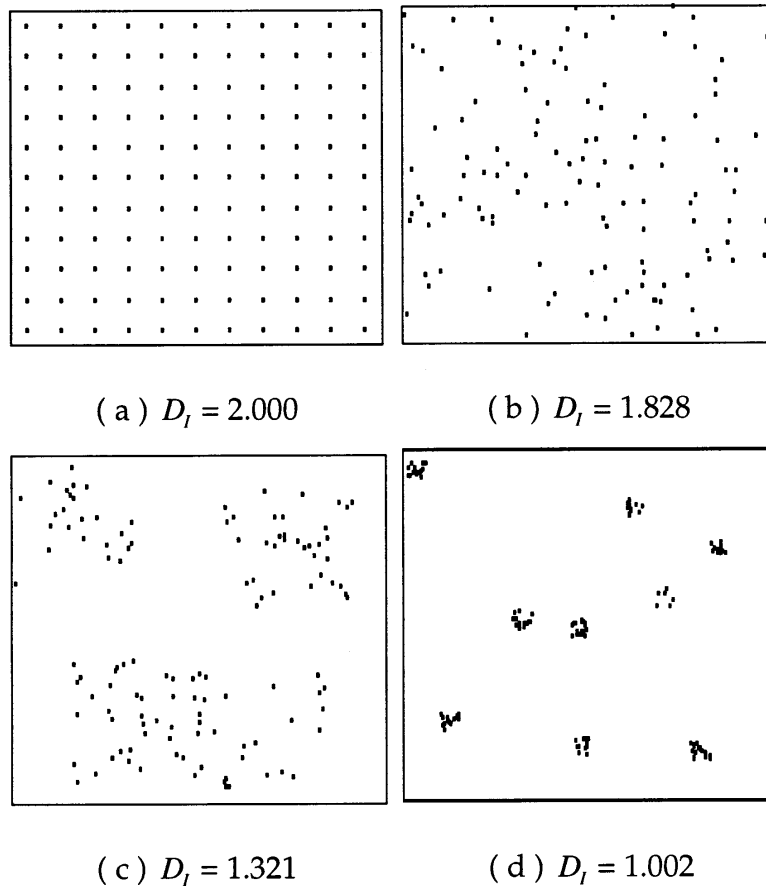


Figure 1.3 Illustration of a regular and evenly distributed structural arrangement (a and b) and a clumped and irregular distribution (c and d) and the respective fractal dimension values as drawn in Li (2000).

By having measurements of porosity and distribution of the pore space of a soil an understanding of proportion and location the pores are in the soil structure is gained. However, there is no information as yet about whether the pore space is made up of many small pores or fewer larger pores.

1.2.3 Pore size distribution

Pore size distribution (PSD) is, as the name suggests, a measure of the frequency of different pore size classes present in the soil volume.

As with porosity and fractal dimension, PSD can be inferred from water retention curves and mercury porosimetry and direct measurements are possible through image analysis (Schjønning *et al.*, 1999; De Gryze *et al.*, 2006; Bird *et al.*, 2008; Papadopoulos *et al.*, 2009; Pires *et al.*, 2010). The distribution of pores determines the availability of nutrients and gases for soil organisms and plants. Preferential flow paths, which are the “paths of least resistance” for chemical and biological processes to occur, are also influenced by pore size distribution through the soil. Of course there is no flow through soil profile if the pore spaces are not connected to each other.

1.2.4 Pore connectivity

Knowing how well connected the pore space is in the soil is key to understanding how water, gases, chemicals etc. are transported throughout the soil profile. It explains how different microorganisms can survive in the same soil volume and yet avoid predation or competition for nutrients or how the concentrations of certain chemicals or metal ions in the soil should be toxic to microbial life and yet microbes survive due to non-connected pore spaces creating barriers between predator and prey, or toxin and organism (Perret *et al.*, 1999; Preston *et al.*, 1999; Al-Raoush and Willson, 2005; De Gryze *et al.*, 2006; Bird *et al.*, 2008; Kilfeather and van der Meer, 2008; Carson *et al.*, 2010).

1.2.5 Cracking analysis

The four structural measurement of the pore space in soil outlined above (i.e.: porosity, fractal dimension, pore size distribution and pore connectivity) provide an overview of the proportion of void to solid space, how the pores are spatially distributed, the range of pore sizes and the connectivity of the pores available for soil processes. These are all within the soil volume and do not necessarily provide information about the surface connected pore space unless undisturbed soil cores have been extracted and the whole volume has been analysed.

In addition to surface connected pores, cracks which are formed as the soil dries and have a significant impact on the soil processes of gas and water flow as well as providing passageways for root development and

microbial processes (Preston *et al.*, 2001). Shrinkage cracks in the soil are pores formed at the surface during drying and are not the same as total porosity in soil (Velde, 1999). All of the structural measurements presented above of porosity, fractal dimension, pore size distribution and pore connectivity can be applied to cracking patterns in soil, allowing an understanding of the surface connected pore space to be elucidated. In addition to the naturally occurring pores connected to the surface, surface cracks formed on drying also introduce external components such as water, chemicals, roots and microorganisms etc. to the soil profile beneath the surface and allow the removal of the same (Guidi *et al.*, 1978; Mele *et al.*, 1999; Preston *et al.*, 1999; Velde, 1999; Horgan and Young, 2000; Li, 2000; Preston *et al.*, 2001; Velde, 2001; Li *et al.*, 2004; Vogel *et al.*, 2005b; Baer *et al.*, 2009).

1.3 Soil hydrodynamics

While structural measurements of the soil matrix can provide information about pore space volume, distribution and connectivity, an understanding of the dynamic flow of water incorporating the movement of chemicals and microorganisms through the soil profile is obtained through measurements of water retention curves, drainage profiles and infiltration, collectively referred to as the soil hydrodynamics.

1.3.1 The water retention curve

A water retention curve (WRC) is a plot of the water content (θ) of a soil volume, either gravimetric (kg kg^{-1}) or volumetric ($\text{m}^3 \text{ m}^{-3}$), against the downward suction pressure (matric potential, MP or Ψ_M , in kPa or pF or -m, matric head, MH or h , in m) exerted on that soil volume. Adhesion and cohesion forces between water molecules and soil particles is known collectively as capillarity and enables soil to retain water against the force of gravity (Doerr *et al.*, 2000). Adhesion is the attraction of the water particles via their H^+ ions to the surface of the soil particle which has a net negative charge due to unsatisfied oxygen anions in the mineral structure. Cohesion is the strong attraction of water molecules for each other which builds layers of water molecules around the soil particle surface (Figure 1.4).

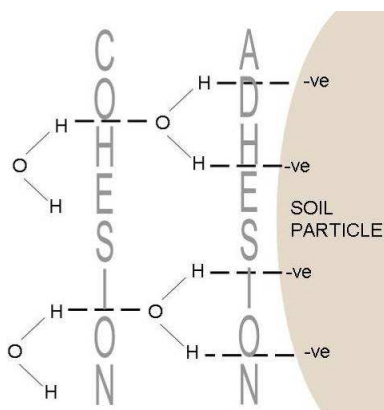


Figure 1.4 Capillarity in soil is due to adhesive and cohesive forces of between the water molecules and the soil particles.

Soil particle sizes determine the amount of water retained due to the surface area. The smaller the particle sizes in a given volume the greater the capillary water retention. As such different soil types have their own typical water retention curves with sandy soil (0.05 mm - 2mm grains) being

the most easily drained and clay (<0.002 mm grains) being the most retentive as illustrated in Figure 1.5.

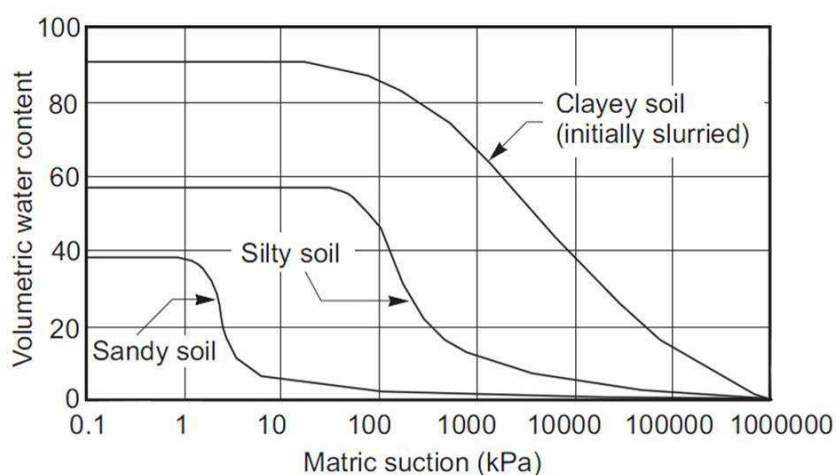


Figure 1.5 Typical water retention curves for sand, silt loam and clay soils from Fredlund and Xing (1994). Saturated water content is indicative of porosity, and the slopes of the curves are representative of variable pore size distributions.

Water retention is the ability of soil to hold or retain water. A soil is described as being saturated when it is retaining water above the normal gravitational pull and this is caused in nature by an impervious layer restricting movement of water in the soil profile, and when there is no evaporation from the surface or uptake by plants in the matrix. As water is drained such as by controlled suction in the laboratory, the ability of soil to retain water is determined by its total soil water potential which is a measurement of the energy that soil water contains. Total soil water potential (Ψ_T) is the sum of three components: (i) the gravitational potential (Ψ_G), which is the pulling force of gravity on the water being held in the pore spaces in soil; (ii) the matric potential (Ψ_M), which is the pulling force of the soil particles on the pore water; and (iii) the osmotic potential (Ψ_O), which is

the pulling force of dissolved salts (ions) on the pore water (Marshall and Holmes, 1979; Hillel, 1998).

The water retention curve (WRC; also known as the Moisture Characteristic, MC) is probably one of the most important functions in soil management. The WRC defines the relationship between the soil's matric potential (ψ_M) and the total moisture content of soil. A schematic of a WRC is illustrated in Figure 1.6.

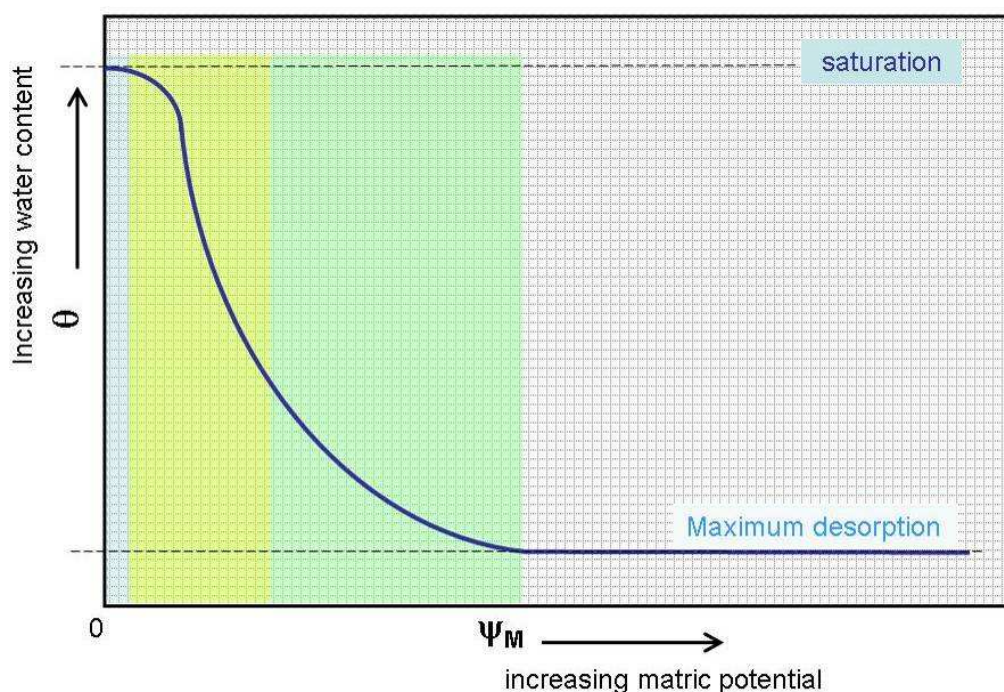


Figure 1.6 Schematic of water retention curve of soil. The drying curve at 0 ψ_M (matric potential) is equivalent to a saturated sample (blue area), where all connected pores are full of water (θ_s). As ψ_M increases the larger pores start to empty and the curve becomes negative (yellow). As the slope of the curve decreases this is indicative of the reflection curve where most of the larger pores are now empty and the smaller pores start to empty (green). θ is soil water content.

Although the WRC curve illustrates the emptying of the pores, it is important to realise that 'empty' does not necessarily mean a pore space is completely

devoid of water, but that a meniscus of water may still exist between the solid materials due to surface tension (capillarity) and a film of fluid will also remain on the surface of the aggregate due to adhesion forces Figure 1.7 (Or and Tuller, 1999).

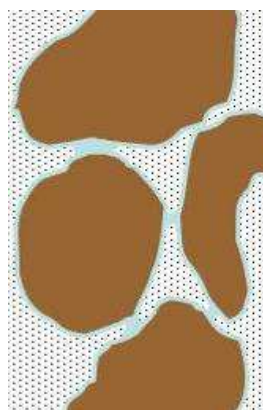


Figure 1.7 Menisci and films of fluid in a drained porous structure. Menisci of water are held in pores by capillarity, whereas the film of wetting fluid on the surfaces of the solid material is held by adhesion. Brown areas represent soil aggregates, blue areas represent water and black dotted areas represent air-filled pore space.

These menisci of water create a mosaic of microenvironments resulting in the heterogeneous distribution of microorganisms in the soil (Young and Ritz, 2000). The micro-niches differ in their physical, chemical and biological properties, and affect bacterial motility, nutrient availability, oxygen availability and hence growth and exudate production by the bacteria (Nunan *et al.*, 2002; Nunan *et al.*, 2003; Ruamps *et al.*, 2011).

Another aspect to consider when investigating water flow through the soil is that of preferential flow whereby the passage of water through the soil matrix is not uniform across the wetting front. These preferential flow

patterns can similarly disrupt the growth and motility of bacteria and their exudate production, either through altering the bacteria's ability to produce the exudates or by sweeping away the products before the bacteria has benefitted from their presence, which in turn negates the energy expenditure of the bacteria in producing these protective compounds (Morales *et al.*, 2010). Whilst the investigation of preferential flow of water through soil was outwith the scope of this study primarily due to the scale and nature of the experimental system, the flow of water into the soil has been investigated by means of a sorptivity assay on the bacteria-treated soils.

1.3.2 Sorptivity

The water retention curve provides static information about the soil matrix, whereas infiltration measurements contain dynamic information related to the capillary drive (Morel-Seytoux and Nimmo, 1999). Infiltration of water into soil is governed by gravity and capillary action and when infiltration (in m) is plotted against time (s) the linear relationship observed in the first 1 to 3 minutes is the sorptivity of the soil ($\text{m s}^{-1/2}$) as illustrated in Figure 1.8.

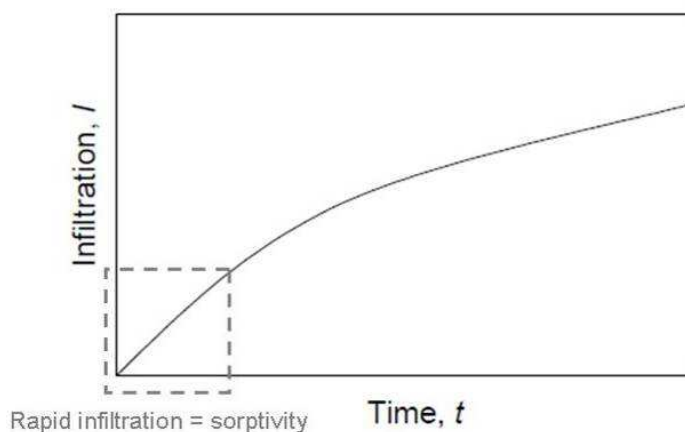


Figure 1.8 Illustration of water infiltration curve highlighting the rapid infiltration rate and linear relationship of the curve in the first 1 to 3 minutes which defines the soil sorptivity. Adapted from Hallett (2007).

Sorptivity (S) is a measure of the capacity of a porous medium to absorb liquid by capillary action (Philip, 1957) and the rapid infiltration at the onset of wetting can be represented by the equation

$$I = St^{\frac{1}{2}} + At$$

Equation 1.1 Representation of Infiltration

Philip's (1957) representation of infiltration where I is infiltration, S is sorptivity, t is time, and A is a curve fitting parameter related to hydraulic conductivity

One of the key determinants in the wettability of soil is the repellency of that soil. Soil repellency can be affected by a soil's antecedent water content, and also by the presence of hydrophobic compounds in the soil matrix (White *et al.*, 2000; Hallett, 2007; Morales *et al.*, 2010)

Antecedent water content of soil has been shown to affect how the water flows through soil particularly in the context of preferential flow. Instead of following a uniform pattern of infiltration into the soil profile, water

follows preferential paths. These paths can be formed by shrinkage cracks, biopores (e.g. created by earthworms and root pathways), by water repellent areas, and by air-entrapment. If a soil has been allowed to significantly dry prior to wetting, there is greater likelihood of these preferential pathways developing (Ritsema *et al.*, 1998; Bauters *et al.*, 2000).

Both water flow (hydraulic conductivity) and sorptivity are controlled by the shape, volume and tortuosity of pores in the soil. Tortuosity is defined as “*the non-straight nature of soil pores*” (SSSA, 2012). Generally a soil with larger pores has a greater hydraulic conductivity but smaller sorptivity than a soil with smaller pores. Antecedent water content and water repellency are also factors in the infiltration of water into soil (Hallett, 2007), and a soil may become water repellent following drying (Bond and Harris, 1964).

1.3.3 Water repellency

Water repellency (soil hydrophobicity), affects plant growth, surface and subsurface hydrology and soil erosion. It is widely accepted that water repellency in soil is caused by the accumulation of long-chained organic compounds on or between soil particles. However, the understanding of the exact chemical composition of these compounds and how they attach to particle surfaces is incomplete (Doerr *et al.*, 2000; Doerr *et al.*, 2002). Repellency is a transient property mainly associated with fluctuations in soil moisture content and follows short-term and seasonal variations. A degree of repellency is a desirable property for soils in that it reduces the structurally disruptive effects of rapid wetting (Hallett and Young, 1999), thereby

increasing aggregate stability. However, if the repellency is too great, as is often observed following wildfire events, then water run-off and overland flow during rainfall events leads to enhanced erosion (DeBano, 2000). The fluctuation in moisture content of soil interacts with the exudates produced by plant roots and some soil microbes, which act to enhance nutrient availability and defend against desiccation (Hallett *et al.*, 2003). These, mostly amphiphilic exudates, are strongly hydrophilic when wet, but below a critical moisture level will bond to each other and the soil particles leaving their hydrophobic components externalised and conveying hydrophobicity to the soil surface. In this thesis the source of these additional exudates is bacterial.

1.4 Bacteria in soil

“In a handful of fertile soil there are more individual [micro-] organisms than the total number of human beings that have ever existed. Yet, due to the inherently large surface area of soil, only $1 \times 10^{-5}\%$ of the total surface area is covered by microbes” (Young, 2010; Li and Zhang, 2011).

In cultivated soil the estimate is 3.5×10^{15} bacterial cells per m^2 soil (Whitman *et al.*, 1998). Bacteria have vital roles in not just the soil ecosystem, but also in the wider ecosystem, for example in the carbon, nitrogen, phosphorous and oxygen cycles. Of the Kingdom *Bacteria* the key phyla in the soil are *Proteobacteria*, *Actinobacteria*, *Cyanobacteria* and *Firmicutes*. Within these phyla are *Nitrosomonas*, *Nitrobacter*, *Actinobacteria*, *Rhizobium* and *Pseudomonas*, which are key bacteria in

nitrogen fixation and mineralization, and organic matter decomposition and humus turnover.

Proteobacteria, and in particular *Pseudomonas* spp. have been shown to be the most abundant phylum and genus respectively in soil (Janssen, 2006; Schloss and Handelsman, 2006; Spain *et al.*, 2009). Proteobacteria are Gram-negative bacteria. Their cell envelope is composed of an inner membrane, followed by a thin periplasmic cell wall, and a semi-permeable outer membrane that is only present in Gram-negative bacteria (Figure 1.9). Gram-negative bacteria are so-called because they do not retain the purple-violet colour Gram stain used in identifying bacteria (Gram, 1884).

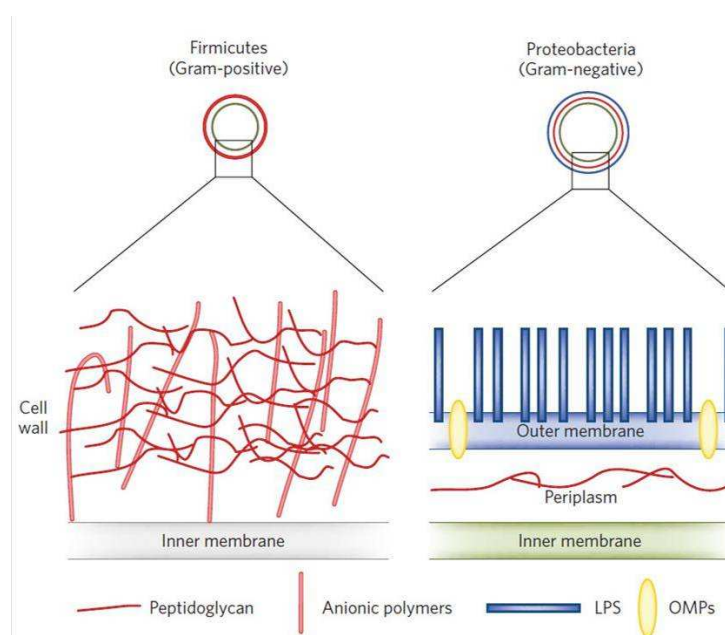


Figure 1.9 Illustration of outer cell envelope of gram-positive and gram-negative bacteria (Figure 1 in Vollmer, 2012). LPS = lipopolysaccharide, OMP = outer membrane protein.

A key structure of interest to this study is the lipopolysaccharide (LPS) which composes the outer leaflet of the outer membrane of Gram-negative bacteria. The two additional bacterial components of interest in this study are

surfactants and exopolysaccharides, which are produced and released from bacteria. Microbial exudates have been shown to play an important role in soil structure (Dorioz *et al.*, 1993; Oades, 1993; Chenu and Cosentino, 2011)

1.4.1 Key bacterial components of interest in this study

1.4.1.1 Lipopolysaccharide

As discussed above, lipopolysaccharides (LPS) are a structural component in the outer leaflet of the Gram-negative outer membrane. Also referred to as surface-active compounds (SAC), these microbial lipids are high molecular weight amphiphilic polymers with a hydrophobic end and a hydrophilic region (Neu, 1996) (Figure 1.10).

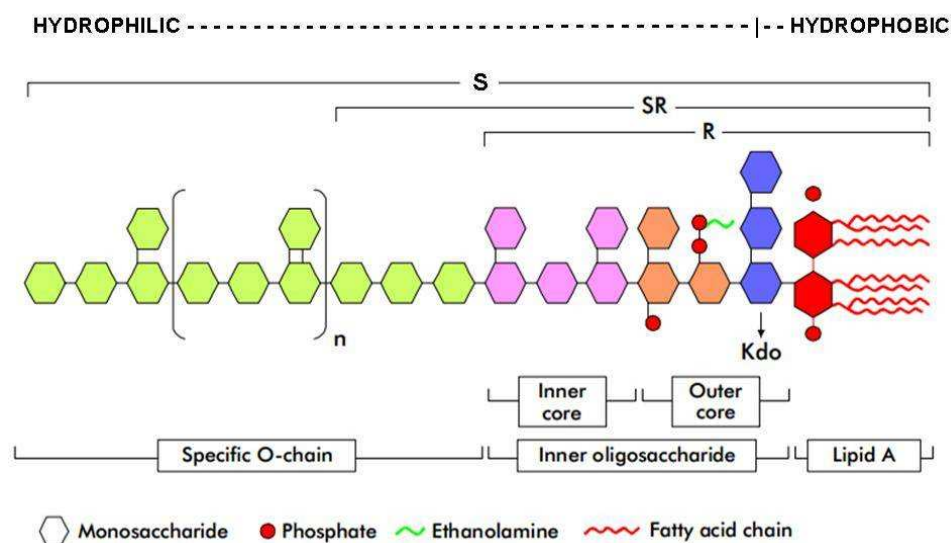


Figure 1.10 General schematic structure of bacterial lipopolysaccharide. Smooth type (S) LPS possess a hydrophilic polysaccharide specific O-chain of 2 or more repetitive units. Semi-rough (SR) type LPS contain a single repetitive unit of specific O-chain. Rough type (R) LPS do not have any specific O-chain units. The hydrophobic Lipid A head is anchored in the bacterial cell membrane. Image adapted from Pupo and Hardy (2009).

Adhesion of LPS-containing microbes to a solid phase, such as soil, will eventually form a layer analogous to a conditioning film that will change the properties of the original surface. Additionally, LPS molecules are continuously released into the environment, not only upon cell death, but also during growth and division (Magalhaes *et al.*, 2007). Williams and Fletcher (1996) discuss the roles of different bacterial compounds on the adhesion and transport of bacteria through porous media and suggest that polymers with non-polar (hydrophobic) sites, like LPS, may dominate in binding to hydrophobic surfaces. The addition of bacterial LPS to clay soil particles has also been shown to increase the water contact angle, thus decreasing wettability and contributing to repellency (Chen and Zhu, 2004).

1.4.1.2 The surfactant viscosin

Surfactants are also amphipathic, with both hydrophilic and hydrophobic regions, which means that they will preferentially gather in areas with different polarities such as at an air-liquid (A-L) interface (Desai and Banat, 1997). The cyclic lipopeptide (CLP) viscosin is a biosurfactant of low molecular weight and although not attached to the cell like LPS, is also considered an SAC (Neu *et al.*, 1990; Neu, 1996; de Bruijn *et al.*, 2007; Saini *et al.*, 2008). Figure 1.11 illustrates its chemical structure.

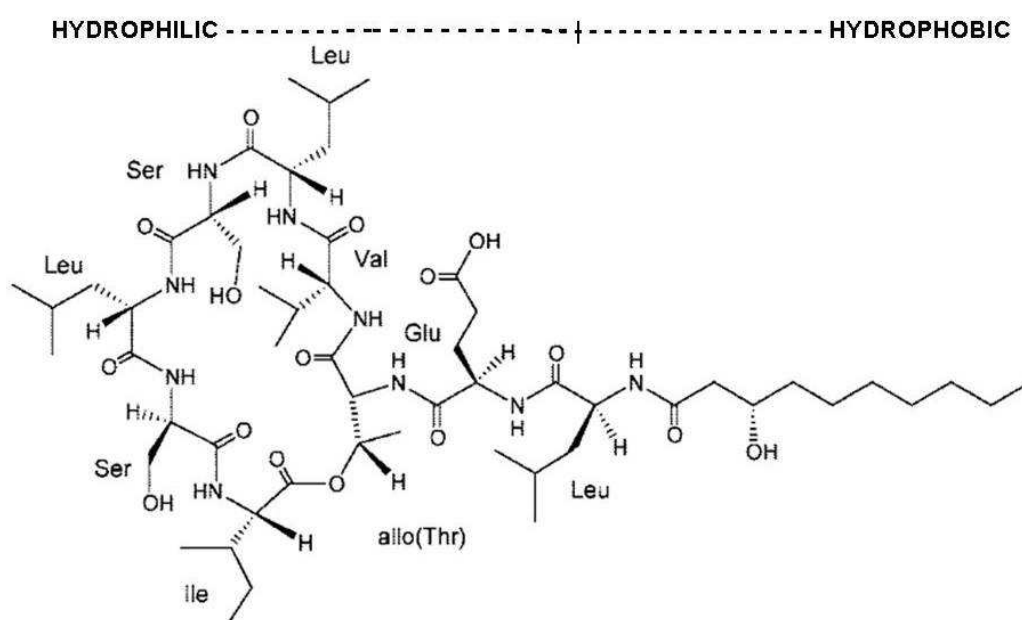


Figure 1.11 Chemical structure of viscosin, a cyclic lipopeptide surfactant. The polar cyclic oligopeptide region is hydrophilic and the non-polar fatty acid (lipid) tail is hydrophobic. Image adapted from Saini *et al.* (2008).

Viscosin was originally isolated from a *Pseudomonas* strain and has been shown to enable wetting of the extremely waxy hydrophobic surface of broccoli leaves by reducing the surface tension of the water (Neu *et al.*, 1990; Laycock *et al.*, 1991; Braun *et al.*, 2001). In addition to the effect of

viscosin on the wettability of solid surfaces, biosurfactants will act to increase the solubility of hydrophobic substances and facilitate their distribution through the soil, which will exacerbate water repellency and produce preferential flow channels for water distribution (Morales *et al.*, 2010). Surfactants have been shown to affect aggregate stability if the concentration of applied surfactant modifies the soil hydrophobicity and the altered soil aggregates stability enables changes in soil porosity and pore size distribution, thereby affecting fluid retention and fluid conductivity of soils (Piccolo and Mbagwu, 1989; Allred and Brown, 1994; Hillel, 1998; Abu-Zreig *et al.*, 2003; Rao *et al.*, 2006).

1.4.1.3 Exopolysaccharides

When bacteria attach to surfaces they form biofilms which provide structured optimal environments for growth, reproduction, exchange of genetic material and protection against desiccation (Donlan, 2002). The biofilm is composed of a mesh of exopolymeric substances (EPS), of which the primary component is the exopolysaccharide matrix (Sutherland, 2001). The role of the exopolysaccharides are to provide structure and protection (i.e.: from both desiccation, since they are usually capable of holding many times their own weight in water and phagocytosis) and may also act as a food source.

In an excellent overview of biofilm exopolysaccharides, Sutherland (2001) discusses the variety of exopolysaccharides synthesized by microbial cells in terms of their composition, chemical and physical structures. Sutherland (2001) states that “*unfortunately, because of the widespread*

study of biofilms produced by alginate-synthesizing strains of *Pseudomonas aeruginosa*, the concept has perhaps arisen that all biofilms contain very highly charged uronic-acid-containing polysaccharides and all biofilm polysaccharides are similar.” In fact, biofilm exopolysaccharides can be neutral macromolecules, polyanionic or even polycationic (Mack *et al.*, 1996; Sutherland, 1997).

Bacterial alginate is produced by *Azotobacter* and *Pseudomonas* and consists of only two uronic acid components, β -(1,4)-linked D-mannuronic acid (M) and α -(1,4)-linked L-guluronic acid (G) in an unbranched polymer chain (Figure 1.12).

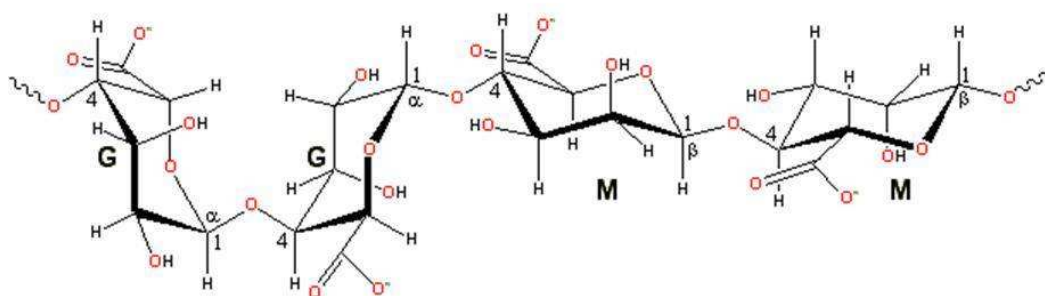


Figure 1.12 The basic chemical structure of alginate ($C_6H_8O_6$)_n. Image from Chaplin (2012).

Alginates differ depending on the source and the proportions of each monomer in the alginate give rise to polymers with very different rheological and physiochemical properties. Alginates are water-insoluble and strongly anionic and therefore will interact with counterions in their environment such as calcium ions (Ca^{2+}) and hydrogen ions (H^+) to form bridges between multiple G-polymer chains in particular resulting in a more rigid gel structure. M-rich polymer chains do not replace the hydrogen bonds with Ca^{2+} ions and

therefore form a softer gel that is more porous and less stable (Remminghorst and Rehm, 2009).

The exopolysaccharide of interest in this study is cellulose. Cellulose is an unbranched polymer of β -1,4-linked glucopyranose residues (Figure 1.13). Multiple glucan chains associate by intramolecular hydrogen bonds to form microfibrils, which is the basic structural unit of cellulose.

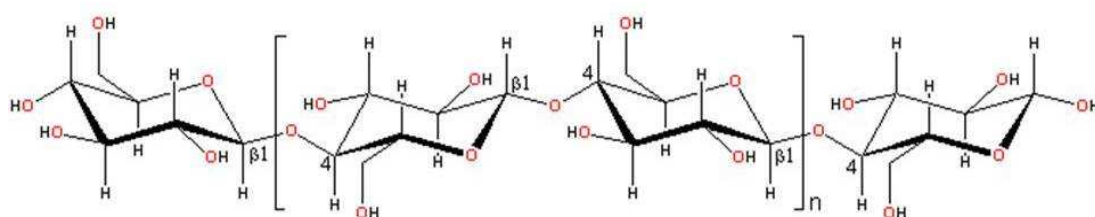


Figure 1.13 The basic chemical structure of cellulose ($C_6H_{10}O_5$)_n. Image from Chaplin (2012).

There are two types of cellulose in nature, cellulose I and II. Cellulose I (Figure 1.14) is the native cellulose produced by bacteria, algae and plants and has two crystalline allomorphs designated I_α and I_β (Figure 1.15).

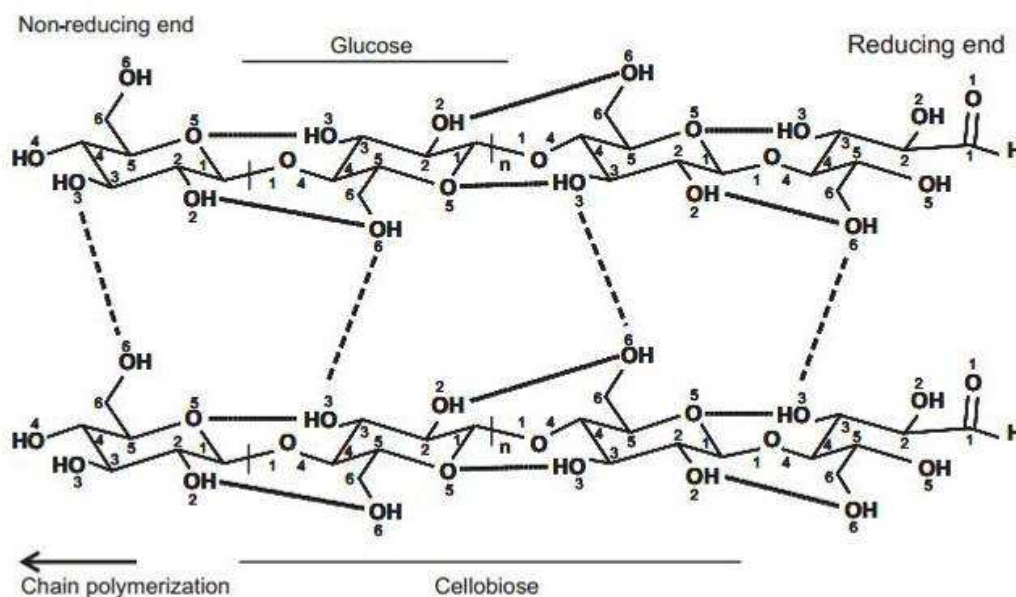


Figure 1.14 The inter- and intra-chain hydrogen bonding in cellulose I. Dashed lines: inter-chain hydrogen bonding. Solid lines: intra-chain hydrogen bonding. Image from Festucci-Buselli *et al.* (2007)

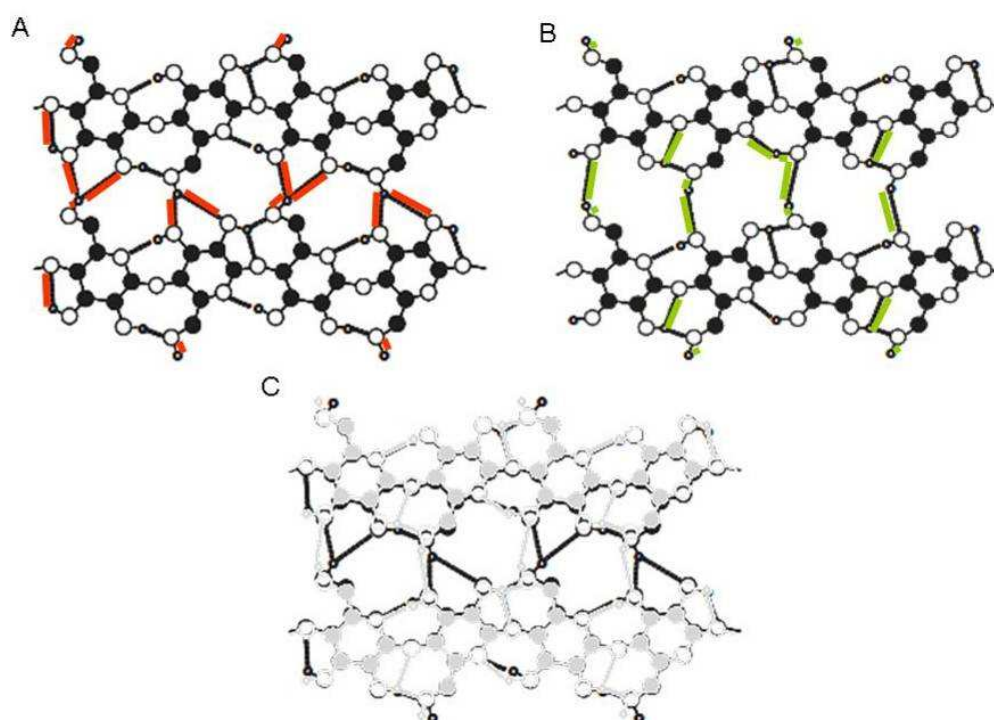


Figure 1.15 Hydrogen-bonding patterns in cellulose I α (A) and I β (B) based on the crystal structures of Nishiyama *et al.* (2002; 2003) adapted from Festucci-Buselli (2007). Differences in hydrogen bonds are represented by coloured lines. (C) is an overlay of I α (A, black) and I β (B, grey).

Bacterial cellulose (BC) is a highly pure form of cellulose and is predominantly cellulose I_α whereas plant cellulose (PC) has a much higher proportion of cellulose I_β and is usually associated with hemicellulose and pectin. The chemical composition of BC is identical to PC, but its macromolecular structure and its properties are different. BC produces subfibrils approximately 1.5 nm in width which crystallise to form microfibrils that then form bundles and finally ribbons (Bielecki *et al.*, 2002). Table 1.1 presents the cellulose structure particular to different bacterial genera.

Table 1.1 Bacterial cellulose producers and their respective cellulose structures. From Bielecki *et al.* (2002) adapted from Jonas and Farrah (1998).

<i>Genus</i>	<i>Cellulose structure</i>
<i>Acetobacter</i>	extracellular pellicle composed of ribbons
<i>Achromobacter</i>	fibrils
<i>Aerobacter</i>	fibrils
<i>Agrobacterium</i>	short fibrils
<i>Alcaligenes</i>	fibrils
<i>Pseudomonas</i>	no distinct fibrils
<i>Rhizobium</i>	short fibrils
<i>Sarcina</i>	amorphous cellulose
<i>Zoogloea</i>	not well defined

Cellulose is detectable using fluorescent microscopy and the stain Calcofluor (Figure 1.16).

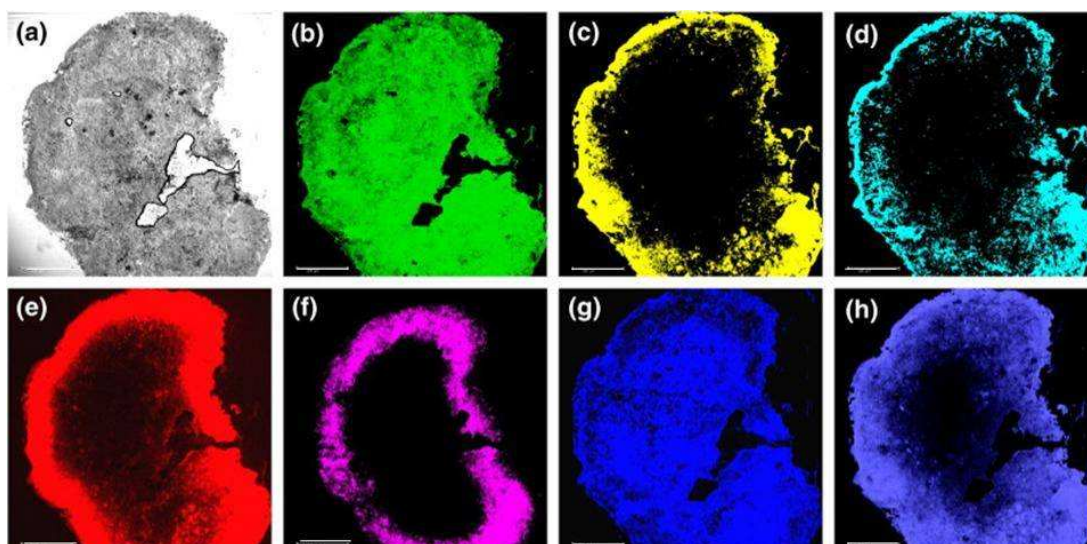


Figure 1.16 Illustration of fluorescent labelling of bioaggregate of *Bacteroides* sp. to visualise exopolymeric substances. (a) Phase contrast image; (b) green (FITC) proteins; (c) yellow (Nile red) lipids; (d) cyan blue (ConA) α -d-glucopyranose polysaccharides; (e) red (SYTO 63) nucleic acids; (f) pink (SYTOX Blue) dead cells; (g) blue (Calcofluor white) β -d-glucopyranose polysaccharides; (h) purple blue (Calcium Green) calcium. Bar = 300 μ m. Image from Adav *et al.* (2010). The reader is directed to image (g) staining of β -d-glucopyranose polysaccharides by Calcofluor white.

The model organism in this study has been shown to produce cellulose in its EPS (Gal *et al.*, 2003; Rainey *et al.*, 2003; Ude *et al.*, 2006). Figure 1.17 shows the Calcofluor white staining of the wrinkly spreader (WS) mutant of *Pseudomonas fluorescens* SBW25 strain.

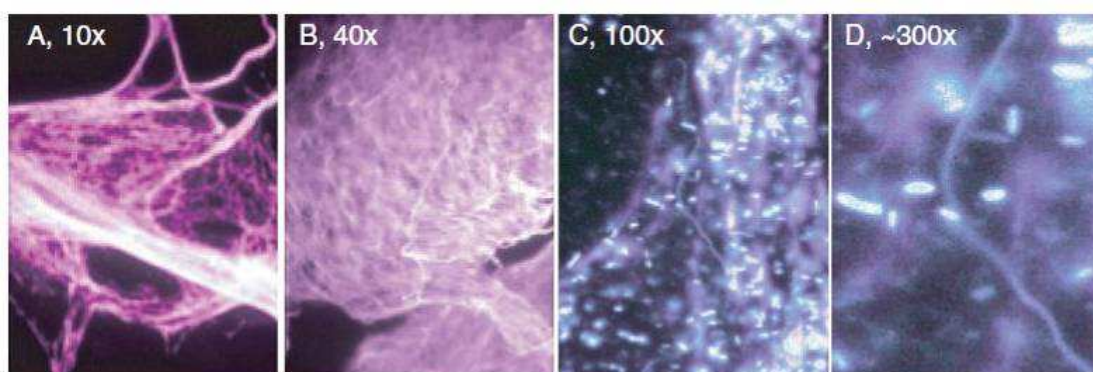


Figure 1.17 Microphotographs for *Pseudomonas fluorescens* SBW25 Wrinkly-spreader (WS) cellulose-overexpressing mutant. The air-liquid interface biofilm samples are stained with Calcofluor highlighting cellulose fibres. A. A large clump of material viewed at low magnification (10x); and B, viewed at medium magnification (40x) showing the variations in structure, including net-like regions, pore and fibres. C. Bacterial cells associated closely with cellulose fibres seen at high magnification (100x). D. Enlargements of the central portion of C showing a single cellulose fibre with a width of approximately the same as that of a cells (<0.02 μm). Note that *P. fluorescens* cells show a high level of autofluorescence. Images and description reused with kind permission from Dr A.J. Spiers (Spiers *et al.*, 2003).

1.4.2 Model organism – *Pseudomonas fluorescens* SBW25

The bacterial model used in the study is *Pseudomonas fluorescens* SBW25, which was isolated from the sugar-beet phyllosphere in Oxfordshire in 1989 (Thompson *et al.*, 1995) and genetically mapped by Rainey and Bailey (1996). It is a Gram-negative, rod-shaped bacterium, given the name *fluorescens* because it secretes a soluble fluorescent pigment (pyoverdine), which is a type of siderophore or proteinaceous iron-chelating compound. The “SBW25” nomenclature is derived from the plant from which the strain was isolated, **s**ugar **b**eet; and **W**ytham, the farm in Oxfordshire where the sugar beet plants grow. The **25**, is the successful isolate number out of 50 that were investigated at the time.

P. fluorescens strains are saprophytic bacteria capable of colonising a variety of ecological habitats, including soil, water, root and leaf surfaces, and internal plant tissues. They are predominantly rhizosphere plant-growth promoting (RPGP) bacteria, despite a close phylogenetic relationship to a number of other *Pseudomonas* spp. that are plant, fungal and animal pathogens. SBW25 is able to colonise the rhizosphere of a number of different plants and readily grows in vermiculite-compost and repacked soil microcosms (Gal *et al.*, 2003; Silby *et al.*, 2009; Fechtner *et al.*, 2011).

The SBW25 chromosome was first mapped by Paul Rainey and Mark Bailey in 1996 (Rainey and Bailey, 1996) and the full genome determined by The Sanger Centre (Silby *et al.*, 2009). The molecular biology of SBW25 has been extensively investigated for plant-microbe interactions (Gal *et al.*, 2003; Preston *et al.*, 2003; Silby *et al.*, 2009) and for bacterial adaptation and biofilm formation (Spiers *et al.*, 2002; Spiers *et al.*, 2003; Ude *et al.*, 2006; Bantinaki *et al.*, 2007; Spiers, 2007). This research has provided a number of genetically-defined mutants which are deficient in the production of components which might be expected to alter soil structure and hydrological behaviour. These include; (i) lipopolysaccharide (LPS) which forms the outer membrane of the bacterial cell; (ii) the glycocalyx (extracellular polymeric substances (EPS), which forms the matrix of air-liquid (A-L) interface biofilms in experimental static liquid microcosms and (iii) and the surfactant viscosin which has multiple antagonistic roles in biocontrol (Healy *et al.*, 1996; Makin and Beveridge, 1996; Williams and Fletcher, 1996; Beech *et al.*, 1999; Gomez-Suarez *et al.*, 2002; Gal *et al.*, 2003; Rainey *et al.*, 2003; Ude *et al.*, 2006).

Five *P. fluorescens* SBW25 strains were used in this study, including wild-type SBW25 and four isogenic mutants, and the key features of these are detailed in the following paragraphs.

Wild-type (or SM) is used to refer to the wild-type *P. fluorescens* SBW25 strain originally isolated by Thompson *et al.* (1995). Wild-type SBW25 grows robustly *in vitro*, in soil and the rhizosphere, and is genetically stable. It is also often referred to as 'SM' (Smooth) after the smooth, rounded colonies it produces on King's B (KB) agar plates. Wild-type SBW25 expresses LPS as part of the normal cell surface (Spiers and Rainey, 2005). It is also able to express viscosin, EPS and attachment factor (Spiers and Rainey, 2005; de Bruijn *et al.*, 2007) under the appropriate conditions. Whilst the environmental signals regulating the expression of these components are unknown, viscosin is known to be expressed in late log-phase KB cultures, and EPS and attachment factor are very poorly expressed in static liquid KB microcosms and KB plates (Spiers *et al.*, 2002; Koza *et al.*, 2009). The attachment factor has not yet been identified, but is probably a pili-like fimbriae. Viscosin is expressed in soil microcosms (Fechtner *et al.*, 2011) and there is evidence for EPS expression on sugar beet roots and leaves, but not in bulk soil (Gal *et al.*, 2003).

ViscA mutant is a deletion-mutant of wild-type SBW25 no longer able to express the surfactant viscosin (de Bruijn *et al.*, 2007). This mutant is genetically stable, is maintained on selective (kanamycin) agar, and grows robustly *in vitro* and in soil. The surfactant-negative phenotype of the *ViscA* mutant is readily seen in the foaming behaviour of over-night KB cultures (Figure 1.18 below). Despite such a simplistic test for viscosin, this

demonstrates that expression is growth phase-dependent, with viscosin only detectable in stationary phase cultures. The *ViscA* mutant is expected to express LPS, cellulose and attachment factor like the wild-type SBW25 under the appropriate conditions.

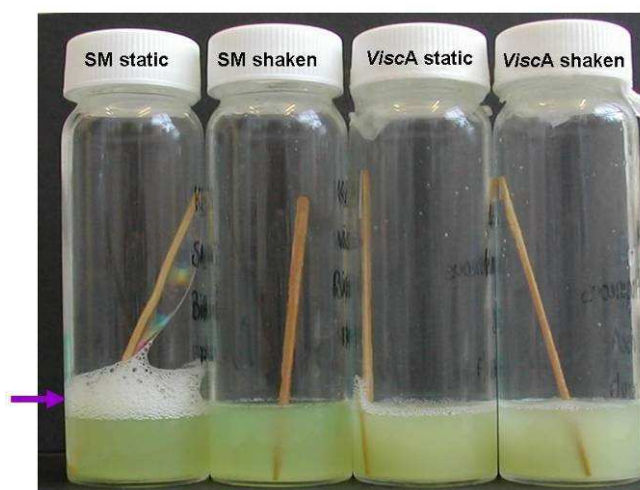


Figure 1.18 Foaming behaviour of wild-type SBW25 in KB cultures. The expression of the surfactant viscosin by wild-type SBW25 is readily demonstrated by the foaming of cultures in comparison with *ViscA* cultures. King's B microcosms were inoculated with wild-type SBW25 ('SM') and the viscosin-deficient mutant *ViscA* and incubated statically or with shaking for 24 hours at 28°C. The microcosms were then briefly shaken together and allowed to settle; the purple arrow highlighting the foaming produced by wild-type SBW25 expressing viscosin. Expression is delayed in shaken microcosms, perhaps because under better aeration conditions the culture has yet to reach stationary phase growth. The *ViscA* mutant shows no sign of foaming in either static or shaken microcosms.

Wrinkly Spreader mutant (WS) is a naturally-occurring mutant of wild-type SBW25 (Bantinaki *et al.*, 2007). This mutant produces wrinkled colonies and forms an A-L interface biofilm in static microcosms (Spiers *et al.*, 2002). The WS phenotype requires the over-expression of cellulose and an unidentified pili-like attachment factor (Spiers *et al.*, 2003). This mutant produces LPS as part of the normal cell surface (Spiers and Rainey, 2005) and viscosin under the appropriate conditions (A. Koza & A.J. Spiers, pers.

comm., 9 August 2007). The WS grows robustly *in vitro* but is known to be genetically unstable under conditions in which the WS phenotype is not advantageous (Spiers, 2007).

WS-4 mutant is a cellulose and attachment factor-deficient mini-Tn5 transposon mutant of the WS (Spiers and Rainey, 2005). In this mutant, the normal genetic expression of the diguanylate cyclase (DCG) response regulator called WspR is prevented. DCG participates in the process required for bacterial biofilm formation and persistence, and as a result, WS-4 no longer expresses cellulose or attachment factor like the WS, but produces smooth wild-type-like colonies on KB agar plates (Spiers *et al.*, 2002; Spiers and Rainey, 2005). In soil, it is likely that WS-4 is unable to express cellulose and attachment factor like wild-type SBW25 due to the disruption of WspR expression. WS-4 grows robustly *in vitro* and is maintained on selective (kanamycin) agar.

WS-5 mutant is an LPS-deficient mini-Tn5 transposon mutant of the WS (Spiers *et al.*, 2002; Spiers and Rainey, 2005). In this mutant, normal membrane function is disrupted, and as a result, WS-5 no longer expresses LPS on the cell surface. However, it still expresses cellulose and attachment factor, and produces smooth wild-type-like colonies on KB agar plates (Spiers *et al.*, 2002; Spiers and Rainey, 2005). WS-5 grows poorly *in vitro* and is maintained on selective (kanamycin) agar.

In a study reporting some of the results obtained in this thesis, it has been found that “*surfactant-expressing pseudomonads could modify local soil-water distributions and that surfactants may therefore play a significant*

hydrological role in soils, in addition to their recognised biological activities" (Fechtner *et al.*, 2011). In this study, the effect of the model organism, *P. fluorescens*, on the properties of the 3D structure of soil was investigated using X-ray computed tomography.

1.5 X-ray computed tomography

1.5.1 X-ray physics

X-rays are a form of electromagnetic radiation emitted by the electrons around the nucleus. In terms of the electromagnetic spectrum, X-rays have shorter wavelengths (higher energies) than UV, but longer wavelengths (lower energies) than γ -rays. Soft X-rays are typically in the range of 0.12 to 12 keV with wavelengths of 10 to 0.10 nm, whereas hard X-rays are typically in the range of 12 to 120 keV with wavelengths of 0.10 to 0.01 nm. In addition to these, very hard X-rays, such as those produced by synchrotron radiation sources, are in the order of approximately 80 keV to 1000 keV (1 MeV). These very high energy X-rays, whilst being in and beyond the energy range of γ -rays, are still defined as X-rays as they originate from the electrons around the nucleus of the atom, whereas γ -rays, by definition, originate from the nucleus.

1.5.2 The CT scanner

In a computed tomography (CT) scanner, X-rays are generated by the high voltage acceleration of electrons released from a hot cathode, the filament,

through the vacuum tube towards an anode, the target. Upon impact of the incident electron beam with the target metal, X-rays are produced via two different atomic processes, X-ray fluorescence and Bremsstrahlung radiation. X-ray fluorescence, also referred to as K-shell emission, is the production of X-rays when electrons on the innermost (lowest state) electron shell (K-shell) are knocked out of the configuration by the incident electrons and outer electrons drop down into the K-shell to replace the scattered electrons, losing energy as they do so, which is released as X-ray photons. The X-rays released are emitted at a single wavelength characteristic to the target element. The discrete energy photon is created with energy equal to the difference in binding energies of the anode material atomic shells. Targets can have different wavelength spikes due to the quantized photons released from electrons dropping from different shell levels to the next as electrons get scattered and others sequentially drop down. Bremsstrahlung radiation is a continuous release of X-ray photons as the incident electrons accelerated towards the target material decelerate upon deflection by the positively charged nuclei. Again this loss of kinetic energy results in X-ray photon generation. However, these X-ray photons have many different wavelengths from just a few keV up to a maximum of the energy of the electron beam. These two atomic processes generate the emission and continuous spectra of the target material as illustrated in Figure 1.19 below.

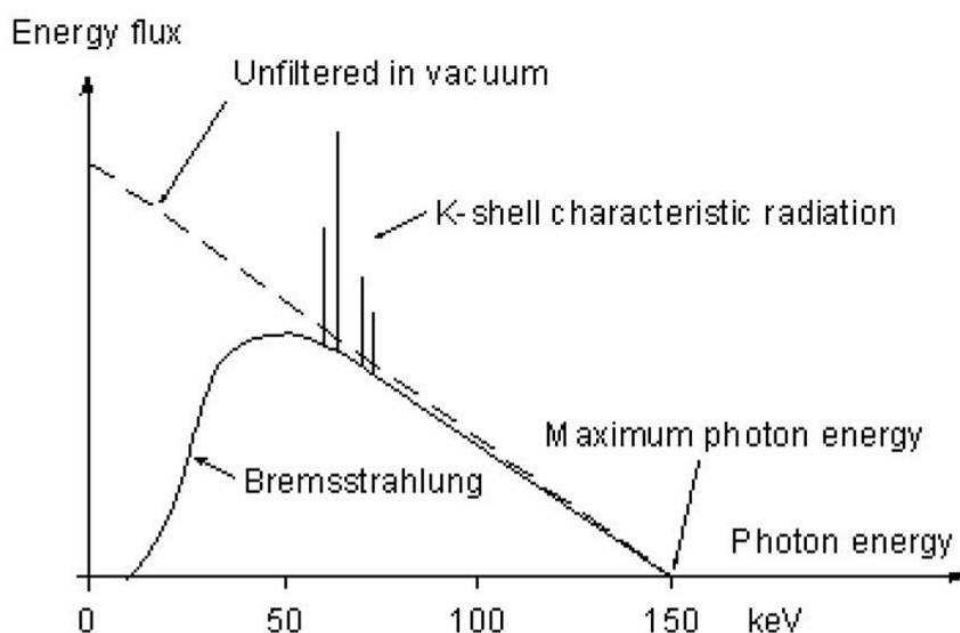


Figure 1.19 Illustration of emission and continuous spectrum of X-rays. K-shell characteristic radiation emission spectrum spikes at single energies and Bremsstrahlung continuous spectrum of photons at a range of energies given off as electrons lose energy upon encountering the target atoms. Maximum photon energy is at the energy of the electron beam. Image courtesy of Andrew Ramsey, Nikon-Metrology, Tring, UK.

In an unfiltered vacuum, as illustrated in Figure 1.19 above, high frequencies of very low energy photons would be present. However, in a typical CT scanner setup several inherent filters are present that remove the lowest energy photons (~1 keV to 15 keV) and significantly reduce the levels of lower energy photons (~15 keV to 50 keV) in the X-ray beam. This process is called beam hardening as the inherent filters remove the softest X-rays at the lowest end of the spectrum. Inherent filters include the target material itself, which will attenuate a proportion of the X-rays, and also the vacuum tube window, usually aluminium or beryllium. In the two scanners used in this study the vacuum tube windows are beryllium.

The spectrum from an X-ray tube can be further modified by the use of additional filters in the experimental setup. These additional filters are thin

sheets of metal inserted in the path of the X-ray beam and can absorb different parts of the beam spectrum resulting in cleaner images due to the absorption of lower energy photons that tend to scatter more. This reduces noise and creates better contrast between materials of different densities in the sample under investigation. High atomic number filters include lead (82), copper (29), silver (47) and tin (50). A lower atomic number filter would be aluminium (13), which was the filter used in this study. The choice of which filter to use depends on the material under investigation and also the target material chosen. In the systems used in this study, the target material was tungsten. Whilst the HMX225 X-ray CT (XCT) scanner (Nikon-Metrology, Tring, UK) has the option of choosing silver, molybdenum, or copper as well as tungsten, the Benchtop XCT system (Nikon-Metrology, Tring, UK) is a fixed tungsten target and hence, tungsten was selected for use in both machines.

The X-ray detector panel on the opposite side of the system from the X-ray gun (Figure 1.20), measures the attenuation of the emitted X-rays and creates a 2D map of the object at each projection which then informs the x, y, z coordinate spatial positioning and the relative greyscale value (density) of the voxel in that location. A voxel is a 3D volume-pixel: A 2D photograph is composed of pixels that have x and y coordinates, whereas in a 3D volumetric rendering the x and y coordinates also have information in the z plane. The reconstruction algorithm, which in this study was filtered back projection, then uses the line integrals of each rotational angle projection to recreate the estimated 3D volume of the object (Amos, 2010).

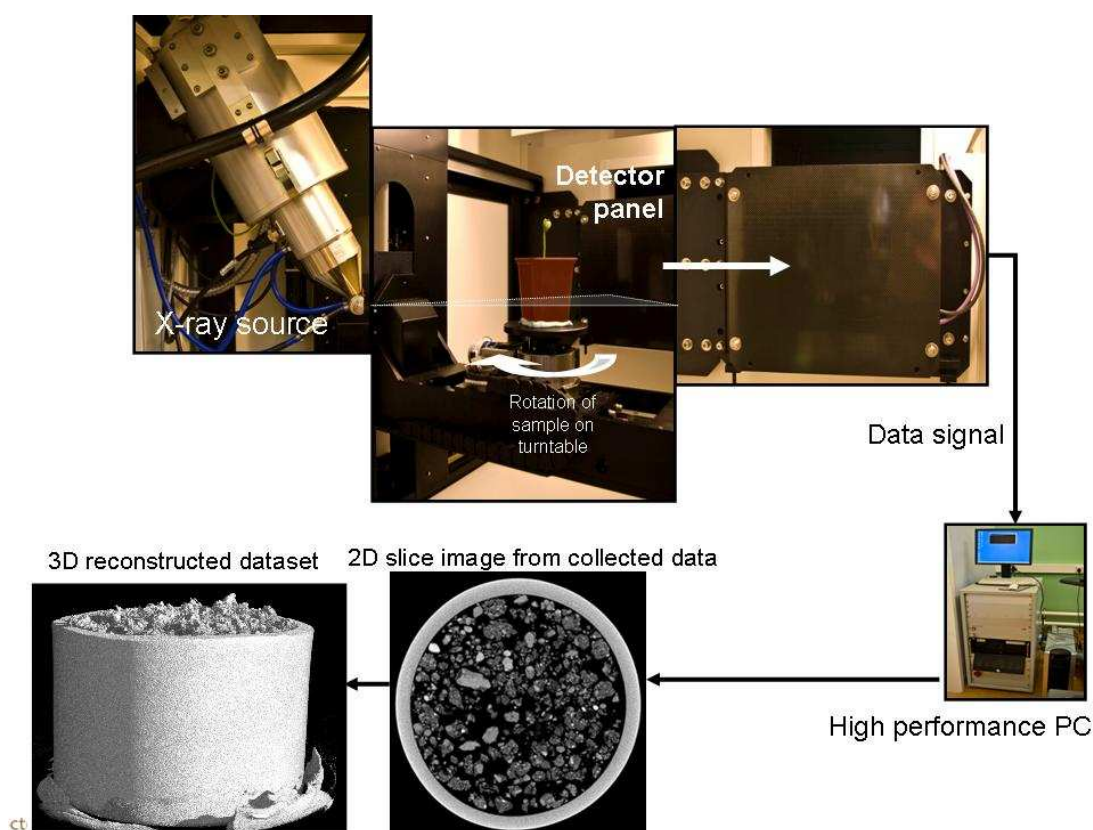


Figure 1.20 From X-ray source to 3D reconstructed dataset. X-rays produced by the X-ray source (gun) pass through the sample which is rotated through 360° and at each rotational angle the detector panel receives X-ray of different intensities (levels of attenuation). The data from each position and rotation of the sample is sent to a high-performance PC which uses computational algorithms to create 2D slice images and the reconstructed 3D datasets.

Synchrotron X-ray computed tomography measurements were performed at Beamline Station 13-BM-D at the Advanced Photon Source (Argonne National Laboratory, IL, USA), operated by GeoSoilEnvironCARS (GeoSoilEnviron = Geophysical and Geochemical Sciences, Soil and Environmental Sciences, CARS = Consortium for Advanced Radiation Sources, GSECARS) of the University of Chicago (Figure 1.21 and Figure 1.22).



Figure 1.21 Aerial view of the Advanced Photon Source at Argonne National Laboratory, Argonne, Illinois. Image credit Argonne National Laboratories.

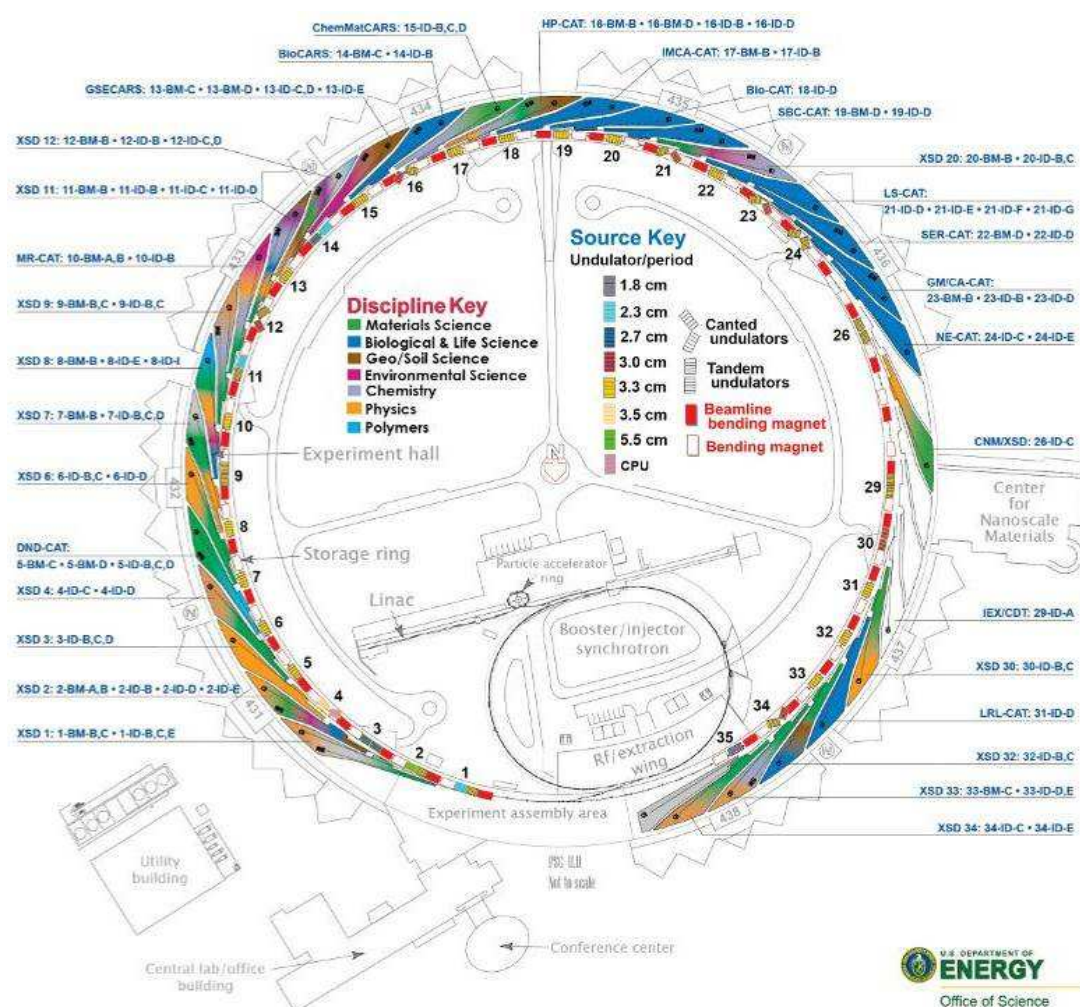


Figure 1.22 Illustration of the 35 beamline sectors around the Advanced Photon Source ring. The studies carried out in this work were undertaken at Beamline Station 13-BM-D. BM = bending magnet. D denotes the end station out of 4 stations at this sector. Image credit Argonne National Laboratories.

The synchrotron-derived, well-collimated, monochromatic X-ray beam passes through each sample mounted on a rotating stage. The energy of the X-ray beam is controlled by the angle of a silicon monochromator crystal, which diffracts the beam. A second monochromator crystal is used to diffract the beam back to the horizontal direction before it is transmitted through the sample. X-rays transmitted through the sample are converted to visible light with a synthetic garnet (YAG) scintillator and the visible light image is magnified with a microscope objective onto a high-speed 12-bit CCD camera (Wildenschild *et al.*, 2001). Figure 1.23, Figure 1.24 and Figure 1.25 illustrate the Advanced Photon Source at Argonne National Laboratories.

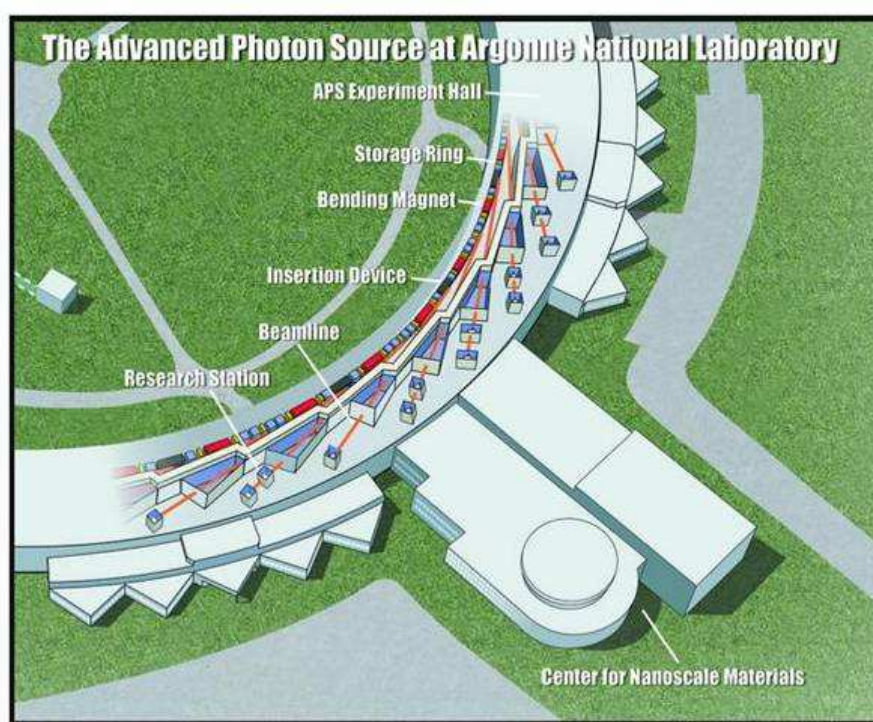
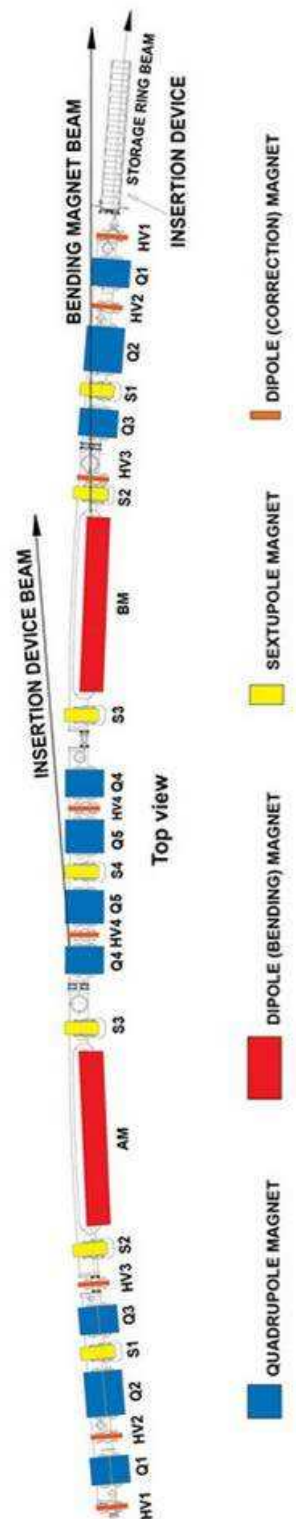


Figure 1.23 Schematics of the beamline sector at the Advanced Photon Source. Image credit Argonne National Laboratories.

Figure 1.24 Schematic of the beamline of the Advanced Photon Source at Argonne National Laboratories.



the photon beam along the
credit Argonne National

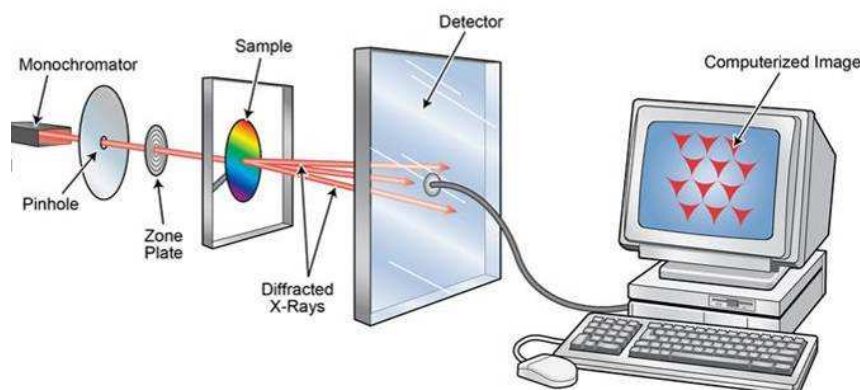


Figure 1.25 Schematic of data acquisition from the monochromatic beam through the sample to the detector. Image credit Argonne National Laboratories.

1.5.3 Applications of XCT in soil analyses

XCT has been used to analyse soil hydro-physical properties as well as the biotic properties of roots and rhizospheres, earthworm burrows, insect activity and microbial habitats. A thorough review of the application of XCT to soil science has been published by Taina *et al.* (2008) as well as a review of 25 years of CT in soil research from the Brazilian perspective by Pires *et al.* (2010).

From the viewpoint of this research, the quantification of soil structure using XCT has been demonstrated by Perret *et al.* (1999), Nunan *et al.* (2006), Tarquis *et al.* (2009), Gibson *et al.* (2006) and Kumar *et al.* (2010). Table 1.2 presents an overview of the scanners, sample size and structural properties under investigation in each of these studies.

Table 1.2 Overview of selected studies using CT to investigate soil structural properties pertinent to this work.

Study	Scanner type	Sample size	Soil structural properties measured
Perret <i>et al.</i> (1999)	whole-body medical scanner	undisturbed cores (800 mm height x 77 mm diameter)	porosity, volume, tortuosity and hydraulic radius of macropore networks
Nunan <i>et al.</i> (2006)	synchrotron XCT at the APS, ANL	naturally cleaved aggregates (1 - 3 mm).	porosity
Tarquis <i>et al.</i> (2009)	micro-CT (μ CT) scanner	undisturbed soil samples (30 cm x 15 cm x 15 cm)	network complexity using fractal dimension
Gibson <i>et al.</i> (2006)	industrial CT scanner	aggregates (2 - 3 mm)	comparison of fractal measurements soil aggregation
Kumar <i>et al.</i> (2010)	μ CT	intact soil cores (76.2 mm height x 76.2 mm diameter)	macropores

1.5.4 Thresholding

A study using CT scanning and subsequent image analysis would not be complete without mentioning the issue of thresholding. Thresholding involves the selection of a greyscale value above which is designated solid phase and below which is designated pore phase (in soil science). In an 8-bit image, greyscale is from 0 - 256 (black to white), and in a 16-bit image, greyscale is from 0 - 65535 (black to white). The human eye can distinguish between 20 and 200 levels of gray and is influenced by adjacent gray levels and the brightness of images (Smith, 1997). The goal is to binarise the image (segmentation) so that pore space is white and solid is black (or vice

versa), which the image analysis programme then uses to perform computerised measurements. The difficulty lies in finding the appropriate threshold level so as not to lose or create false pore space (Figure 1.26).

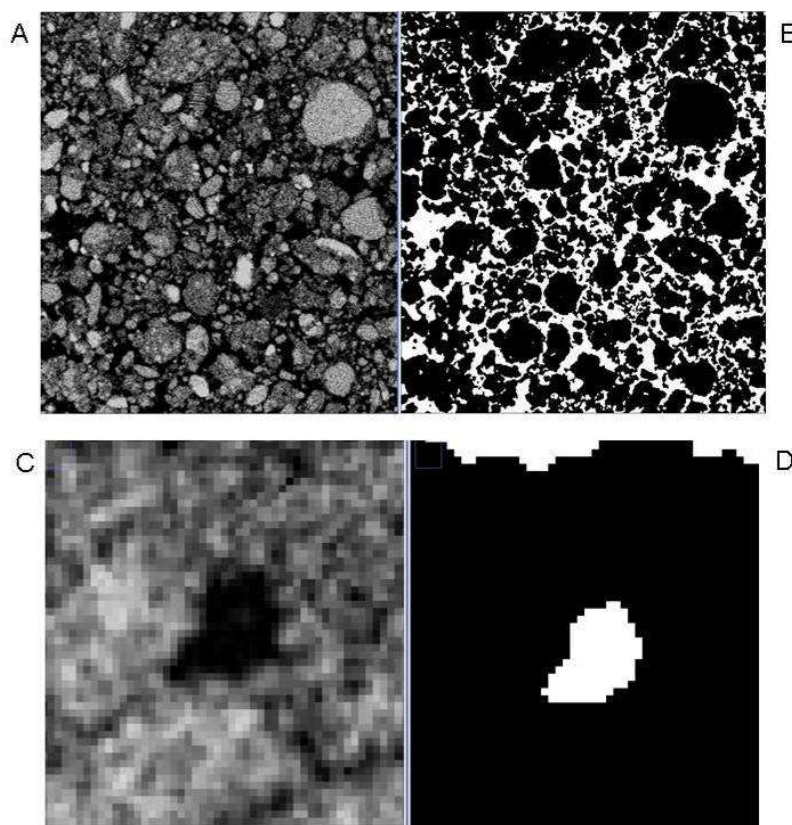


Figure 1.26 Thresholding of a greyscale image to a segmented black and white image. A is an 8-bit greyscale image of a soil matrix and B is the segmented image following thresholding. C is a magnified image of a region of a soil matrix, notice the individual pixels visible, and D is the resultant thresholded and segmented image.

In an image where the solid phase is composed of a single. X-ray dense material type e.g. a metal composite, thereby producing an obvious distinction between solid and background air the binarisation process is a simple case of selecting the clearly defined greyscale value above which is reported as solid, and below which all pixels or voxels are “switched” to black indicating pore space. The heterogeneous nature of soil does not lend itself

easily to the binarisation process. The varied and low X-ray densities of the composite materials of the solid phase produce the many different levels of gray as observed in the greyscale image (Figure 1.26, A). The distinction between low-X-ray density solid material and pore space is not readily made. Nor are the solids evenly dispersed throughout the soil matrix and the edges of pores are not straight lines like the boundaries of the voxels. In the study by Tarquis *et al.* (2009) (Table 1.2), fractal measurements obtained were shown to be threshold dependent. The higher the threshold value, the greater the reported proportion of black pixels and vice versa for a lower threshold value. Iassonov *et al.* (2009) present an excellent discussion and review of recent efforts to develop adequate segmentation techniques of XCT images of porous materials, not just soil. Baveye *et al.* (2010), on which the author of this study was a contributor, presents the observer-dependent nature of thresholding through the use of images that were thresholded by 15 different image analysis experts and the resultant threshold levels were scrutinised for variability. In this study, the issue of variability in thresholding is addressed within the relevant chapters.

1.6 Aims of study

The aims of this study are to examine the impact that bacteria have on soil. Using soil inoculated with different strains of *Pseudomonas fluorescens* SBW25 with particular properties in the production of specific extracellular (EC) components (cellulose, LPS and viscosin), moisture release curves and sorptivity analyses will be used to determine changes in water retention and

flow. 3D X-ray computed tomography and 2D surface-crack pattern analysis will be used to elucidate changes in the physical properties of the pore networks.

The hypothesis is that the presence of bacteria and bacterial legacy materials affects the biophysics of water retention and flow in soil. In this work, the term bacterial legacy is used to refer to all aspects of bacterial activity. Bacterial legacy consists of (i) exudate compounds produced by the bacteria and released into the immediate environment, (ii) cell debris released when bacteria die, and (iii) the footprint left behind when a bacterium attaches to and detaches from a surface.

The changes in the physical properties of the soil are hypothesised to be due to the presence of the bacteria and their extracellular (EC) components in the pore networks affecting the polarity of the solid phase and physically interfering with water flow by blocking narrow pore passages. The chemical properties of the bacterial legacy will also affect aggregate stability and result in the structural rearrangement of the soil matrix.

CHAPTER 2

2 Methodological approaches used in this thesis**2.1 Introduction**

In order to assess the effect of bacteria on the structure of soil a model soil core (microcosm) experimental system was designed. These experimental cores were incubated with a set of bacterial strains and maintained at a variety of pre-selected water potentials. These were then assayed to determine changes in soil structure and hydrological behaviour, to allow an investigation of the impact of bacteria on the biophysics of water retention and flow in soil.

In this work the soil and plant-associated *Pseudomonas fluorescens* SBW25 was used as a representative aerobic rhizosphere bacterium (e.g. exopolymeric substances, lipopolysaccharide, viscosin) that might be expected to alter soil structure and hydrological behaviour. SBW25 mutants deficient in the production of these compounds were available for use and could be compared directly with the wild-type strain as a set of defined isogenic strains. Experimental cores inoculated with these bacteria, assayed for changes in soil structure and hydrological behaviour and evaluated by the appropriate pairwise statistical analysis, would allow an investigation of whether specific bacterial components could alter soil structure and hydrological behaviour. Possible mechanistic explanations for any alterations would then come from an understanding of the biochemistry and behaviour of these components, as well as hypothesised soil-component interactions.

This chapter describes the experimental system, order of experiments and assays used in this study. The following three research chapters then describe the results of this work.

2.2 The experimental cores

Standard experimental cores used for the investigation of soil characteristics are usually in the range of 2.5 – 10 cm in height and diameter (Messing and Jarvis, 1995). In this study, smaller experimental cores of 1.5 cm high x 2 cm diameter were chosen for two practical reasons. The reasons for this change in size were that firstly, the 10 core replicates could be assayed on each of the Haines apparatus tension tables available for use in the Soil Laboratory of The SIMBIOS Centre. Secondly, smaller cores allowed the use of a higher magnification during micro-X-ray computed tomography (μ XCT) scanning which improved the resolution of soil structures.

When standard cores (2.5 - 10 cm height x 5 cm diameter) were used a maximum resolution of 30 μ m could be achieved with the HMX225 scanner (Nikon Metrology, UK) (Pajor *et al.*, 2010). However with smaller experimental cores, such as those used in this study (1.5 cm high x 2 cm diameter), a maximum resolution of 13.2 μ m could be obtained, as the reduction in source to sample distance resulted in a greater magnification, and thus improved resolution.

The destructive sampling of a subset of soil cores also allowed microscale analysis of 3D structure following synchrotron- μ XCT imaging of 2 mm aggregates with a maximum resolution of 5.4 μ m (this imaging was

performed at the Advanced Photon Source, Argonne National Laboratories, USA).

2.3 The soil

The soil type selected for the experimental cores used in this research was Labfield soil, a local arable sandy loam (WRBⁱ classification: Eutric cambisol) soil from an experimental site at The James Hutton Institute (JHI) (Invergowrie, UK). This Macmerry Series soil has been used in a number of research studies (e.g. Hallett and Young, 1999; Fechtner *et al.*, 2011). A second arable sandy loam soil (also Eutric cambisol) from the JHI was used for 2D cracking analysis in addition to the Labfield soil. This soil, known as Bullionfield, is a Carpow Series soil and has been used extensively in studies at The SIMBIOS Centre and at the JHI (White *et al.*, 2000; Harris *et al.*, 2002b; Harris *et al.*, 2003; Feeney *et al.*, 2006a; Pajor *et al.*, 2010). The compositions of these two soils are shown in Table 1.1.

ⁱ World Reference Base for Soil Resources

Table 2.1 Composition of the Labfield and Bullionfield soils

Component	Labfield	Bullionfield
organic matter	6.3%	2.6%
sand	59%	71%
silt	34%	19%
clay	7%	10%

Data from Hallett and Young (1999) and White et al., (2000).

Both the Labfield and Bullionfield soils are particular to the Dundee area. The majority of previous studies on hydrodynamic flow in soils undertaken at The SIMBIOS Centre have used Bullionfield soil (see references above). The choice of Labfield soil for this work will allow possible future comparisons to be made between these two soils (this comparison is not part of this research work). Both Labfield and Bullionfield were selected for cracking analyses as previous studies had used a soil not particular to the Dundee area (Preston *et al.*, 2001).

Experimental cores can contain undisturbed soil samples or can be packed with soil aggregates. The use of undisturbed natural soil cores may be of greater value when investigating natural variation between sites and soils, but the presence of indigenous biomass and biota cannot be easily controlled and may interact negatively with study organisms. Artificial experimental cores, constructed by the appropriate packing of soil aggregates, allow the production of replicate cores with minimal between-core structural variation. The preparation of the aggregates from sampled soils also allows the exclusion of unwanted biomass such as plant roots,

rotting material, earthworms, etc. In this work, sterilised sieved soil was chosen to provide repacked experimental cores with consistency in particle size, soil density, and structure ready for inoculation with the experimental bacterial strains.

A concurrent study carried out in The SIMBIOS Centre using larger experimental cores has investigated the problems encountered during the packing of soil aggregates and resultant μ XCT image packing artefacts (R. Pajor, pers. comm., 14 Feb 2007). However, the size of the cores employed in this study was small enough to allow homogeneous compression of soil during packing as shown by White *et al.* (2000). This was proven to be valid in this work, as the experimental cores were not observed to have striated, delineated packing structures when visualised by μ XCT (see Figure 2.1).

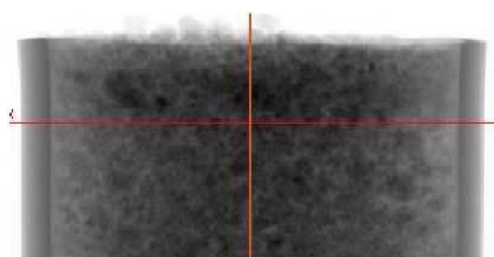


Figure 2.1 Sagittal radiographic image of an experimental soil core. An experimental core packed with Labfield soil has been imaged using The SIMBIOS Centre CT HMX scanner and processed by CTPro software. A sagittal section is shown. The darker vertical lines visible on the outer edges of this image are the plastic ring used to hold the core. The red crosshairs represent the rotational axes used in the 3D reconstruction process by the CTPro software.

2.4 The bacteria

The *Pseudomonas fluorescens* wild-type SBW25 strain is used in this work for two key comparisons: firstly, against the bacteria-free dH₂O control

in order to determine whether the presence of bacterial activity (metabolism, uptake of local nutrients, alteration of local pH, production of biomass, production of cell debris following cell death and lysis, etc.) in of itself has an impact on soil structure and hydrological behaviour. Secondly, it can be compared to each of the isogenic mutants to establish whether LPS, cellulose, attachment factor or viscosin impact on soil structure and hydrological behaviour individually.

SBW25 has been previously shown to survive incubation in soil for 1 to 4 weeks (Gal *et al.*, 2003) and preliminary work undertaken at the beginning of this study by fellow researchers at The SIMBIOS Centre had shown that it could survive and grow in experimental cores similar to the ones described here over 2 week periods (subsequently published in Fechtner *et al.*, 2011).

2.5 Sterilisation

The central aim of this research was to investigate the impact of bacteria on soil structure and hydrological behaviour. In order to be able to conclusively attribute the effects observed to the bacterial components tested, it was necessary to have a sterile soil system in which no other viable microorganisms were present, and a sterilisation system that could be used to halt microbial activity at the end of the incubation period.

Autoclaving is the most commonly used technique for the sterilisation of soil (Berns *et al.*, 2008), although sterilisation with dry heat, microwave and γ -radiation, and the use of chemicals have been used by others (Trevors, 1996). Whilst each of these techniques has the potential to affect

soil chemical composition in terms of the soil organic matter (SOM), no effect on physical structure has been shown to date (Wolf *et al.*, 1989; Trevors, 1996; McNamara *et al.*, 2003; Colman *et al.*, 2007; Razavi Darbar and Lakzian, 2007).

For the purposes of this research, the initial sterilisation of the soil samples, before core packing, was performed by a double autoclaving procedure (as described in Section 3.4). After the first autoclaving, soil samples were maintained at room temperature for 48 hours to allow the germination of any remaining heat-resistant bacterial and fungal spores. These were then destroyed by the second autoclaving cycle.

The experimental cores were re-sterilised at the end of the two week incubation period in order to prevent further growth or activity of the model bacteria during the assay processes. This sterilisation step was performed using two methods: standard autoclaving and chemical sterilisation using selected antibiotics (cycloheximide – antifungal, streptomycin – antibacterial) (West, 1986). The rationale behind choosing two dissimilar methods was that this enabled a comparison of sterilisation techniques within the experimental design. This comparison could indicate whether soil structure and hydrological behaviour were significantly affected by sterilisation technique. However, both methods have been used extensively in separate studies carried out by the SIMBIOS Centre (White *et al.*, 2000; Feeney *et al.*, 2006a; Feeney *et al.*, 2006b; Feeney *et al.*, 2006c; Pajor *et al.*, 2010) without causing obvious experimental problems.

2.6 Statistical analyses

The data from the analyses in this study were clustered as the measurements shared common characteristics in terms of matric potential for the water retention assays, sterilisation method, and cycle. The data were also longitudinal in the water retention assays as there were repeated measurements within each cycle. As such, Generalised Estimating Equations (GEE) were used for analysing statistical significance as unknown correlations were present in Generalized Linear Models (Liang and Zeger, 1986; and Zeger and Liang, 1986 cited in: Ziegler *et al.*, 1998).

All factors were presented in the GEE analysis and, in a stepwise regression pattern, terms were tested for their interaction effects. As interactions were ruled out ($p > 0.05$), those terms were removed. If interactions were demonstrated ($p < 0.05$) the analyses were split according to individual factors levels. This process continued until there were no further levels available for separation, or until interactions were statistically ruled out. Effectively, a hierarchical representation of effects was applied, whereby all terms were collectively tested for interactions and splits were made, where $p < 0.05$, in a logical fashion depending on the experimental aim of the particular research question. As the aim of this study overall was to look at the impact of bacterial treatment on soil then treatment type (tt) was always the last term in the tree. A simplified, descriptive illustration is presented below (Figure 2.2).

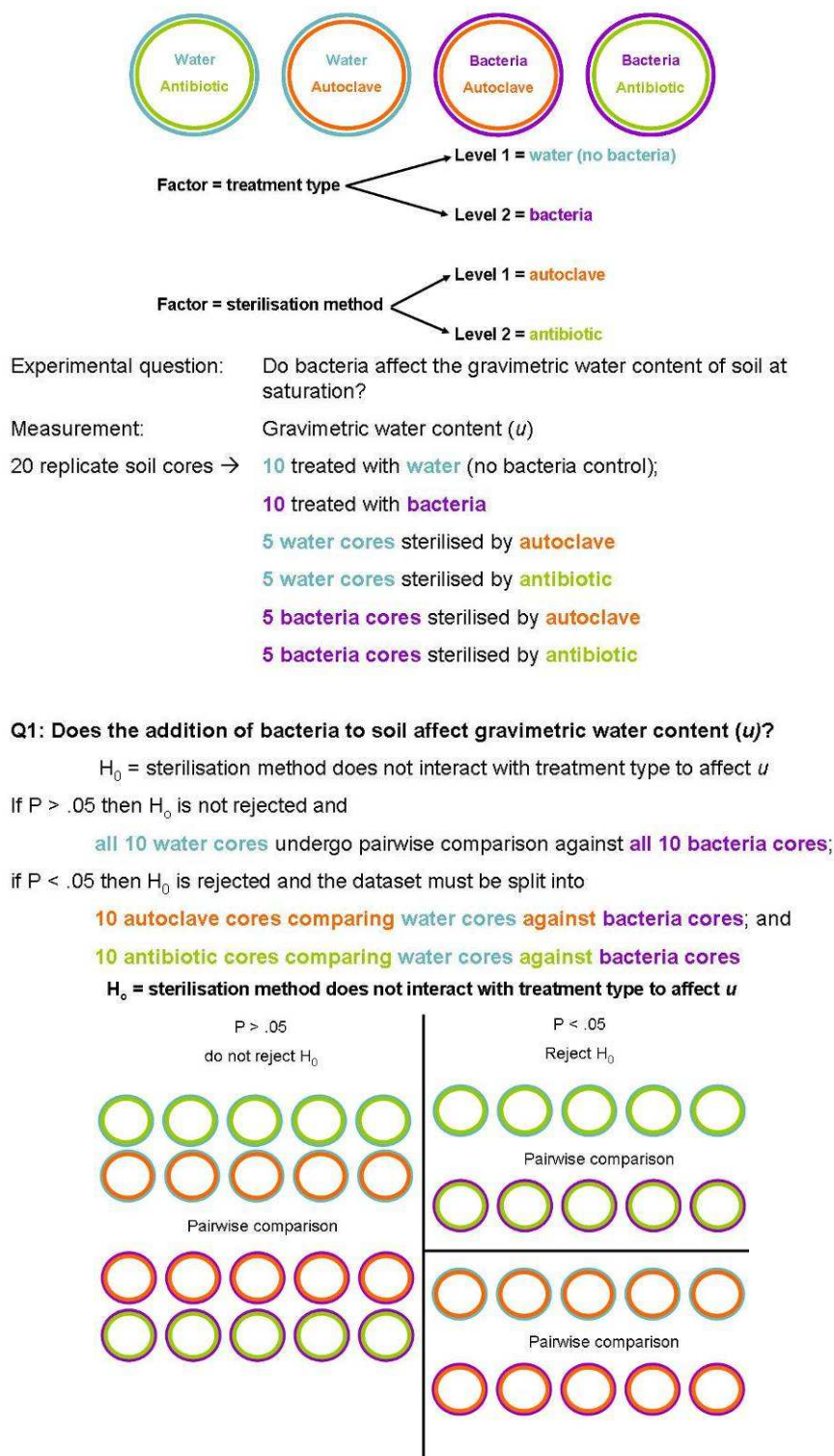


Figure 2.2 Simplified schematic of statistical analysis of interactive effects of factors in the experimental system leading to pairwise comparison of treatment types

2.7 Experimental design

The key experimental design used for the research presented in the Thesis is outlined in Figure 2.3. This involved two experimental programs. The first (the left-hand section of Figure 2.3) investigating the hydrodynamics and structural properties of soil in cores, and the second (the right-hand section of the figure) investigating the structural properties of soil following slurring and cracking.

Replicate soil cores were inoculated and incubated with the *Pseudomonas fluorescens* SBW25 isogenic strains, or with distilled water as a bacteria-free (dH₂O) control, then subjected to either autoclave or antibiotic sterilisation. The experimental cores were then subjected to two wetting-drying cycles (Cycle A & B). During these cycles, three key assays were undertaken: (i) the measurement of water retention characteristics, (ii) the measurement of sorptivity and (iii) 3D structural measurements following μ XCT imaging. These assays are reported in **Chapter 4: Soil Hydrodynamics**, and in **Chapter 5: Microtomographic analysis of 3D soil structure**, respectively. Following Cycle B, a subset of cores was destructively sampled to obtain 2 mm aggregates for synchrotron- μ XCT imaging and 3D structural analysis at the microscale. The results of this are also presented in Chapter 5. Finally, an investigation into the impact of bacteria on the cracking behaviour of soil was conducted using 2D analysis. The results of this are presented in **Chapter 6: 2D analysis of soil structure**.

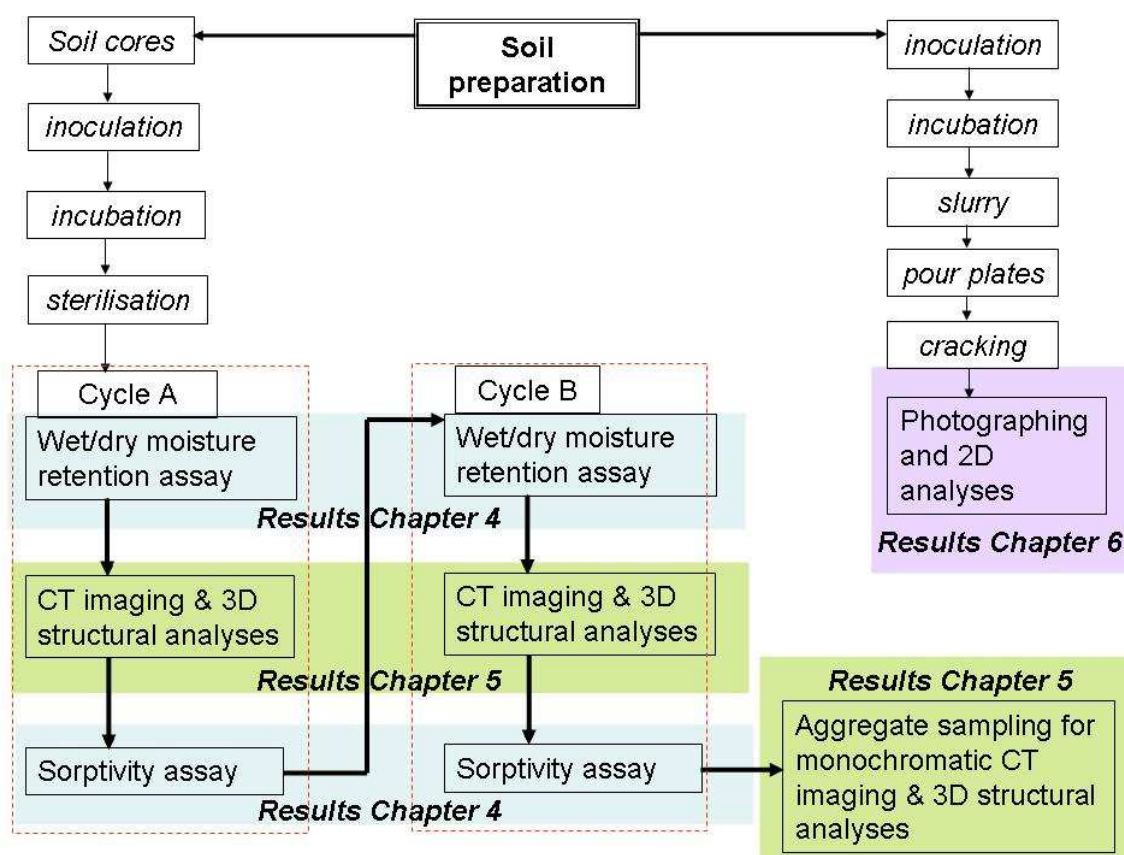


Figure 2.3 Schematic overview of experimental design process and associated Results chapters. Soil preparation involved initial sterilisation steps to eradicate native soil biota so as to start experimental processes with a control soil free from influences extraneous to those being investigated.

CHAPTER 3

3 Materials and Methods

3.1 Chemicals, reagents and buffers

All general chemicals were of molecular biology grade and obtained from Sigma, UK unless otherwise stated.

3.2 Bacterial strains and growth media

Pseudomonas fluorescens SBW25 strains were kindly provided by Dr AJ Spiers. Isogenic mutant strains were selected for their differential surface and exudate properties. Table 3.1 below details the genotype of each strain.

Table 3.1 *P. fluorescens* SBW25 strains used in this work detailing designation, genotype and reference.

Strain/Designation	Genotype	Source/Reference
SM	Wild-type <i>Pseudomonas fluorescens</i> SBW25	Rainey and Bailey (1996)
<i>ViscA</i>	Mutant that does not express viscosin, SBW25 <i>viscA</i> ::TnMod-OKm, Km ^R .	de Bruijn <i>et al.</i> , (2007)
WS and mutants		
WS	Biofilm forming strain (PRI200) evolved from SM	Spiers <i>et al.</i> , (2002)
WS-4	WS <i>wspR</i> ::mini-Tn5; isolated from a mini-transposon screen of WS	Spiers <i>et al.</i> , (2002)
WS-5	WS <i>tol</i> ::mini-Tn5; isolated from a mini-transposon screen of WS; mini-Tn5 is immediately upstream of <i>ybgC</i> , the first gene of the <i>tol</i> cluster	Spiers <i>et al.</i> , (2002)

Km^R, kanamycin resistant

Bacterial strains were grown in King's B (KB) medium (10 g glycerol; 1.5 g K_2HPO_4 (anhydrous); 1.5 g $MgSO_4 \cdot 7H_2O$; 20 g proteose peptone)ⁱⁱ (King *et al.*, 1954). KB plates contained 1.2% w/v agar. The antibiotic kanamycin was made at a stock concentration of 100 mg/ml and used at a final concentration of 25 µg/ml.

3.3 Bacterial culture conditions

All cultures were incubated at 28°C. All experimental cultures were started from 6 ml overnight, shaken cultures in 30 ml Universal glass vials (hereafter referred to as culture vials) inoculated from -80°C glycerol stocks. Bacteria were grown in planktonic, sessile and simulated complex structure cultures at different times during the experimental process. Planktonic cultures were either shaken or static. Shaken liquid cultures were oscillated at 200 rpm (SI500 Orbital Shaker, Stuart, Staffordshire, UK), to ensure adequate aeration. Static liquid cultures were incubated in the same incubator without oscillation. Sessile cultures were grown on agar plates at 28°C, 5% CO_2 . Sterilised glass beads (2 g of 1.5 – 2.5 mm beads (BDH, VWR International, UK) were submerged in 6 ml KB media in culture vials to simulate a complex structure growth environment. Structured cultures were either static or shaken as detailed above for planktonic growth.

Permanent stocks of the *P. fluorescens* SBW25 strains used in this study were produced by inoculation of 6 ml KB medium with a single colony in a 30

ⁱⁱ Proteose peptone was Bacto™ Proteose peptone No.3 (BD Biosciences, UK)

ml glass Universal vial which was incubated overnight at 28°C, 200 rpm oscillation. The resultant culture was aliquoted (1 ml) into cryotubes containing 400 µl sterile 50% w/v glycerol, mixed rapidly and frozen at -80°C.

3.4 Sampling and preparation of soil

Two arable soils from the Labfield and Bullionfield experimental sites at the Scottish Crop Research Institute (Invergowrie, Dundee, UK; 56°27.318N, 3°4.796W) were used in this study.

Labfield is a Macmerry series Eutric cambisol (organic matter, 6.3%; sand, 59%; silt, 34%; clay, 7%) (Hallett and Young, 1999), and Bullionfield is a Carpow series Eutric cambisol (organic matter, 2.6%; sand, 71%; silt, 19%; clay, 10%; pH 6.2) (Harris *et al.*, 2002a).

Soil was sampled from approximately 30 cm depth and sieved while at a field moisture content of about 12% to an aggregate size of less than 2 mm. The sieved soil was then air-dried at 20°C in a temperature controlled laboratory overnight, and sterilised by autoclaving twice at 120 °C, 1 hour, 15 psi with a 48 hr interim incubation period at room temperature before being batch-stored at 4°C in sterile conditions.

Labfield soil was used for core, aggregate and cracking studies; Bullionfield soil was additionally used for cracking analysis.

3.4.1 Soil cores

Plastic cores (20 mm \varnothing x 15 mm d) were sealed on one end with a voile retaining mesh (< 0.1 mm) to prevent loss of soil and packed with sterile Labfield soil to an average dry bulk density of 1.2 g cm⁻³. Bulk density of the Labfield sampled soil was also determined by the standard oven-drying method (105°C, 24hrs): bulk density = mass of oven dry soil/core volume

Equation 3.1

$$\rho = \frac{M_s}{V_t}$$

Equation 3.1 Bulk density

Soil cores were inoculated with 1.6×10^7 bacteria g⁻¹ soil and taken to -0.2 kPa to ensure maximum distribution of the bacterial culture throughout the pores of the soil. This resulted in a soil moisture content of 0.29 g g⁻¹ (Hallett and Young, 1999) (as per previous studies in The SIMBIOS Centre where the work in this thesis was carried out), and incubated for 2 weeks at 28°C in a dark, humidified environment. The bacteria used to inoculate the soil were resuspended in 1 ml distilled H₂O (dH₂O). This process is schematically illustrated in Figure 3.1.

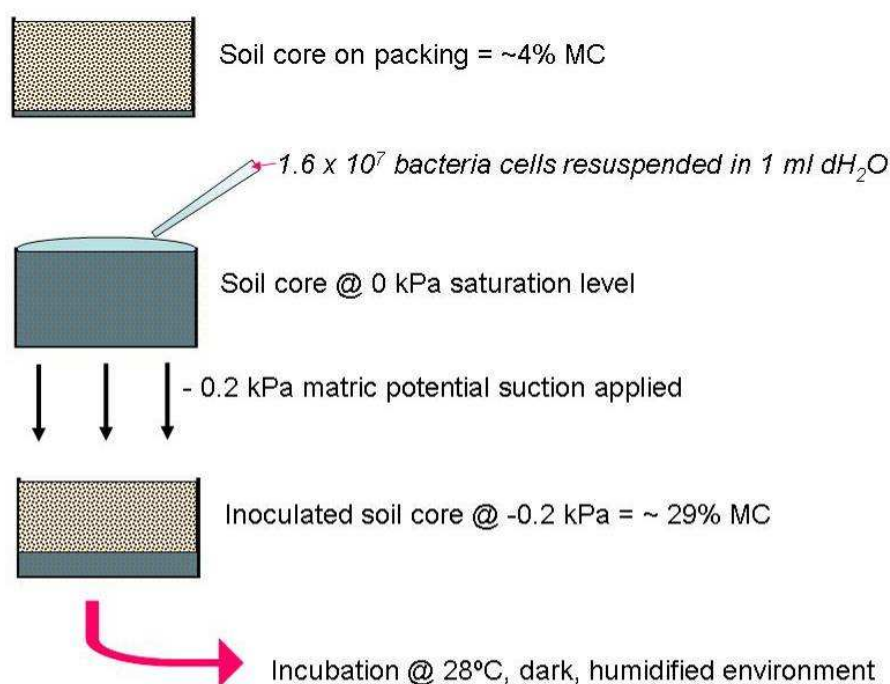


Figure 3.1 Schematic representation of moisture content of soil cores for inoculation with bacteria.

Sterilisation of the cores subsequent to incubation was carried out to ensure that continued bacterial growth would not affect the hydrodynamic measurements. Half of the samples (30) were sterilised by autoclaving at 115°C, 120 psi, 1 hr; the other half were sterilised by semi-submersion in an antibiotic solution of 50:50 (0.6% w/v) cyclohexamide/streptomycin (cycloheximide – antifungal; streptomycin – antibacterial) (West, 1986). So as not to disturb the soil cores, the antibiotic solution was slowly added to a container containing the cores, and the solution allowed to absorb into the cores from the bottom up. The solution was seen to rise to the surface of the cores by capillary action, at this point no more antibiotic solution was added to the container and the cores left to sterilise for 24 hours (West, 1986).

3.4.2 Soil slurries for cracking plates

Sieved, autoclaved soils (Labfield and Bullionfield) were inoculated with 1.6×10^7 bacteria in $\text{dH}_2\text{O g}^{-1}$ soil adjusted to 0.29 g g^{-1} soil moisture content with dH_2O in vented plastic tubs (Nalgene® PFA straight-side jars with a foam plug in centre of lid to allow gaseous exchange). Tubs were then incubated at 28°C , 5% CO_2 , 2 weeks in a dark, humidified environment.

Incubated soil was saturated with deionised water and placed in a Stomacher Lab Blender 400 (Colworth, UK), for 60 s to produce a homogeneous soil slurry. Aliquots equivalent to 25 g oven weight dry soil were then poured into Petri dishes (8.6 cm \varnothing)

Seven replicate plates per treatment (SM, WS, *ViscA*, WS-4, WS-5 as described in Table 3.1) plus 7 plates dH_2O incubated, bacteria-free control were prepared and allowed to dry in a force-ventilated room at $20 \pm 2^\circ\text{C}$. To ensure that the 2-week incubation alone did not have an effect on the genesis of cracks, an incubation control of untreated soil saturated with dH_2O was included for each of the soil types. These samples were immediately saturated without incubation period, homogenised, aliquoted and allowed to air-dry as described above.

3.4.3 Preparation of aggregates

Aggregates were decanted from repacked cores after completion of hydrodynamic analyses and polychromatic scanning. Five cores from each of dH_2O , SM and WS-4 were sampled 3 times each. The 2 mm aggregates were mounted on toothpicks using superglue for the purposes of synchrotron

x-ray scanning at Station 13-BM-D at the Advanced Photon Source (Argonne National Laboratory, USA). Figure 3.2 shows a 2 mm aggregate mounted on a toothpick.

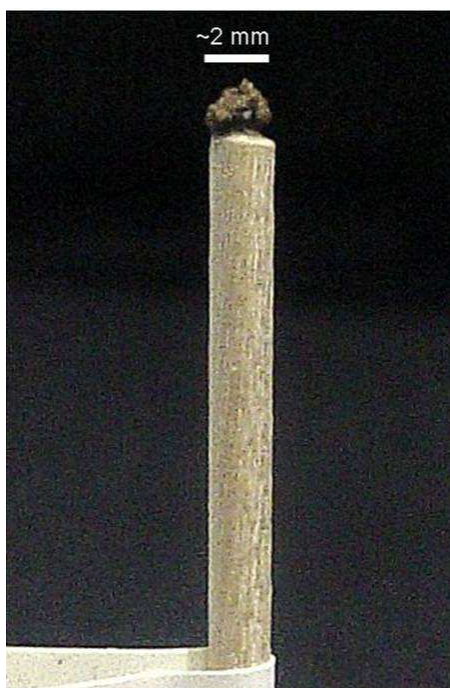


Figure 3.2 Mounted ~ 2 mm sieved aggregate. Close-up of mounted aggregate from sieved Labfield soil (~ 2 mm)

3.5 Hydrodynamic analyses

3.5.1 Water retention

The water retention curve of the soil cores was measured using a modified Büchner-Haines apparatus setup- a tension table and hanging water head column method as originally described by Haines (1930). The tension table and hanging column consisting of a glass Büchner funnel containing a sintered glass filter, rubber tubing, and a glass burette mounted on a boss-

and-clamp stand rigging, as illustrated in Figure 3.3, was used to measure soil water content at gradually decreasing matric potentials (0 to -10 kPa).

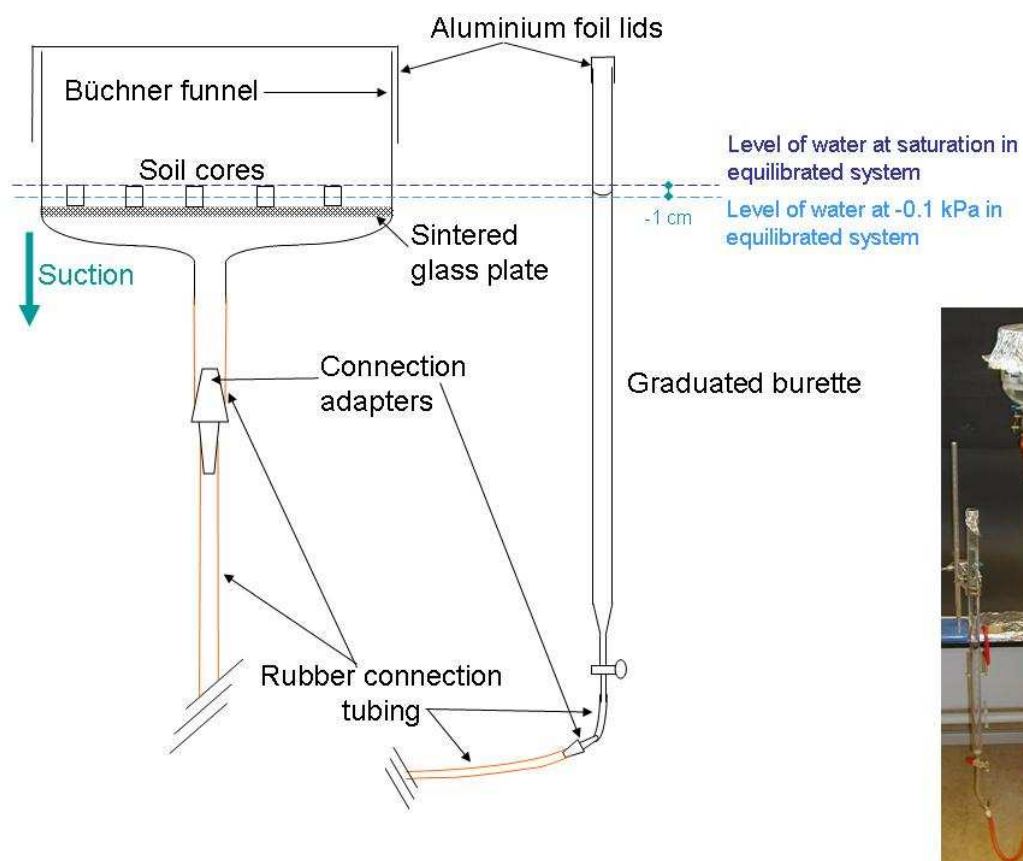


Figure 3.3 Water retention apparatus schematic and photograph

The apparatus was set up in a temperature controlled laboratory (20 ± 2 °C) which was darkened for the duration of the analysis. Tap water was de-aired by boiling twice and used to fill the apparatus. Sterilised filter paper discs (Whatman No.3 cut to the same diameter as the cores, ~20 mm \varnothing) were used to ensure good hydraulic contact between the soil cores and the sintered glass filter. An aluminium foil lid for each funnel was applied to prevent evaporation from the cores or contamination from the air. Each core

was gently twisted each time it was placed onto its filter disc to disrupt any surface tension in the soil-water interface that would interfere with proper drainage. The cores were saturated by raising the level of the water in the funnel to approximately 2 mm below the upper edge of the core and allowed to equilibrate at this level for several hours. The surface water above the glass plate was then removed and the cores were removed from the apparatus and individually weighed. The glass burette was lowered gradually over time to each desired matric potential, and once equilibration had been achieved (several hours) each core was removed and weighed. The water content of the cores at given points on the water desorption curve at the set potential was obtained as illustrated in Figure 3.4.

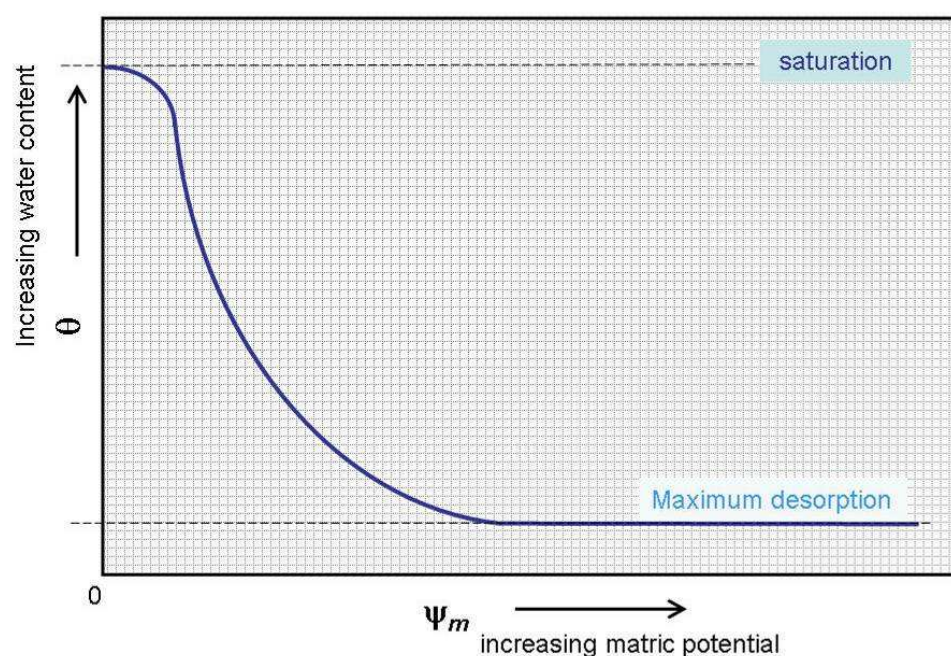


Figure 3.4 Schematic of water retention curve. At each matric potential the water content was plotted giving the characteristic water retention curve.

The lowest matric potential in this study was -10 kPa (-100 cm). The cores were then oven-dried at 40°C overnight to obtain a dry weight measurement of the soil to enable calculation of the gravimetric water content.

3.5.1.1 Calculation of gravimetric water content

Gravimetric water content (u) was calculated by Equation 3.2 below.

$$u = \frac{(m_w - m_d)}{m_w}$$

Equation 3.2 Gravimetric water content of soil

Where u is gravimetric water content (g water.g soil⁻¹), m_w is mass of wet soil (g), and m_d is mass of oven-dried soil (g).

An important aspect is the scale of the pores being discussed in this study. The soil cores samples were 20 mm in diameter, composed of repacked 2 mm aggregates. In this study, macropores are defined as pores greater than approximately 300 µm in diameter and drained at -10 cm matric head, and mesopores are defined as pores approximately 30 µm and up to 300 µm in diameter and drained at -80 cm matric head. Figure 3.5 illustrates the scale relationship schematically.

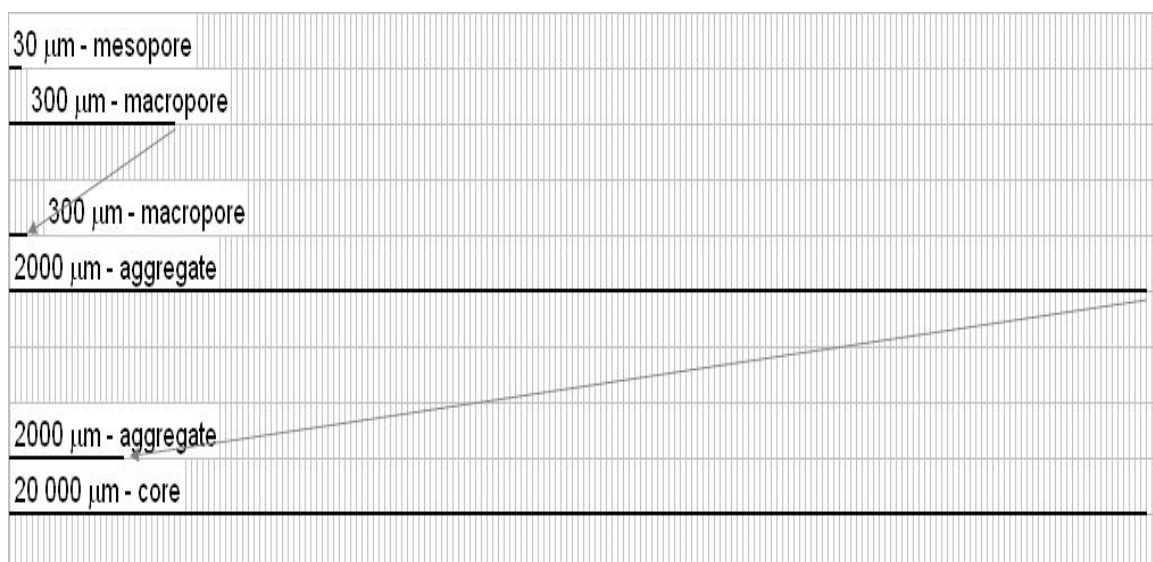


Figure 3.5 Schematic illustration of the pore, aggregate and core scale relationships. Water flow would be expected to be unhindered by bacterial presence in the pores between the aggregates. Macropores are defined in this study as being $>300 \mu\text{m}$ and mesopores as being $30 - 300 \mu\text{m}$.

3.5.1.2 Calculation of absolute drainage

Absolute drainage at macropore (Δ_{mac}) and mesopore (Δ_{mes}) levels were calculated by Equation 3.3 and Equation 3.4 below.

$$\Delta_{mac} = GWC_{sat} - GWC_{mac}$$

Equation 3.3 Calculation of Δ_{mac}

$$\Delta_{mes} = GWC_{mac} - GWC_{mes}$$

Equation 3.4 Calculation of Δ_{mes}

3.5.1.3 Calculation of percentage drainage

Macropore, mesopore and total drainage as a percentage of the GWC at saturation were calculated by Equation 3.5, Equation 3.6 and Equation 3.7 below.

$$\% \text{ water drainage from macropores} = \left(\frac{GWC_{sat} - GWC_{mac}}{GWC_{sat}} \right) \times 100$$

Equation 3.5 Percentage macropore drainage

$$\% \text{ water drainage from mesopores} = \left(\frac{GWC_{mac} - GWC_{mes}}{GWC_{sat}} \right) \times 100$$

Equation 3.6 Percentage mesopore drainage

$$\% \text{ total water drainage} = \left(\frac{GWC_{sat} - GWC_{mes}}{GWC_{sat}} \right) \times 100$$

Equation 3.7 Percentage total drainage

3.5.2 Sorptivity

The water sorptivity was measured using a modified miniature infiltration device as described by Leeds-Harrison *et al.*, (1994) and Hallett *et al.*, (2004) and illustrated in Figure 3.6.

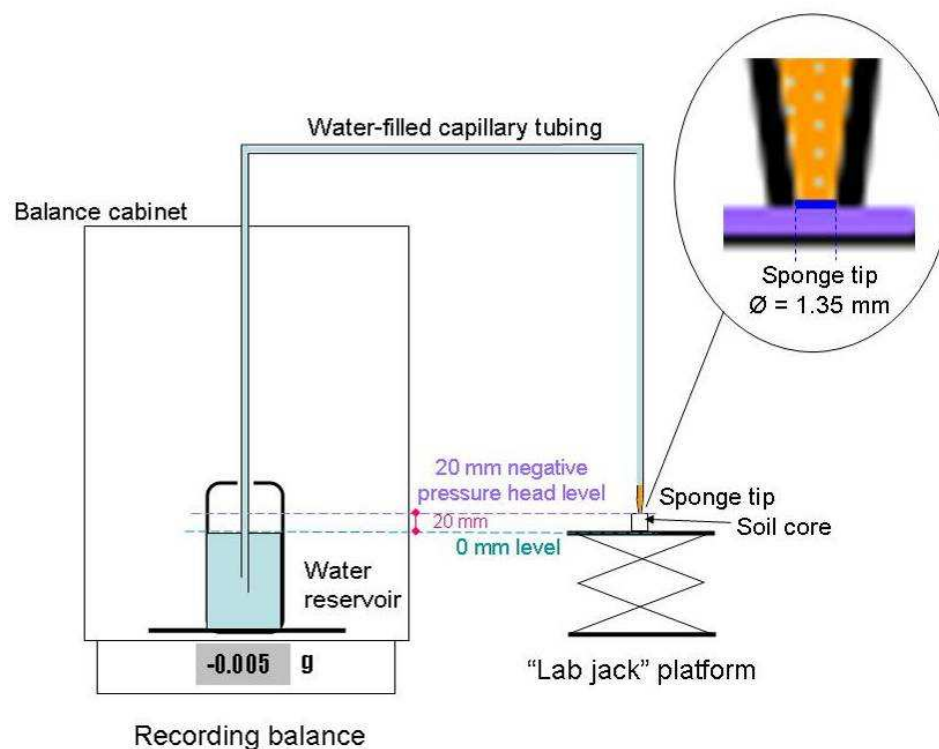


Figure 3.6 Schematic of miniaturised infiltrometer to measure sorptivity. Mass loss from the water reservoir on the balance due to water uptake by the soil core through the conductance tube was recorded at 2 second intervals using Ohaus® BalanceTalk software

The infiltration of the water occurred via a circular sponge-filled tip (1.35 mm diameter), which when connected to the aggregate surface allowed the flow of liquid from the capillary tube, drawing water from the reservoir on the Adventurer™ recording balance (Ohaus® AR2140) capable of accurate recording to 0.1 µg. The sponge-tip provided good soil contact and the set-up allowed for a negative head of 20 mm to reduce macropore flow. Thus any infiltration was via mesopores in the aggregates. The reduction in mass of the water reservoir was recorded by Ohaus® BalanceTalk v4.0 9-ch (Labtronics Inc., Guelph, Ontario, Canada) as a function of time (t).

3.5.2.1 Calculation of sorptivity

Sorptivity, S was calculated using a formula presented by Leeds-Harrison *et al.*, (1994) as

$$S = \sqrt{\frac{Qf}{4br}}$$

Equation 3.8 S , Sorptivity

Where S = sorptivity [$\text{mm } \sqrt{\text{s}^{-1}}$]; Q = rate of infiltration of water [$\text{mm}^3 \text{ s}^{-1}$]; f = fillable (air-filled) porosity calculated using the dry bulk density (1.2 g cm^{-3}) and the specific density of soil material (taken as 2.65 g cm^{-3}) to obtain total pore volume, then subtracting the water-filled volume of pores.

In this study the cores had been oven-dried at the end of the water retention curve experiment to obtain the dry soil mass and kept in the desiccator between experiments therefore the fillable porosity (f) is the total porosity; $b = 0.55$ (average value of parameter based on soil-water diffusivity function as suggested by White and Sully (1987); r = radius of infiltrometer tip [mm]. In this study, f was calculated by

$$\begin{aligned} f &= 1 - \left(\frac{\text{dry bulk density}}{\text{specific density of soil}} \right) \\ &= 1 - \left(\frac{1.2 \text{ g / cm}^3}{2.65 \text{ g / cm}^3} \right) \\ &= 0.55 \end{aligned}$$

Equation 3.9 f , fillable porosity

and S was calculated by

$$S = \sqrt{\frac{Q \times 0.55}{4 \times 0.55 \times 0.675}} \text{ mm.s}^{-1/2}$$

Equation 3.10 S, Sorptivity in this study

Q for each replicate was calculated from the slope of the mass loss on the balance (g) once steady-state flow was reached, after about 30 seconds, against time lapsed in seconds, using equation 2.7.

$$Q = ABS(SLOPE(y's, x's)) \times 1000$$

Equation 3.11 Q, rate of infiltration

3.6 Imaging for structural analyses

3.6.1 Computed tomography (CT)

X-ray computed tomography at micron-scale (μ XCT) was undertaken in this study using two types of X-ray beam, polychromatic μ XCT at The SIMBIOS Centre (University of Abertay, Dundee) and monochromatic synchrotron-XCT at the Advanced Photon Source (APS) (Argonne National Laboratory, USA).

Two X-ray computed-tomography polychromatic scanners, the Benchtop and the HMX-225, were used during the course of this study (Nikon-Metrology, Tring, UK). Experimental conditions were 110-115 kV, 75-99 μ A, 1 frame per second and 1169 projections, using a 0.1 mm aluminium filter.

Synchrotron X-ray computed tomography measurements were performed at Beamline Station 13-BM-D at the Advanced Photon Source

(Argonne National Laboratory, USA), operated by GeoSoilEnvironCARS (GSECARS) of the University of Chicago. The experimental conditions were 20 keV monochromatic X-rays, 1 s exposure time per projection, 720 projections and 696 x 520 pixels per projection.

3.6.2 Photographing of cracked plates

Petri dishes of cracked soil slurries were photographed using an AxioCam MRc 5 and associated AxioVision software (both Carl Zeiss MicroImaging GmbH, Munich, Germany).

3.7 Image processing

3.7.1 3D-image reconstruction

Datasets from the SIMBIOS μ XCT scanners were reconstructed using CT Pro (Nikon-Metrology, Tring, UK). Datasets from the synchrotron CT facility were reconstructed using IDL (interactive data language) Tomography Processing. X-Tek CT-*Pro* (Nikon-Metrologyⁱⁱⁱ, UK) was used to reconstruct the 2D images from the μ XCT scanner into a 3D image. The parameter file (.par) was imported into CT-*Pro* and reconstructed at a resolution of 13.2 μ m for the datasets from the HMX-225, and 28.4 μ m for those from the Benchtop. At the experimental stage of this study, CT-*Pro* reconstruction

ⁱⁱⁱ X-Tek Systems Ltd. is a wholly owned subsidiary of Metris as of January 2008. Metris is wholly-owned subsidiary of Nikon as of October 2009; rebranded as Nikon-Metrology, November 2009.

was not automated; therefore the centre of rotation (COR) for optimal 3D reconstruction was determined using dual-mode settings in the COR-wizard feature of *CT-Pro*.^{iv}

Automated reconstruction of the CT data from the synchrotron was carried out using a Fourier Transform algorithm. Pre-processing to correct for dark and flat-fields and to remove artefacts was done using software written in interactive data language (IDL). The charged-coupled device (CCD) data from the .spe file output by the image collection software (IDL Tomography Collection) was taken by the IDL Tomography Processing software, and the corrected data written to a 3D volume file for reconstruction^v purposes.

Following reconstruction in *CT-Pro*, the reconstructed volumes were optimised in VGStudio MAX (VGSM) v.1.2 (Volume Graphics GmbH, Heidelberg, Germany). This is a powerful, 3D visualisation tool for volume graphics. In this study VGSM was used to visually assess the reconstructed 3D image and to output axial slice image stacks of the reconstructed volume as jpeg files for use in ImageJ processing. Figure 3.7 illustrates the image stack creation process in the cores.

^{iv} The process from scan to reconstructed volume is now fully integrated between the Inspect-X scan software and *CT-Pro*, via new software (CT Agent); and as such the user now simply scans and moves straight to VG Studio Max (VGSM) for 3D image processing.

^v (<http://cars9.uchicago.edu/software/idl/tomography.html>)

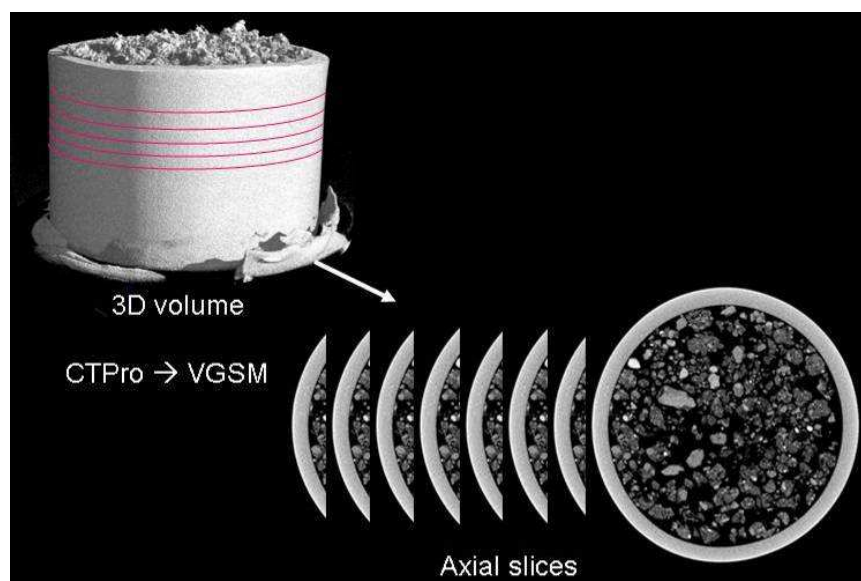


Figure 3.7 Illustration of axial image stack creation from a soil core by VGStudio Max. The 3D volume was sliced on the axial plane by VGSM to create individual sequential tiff files for import into ImageJ.

3.7.2 ImageJ despeckling and thresholding

ImageJ is public domain image analysis software developed by Wayne Rasband (Rasband, W.S., ImageJ, U. S. National Institutes of Health, Bethesda, Maryland, USA, <http://rsb.info.nih.gov/ij/>, 1997-2007; version 1.39q). 2D image slices were imported into ImageJ for core and aggregate image processing. For the soil core image processing, starting at slice 100, equivalent to a depth of 2.84 mm in Benchtop-scanned cores and 1.35 mm in HMX-scanned cores, 200 axial slice images created in VGSM were imported into ImageJ. This gave a representative volume of soil within reasonable computational time-constraints as determined by initial trials to optimise the representative volume versus processing time required (data not shown). The imported circular core was then cropped in ImageJ to remove the plastic core from the analysis area.

Figure 3.8 illustrates the central, cuboid volume of approximately 10 x 11 x 2.6 mm that was analysed from each core to reduce processing time and computer random access memory (RAM) requirements.

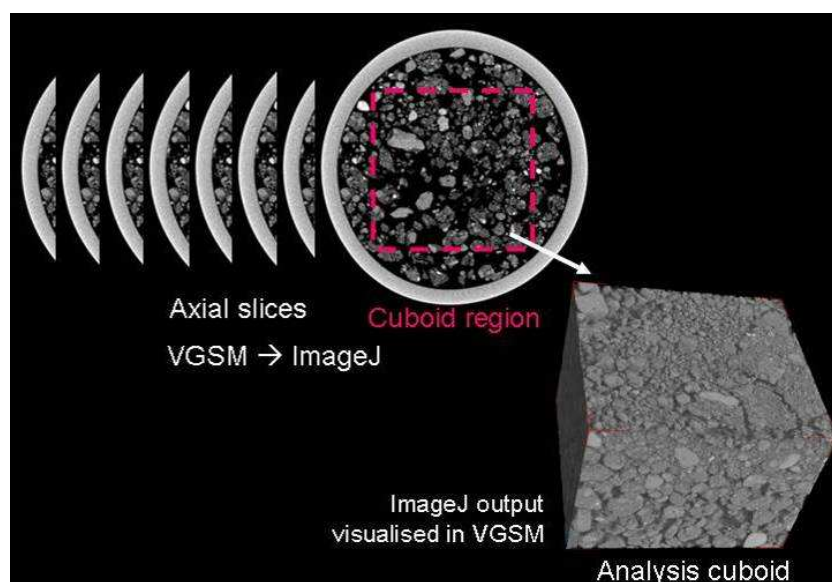


Figure 3.8 Schematic of soil core analysis cuboid. The central cuboid was selected to reduce processing time and RAM requirements.

For the aggregates, the irregular shape of the aggregates meant that the starting import slice had to be manually found for each aggregate. Once the appropriate starting slice containing only soil was found, 150 slices were

imported and an area 150 x 150 pixels was selected from each aggregate. This gave an overall cuboid volume for each aggregate of 0.831 x 0.831 x 0.831 mm (based on synchrotron-CT resolution of 5.54 μm) (Figure 3.9).

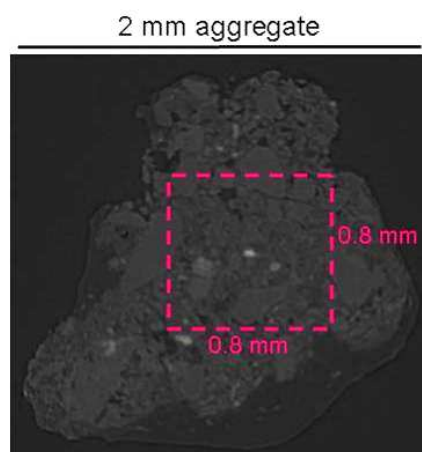


Figure 3.9 Illustration of analysis cuboid from soil aggregate

Two processing steps were undertaken in ImageJ, these were despeckling, to reduce noise, and thresholding to segment background from material. Noise reduction was carried out using the despeckling tool in ImageJ which applied a median filter to the image. Each pixel image was replaced with its median value in a 3 x 3 pixel neighbourhood (Figure 3.10 plate B). Threshold value to delineate pore space from soil matrix was ultimately determined by visual inspection and comparison of μXCT images and binarised images. Optimum threshold values were visually determined to be approximately 20 for Benchtop-scanned cores, and approximately 40 for HMX-scanned cores (Figure 3.10 plate C).

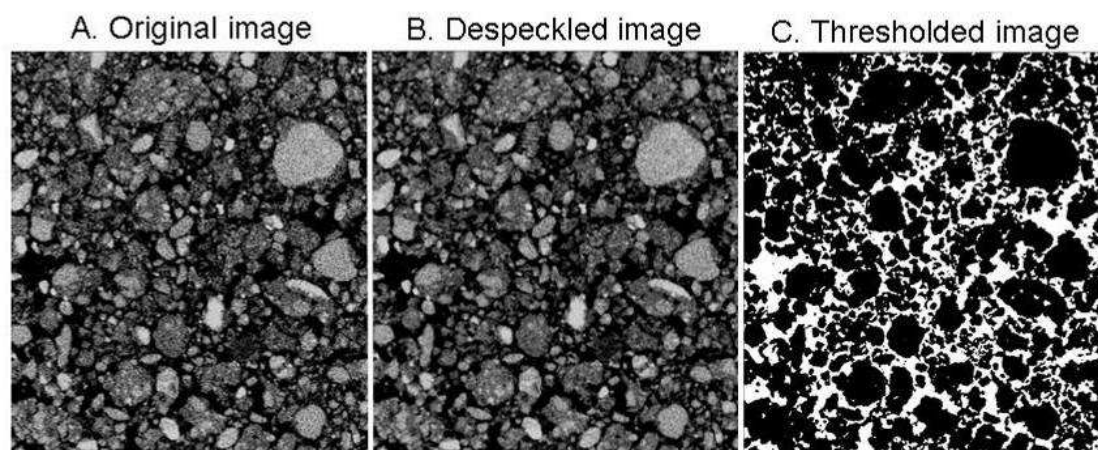


Figure 3.10 Despeckled and thresholded image in ImageJ

This thresholded binary image sequence was then analysed by SCAMP v1.1 (Simbios CT Analysis and Manipulation Plugin, UAD).

3.7.3 2D Image processing

The photographs of the soil cracking plates were imported directly into ImageJ for processing. Processing of the photographed cracking plates was in two stages. First, the images were thresholded by selection of the appropriate greyscale value which delineated pore space from soil matrix and set so as to defined pores as black and soil as white (also known as segmentation). Then the images were despeckled to clean up the images and remove falsely represented pore space caused by shadows in the photograph and bumps in the soil surface. Despeckling involved highlighting the crack patterns using the wand tracing tool, followed by the ‘clear outside’ inbuilt software function which removes the pixels not selected in the crack-highlighting procedure. Final cleanup was performed using the eraser tool.

Figure 3.11 illustrates the thresholding process and Figure 3.12 illustrates the subsequent despeckling process.

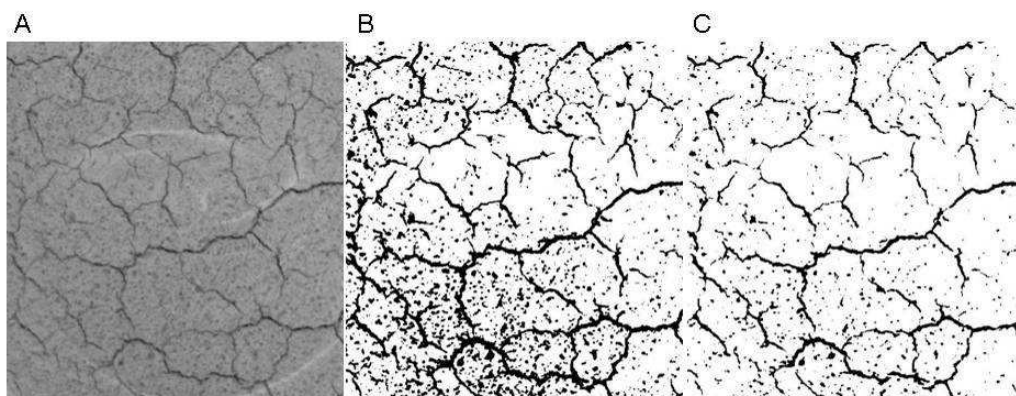


Figure 3.11 Labfield soil; cracking plate thresholding. A. Original photograph; B. ImageJ-suggested threshold value of 128; C. Amended threshold value of 118.

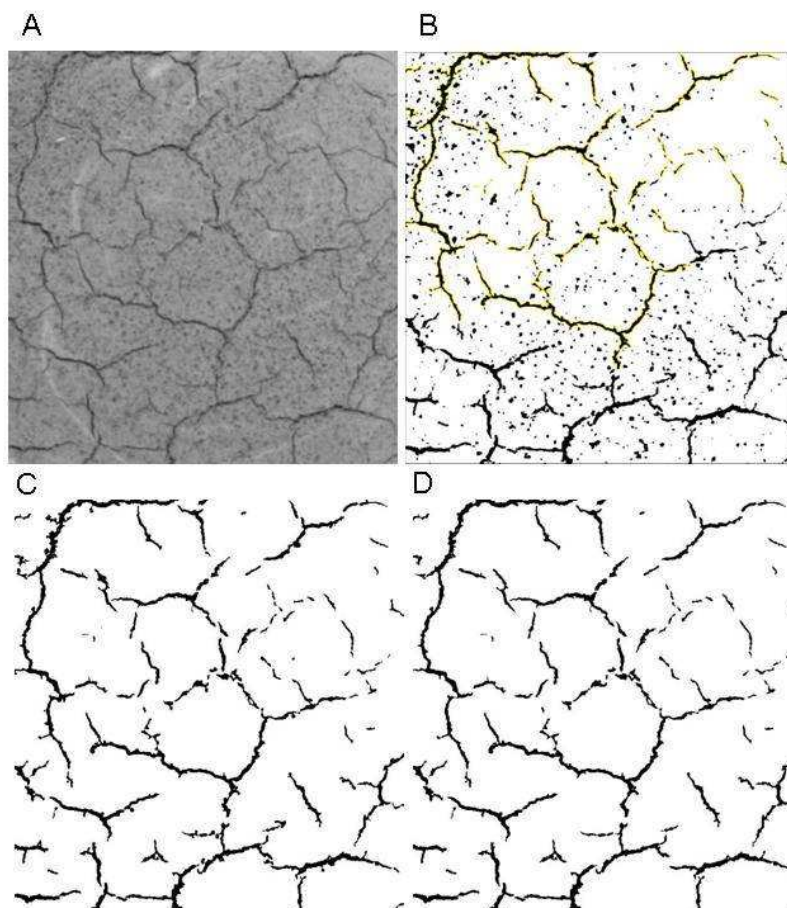


Figure 3.12 Labfield soil; cracking plate despeckling. A. Original photograph; B. Despeckling stage 1 – selection of cracks using wand (tracing) tool in ImageJ (screenshot); C. Despeckling stage 2 – clear outside function applied to the wand-selected image; D. Despeckling stage 3 – eraser tool used to remove final noise interference.

Labfield plates were thresholded at a greyscale value of 118. However, when this value was applied to the Bullionfield soil plates, the cracking patterns were grossly under-represented. A threshold value of 136 was determined to be more accurate for the Bullionfield plates (Figure 3.13).

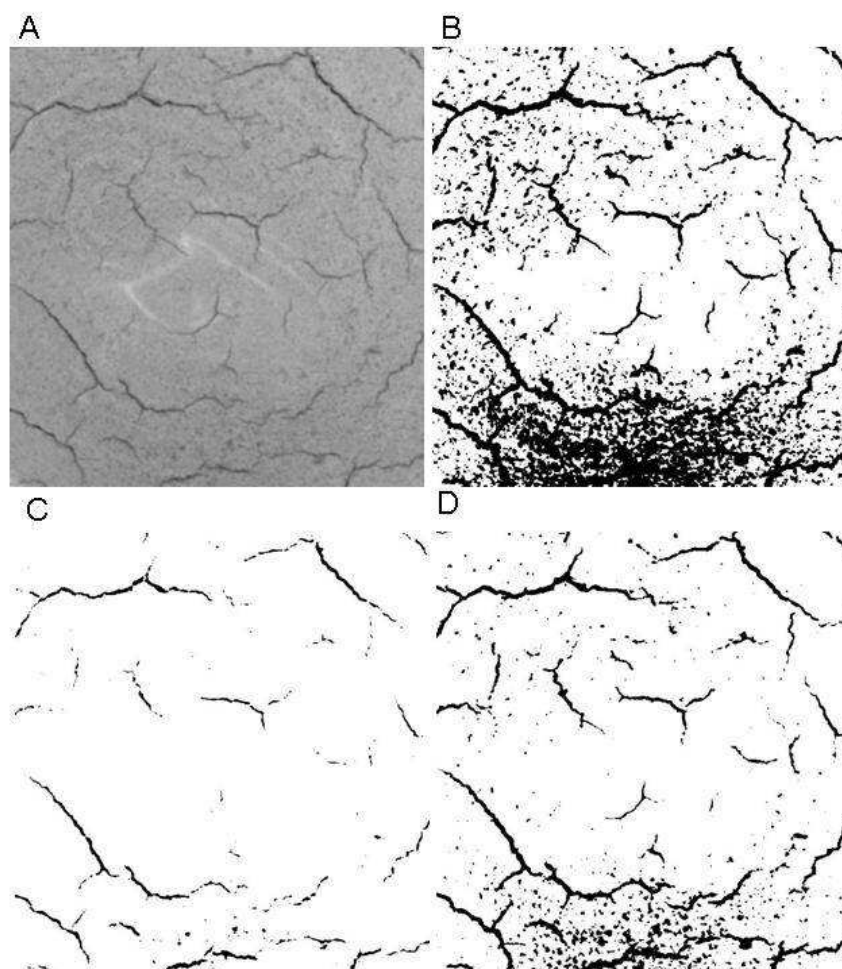


Figure 3.13 Bullionfield soil; cracking plate image thresholding. A. Original photograph; B. ImageJ-suggested threshold value of 146; C. Labfield-threshold value of 118; D. Amended threshold value of 136 (uncleaned).

The same final cleaning steps were carried out on the thresholded and partially cleaned images for the Bullionfield plates as was performed on the Labfield plates using the eraser tool (as described in Figure 3.11). The

cleaned images were then subjected to SCAMP v1.1 analysis of porosity, fractal dimension and pore connectivity, and analysed for impact of bacterial treatments on the formation of cracks in the two different soils. The spatial resolution of the images was determined by photographing a plate with a ruler and calculating resolution using ImageJ (Figure 3.14).

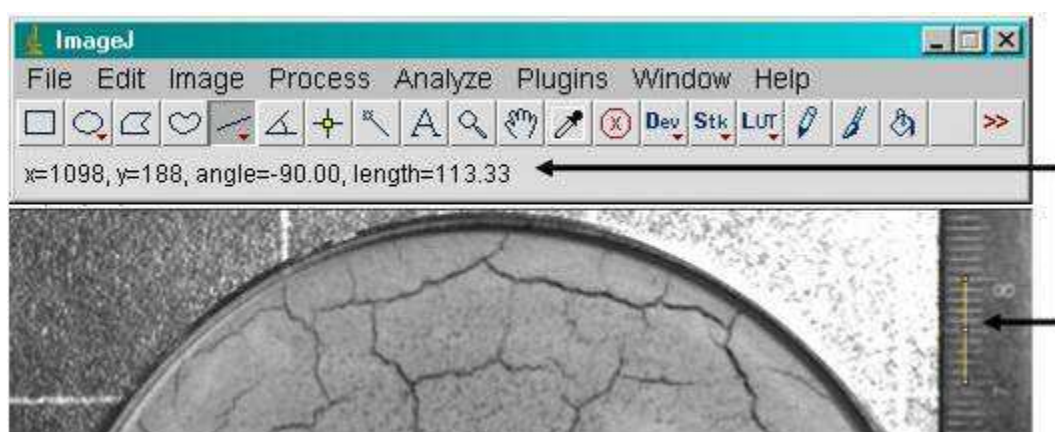


Figure 3.14 Determination of resolution of cracking plate images using ImageJ and ruler image. By drawing a straight line of known length (1 cm) in ImageJ (yellow line indicated by lower arrow); pixel length (113.33) is presented in the information bar of the ImageJ interface (indicated by upper arrow).

The resolution of the crack plates was determined to be 88.495 μm .

3.8 3D and 2D physical measurements using SCAMP v1.1

SCAMP v1.1 (SIMBIOS CT image Analysis and Manipulation Plug-in), an in-house developed analysis software plug-in for ImageJ, was used to measure porosity, fractal dimension, pore-size distribution, and pore connectivity in the cores, aggregates and cracking plates.

3.8.1 Porosity

Porosity was measured in each sample by setting the pore colour and threshold value. Porosity is reported as observed porosity in this study, since pores smaller than the resolution of the images are not resolved. The reported observed porosity value is the percentage of void space in the volume overall.

3.8.2 Fractal dimension

Fractal dimension in this study was measured using a box-counting method as described in Figure 3.15 and calculated using the linear regression equation for the line of the log-log plot of box count against box size as illustrated in Figure 3.16.

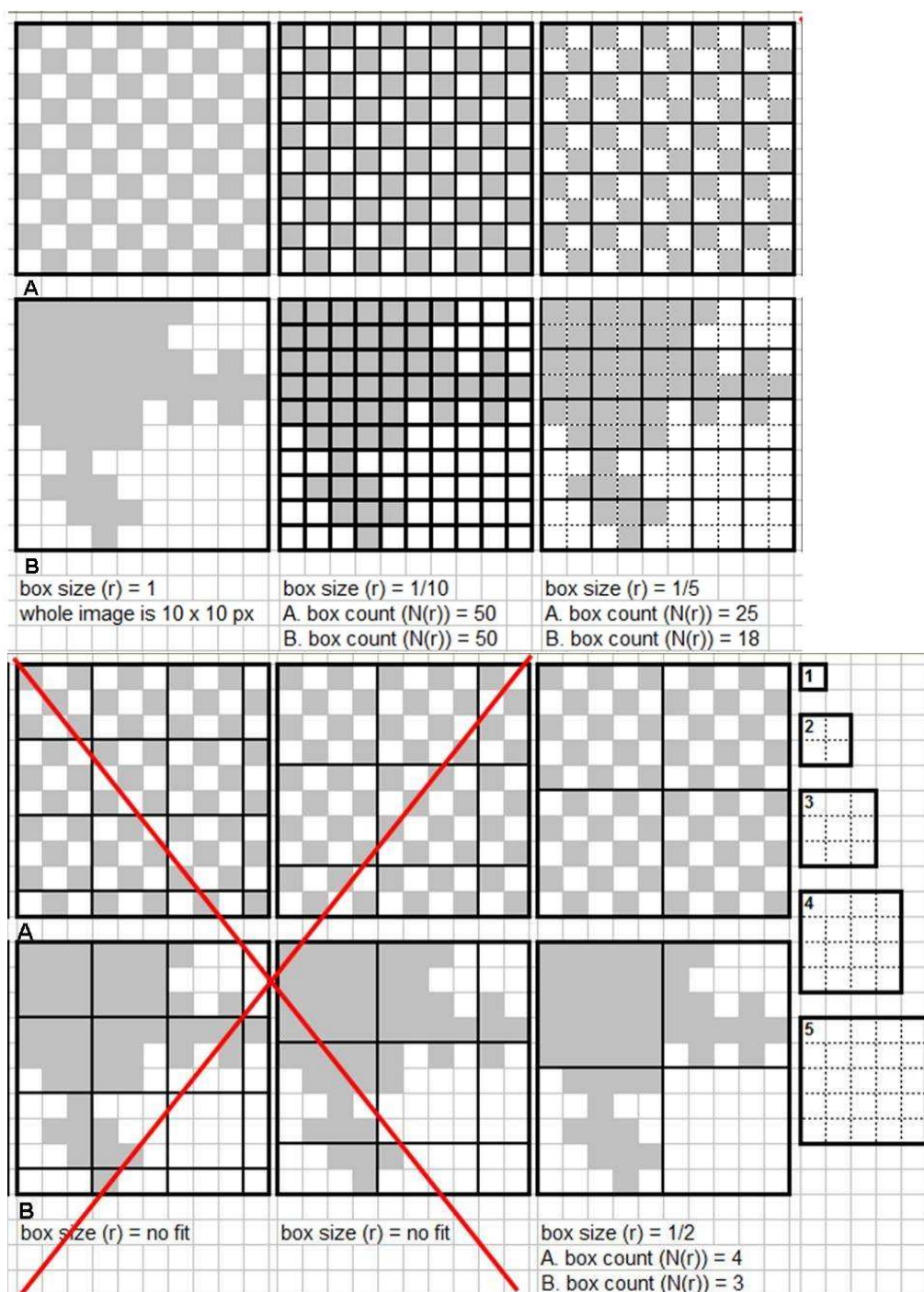


Figure 3.15 Schematic illustration of box counting method for fractal dimension on representative images of A. homo- and B. heterogeneity. Box size (r) = 1 is the smallest box that will cover the whole image. The image is then magnified to its maximum resolution (= pixel size) so that the box size is now 1/pixel size (1/10) and the number of 1/10 boxes containing pore pixels is counted ($N(r)$). The magnification is then reduced until the next box size that covers the image evenly is reached (here 1/5) and the $N(r)$ is counted again. This process is repeated with the final $N(r)$ count being for the maximum box size, which will be the total number of pixels of shortest side of the image divided by 2 (here 5 pixels wide) and therefore $r = 1/2$.

r	$-\log(1/r)$	N(r)		$\log(N(r))$	
		A	B	A	B
1/10	1	25	25	1.4	1.4
1/5	0.699	25	18	1.4	1.3
1/2	0.301	4	3	0.6	0.5

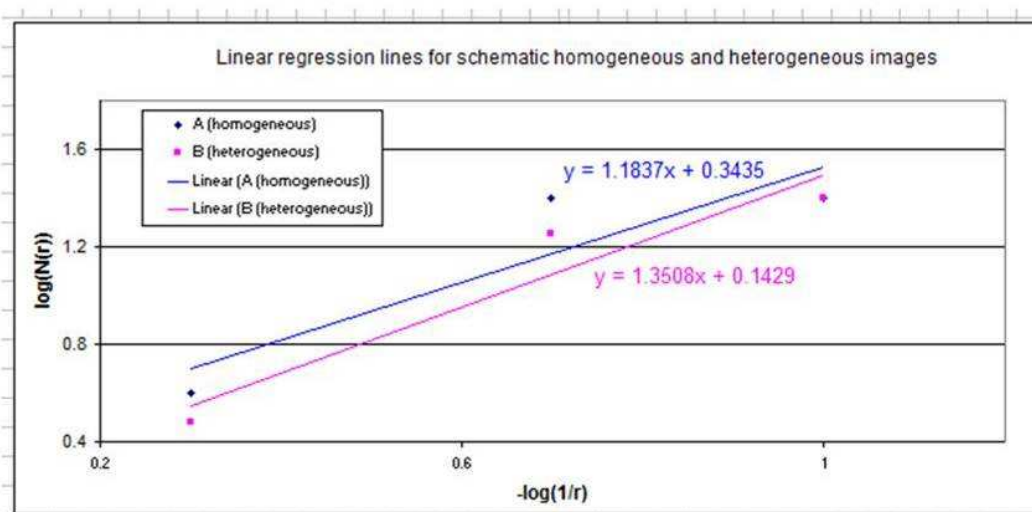


Figure 3.16 Illustration of calculation of fractal dimension for representative homo- and heterogeneous images. The linear regression equation for the line of log-log plot of box count against box size [$\log(N(r)) / -\log(1/r)$] is determined and fractal dimension is the slope of the line. Here the graph demonstrates the heterogeneous image of clustered pores has a higher fractal dimension (1.35) than the homogeneous image of uniformly distributed pores (1.18).

3.8.3 Pore-size distribution

Pore-size distribution required input of the scanner resolution value and pore colour. The number of pores at each radius is counted and the mean pore size reported. When pore-size distribution (reported as a single mean pore size in SCAMP V1.1) is selected, the software puts down spheres (dictated by the pixel size height, width and depth input by the user) and enlarges the sphere within each pore space. Once the sphere encounters soil on its opposite edge then the size of the sphere at that point is recorded as for

example, “1 pore at size x”. This frequency is reported as percent coverage, meaning that the recorded percentage of the total porosity is within pore size class x. This is done for all void spaces and creates a profile of percentage of the total porosity is at size 1x, 2x, 3x etc. Figure 3.17 illustrates this process schematically and presents the input and output interfaces in SCAMP v1.1.

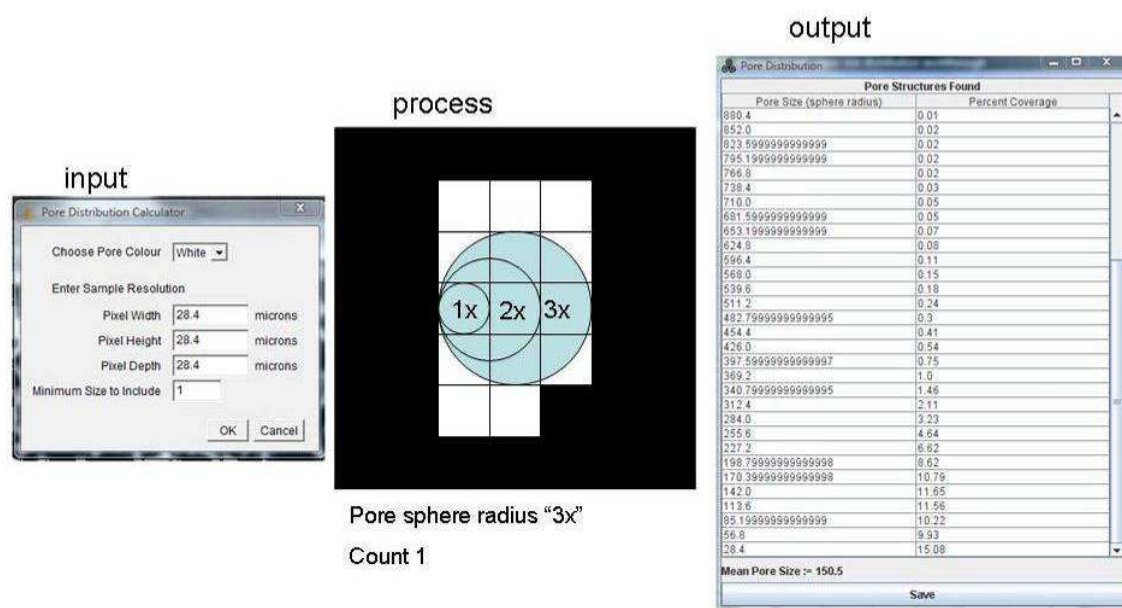
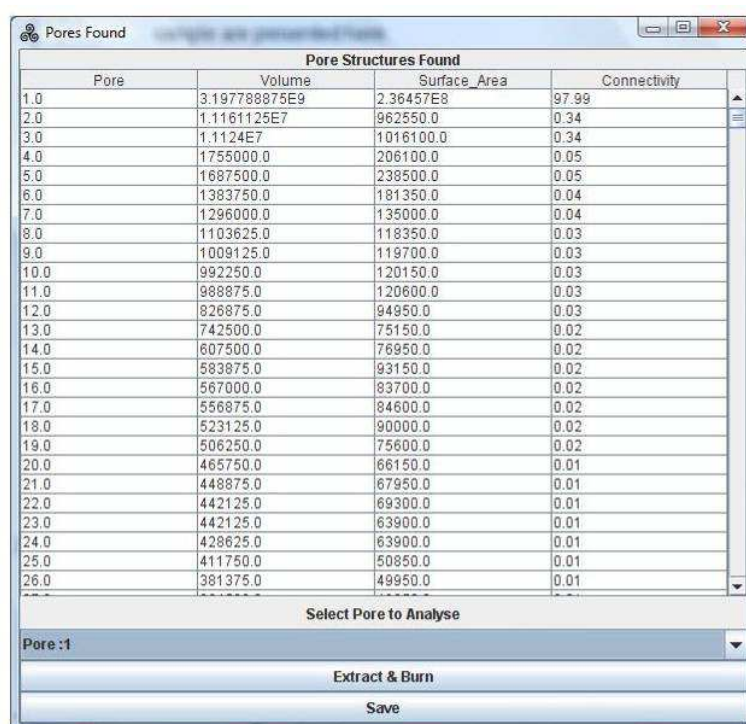


Figure 3.17 Schematic representation of calculation of pore-size distribution in SCAMP V1.1. The user selects the pore colour, enters sample resolution (28.4 μm in this example) and minimum sphere size to include. SCAMP V1.1 puts down spheres inside each pore space and “inflates” the sphere in integer multiples until soil is encountered on the opposite side. This is then recorded as percentage coverage of total pore space at sphere radius e.g. “3x”. This continues throughout the segmented volume until all pore spaces have been counted. A table of pore size percentage coverage is generated and the “mean pore size” is calculated.

3.8.4 Pore connectivity

Due to the time-consuming nature of this procedure and computational limitations of the current system, the pore connectivity of the 3D cores were not analysed. Pore connectivity in the 2 mm aggregate data from the APS experiments and in the crack plate analyses were carried out since these

dataset volumes were not computationally onerous. Pore connectivity is estimated by random walkers placed within the pores and is presented, in SCAMP v1.1, in several ways. For each connected pore found, pore volume, and connectivity (as a percentage of total pore volume) is returned. Figure 3.18 illustrates the output from a typical analysis.



Pore Structures Found			
Pore	Volume	Surface Area	Connectivity
1.0	3.197788875E9	2.36457E8	97.99
2.0	1.1161125E7	962550.0	0.34
3.0	1.1124E7	1016100.0	0.34
4.0	1755000.0	206100.0	0.05
5.0	1687500.0	238500.0	0.05
6.0	1383750.0	181350.0	0.04
7.0	1296000.0	135000.0	0.04
8.0	1103625.0	118350.0	0.03
9.0	1009125.0	119700.0	0.03
10.0	992250.0	120150.0	0.03
11.0	988875.0	120600.0	0.03
12.0	826875.0	94950.0	0.03
13.0	742500.0	75150.0	0.02
14.0	607500.0	76950.0	0.02
15.0	583875.0	93150.0	0.02
16.0	567000.0	83700.0	0.02
17.0	556875.0	84600.0	0.02
18.0	523125.0	90000.0	0.02
19.0	506250.0	75600.0	0.02
20.0	465750.0	66150.0	0.01
21.0	448875.0	67950.0	0.01
22.0	442125.0	69300.0	0.01
23.0	442125.0	63900.0	0.01
24.0	428625.0	63900.0	0.01
25.0	411750.0	50850.0	0.01
26.0	381375.0	49950.0	0.01

Select Pore to Analyse

Pore:1

Extract & Burn

Save

Figure 3.18 Typical output from pore connectivity analysis in SCAMP v1.1. Each connected pore is reported in terms of volume, surface area and connectivity. The connectivity is representative of “percentage of total sample pore volume in the associated pore”.

3.9 Statistical analyses

SPSS v16 and latterly v17 statistical software was used throughout the study. Generalised estimating equations (GEE) were used for analysing statistical significance as unknown correlations were present in Generalized Linear Models. All factors were presented in the analysis and, in a stepwise

regression pattern, terms were tested for their interaction effects. As interactions were ruled out, those terms were removed or if interactions were demonstrated then the analyses were split according to individual factors levels. This process continued until there were no further levels available for separation, or until interactions were statistically ruled out. Effectively a hierarchical representation of effects was applied; and as the aim of this study was to look at the impact of bacterial treatment on the soil then that was always be the last term in the tree. Figure 3.19 illustrates this diagrammatically.

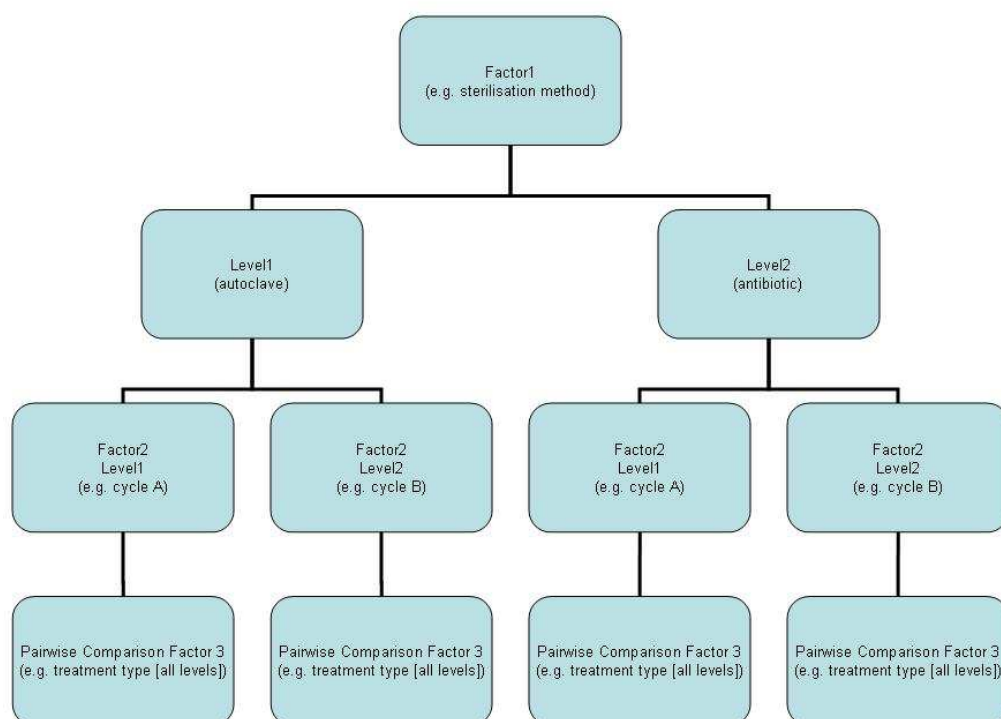


Figure 3.19 Diagrammatic representation of statistical hierarchy

Overall test results are reported according to the Wald chi-square test. This test is based on the linearly independent pairwise comparisons among the estimated marginal means of the dependent variable. The pairwise comparisons of estimated marginal means are based on the original scale of the dependent variable.

CHAPTER 4

4 Studies on the effects of *Pseudomonas fluorescens* SBW25 and key mutants on selected soil hydrodynamics**4.1 Introduction**

Water flow in soil governs the movement of solutes, nutrients, and microbes through the soil profile. As such, understanding the hydrodynamics of the soil enables a greater understanding of its internal architecture (Crawford *et al.*, 2005; O'Donnell *et al.*, 2007). In order to postulate on how bacteria can influence the movement of water through the soil it is necessary to determine the differences between treated soils in terms of their ability to retain water and the drainage profile. This study looks at the unsaturated zone where the soil pores contain both air and water.

4.2 Chapter aims and research objectives

The aim of this research chapter is to ascertain the impact of bacteria and bacterial activity on the hydrodynamics of water flow and retention in soil. In this work, the term bacterial legacy is used to refer to all aspects of bacterial activity. Bacterial legacy consists of (i) exudate compounds produced by the bacteria and released into the immediate environment, (ii) cell debris released when bacteria die, and (iii) the footprint left behind when a bacterium attaches to and detaches from a surface.

In order to determine if differences in the hydrodynamic properties of the soil can be attributed to bacterial legacy, prepacked sandy loam soil

cores were treated with different strains of *Pseudomonas fluorescens* SBW25 and subjected to two wet/dry cycles to produce water retention curves (WRCs) for each treated soil, and also to a sorptivity assay to determine the wettability of the treated soils.

Research objectives:

1. Characterisation of the impact of the different bacterial legacies on the gravimetric water content of the soil at key points in the WRC (saturation^{vi}, macropore drainage point, and mesopore drainage point).
2. Characterisation of the impact of the different bacterial legacies on the absolute drainage of the soil at the key points in the WRC.
3. Characterisation of the impact of the different bacterial legacies on the percentage drainage of the soil at the key points in the WRC relative to the initial saturation level.
4. Characterisation of the impact of the different bacterial legacies on the wettability of the soil following drying after each wet/dry cycle.

The hydrodynamics of experimental cores under different bacterial treatments were investigated using water retention curves. The cores were subjected to two wet/dry cycles, cycle A and cycle B. Each cycle also included analysis by μ XCT (results reported in Chapter 5) and a sorptivity

^{vi} The term “saturation” is used in this study to refer to the near-saturation level found at a matric head of 0 cm

assay (results reported in this Chapter 4) as illustrated again for reference in Figure 4.1 below.

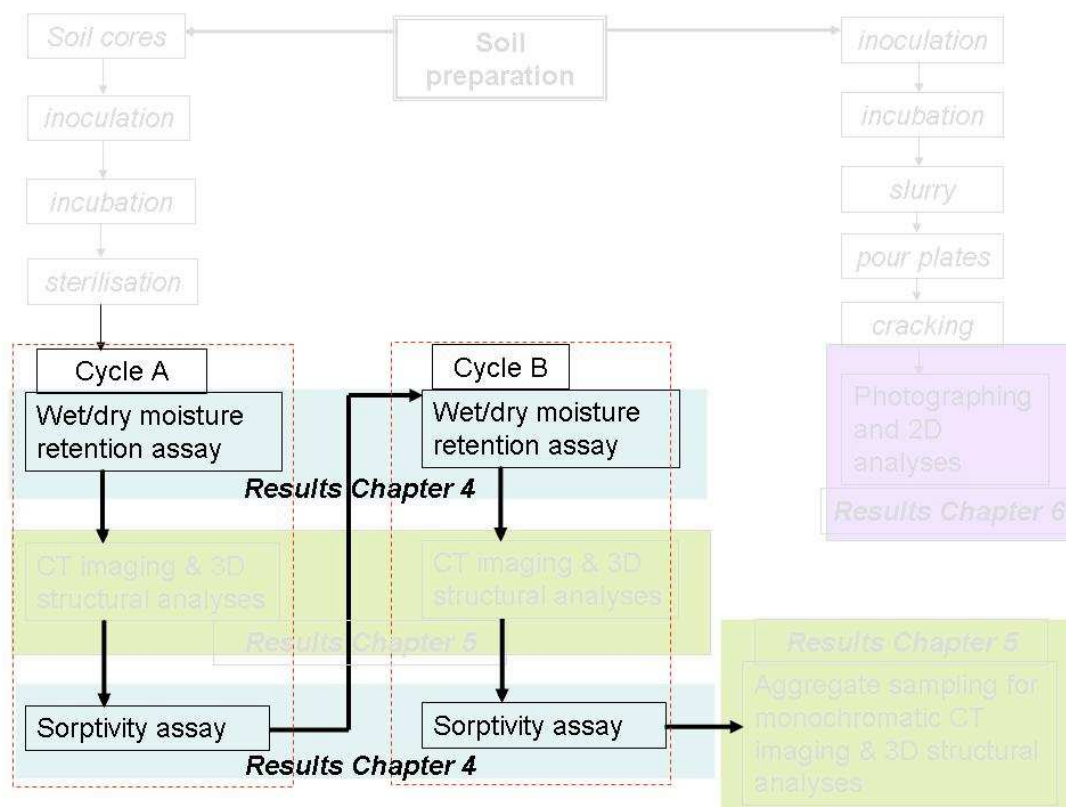


Figure 4.1 Schematic of experimental design highlighting moisture retention assay used to produce data for the water retention curves.

4.3 Results

4.3.1 Water retention curves

4.3.1.1 Introduction

Experimental cores packed with Labfield soil were incubated with different bacterial treatments then, following sterilisation, were subjected to a water retention assay in which gravimetric water content ($u \text{ g g}^{-1}$) was determined

at equilibrated matric potentials from -1 cm to -100 cm (where -1 cm = -0.1 kPa, and -100 cm = -10 kPa matric pressure) of a wet/dry cycle (Cycle A) shown in Figure 4.2 and a second wet/dry cycle (Cycle B) shown in Figure 4.3 below.

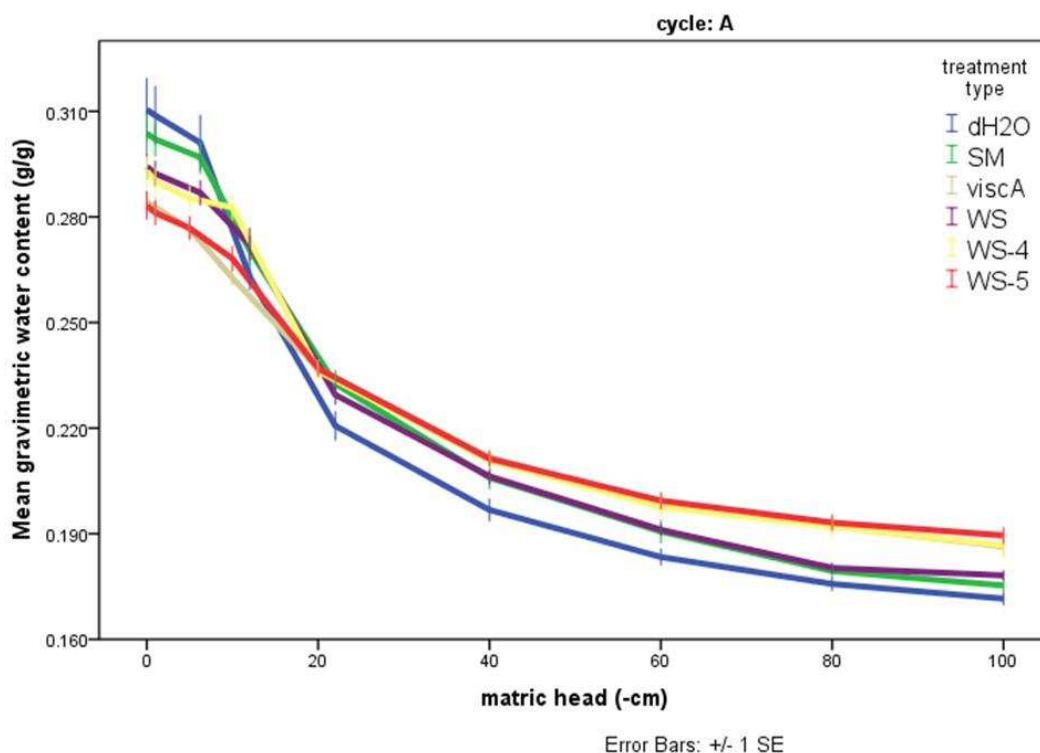


Figure 4.2 Water retention curve of wet/dry cycle A for sandy loam (Labfield) soil with different bacterial legacies. Mean gravimetric water content of the soil cores plotted against the equilibrated matric head level shows the characteristic water retention curve. dH₂O = bacteria-free control soil, SM = wild-type bacteria-control soil, *ViscA*, WS, WS-4 and WS-5 = bacteria treatments. Error bars were calculated as the standard error of the means of each treatment type (n = 10).

Bacterial treatments showed varying degrees of impact on the water retention curve in Cycle A with *ViscA* and WS-5 treatments (buff and red lines respectively) presenting the most notable effects at near-saturation level (0 cm), and WS-5 and WS-4 treatments (red and yellow lines

respectively) presenting the most notable effects at mesopore level (-80 cm to -100 cm).

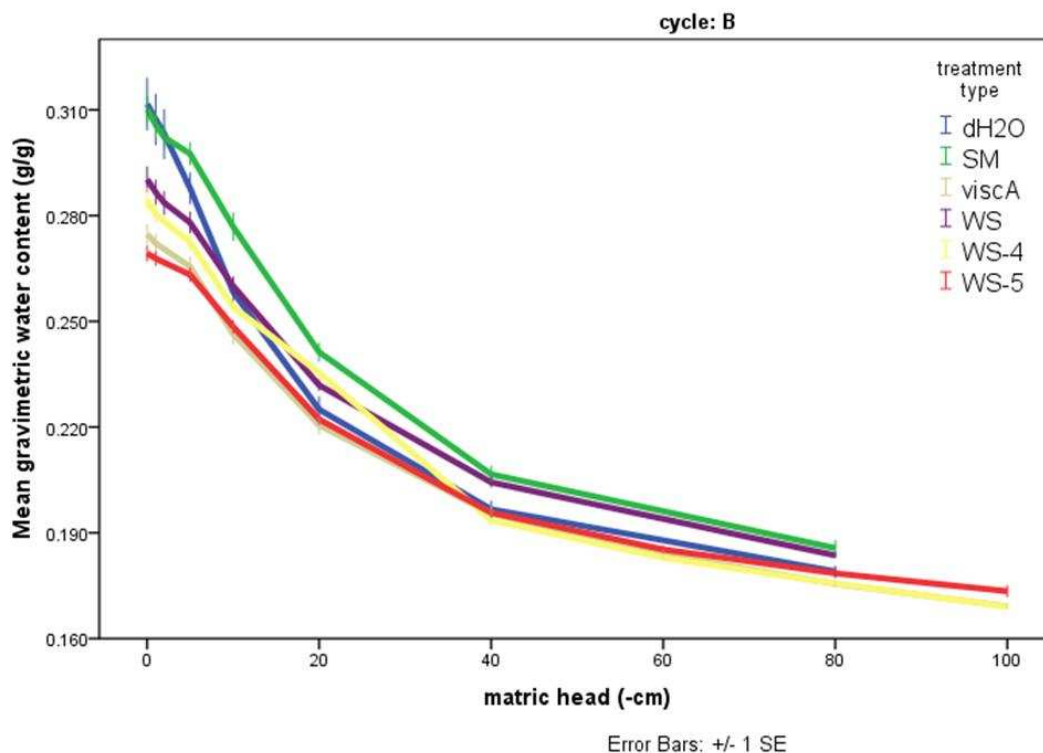


Figure 4.3 Water retention curve of wet/dry cycle B for sandy loam (Labfield) soil with different bacterial legacies. Mean gravimetric water content of the soil cores plotted against the equilibrated matrix head level shows the characteristic water retention curve. dH₂O = bacteria-free control soil, SM = wild-type bacteria-control soil, *ViscA*, WS, WS-4 and WS-5 = bacteria treatments. Error bars were calculated as the standard error of the means of treatment types (n = 10).

Bacterial treatments showed varying degrees of impact on the water retention curve in Cycle B, most notably at 0 cm matrix head (near-saturation) where all but the SM (green line) treatments appeared to reduce the gravimetric water content of the soil in comparison to the bacteria-free dH₂O control (blue line).

Analysis of the gravimetric water content at all points of equilibrium would have been extremely time-consuming, therefore analysis of

gravimetric water content at key matric heads was carried out to provide an insight into the effect of bacterial legacy on these key water-filled and drainage points. In this study, three approaches to analysing the water retention curves were undertaken to investigate the impact of bacteria on the hydrodynamics of the soil.

1. The absolute gravimetric water content at 0 cm, -10 cm, and -80 cm^{vii} matric head points representing water-filled soil, macropores drainage and mesopore drainage points (results reported in Section 4.3.1.2);
2. The absolute drainage of water from macropores and from mesopores (results reported in Section 4.3.1.3); and
3. The drainage from macropores and from mesopores as a percentage of initial water content (saturation) (results reported in Section 4.3.1.4).

4.3.1.2 Investigation of the impact of bacteria on GWC

Three key points on the water retention curve were selected for analysis of gravimetric water content to determine the impact of bacteria on the water retention ability of the soil. Matric head (MH) impacts a negative pressure head (suction) value on the soil water flow. Levels are reported as matric head 0 cm (near saturation point), -10 cm (macropores drained) and -80 cm

^{vii} Typically the mesopore drainage point would be reported at -100 cm matric head, however, this study uses the -80 cm matric potential head (-0.8 kPa) as the mesopore value, as the glass burette on one of the tension tables broke when being adjusted to -100 cm in the final equilibration step of cycle B

(in this study taken to be mesopores drained). Tests of model effects indicated necessary splitting of the data by cycle and then by matric head within each cycle. The sterilisation method was shown not to have a statistically significant effect on gravimetric water content at all matric heads ($p > 0.156$).

For cycle A, mean gravimetric water contents for each treatment type are shown in Figure 4.4 and the results of the pairwise comparison of treatment types at each matric head, within each cycle are shown in Table 4.1.

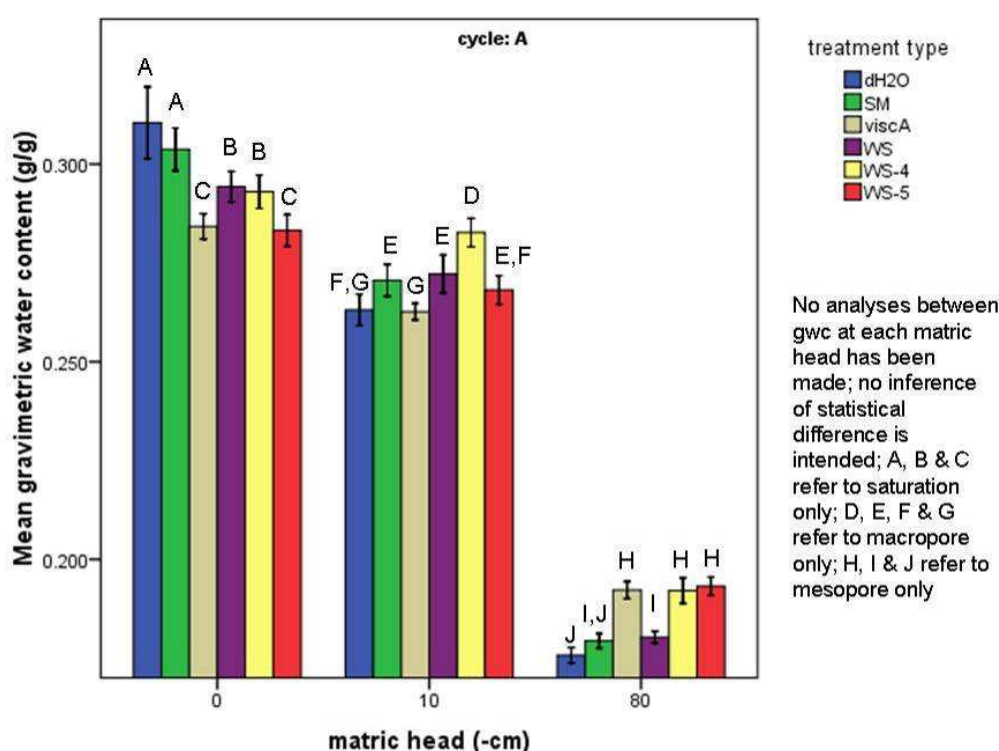


Figure 4.4 Mean GWC at key matric head levels for soils under different treatment types in cycle A. Error bars were calculated as the standard error of the means of treatment types ($n = 10$).

The presence of the bacterial legacy from the mutant strains considerably reduced the GWC of the soil at saturation level (0 cm). Macropore (-10 cm)

GWC was increased by SM-treatment, this response was then reduced by *ViscA*, but greatly increased by WS-4. Mesopore (-80 cm) GWC was unaffected by SM-treatment but greatly increased by all mutant strain legacies except WS.

Table 4.1 Pairwise comparison of the effect of bacterial treatment type on gravimetric water content of Labfield soil in cycle A

Key matric head level				
		saturation (0 cm)	macropore (-10 cm)	mesopore (-80 cm)
pairwise treatment types	dH ₂ O vs. SM	0.363	↑ 0.047	0.099
	SM vs. mutants	↓ < 0.025	<i>see below</i>	↑ < 0.001 (Except WS)
	SM vs. <i>ViscA</i>	↓ < 0.001	↓ 0.006	↑ < 0.001
	SM vs. WS	↓ 0.024	0.698	0.645
	SM vs. WS-4	↓ 0.022	↑ 0.001	↑ < 0.001
	WS vs. WS-4	0.729	↑ 0.018	↑ < 0.001
	SM vs. WS-5	↓ < 0.001	0.452	↑ < 0.001
Bold type indicates statistical significance ($p < 0.05$); ↓ indicates decreased GWC compared with control; ↑ indicates increased GWC compared with control; first term in treatment type column indicates control for comparison				

At saturation, whilst the treatment of the soil with the SM control bacteria did not affect GWC compared with the bacteria-free dH₂O control, all mutant strains decreased the water-holding capacity of the soil compared with the SM control. At macropore level, the impact of bacteria on the soil was an increase in GWC with the SM treatment compared with the bacteria-free dH₂O control, and also with the WS-4 treatment compared with the SM control, whereas *ViscA* decreased the soil GWC compared with the SM control. At mesopore level, where an effect was observed, a more

consistent response was noted. Water levels were elevated by impacting bacterial treatments compared with the respective controls. In addition to these observations that whilst treatment of the soil with the different bacterial strains did elicit an impact on the water holding capacity of the soil, the overall effects were not consistent across the different pore sizes e.g. WS-4 treated soil held less water than the SM control soil at saturation, but at macropore and mesopore levels, the water levels were comparably increased. Whereas with WS-5 treatment, GWC at saturation was again less than the SM control, no difference was observed at macropore level, but at mesopore level WS treated soil held more water than the SM control. The impact of the different legacies left in the soil by the bacterial treatments was varied at the different key matric potential measurement levels in cycle A.

For cycle B, mean gravimetric water contents for each treatment type are shown in Figure 4.5 and the results of the pairwise comparison of treatment types at each matric head, within each cycle are shown in Table 4.2.

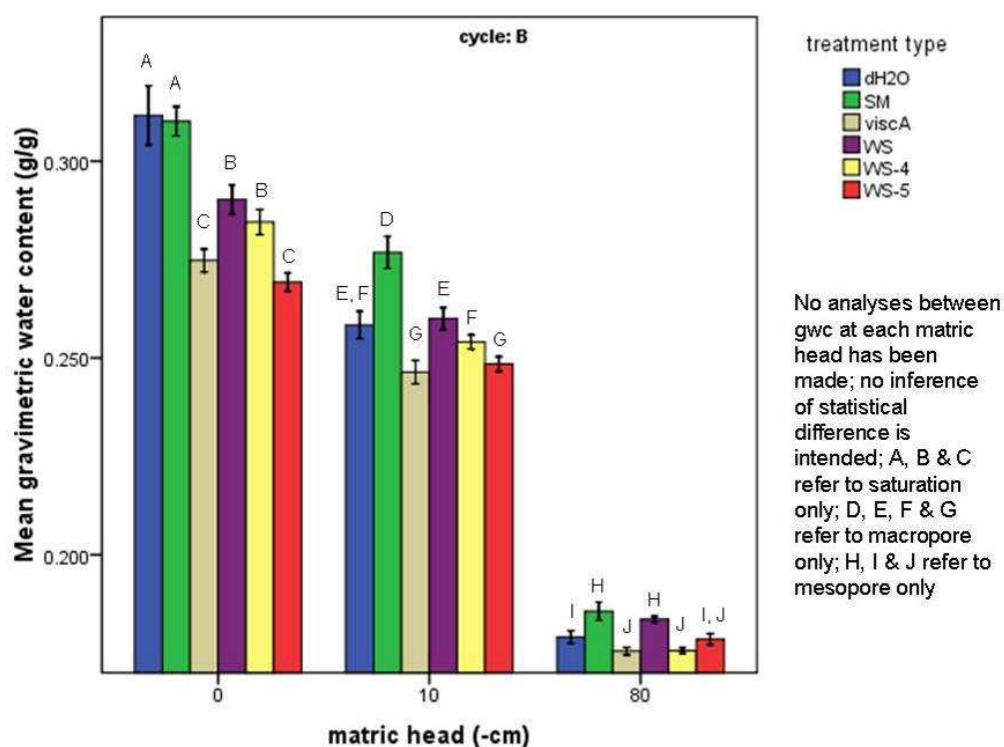


Figure 4.5 Mean GWC at key matric head levels for soils under different treatment types in cycle B. Bacterial legacy of the mutant strains considerably reduced the GWC of the soil at saturation level (0 cm). Macropore (-10 cm) and mesopore (-80 cm) GWCs were increased by SM-treatment, but reduced by some of the mutant-strain treatments. Error bars were calculated as the standard error of the means of each treatment type ($n = 10$).

Table 4.2 Pairwise comparison of the effect of bacterial treatment type on gravimetric water content of Labfield soil in cycle B

		Key matric head level		
		saturation (0 cm)	macropore (-10 cm)	mesopore (-80 cm)
pairwise treatment types	dH ₂ O vs. SM	0.840	↑ < 0.001	↑ 0.013
	SM vs. mutants	↓ < 0.001	↓ < 0.001	see below
	SM vs. <i>ViscA</i>	↓ < 0.001	↓ < 0.001	↓ < 0.001
	SM vs. WS	↓ < 0.001	↓ < 0.001	0.369
	SM vs. WS-4	↓ < 0.001	↓ < 0.001	↓ < 0.001
	WS vs. WS-4	0.183	↓ 0.018	↓ < 0.001
	SM vs. WS-5	↓ < 0.001	↓ < 0.001	↓ 0.005

Bold type indicates statistical significance ($p < 0.05$); ↓ indicates decreased GWC compared with control; ↑ indicates increased GWC compared with control; first term

in treatment type column indicates control for comparison

As seen with cycle A, SM-treated soil in cycle B showed no difference in GWC at saturation level compared with the bacteria-free dH₂O control soil; and once again all the mutant strains showed decreased GWC compared with the SM control soil. The pattern of decrease in GWC of cycle A was also echoed in cycle B, with the *ViscA* and WS-5 soils showing a comparable greater decrease in GWC than the comparable decrease observed in the WS and WS-4 soils.

In cycle A, where a difference was noted in the GWC at macropore and mesopore levels compared with the controls, that difference was an increase in GWC (with the exception of *ViscA* soil at macropore). However, the overall impact of the mutant bacteria on the GWC of soil in cycle B compared with the SM control is a decrease at both macro- and mesopore levels (with the exception of WS at mesopore which showed no difference to the SM control); and interestingly at both macropore and mesopore levels, SM soil was observed to have an increased GWC compared with the bacteria-free dH₂O control soil.

4.3.1.3 Investigation of the impact of bacteria on absolute water drainage

In order to assess the impact of bacteria on the absolute drainage of water from the soil the change in water content between the points on the WRC were calculated. Macropore drainage, Δ_{mac} , was calculated by subtracting the GWC at macropore level (GWC_{mac}) from the GWC at saturation level

(GWC_{sat}). Mesopore drainage, Δ_{mes} , was calculated by subtracting the GWC at mesopore level (GWC_{mes}) from the GWC_{mac} . Overall, all soils presented greater drainage from mesopores than from macropores ($p < 0.05$) as shown in Figure 4.6.

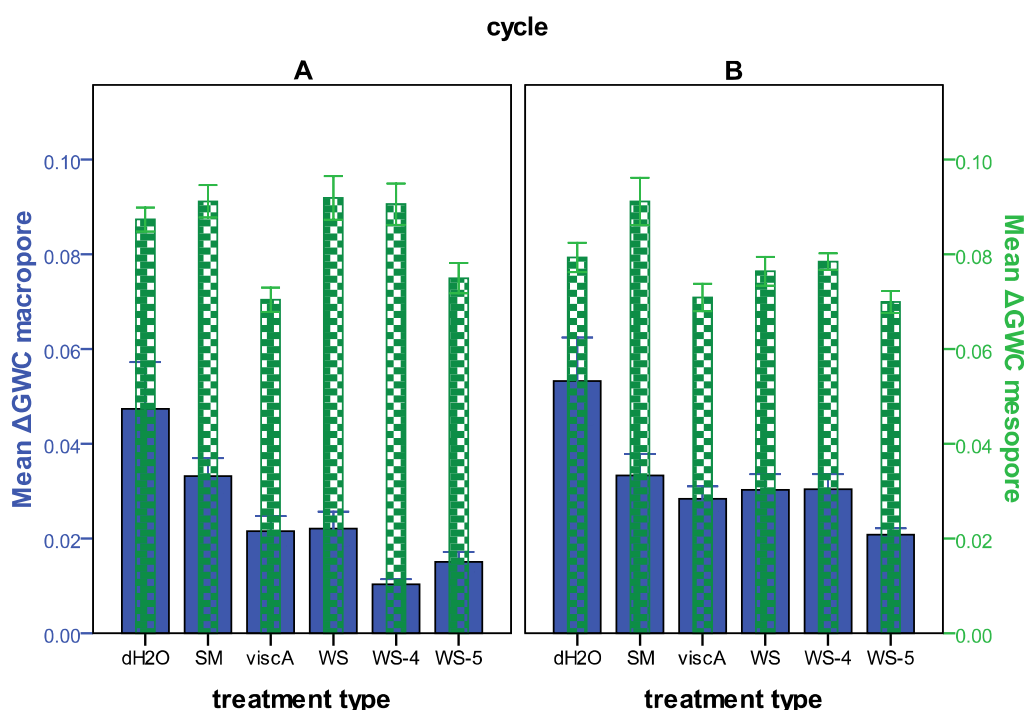


Figure 4.6 Overview of drainage from macropores and mesopores for soil cores under different treatment types. Blue bars represent mean macropore drainage (g/g) and green bars represent mean mesopore drainage (g/g) for each treatment type-soil, in cycle A and cycle B. Error bars were calculated as the standard error of the means of each treatment type ($n = 10$).

Sterilisation method was shown to not have a statistically significant interactive effect on treatment type ($p = 0.787$) therefore all cores within treatment types were analysed together. Cycle and treatment type were shown to be interacting terms in both Δ_{mac} ($p < 0.001$) and Δ_{mes} ($p = 0.003$) therefore both the analyses were split into cycle A and cycle B.

Results for Δmac and Δmes are shown in Figure 4.7 and Figure 4.8 below; and the pairwise comparisons of treatment types within each cycle are highlighted in Table 4.3 and Table 4.4.

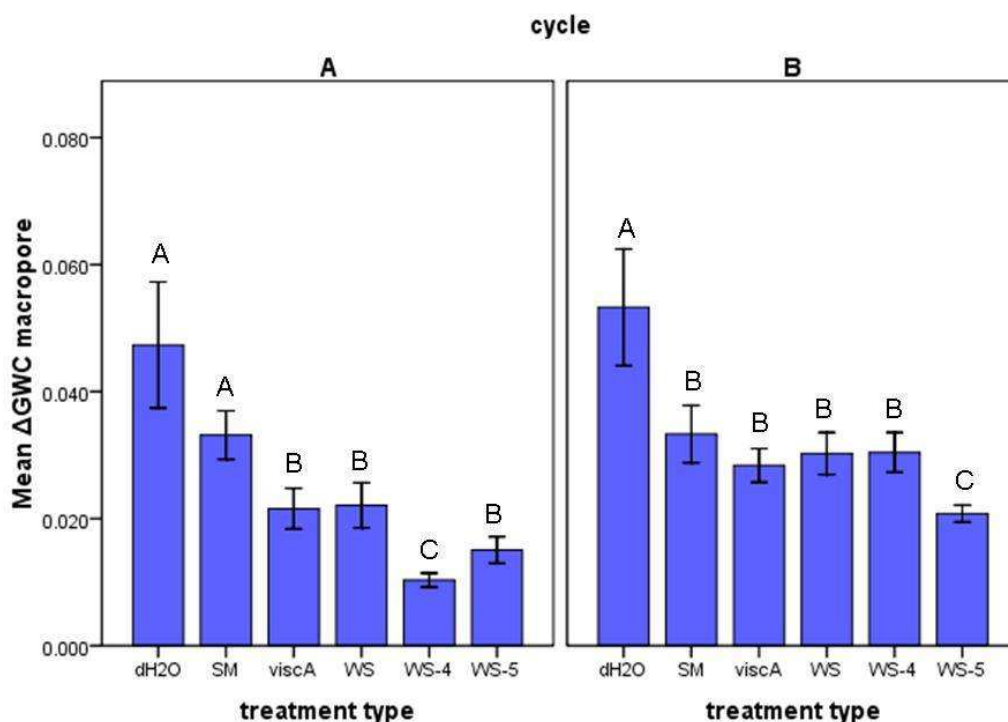


Figure 4.7 Macropore drainage for soil cores under different treatments. Significantly different ($p < 0.05$) treatments are indicated by lettering within each cycle. No statistical comparison has been made between cycles and as such no inference is intended between cycle A and cycle B. Error bars were calculated as the standard error of the means of each treatment type ($n = 10$).

In cycle A, soils with mutant-strain legacies drained less readily than the SM control soil. In cycle B, macropore drainage was decreased by SM treatment compared with the bacteria-free dH₂O control, but only the WS-5 reduced the macropore drainage ability from that of the SM control soil.

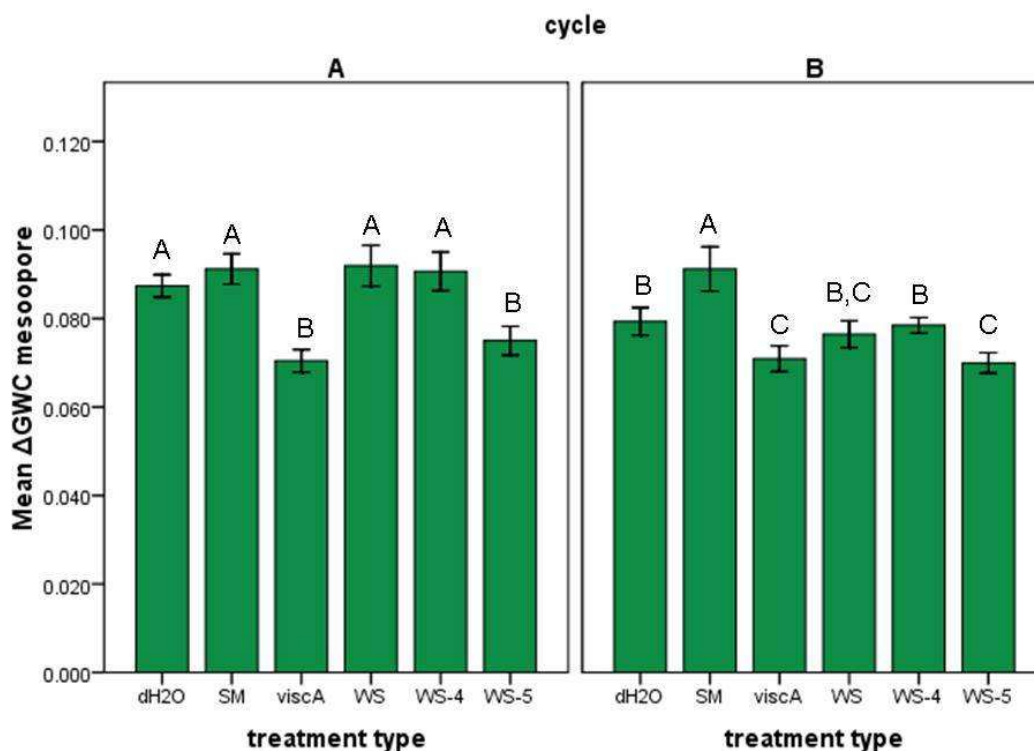


Figure 4.8 Mesopore drainage for soils under different treatments. Significantly different ($p < 0.05$) treatments are indicated by lettering within each cycle. No comparison has been made between cycles at this stage and as such no inference is intended between cycle A and cycle B. Error bars were calculated as the standard error of the means of each treatment type ($n = 10$).

In cycle A only the soil treated with mutant strains *ViscA* and WS-5 drained less readily at mesopore level than the SM control soil. In cycle B, all bacterial mutant-strain treatments decreased the mesopore drainage of the soils from that of the SM control soil, which showed greater drainage than the bacteria-free dH₂O control soil.

Table 4.3 Pairwise comparison of the effect of bacterial treatment type on absolute drainage of Labfield soil in cycle A

pairwise treatment types		Δ_{mac}	Δ_{mes}
	dH ₂ O vs. SM	0.160	0.342
	SM vs. mutants	↓ < 0.025	<i>see below</i>
	SM vs. <i>ViscA</i>	↓ 0.014	↓ < 0.001
	SM vs. WS	↓ 0.025	0.894
	SM vs. WS-4	↓ < 0.001	0.913
	WS vs. WS-4	↓ 0.001	0.829
	SM vs. WS-5	↓ < 0.001	↓ < 0.001

Bold type indicates statistical significance ($p < 0.05$); ↓ indicates decreased drainage compared with control; ↑ indicates increased drainage compared with control; first term in treatment type column indicates control for comparison

In cycle A (Table 4.3 above) bacteria are shown to have a greater impact on drainage at the macropore level; whereas in cycle B (Table 4.4 below), bacteria are shown to have a greater impact on drainage at the mesopore level.

Table 4.4 Pairwise comparison of the effect of bacterial treatment type on absolute drainage of Labfield soil in cycle B

pairwise treatment types		Δ_{mac}	Δ_{mes}
	dH ₂ O vs. SM	↓ 0.040	↑ 0.034
	SM vs. mutants	<i>see below</i>	<i>see below</i>
	SM vs. <i>ViscA</i>	0.321	↓ < 0.001
	SM vs. WS	0.566	↓ 0.008
	SM vs. WS-4	0.581	↓ 0.011
	WS vs. WS-4	0.968	0.540
	SM vs. WS-5	↓ 0.005	↓ < 0.001

Bold type indicates statistical significance ($p < 0.05$); ↓ indicates decreased drainage compared with control; ↑ indicates increased drainage compared with control; first term in treatment type column indicates control for comparison

4.3.1.4 Investigation of impact of bacteria on percentage water drainage

Having considered the values of GWC, it became apparent that although a soil may present a lower ΔGWC for either macro- or mesopore drainage, if that particular soil originally exhibited less water at saturation, then it would stand to reason that less water would be observed to drain at any particular potential. Therefore, drainage from macro- and mesopores, and total drainage were subsequently calculated as a percentage of the GWC of each treatment type. Tests of model effects indicated sterilisation method did not have a statistically significant effect on percentage water drainage for all analyses ($p > 0.217$ n.s.). Cycle and treatment type were shown to be interacting terms in both percentage total drainage and percentage mesopore drainage therefore these analyses were split at the cycle level. Following this split, sterilisation was shown not to have an interacting effect with treatment type ($p = 0.428$ n.s., cycle A; $p = 0.780$ n.s., cycle B); and in percentage mesopore drainage ($p = 0.351$ n.s., cycle A; $p = 0.218$ n.s., cycle B).

Overall profiles of total, macropore and mesopore percentage drainage are presented in Figure 4.9 and results are presented in Table 4.5 for total percentage drainage, Table 4.6 for percentage macropore drainage and Table 4.7 for percentage mesopore drainage below.

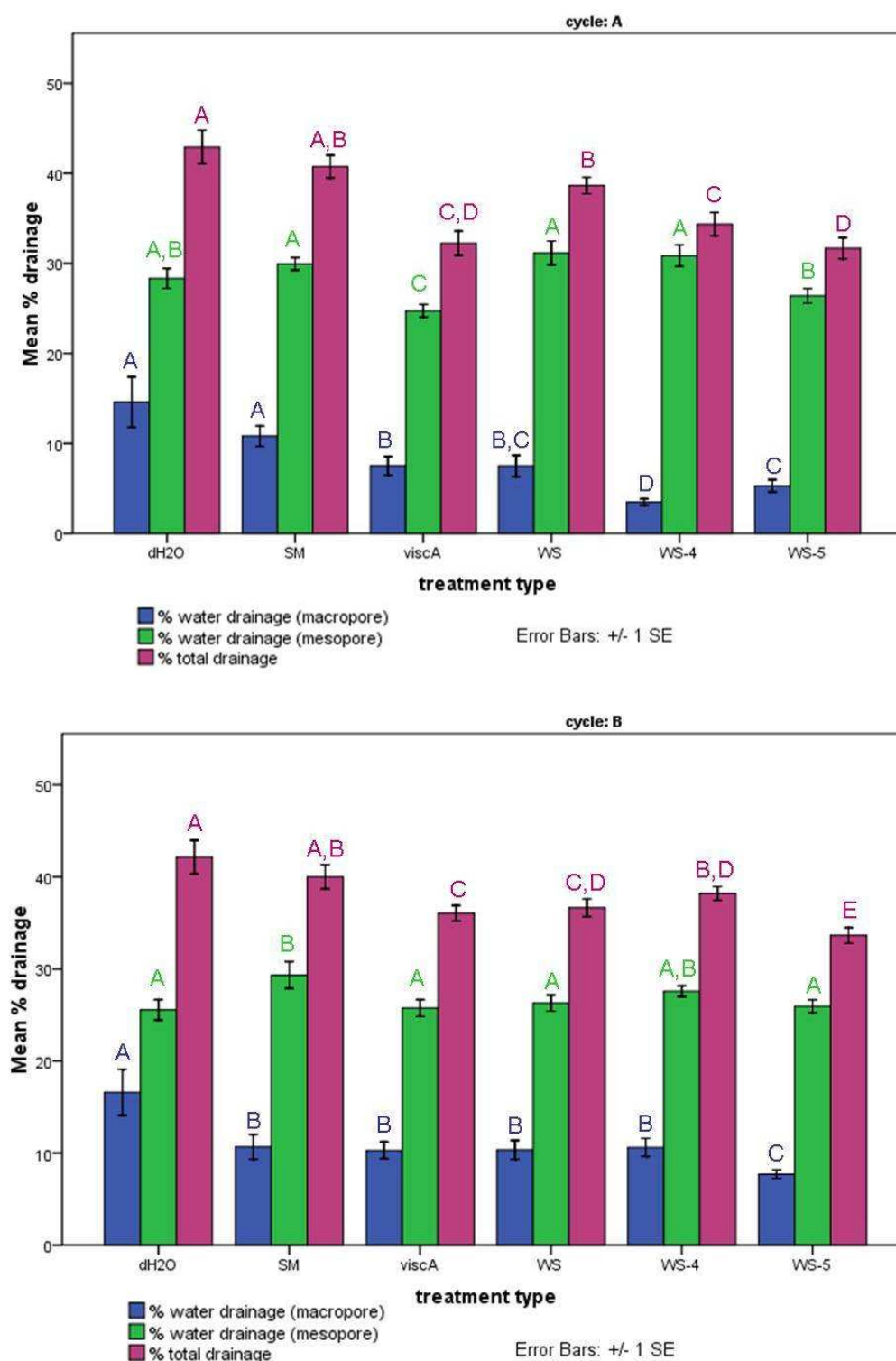


Figure 4.9 Percentage drainage from pores of soil with different bacterial legacies. Mean percentage drainage for each experimental soil-treatment type is plotted showing total, macropore and mesopore percentage drainage within Cycle A (top) and Cycle B (bottom). Statistical differences between the percentage water loss from soils with different bacterial legacies are indicated by the corresponding coloured letters for each drainage analysis ($p < 0.05$). Error bars were calculated as the standard error of the means of each treatment type ($n = 10$).

Total drainage from macropores and mesopores in both cycles for all cores was less than 45% of the saturated gravimetric water content. Approximately 30% water loss was from mesopores alone, and between approximately 5 and 15% was from macropores alone.

Table 4.5 Pairwise comparison of the effect of bacterial treatment type on % total drainage of Labfield soil for cycles A and B

		% total drainage	
		cycle A	cycle B
pairwise treatment types	dH ₂ O vs. SM	0.269	0.307
	SM vs. mutants	<i>see below</i>	<i>see below</i>
	SM vs. <i>ViscA</i>	↓ < 0.001	↓ 0.009
	SM vs. WS	0.132	↓ 0.028
	SM vs. WS-4	↓ < 0.001	0.209
	WS vs. WS-4	↓ < 0.001	0.163
	SM vs. WS-5	↓ < 0.001	↓ 0.001
Bold type indicates statistical significance ($p < 0.05$); ↓ indicates decreased % drainage compared with control; ↑ indicates increased % drainage compared with control; first term in treatment type column indicates control for comparison			

Table 4.6 Pairwise comparison of the effect of bacterial treatment type on % macropore drainage of Labfield soil for cycles A and B

% macropore drainage			
		cycle A	cycle B
pairwise treatment types	dH ₂ O vs. SM	0.178	↓ 0.028
	SM vs. mutants	↓ < 0.038	<i>see below</i>
	SM vs. <i>ViscA</i>	↓ 0.019	0.804
	SM vs. WS	↓ 0.037	0.836
	SM vs. WS-4	↓ < 0.001	0.970
	WS vs. WS-4	↓ 0.001	0.844
	SM vs. WS-5	↓ < 0.001	↓ 0.023

Bold type indicates statistical significance ($p < 0.05$); ↓ indicates decreased % drainage compared with control; ↑ indicates increased % drainage compared with control; first term in treatment type column indicates control for comparison

Table 4.7 Pairwise comparison of the effect of bacterial treatment type on % mesopore drainage of Labfield soil for cycles A and B

% mesopore drainage			
		cycle A	cycle B
pairwise treatment types	dH ₂ O vs. SM	0.208	↑ 0.019
	SM vs. mutants	<i>see below</i>	<i>see below</i>
	SM vs. <i>ViscA</i>	↓ < 0.001	↓ 0.024
	SM vs. WS	0.354	↓ 0.035
	SM vs. WS-4	0.371	0.216
	WS vs. WS-4	0.804	0.162
	SM vs. WS-5	↓ < 0.001	↓ 0.016

Bold type indicates statistical significance ($p < 0.05$); ↓ indicates decreased % drainage compared with control; ↑ indicates increased % drainage compared with control; first term in treatment type column indicates control for comparison

Taking the percentage drainage in its entirety, the observed impact of the treatment of soil with the wild-type SM bacteria compared with that of untreated soil was none. However, by looking at the percentage drainage at

the difference pore scales in cycle B, it was observed that SM decreased the drainage capacity of the soil at macropore level, but increased the drainage capacity at mesopore level. These two opposite impacts on the whole soil core have served to cancel the observed response, misleadingly appearing as no impact overall. In cycle A no impact was observed in percentage drainage overall, nor at macro- or mesopore scale.

Interestingly, all mutant strains effected a reduction in drainage capacity to differing extents at macropore, or mesopore, or both and overall, compared with the SM control soil.

4.3.1.5 Summary of the observed impact of bacteria on water retention curves

The analysis of experimental soil microcosms under different bacterial treatments by water retention curves has shown that overall in the first wet/dry cycle (cycle A) the addition of wild-type bacteria to sterile soil has no impact on GWC, absolute or percentage drainage measured, with the exception of macropore GWC which only showed a marginal increase in GWC ($p = 0.047$), where if $p = 0.05$, the observed response would have been declared not significant.

Repeating the wet/dry cycle (cycle B) resulted in observed impact of addition of wild-type bacteria to sterile soil by way of an increase in GWC at macropore and mesopore scale and similarly increased drainage at the mesopore scale. At the macropore scale in cycle B the release of water from

the bacteria soil system was reduced compared with the bacteria-free dH₂O control soil system.

A greater impact of bacteria on soil water retention curves is observed when looking at a comparison of systems containing the different bacterial treatment regimens. The overriding observation is that where the production of an expressed component is disturbed, for the most part the GWC of that soil system is reduced and the release of the water from that soil system is reduced.

4.3.2 Sorptivity

4.3.2.1 Introduction

The oven-dried cores from the water retention experiment were wetted using a mini-infiltration setup. The increasing weight of the cores due to water ingress was deduced from the loss of water from the reservoir on an automated high precision balance over a period of 2.5 min (steady-state flow). Sorptivity was calculated by the weight loss from the reservoir as a function of time and reported as rate of infiltration of water into the soil via the 1.35 mm sponge-filled tip ($\text{mm s}^{-1/2}$). No statistical interactions between cycle, sterilisation and treatment type were observed. Therefore mean sorptivity of the soil cores under different bacterial legacies is presented in its entirety in Figure 4.10 below and pairwise comparisons of the treatment types are presented in Table 4.8.

4.3.2.2 Investigation of the impact of bacteria on sorptivity

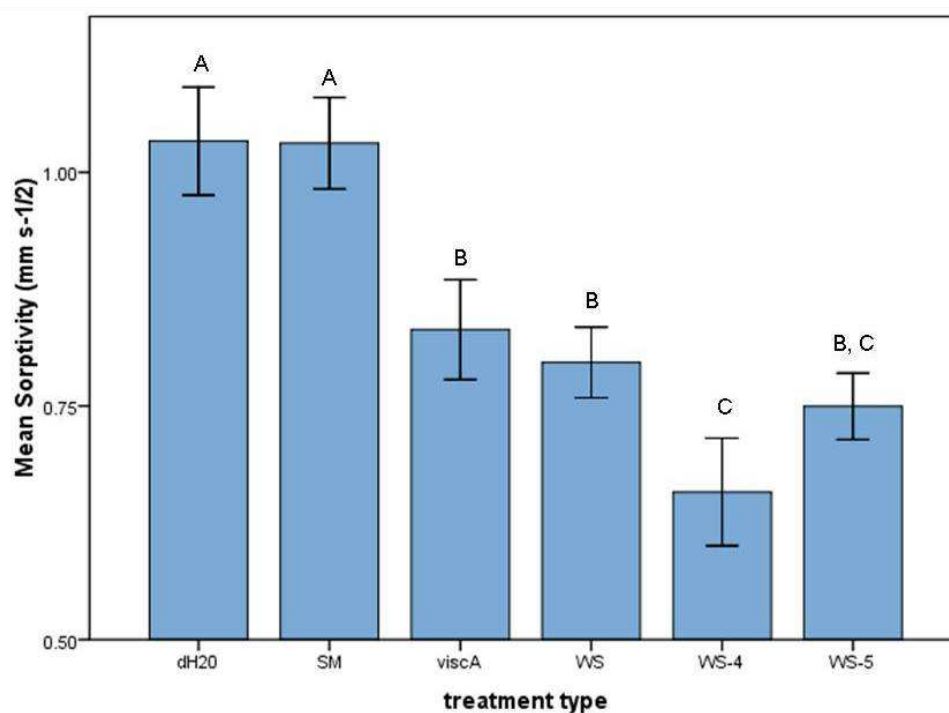


Figure 4.10 Sorptivity of sandy loam soil with different bacterial legacies. Mean sorptivity is shown for each experimental core under different bacterial treatments. Statistical differences between measured sorptivities are indicated by the different letters ($p < 0.05$). Error bars were calculated as the standard error of the means of each treatment type ($n = 10$).

Table 4.8 Pairwise comparison of the effect of bacterial treatment type on sorptivity of Labfield soil

		sorptivity
pairwise treatment types	dH ₂ O vs. SM	0.976
	SM vs. mutants	↓ < 0.009
	SM vs. <i>ViscA</i>	↓ 0.008
	SM vs. WS	↓ < 0.001
	SM vs. WS-4	↓ < 0.001
	WS vs. WS-4	↓ 0.036
	SM vs. WS-5	↓ < 0.001

Bold type indicates statistical significance ($p < 0.05$); ↓ indicates decreased sorptivity compared with control; ↑ indicates increased sorptivity compared with control; first term in treatment type column indicates control for comparison

Treatment of soil with the wild-type SM strain demonstrated no impact on the sorptivity of the soil when compared with that of the bacteria-free dH₂O control soil. Whereas the mutant strain treatments all decelerated the infiltration of water into the soil compared with the sorptivity observed for the SM control soil, with the most effective being the WS-4-legacy.

4.3.2.3 Summary of observed impact of bacteria on sorptivity

The analysis of experimental soil microcosms by sorptivity has shown that when complete bacteria are added to sterile soil there is no impact on the sorptivity of the soil system; but that when the production of bacterial exopolymers is disturbed an overall reduction in sorptivity is observed compared with the complete-bacteria experimental soil system.

4.4 Summary of studies on the effects of bacteria on soil hydrodynamics

Sandy loam soil was sieved to 2 mm aggregates, sterilised and repacked into identical cores in order to produce uniformly structured environments for the testing of the impact of bacterial legacy on the hydrodynamics of soil. In sample replicates (10 each), the cores were inoculated and incubated for 2 weeks then sterilised again to kill the bacteria and halt bacterial action of the applied treatment types on the soil. Thus any effect observed is attributable to the bacterial activity on the soil during the incubation period, or the bacterial legacy during the course of the WD cycles. Bacterial legacy consists of (i) exudate compounds produced by the bacteria and released

into the immediate environment, (ii) cell debris released when bacteria die, and (iii) the footprint left behind when a bacterium attaches to and detaches from a surface.

The bacteria-free dH₂O control system was distilled water treatment under the same conditions as the bacterial soil treatments. The bacterial strains used were chosen based on availability of strains that were genetically modified to heighten or suppress the expression of a key component of interest in hydrodynamic and structural impact on soil i.e. surfactant, cellulose and lipopolysaccharide. Table 4.9 reiterates the names used in this study for each of the strains, and their key legacy property of interest.

Table 4.9 Legacy property of interest for each bacterial strain used in this study. All bacteria are strains of *Pseudomonas fluorescens* SBW25, with SM being the wildtype control capable of producing all properties listed depending on growth conditions. Each of the other strains are isogenic mutants of the SM strain. Detailed genotypic information is presented in Table 3.1

Strain reference name	Key legacy property
SM	complete bacterium
<i>ViscA</i>	surfactant deficient
WS	cellulose-overexpressing
WS-4	cellulose-deficient
WS-5	lipopolysaccharide (LPS) deficient

Figure 4.11 schematically details the possible states of the key components of the *Pseudomonas fluorescens* SBW25 bacteria at different stages of the experimental process.

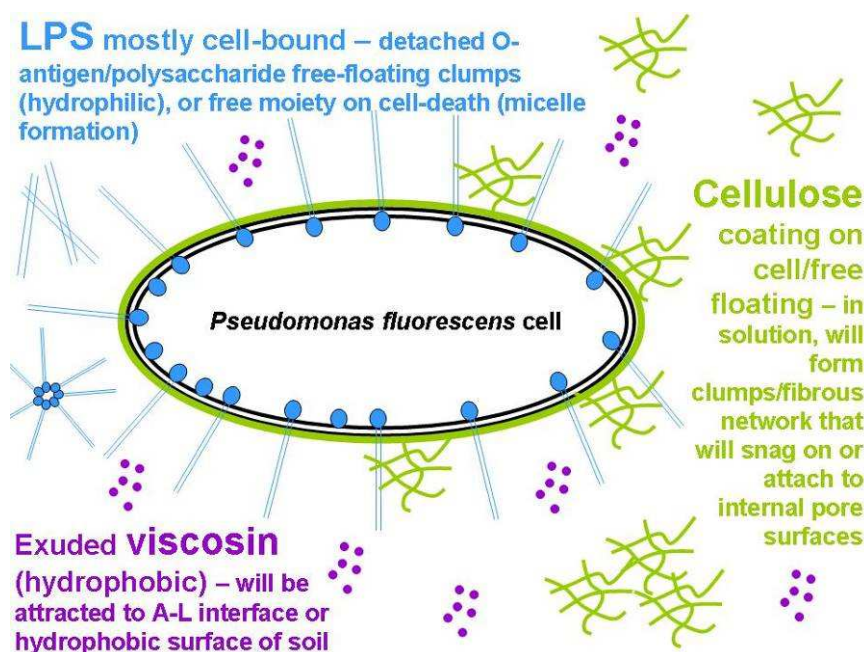


Figure 4.11 Schematic illustration of the key bacterial components under investigation. LPS (lipopolysaccharide) is composed of hydrophilic polysaccharide tail and hydrophobic lipo-head unit making the compound amphiphilic overall; cellulose is amphiphilic with both polar and non-polar side chains; and viscosin comprises a cyclic peptide head unit with a non-polar fatty acid tail resulting in an overall hydrophobic compound. Moieties are not scaled.

Following sterilisation, the cores were subjected to 2 wet/dry cycles (A and B), where the cores were saturated, drained steadily to equilibrium at incremental matric heads (i.e. suction pressure values), then dried overnight at 40°C to obtain dry soil weight for subsequent calculations (cycle A); and the whole cycle repeated (cycle B).

Table 4.10 summarises the key stages in the experimental setup as well as the water status of the cores and the assumed bacterial and bacterial legacy states at each point. Table 4.11 presents an overview of the changes in hydrodynamic response observed during this study.

Stage	water state of core	assumed bacterial/legacy state
s	t u p	
inoculation	saturation + 1 ml inoculum	growing, live, intact bacteria
drainage to -20 cm	~24% moisture content (MC) – aim was for 29%, post-inoculation calculation by weight showed 24% average MC was actually achieved	possible biofilms and sloughed off bacterial compounds particularly hydrophobic components present in areas of low water content (macropores); bacteria intact and growing in water-filled mesopores
incubation (2 weeks, 28°C, dark, humidified environment)	~24% MC	normal growth/death of planktonic and biofilm bacteria; compounds exuded & sloughed off; mesopores water-filled containing predominantly hydrophilic components; macropores drained containing predominantly hydrophobic components
sterilisation	autoclave (120°C, 15 psi) steam-containing cores; antibiotic – cores saturated	death of bacteria – rupturing of cell membranes by either heat/pressure, or by antibiotic disruption, release of cell membrane components & intracellular material
c	y c i e	A
saturation	all pores water-filled	hydrophobic cpds seek out hydrophobic pore surfaces or form micelles; hydrophilic cpds in solution
-10 cm MH	macropores drained; mesopores water-filled	hydrophobic cpds on macropore surfaces/seek out A-L interfaces; hydrophilic cpds in solution in mesopores, micelles in mesopores
-80 cm MH	macropores & mesopores drained	hydrophobic cpds on hydrophobic surfaces throughout pores; micelles and hydrophilic cpds clumped in small pockets of water on pore surfaces and in pore necks
oven-drying (O/N 40°C)	soil cores desiccated	desiccation of all cellular components and cpds; most likely to be some form of destruction of the physical structure of some of the cpds; cpds may form coating on pore surfaces/plugs in pore necks
c	y c i e	B
saturation	all pores water-filled	if pore necks are blocked by desiccated cpds, resaturation of cores will be reduced or slowed; rehydratable cpds will allow reswelling of the soil; non-rehydratable cpds will not allow reswelling and may create tension on the pore surface against the underlying soil aggregates resulting in change in soil pore/aggregate structure
-10 cm MH	macropores drained; mesopores water-filled	exopolymer/cell debris not rehydrated in this cycle but dislodged by saturation step may now become trapped in pore necks or deposited loose in macro- and larger pores as water drains from macropores; hydrophobic cpds on macropore surfaces/seek out A-L interfaces; hydrophilic cpds in solution in mesopores, micelles in mesopores
-80 cm MH	macropores & mesopores drained	exopolymer/cell debris not rehydrated or trapped in pore necks will be left behind in mesopores as with macropores; hydrophobic cpds on hydrophobic surfaces throughout pores; micelles and hydrophilic cpds clumped in small pockets of water on pore surfaces and in pore necks
oven-drying (O/N 40°C)	soil cores desiccated	desiccation of all cellular components and cpds; previously rehydrated cpds may now become trapped by the relocated clumps of non-hydrated cpds from the desiccation step at the end of cycle A forming larger masses within the soil pore network

Key: cpds = compounds, MH = matric head, MC = moisture content

SOIL TREATMENT-TYPE	HYDRODYNAMIC RESPONSE																
	GWC						ΔGWC (ABSOLUTE DRAINAGE)				% DRAINAGE					SORPTIVITY	
	cycle A			cycle B			cycle A		cycle B		cycle A			cycle B			
	saturation	macropore	mesopore	saturation	macropore	mesopore	Δmacropore	Δmesopore	Δmacropore	Δmesopore	total	macropore	mesopore	total	macropore		mesopore
IMPACT OF BACTERIA SM	•	↑	•	•	↑	↑	•	•	↑	↑	•	•	•	•	↑	↑	•
SURFACTANT DEFICIENT VisCA	↑	↑	↑	↑	↑	↑	↑	•	↑	↑	↑	↑	↑	↑	•	↑	↑
CELLULOSE OVEREXPRESSION WS	↑	•	•	↑	↑	•	↑	•	↑	↑	•	↑	↑	↑	•	↑	↑
CELLULOSE DEFICIENT WS-4	↑	↑	↑	↑	↑	↑	↑	•	↑	↑	↑	↑	•	•	•	•	↑
COMPARATIVE WS VS WS-4 RESPONSE	•	↑	↑	•	↑	↑	↑	↑	•	•	↑	↑	•	•	•	•	↑
LPS DEFICIENT WS-5	↑	•	↑	↑	↑	↑	↑	↑	↑	↑	↑	↑	↑	↑	↑	↑	↑

Table 4.11 Impact of bacteria on soil hydrodynamic responses. SM response is compared with that of bacteria-free dH₂O control response. For the response of mutant bacteria treatments compared against SM control response, except where stated. • indicates no effect observed; ↓ indicates reduced response observed; ↑ indicates heightened response observed by the removal of one of the key exopolymers from the soil treatment.

For convenience, Table 4.12, summarises and describes the hydrodynamic measurements taken and subsequent calculations from those measurements.

Table 4.12 Summary and description of hydrodynamic measurements and calculations

measurement	description
GWC_{sat}	how much water was in the whole system
GWC_{mac}	how much water was left after macropores had been drained
GWC_{mes}	how much water was left after mesopores had been drained
Δ_{mac}	how much water the macropores contained
Δ_{mes}	how much water the mesopores contained
% total	what % of water in total was drained from the saturated system
% macropore	what % of water drained was from the macropores
% mesopore	what % of water drained was from the mesopores
The GWCs were measured responses; the remaining responses were calculated using Equation 3.5 to Equation 3.7 from Section 3.5.1. p68	

4.5 Chapter discussion

4.5.1 Discussion

In nature, at any given time a soil bacterium and its associated biofilm or colony, and its resultant bacterial legacy, can be in a state of “cycle A” or “cycle B”, therefore both scenarios presented become relevant in the real world of the vadose zone, representing the layer of the earth’s crust above the permanent water table. Traditionally, the perspective of soil scientists has been to ignore cycle A in a wetting/drying experiment as the hydraulic

stresses of WD cycles serve to improve tensile strength through the formation of bonds between soil particles leading to the formation of water-stable aggregates and new pores as a consequence of crack formation (Czarnes *et al.*, 2000; Horn and Baumgartl, 2002). However, the addition of living, evolving, interacting and dying microorganisms means that each cycle in terms of the organisms and their effect on the biophysics of the soil becomes relevant inasmuch as there will always be bacteria that are in a state of cycle A that have not been dried in the natural course of the soil's cycles and similarly with cycle B. Therefore, it becomes important to look at the hydrodynamic responses of the soils in the context of both cycles. In addition, whilst biopores are not of concern in this study, as the soil under investigation was sterile, sieved and repacked in cores; shrinkage cracks, and air-entrapment need to be considered in the evaluation of the results particularly following the drying process at the end of cycle A and rewetting process at the start of cycle B, and the creation of water repellent areas in the treatment process.

In order to hypothesise the effects of the bacteria on the water in the soil it is necessary to understand the chemistry of the components of interest, both of the bacteria and of the soil itself. Figure 4.12 illustrate the whole and component parts of viscosin, lipopolysaccharide (LPS) and cellulose, as well as detailing their expected behaviour in water and in pore spaces.

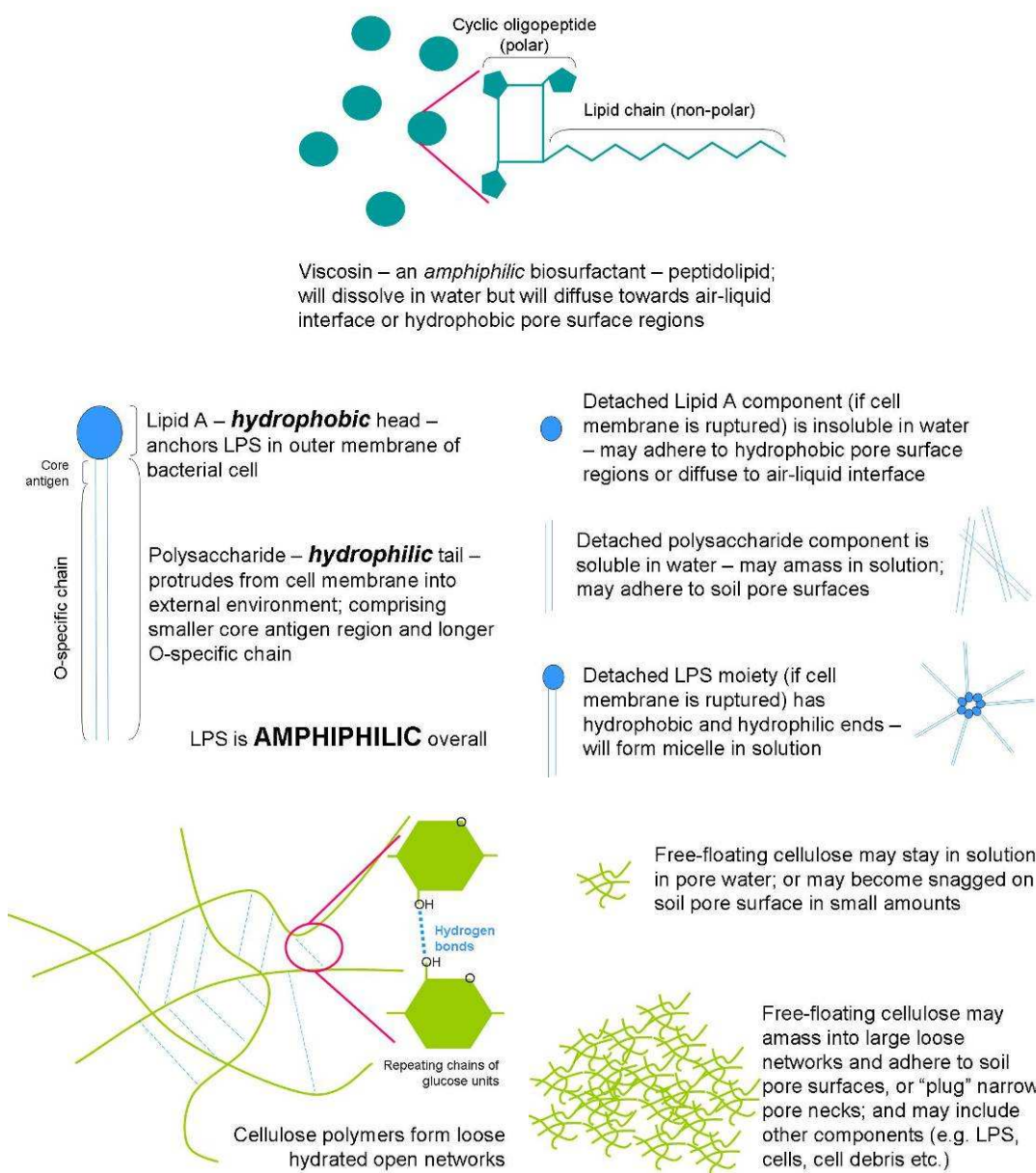


Figure 4.12 Schematic representation of the chemical and conformational structures of viscosin (top), lipopolysaccharide (middle) and cellulose (bottom). Figure drawn by PDSterpaio. Viscosin (Saini *et al.*, 2008) and LPS are amphiphilic overall due to their hydrophobic and hydrophilic component parts, and cellulose is highly insoluble and inelastic (Ross *et al.*, 1991)

A hydrophilic surface will allow water to spread over it in a continuous film, whereas a hydrophobic surface causes the water to form individual droplets.

For water to spread on a surface, the adhesive forces between the water and the surface must exceed the cohesive forces within the body of water.

Water's surface tension at 20 °C, 1 atm is $72.75 \times 10^{-3} \text{ N m}^{-1}$, and if the surface tension (surface free energy) of the solid is greater than $72.75 \times 10^{-3} \text{ N m}^{-1}$ then it will attract water and will be hydrophilic. The higher the surface tension of the surface the greater the attraction. In soil grains there are hydrophilic minerals and hydrophobic organic solids and if the minerals are coated by the organic solids the surface presented to the water is therefore hydrophobic (Doerr *et al.*, 2000).

In this study the soil used has not been stripped of all additional organic material that may have been present in the soil at the point of sampling, therefore the presence of organic compounds derived from plants or microorganisms prior to preparation of the soil cores must be acknowledged. Doerr *et al.*, (2000) categorise these compounds from water repellent soils into two groups:

- i) The aliphatic hydrocarbons (non-polar), which are almost insoluble in water.
- ii) Amphiphilic structured polar substances, which as compounds are generally water soluble. However, depending on the orientation of the polar ends on the surface they can render the surface hydrophobic. Alternatively, if the critical moisture point is reached the coating inverts due to the attractive forces of the water, rendering the surface wettable and therefore hydrophilic.

Whilst it is difficult to finally ascertain the physical associations of these compounds to the soil particles, since the natural abundance of various, potentially interactive substances complicates studies, all soil cores in this study were prepared replicates prior to treatment with the model bacteria. Therefore, any subsequent variation observed in hydrophobicity, hydrophilicity, repellency or retention of water can be attributed to the bacterial legacy in question.

4.5.2 The impact of bacteria on the hydrodynamics of cycle A

In cycle A, the bacteria and bacterial legacy would still have been in its native biochemical and biophysical state i.e. not having undergone the drying process which would have occurred at the end of the drainage cycle. Therefore bacterial effects on the water in the soil would be expected to reflect the native properties of that component. As such, the surfactant viscosin would be expected to reduce the surface tension of the water in its environment. The amphiphilic cellulose would be expected to attract or repel water depending on the orientation of its hydrophobic ribbons. Similarly amphiphilic lipopolysaccharide, while still attached to the bacteria, would be expected to attract water due to its hydrophilic O-polysaccharide chains protruding from the cell membrane. However, its lipo-heads, if released from the cell membrane through cell rupture, would add to the hydrophobicity to the inner pore environment. The permanent physical changes to the structure of the pore network in cycle A would be expected to be minimal as the bacterial compounds would only be coating the surface of the network.

Whilst the mineral grains in soil are hydrophilic, it is the hydrophobic organic matter naturally present in the interstitial matrix and coating the grain surfaces that confer water repellency and reduce the wettability of the soil (Doerr *et al.*, 2000).

In this study the bacteria-free dH₂O control soil cores provide the information about the hydrodynamic responses of the soil due to the wet/dry cycles alone. They are also the cores against which the SM control is compared so as to provide information about the changes observed in soil in the presence of the wild-type model bacteria. The SM control soil cores provide the information about the hydrodynamic responses of the soil during the wet/dry cycles in the presence of the wild-type bacteria against which the mutant strain legacies are compared. The response expected would be where the added hydrophobic compounds attach to hydrophobic surfaces of the soil within the pores and narrower pore necks connecting adjacent pores, or, where the hydrophobic compounds on the air-liquid interface of the water front could potentially block the passage of water if the neck or pore was narrower than the accumulated exopolymer mass then it would be reasonable to assume that the direction of flow would be diverted away from the blockage, most likely leaving the hydrophobic mass behind. While this may not impact directly on the specific pore that the water body is entering or draining from, unless of course it is the only directional exit or inlet for the water; it is the pores beyond this blockage that would be affected. These neighbouring pores could be large macropores or smaller mesopores.

In terms of water ingress, a reduced response would be expected in terms of total water capacity (GWC_{sat}) and sorptivity rate. However, in a

drainage experiment or situation this could result in greater retention (GWC_{mac} , GWC_{mes}) of water by a predominantly hydrophobic system as these blockages would prevent or reduce water egress from the system (ΔGWC , percentage drainage). This would be contrary to immediate perception that hydrophobic systems would repel water more quickly than hydrophilic systems.

In a predominantly hydrophilic system, where dissolved or suspended compounds in the water present a blockage in the narrowest necks of the network, water should still be able to flow between molecules of the hydrophilic components as they would not present repulsive forces to the water molecules. Water movement would be merely slower until such a point where larger compounds, such as cell debris or perhaps micelles of LPS complete the blockage entirely. This would mean that a hydrophilic system would be expected to continue drainage in a similar fashion to an untreated system, which would present no physical hindrances to water flow. As such, the expected pattern in hydrodynamic response would be that a predominantly hydrophobic system would be most resistant to water flow, followed by a hydrophilic system which would be expected to closer in response to an untreated system.

Upon addition of the wild-type bacteria (SM) possessing both hydrophilic and hydrophobic properties, with the exception of the measured macropore GWC, no effect was observed compared with the responses observed for the untreated system, neither in water ingress (GWC_{sat} and sorptivity), retention (GWC_{mes}), nor egress (ΔGWC , percentage drainage).

It could be interpreted that the wild-type SM bacteria system is so mildly hydrophilic that the hydrodynamic responses of the complete bacteria system are not sufficiently different from the untreated system to be observable in all but the macropore measurements which showed an increased GWC, as would be expected in a hydrophilic system. Equally, it could be argued that, in the presence of both hydrophobic and hydrophilic compounds the reduction in water flow response could be expected to be cumulative. However, the experimental observations would appear to point towards a null-effect, whereby the balance of water-attracting/repulsing forces of the compounds have effectively cancelled each other out resulting in no observed difference between bacteria-free dH₂O control and SM control systems. It is only when the balance of these compounds in the system was disturbed, through treatment of the soil with bacteria genetically mutated to be deficient in one of these key exopolymer or membrane-bound compounds, that the expected effects of a hydrophilic or hydrophobic system were observed. Interestingly in the WS (cellulose over-expressing) and WS-4 (cellulose deficient) systems, where it would be reasonable to expect opposite effects in hydrodynamic responses when compared against the SM control system, the observations are predominantly the same for both organisms. It is only through a further evaluation of the WS-4 system against the WS that a more detailed understanding of what is occurring can be elucidated.

The gravimetric water content (GWC) measurements represent the actual water content of the soil. In cycle A, although the initial saturation level water content was consistently less in soils treated with the mutant

bacteria than the complete bacteria systems (Table 4.11), macropores contained more water than the complete bacteria control soil when cellulose levels were changed (either increased or decreased). This increase in macropore GWC was also observed in the complete bacteria system compared with the bacteria-free dH₂O control. However, no difference in macropore GWC compared with SM control soil was observed due to change in surfactant or LPS levels.

Mesopores in the mutant bacteria systems consistently demonstrated higher GWC than the untreated and complete bacteria systems; and, as would be expected given the saturation observations, sorptivity for all of the mutant systems were reduced compared with the dH₂O and SM bacteria controls. The Δ mesopore, which measures the change in GWC attributable to the mesopores, showed no difference compared with untreated or complete bacteria systems when the cellulose levels were changed suggesting that cellulose did not affect the mesopores in the soil system. Similarly, percentage drainage from mesopores was unaffected in the cellulose-altered systems, and also in the LPS-altered system.

These observations support the hypothesis that blockages - both complete and partial - due to compounds in the narrowest pores and necks of the soil pore network are creating resistance to pore water flow for both ingress resulting in lower saturated water content and sorptivity rates, and also egress from the narrowest paths of the network, the mesopores.

In order to assess the individual impact each of the key exopolymers, comparison of the mutant response against the SM control system was also performed (Table 4.11). At saturation, the mutant bacteria systems

demonstrated a lower GWC than the control system which would suggest that the loss of one of exopolymers has upset the hydrophobic/hydrophilic balance exhibited by the complete bacteria system, and as such, reduced the water ingress capability of the soil. This observation was echoed in the sorptivity response, wherein a reduction in rate of water ingress was observed across all mutant systems.

Macropores demonstrated variability in their GWC depending on the exopolymer that had been removed i.e. the surfactant-deficient system demonstrated a reduced GWC, the cellulose-deficient system demonstrated an increased GWC and the LPS-deficient system demonstrated no effect on macropore GWC compared with the control system.

In a surfactant-deficient system, where surface tension of the water in the system would be expected to be higher than in a surfactant-producing system, the observed reduction in water content at macropore level could be expected as the water flow would be expected to be reduced due to the higher attractive forces of the water molecules to themselves.

In the cellulose-deficient system, the increased GWC observed at macropore level can be reasonably attributed to the fact that the amassed networks of cellulose fibres that would be expected to be most prolific at blocking small pores and necks from filling with water are not present. This however, contradicts the finding of reduced GWC at saturation, which if the absence of blocking-material explanation is to be accepted, would suggest a similar increase in GWC at saturation compared with the SM control system should be observed.

In the LPS-deficient system, the fact that there was no observed difference between the SM control and the LPS-deficient systems suggests that the effects of LPS on the hydrodynamics of the soil are limited to the mesopore level.

At mesopore level, all the mutant strains exhibited greater GWC than the SM control system. This fits with the hypothesis that by upsetting the hydrophobic/hydrophilic balance seemingly observed in the SM control system, the pore water flow has been affected by the hydrophobic and hydrophilic biocolloids (cellulose, LPS and viscosin) and their deposition on the soil grains and in the pore necks both of which are most likely to be observed in the smallest pores, the mesopores in this study (Elliott and Coleman, 1988).

Where the ingress of water (GWC_{sat} and sorptivity) was reduced in all the mutant strain systems compared with the SM bacteria system, subsequent water retention observed in macropores and mesopores was variable when looking at GWC alone. Calculation of change in water content (ΔGWC), with the exception of the cellulose-deficient system Δ_{mesopore} , indicated a reduction in the ability of the mutant soil-systems to retain water compared with the complete-bacteria system. This reduction was also observed, again with the exception of the cellulose-deficient system at mesopore level, in the egress of water from the system (percentage drainage).

If a system starts out with less water compared with the SM control system, but ends with greater water retention at the mesopore level (all mutant systems), then the observed reduction in egress would be expected;

as would the reduction in change in water content between the levels. Cellulose deficiency appears to be more significant at macropore level than at mesopore level. This conclusion is drawn from the observations that the cellulose-deficient system showed greater water content at macropore level as well as the mesopore level and that no difference in retention (Δ_{mes}) or water egress (% mesopore) was observed between the SM control system and the cellulose-deficient system at mesopore level.

4.5.3 The impact of bacteria on the hydrodynamics of cycle B

In cycle B, responses observed would be mainly due to physical changes to the soil grain/pore network structure. Structural reorganisation of soil aggregates following wet/dry cycles is well documented. The bacterial compounds present in each of the pore structures i.e. macropores, mesopores, pore necks and smaller network structures etc., will have been desiccated during the oven-drying process, which serves to represent a natural drying process that occurs during periods of no rainfall or snowmelt. This is when shrinkage of the grains will occur resulting in cracking of the aggregates and restructuring of the pore networks. The biocolloids deposited on the grain surfaces could serve as scaffolding to hold grains together, either intra- or intergranularly. The substances that would be most expected to perform this scaffolding role would be the hydrophobic compounds since these would not contain water molecules within their structure, and as such, upon removal of water from the surrounding area would start to attach to desiccated grain surfaces as contact is made. This is dependent on the polarity of the grain surface as well. If the grain surface is

non-polar then hydrophobic compounds are not going to attach and will most likely rest, unattached against the surface until porewater flow is reinstated at which point these compounds will re-enter suspension in the water until they encounter a suitable hydrophobic grain surface onto which they can attach or move to the air-liquid interface until they are physically blocked from progressing through the pore network by narrowing of the conduits or the arrival at an air-bubble which prevents further transport.

Another possibility is that rehydratable compounds, the hydrophilic and hygroscopic compounds, will rehydrate (and swell) more quickly than the aggregates, and, if not attached to a grain surface, will mobilise with pore water flow and upon encountering narrow conduits in the pore network will block the subsequent rehydration of these passageways in the system.

Taking all the factors into account, it is expected that the dried systems, in the presence of these biocolloids would resist rehydration either through polar “gluing” of aggregates or hydrophilic blocking of network conduits. As such, level of soil core saturation would be expected to be reduced, as would sorptivity (both measures of water ingress); retention observations (GWC_{mac} , GWC_{mes} , and ΔGWC) would vary depending on the balance of the hydrophobic/hydrophilic interactions of the biocolloids and the grain surfaces, as well as the pore sizes being observed and water egress would be expected to be reduced (percentage drainage) as a result of cumulative deposition of suspended hydrophobic and precipitated hydrophilic biocolloids in the narrow conduits as the porewater levels decrease.

Overall the observed effect of the presence of bacteria, versus the bacteria-free dH_2O control soil system, was that the mutant bacteria

demonstrated reduced responses across the board. However, unlike in cycle A where the complete bacteria largely showed no significant difference from the untreated system, in cycle B, there was greater variability in the responses.

Whilst saturation and sorptivity, water ingress, were unaffected by the presence of the complete bacteria, GWC_{mac} and GWC_{mes} were elevated, suggesting a better retention of the (reduced-overall) quantity of water taken in by the complete bacteria system. Upon closer inspection of the retention data, by looking at the change in water content attributable to macropores and mesopores individually ($\Delta_{macropore}$, $\Delta_{mesopore}$ respectively), the evidence suggests that less water is lost from the macropores ($\Delta_{macropore}$ is reduced) and that the majority of water drainage occurs from the mesopores ($\Delta_{mesopore}$ is elevated compared with the untreated system). These findings are further supported upon consideration of the egress calculations (percentage drainage). These findings would suggest that the presence of biocolloids in the bacterial system promotes water retention in the soil.

The mutant bacterial systems demonstrated that upsetting the balance of any of the key exopolymers under investigation in this study (cellulose, LPS or surfactant) results in reduction of level of saturation compared with the untreated system. Given that the exopolymers present varying levels of both hydrophilic and hydrophobic properties, it would seem that the physical effect of these polymers on the soil grains is again more important at mesopore level, as was observed with cycle A. This theory is

further supported by examining the responses at the mesopore level, GWC_{mes} and percentage drainage of the cellulose-deficient, LPS-deficient and cellulose overexpressing systems, and $\Delta_{mesopore}$ of both cellulose-altered systems.

Looking more closely at the specific response of mutant bacterial systems versus the complete bacteria system provides more insight into the particular effect of each exopolymer in question. Most interesting, in contrast with the cycle A finding, the cellulose deficient system showed no significant difference in percentage drainage compared with the SM control suggesting that lack of cellulose, after desiccation, has no bearing on water egress in bacterial systems.

Cellulose is hygroscopic, and has been shown to be a key component of biofilms (Ross *et al.*, 1991), specifically having a role in resisting desiccation by creating a gel-like mesh within which the bacteria can survive periods of drought. In a soil system, cellulose would be expected to carry out a similar role. Therefore the observation that following desiccation, lack of cellulose in a bacterial soil system has no bearing on the egress of water from that system is contradictory to the expected response. A system containing cellulose would be expected to resist water egress in a bid to maintain water levels in a bacterial environment and a system lacking cellulose would be expected to have no effect on water egress. This conflicting observation suggests that following desiccation, the chemical and physical properties of cellulose have been changed so as to not behave in the manner expected.

Removal of surfactant from the bacterial soil system reduced water ingress (GWC_{sat} and sorptivity), and also retention and egress of water at mesopore level, but not at macropore level when calculated as $\Delta_{macropore}$ and percentage drainage respectively. The GWC_{mac} was reduced compared with that of the complete bacterial system.

In the complete bacterial system, the production of surfactant would be expected to reduce the surface tension of water if still in its native surfactant chemical state. However, in cycle B any surfactant produced in cycle A has undergone drying. If the water-tension reducing surfactant properties had been nullified by the drying process then the expected observation would be that the complete bacteria system would not possess the ability to reduce the surface tension of the water and as such behave more like the surfactant-deficient bacterial system, this was not observed. Removal of surfactant from the bacterial soil system demonstrated a reduced capacity for water ingress, reduced capacity for water retention based on GWC measurement alone, but the calculated change in water retention at macropore level ($\Delta_{macropore}$) reflected no difference compared with the complete bacteria system, leaving the reduction in change in water retention to be observed only in the $\Delta_{mesopore}$ calculation. This observation was echoed in the percentage drainage calculation, wherein, total percentage drainage was reduced and seemingly is only attributable to reduced mesopore drainage.

The LPS-deficient soil system in cycle B showed a complete reduction in all hydrodynamic responses compared with the complete bacteria soil

system. Following the sterilisation of the systems in cycle A, the components of LPS may have been released into the internal pore network (as observed in medical LPS-release studies into septic shock (Eng *et al.*, 1993; Horii *et al.*, 1998; Horii *et al.*, 2000; Tsumura *et al.*, 2003). The individual hydrophobic lipid A heads would have sought out air-liquid interfaces and hydrophobic grain surfaces. Hydrophobic heads still attached to the polysaccharide tails would have formed micelles and been suspended in pore water, and the detached polysaccharide tails would have dissolved in the pore water. Upon draining, the hydrophobic moieties would have been attracted to air-liquid interfaces and hydrophobic grain surfaces initially of macropores and then of the mesopores upon drying. Whereas the hydrophilic moieties would have remained dissolved and moved through the pore network with the water until the conduits became too narrow, blocked by deposited biocolloids or air-bubbles, or until the concentration of water became so low that precipitation occurred. As such, the hydrophobic effects of LPS would be expected to be more pronounced in macropores, and its hydrophilic effects more pronounced in mesopores. Removal of LPS from the soil system would be expected to return a balanced overall effect to the pore levels dependent solely on the other biocolloid effects of the bacteria.

The observation that removal of LPS from the bacterial soil system reduced all responses compared with those of the complete bacterial system, would support the theory that the hydrophobic-macropore/hydrophilic mesopore imbalance has been nullified, and that the overall effect of the remaining biocolloids in the LPS-deficient bacteria soil

system is that of, most likely, blocking the flow of water in and out of the soil following a drying cycle.

4.5.4 This research in context

Peng *et al.*, (2011) carried out extensive physical testing of rigid and non-rigid soil in response to amendment with analogues of biological exudates. Using dextran and xanthan as analogues for bacterial exopolysaccharides and lecithin as an analogue for phospholipid surfactants, they measured water sorptivity, water content (at saturation) and porosity, as well as water repellency, tensile strength and aggregate stability. The Gleysol, a non-rigid soil, in their study is comparable to the non-rigid Cambisol used in this research and their WD cycles 0 and 1, are comparable with cycle A and cycle B in this research. Like the findings in this study, effects were noticed in the measurements of saturated water content and water sorptivity between treatments. Lecithin, (surfactant-analogue) was shown to reduce the saturated water content of the Gleysol; and demonstrated the greatest reduction in water sorptivity (S_w). It was noted that with increasing WD cycles S_w gradually rose. Xanthan- and dextran-amended soils demonstrated a slight increase in the early WD cycles, followed by a decrease; Xanthan, like lecithin, decreased S_w , whereas dextran increased S_w . Making a direct comparison between this study and that of Peng *et al.* (2011), the ability of the SM bacteria to produce viscosin would be expected to reproduce the findings of the lecithin-amended soil. However, the SM soil showed no difference to the dH₂O soil in terms of saturated water content or

sorptivity. This could be attributed to the growth conditions not being conducive to viscosin production by the SM bacteria; or that the combination of other biological exudates masked this expected behaviour.

Peng *et al.* (2011) used the physical properties of the biological exudates to formulate links between the behaviour of the exudates in soil and their effects. One of the physical measurements taken was the surface tension of the exudates, which was also measured as part of the bacterial characterisation experimentation in this study (summary data in Section 8). For their study, Peng *et al.*, used solutions of the chemicals in water, whereas in this study the exudate properties were measured on cell-free extract which was in KB growth media. The KB control was shown to have a surface tension of 51.44 nM m^{-1} (water control 72.52 nM m^{-1}), while the bacterial exudate solutions were shown to *increase* the surface tension of the KB media. This observation would appear to support the hypothesis that whilst individual effects of the bacterial legacy components may be expected to cause a certain response, the interaction of these components with each other and with their environment may indeed cause an opposite or no effect.

4.5.5 Summary statement

The impact of the SM control on hydrodynamic response of soil compared with the bacteria-free dH₂O control has been observed to be predominantly a nil response in the first WD cycle (cycle A) but following a drying and rewetting episode, an increased water content is observed at macro- and mesopore levels (cycle B), indicating that the presence of bacteria in the soil

system causes an increase in the ability of that soil to retain water. Furthermore, investigations of the drainage points of the soil indicate that the bacteria cause reduction in the drainage capability of the macropores but increase the drainage from the mesopores. The SM control strain did not have any impact on the sorptivity of the soil system. The mutant strains were observed to have an overall reductive effect on the hydrodynamic responses measured in this part of the study. Most notably the sorptivity of the soil systems was decreased irrespective of the altered bacterial legacy component; whilst this is counterintuitive to the known chemistry of the compounds, it is aligned with the measured surface tensions of the cell-free extracts from the bacterial growth systems which all indicated an increased surface tension (data not shown) thereby indicating an expected reduction in the wettability of the soil.

Bacteria have been shown to impact the hydrodynamics of soil, however in order to ascertain more definitive answers to the specifics of what bacterial component alters what aspect of the hydrodynamics, and in what way, a greater understanding of the interactions of the bacterial legacy within itself and with the soil is required.

4.6 Future work

Doerr *et al.*, (2000) make the point that there is great difficulty in ascertaining the physical association of hydrophobic compounds to the soil particles since the natural abundance of various hydrophobic substances complicates studies.

The interpretation of the observations in this study is focussed on whether or not the system is predominantly hydrophobic or hydrophilic, and many other contributing factors ought to be taken into account, such as ionic strength of the water in the system, the presence of air-liquid interfaces, air entrapment; surface water-film strength, mineral biocolloids that naturally occur as an unsaturated porous medium becomes water-filled and then drains again, and so on. Ideally each of these many additional properties should be fixed, in turn, in a known experimental environment, allowing for the individual effects to be elucidated, such as was carried out in this study for the key components of the bacteria. Then the biological, chemical and physical interactions of each additional property determined in a logical stepwise fashion.

The bacteria themselves do not behave in a known manner in soil. The growth conditions of bacteria *in vitro* can alter the exudate production levels, viscosin only being produced in late log phase of *Pseudomonas fluorescens* SBW25 grown on solid media being a prime example (Spiers *et al.*, 2002; Koza *et al.*, 2009). Control of all these conditions is not likely to ever be achievable in an experimentally designed unsaturated, porous medium such as that found in the vadose zone of soil; and as such true understanding of the exact nature of the biophysical interactions at this level is similarly unlikely. However, the results presented above serve as a solid, starting point for further investigation into the effect of bacteria on the hydrodynamics of soil in an unsaturated environment.

The data in this part of the study has, for the most part, only been presented and interpreted in this thesis using comparisons of the bacteria-

free dH₂O treated and wild-type SM treated soil systems, and of the wild-type treated and mutant treated soil systems. However, the statistical analyses were designed so that pairwise comparisons were made between every permutation of the experimental design and whilst outwith the scope of this thesis, the data is available for future interpretation looking at the level of response of each of the bacterial strains against the bacteria-free dH₂O control soil and also against each other. A question that would be worth asking would be: Does the removal of any of the key legacy compounds negate the presence of the bacteria in terms of their effect on the hydrodynamics of the soil? This could serve to inform field scale studies of bioaugmentation or bioremediation.

The observations in this Chapter have looked at the impact of bacteria on the hydrodynamic responses of the soil from the perspective of the bacterial legacy on the soil after live bacterial action had been halted by the sterilisation process. In other words, the effect of the exudate compounds on the surfaces of the soil grains and in the pore networks. However, the effects on the soil also include those elicited on the physical structure of the aggregates and the interaggregate spaces during the incubation period need to be considered in terms of formation of different bonding strengths mediated by the presence or absence of exudate compounds leading to different porosities, heterogeneity of pore distribution, and connectivity of the pore spaces in the soil systems. As such, these structural properties need to be measured and considered in building a picture of the impact of bacteria on the biophysics of the soil. Chapter 5 investigates the structural properties

of the soil systems using μ XCT scanning and 3D image analysis of both core scale and aggregate scale soil in this study.

CHAPTER 5

5 The use of microtomography in the investigation of the effects of *Pseudomonas fluorescens* SBW25 and key mutants on Labfield soil**5.1 Introduction**

Soil structure controls and modulates water flow, which in turn governs the movement of solutes, nutrients, microbes and gases through the soil profile (Young *et al.*, 2001). In order to consider how bacteria can influence the soil structure it is necessary to determine the differences between treated soils in terms of their porosity, the heterogeneity of this porosity, pore-size distribution and pore connectivity. The porosity of soil is defined as the *“volume of pores in a soil sample (nonsolid volume) divided by the bulk volume of the sample”* (SSSA, 2012). Pores can be either air or water filled in the unsaturated zone. Depending on the type of soil in question, the grain size (silt, clay, sand) and the physical arrangement of the soil grains in that soil, porosity can vary greatly between samples. In this study, the Labfield soil grains were sieved to uniform 2 mm aggregates. Therefore, the physical arrangement of the soil aggregates will be impacted on by the presence of bacteria and will highlight differences in soil structure as a result of the presence of these bacteria. The heterogeneity and complexity of the distribution patterns of the pores in the soil is reported in this study as a fractal dimension (FD) value. Fractal dimension is defined as *“a measure of the dimensionality of a fractal object or function. Its value is generally a fractional number that is either less to or greater than the Euclidian dimension of the space in which the fractal is embedded”* (SSSA, 2012). A

lower FD value is characteristic of uniform distribution pattern ($FD = 2$) and a higher value is characteristic of clumped distribution pattern ($FD = 3$). The heterogeneity of the distribution of the pore volume has been shown to impact on the hydraulic conductivity of soil (Young and Crawford, 1991; Young *et al.*, 2001; Dathe and Thullner, 2005). Another measurement of interest in understanding the structure of soil is the pore-size distribution described by Nimmo (2004) as “*the relative abundance of each pore size in a representative volume of soil*” which as such, adds architectural information to the porosity value and clustering distribution elucidated by the fractal dimension measurement. Each of these three measurements when taken from images of the soil volume will report the totality of the void spaces present in the soil, observed above the imaging resolution. These measurements do not take into account the existence of vesicles in the soil which are non-connected void spaces often created by wetting fronts and soil particle movement entrapping air and or water. In order to differentiate between total porosity-based measurements and effective porosity in which water, solute and biomass movements can occur, pore connectivity measurements provide information about the accessible pore spaces with continuity to the boundaries of the medium.

Whilst valuable information about pore space geometry can be provided by 2D image analysis of thin soil sections (Czarnes *et al.*, 2000; Nunan *et al.*, 2001; Nunan *et al.*, 2002; Harris *et al.*, 2003; Nunan *et al.*, 2003) recent advances in visualisation techniques such as XCT has enabled true 3D structural information to be obtained (Anderson *et al.*, 1990; Pierret *et al.*, 2002; De Gryze *et al.*, 2006; Sleutel *et al.*, 2008; San José Martínez *et*

al., 2010). In this study, micro-X-ray computer tomography (μ XCT) has been used to visualise the inner space of the soil cores and aggregates and, thanks to the non-destructive nature of μ XCT on the original sample cores, it is possible to repeatedly record and, using sophisticated image analysis software, analyse the structure of soil before, during and after experimental treatments on the same sample. This approach allows for actual measurements to be made and accurately visualised as the soil changes. This part of the study looks at the microscale effects of microbes and specifically their bacterial legacy, on the 3D physical structure of sandy loam soil at the core and aggregate scale.

5.2 Chapter aims and research objectives

The aim of this research chapter is to ascertain the impact of bacteria and bacterial activity on the pore structure and related phenomena of soil. In this work, the term bacterial legacy is used to refer to all aspects of bacterial activity. Bacterial legacy consists of (i) exudate compounds produced by the bacteria and released into the immediate environment, (ii) cell debris released when bacteria die, and (iii) the footprint left behind when a bacterium attaches to and detaches from a surface.

In order to determine if differences in the structural properties of the soil can be attributed to bacterial activity, prepacked sandy loam soil cores were treated with different strains of *Pseudomonas fluorescens* SBW25 and subjected to two wet / dry cycles and at the end of each cycle μ XCT

scanning was carried out to obtain 3D volumetric datasets from which physical measurements were taken.

Research objectives:

1. Characterisation of the impact of the different bacterial legacies on the porosity of the soil at core and aggregate scale.
2. Characterisation of the impact of the different bacterial legacies on the fractal dimension of the soil at core and aggregate scale.
3. Characterisation of the impact of the different bacterial legacies on the pore-size distribution of the soil at core and aggregate scale.
4. Characterisation of the impact of the different bacterial legacies on the pore connectivity of the soil at core and aggregate scale.

5.3 Results

The structural properties of experimental cores under different bacterial treatments were investigated using μ XCT. The cores were subjected to two wet / dry cycles, cycle A and cycle B. Each cycle also included analysis by WRC and a sorptivity assay (Results reported in Chapter 4) as illustrated again for reference in Figure 5.1.

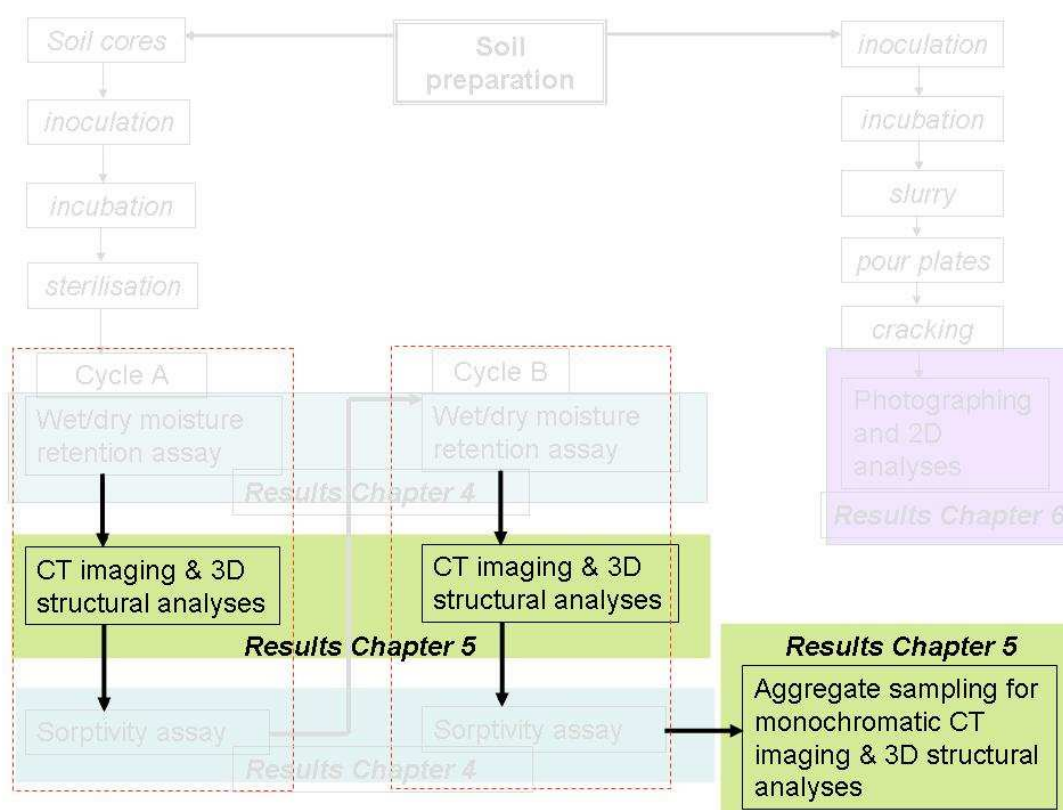


Figure 5.1 Schematic of experimental design highlighting CT imaging and 3D structural analyses

5.3.1 Resolution variability in acquired data

At the time when these samples were being scanned and analysed, it was thought that the differences in scanner resolution as a result of scanner functionality would be able to be accounted for in the post-analyses calculations. Subsequently this was found not be the case. Assumptions were made based on the automatically generated outputs of the software by the algorithms in the image manipulation and physical analysis software. In hindsight, and with recent developments in the field, it has been possible to identify the need for samples to be, if not scanned at all the same resolution, at the very least to be reconstructed at the same resolution so as to negate misinterpretation of results output by the software.

The reason for using the different scanners was due to functional availability at the time of the experimental phase of this study and there is an obvious discrepancy in the effect of the higher resolution HMX scanner (Nikon Metrology, Tring, UK) versus lower resolution Benchtop scanner (Nikon Metrology, Tring, UK) on the output. The Benchtop was used to scan the first 30 samples (dH₂O, SM and WS in Cycle A) at 15.3 μm and the last 30 samples (*ViscA*, WS-4 & WS-5 in Cycle B) at 24.8 μm resolution. Therefore any pores smaller than 15.3 μm and 24.8 μm respectively would not be observed. Whereas the HMX would have detected pore space down to 13.2 μm (used to scan the *ViscA*, WS-4 and WS-5 cores in cycle A; and the dH₂O, SM and WS cores in cycle B).

5.3.1.1 The expected effect of different resolutions on porosity measurements

The samples scanned at higher resolution would be expected to report higher porosity. We know that smaller pores exist in the soil and we are only limited to their discovery by the resolution of the scan. ImageJ (Rasband, W.S., ImageJ, U. S. National Institutes of Health, Bethesda, Maryland, USA, <http://rsb.info.nih.gov/ij/>, 1997-2007; version 1.39q) and subsequently SCAMP v1.1 (SIMBIOS CT image Analysis and Manipulation Plug-in), will only differentiate black and white in a thresholded image. When an image is thresholded (binarised) pore colour is set to black and soil colour is set to white. If the scan resolution means that more black pixels are distinguishable then porosity could be expected to be higher. The question, at this point, is

how much higher would the reported porosity be, considering that the 'missed' pores are the smallest? Therefore, how much would their discovery add to the overall porosity of the soil sample? Additionally, would the observed difference have a significant impact on the comparison of the different soil-system treatments?

In the context of this study, a voxel of sample of soil scanned at 28.4 μm could be reported as 100% black (pore) or 100% white (solid). However, the heterogeneous nature of the sample and partial volume effects, could mean that the voxel is 52% black and being reported as being 100% black or only 48% black and being reported as being 100% white. In the same 28.4 μm voxel sample, had it been scanned and reconstructed at 15.3 μm , that 28.4 μm voxel cube would be effectively quartered. In this case, the 52% black could be composed of 2 black 15.3 μm voxels and 2 white 15.3 μm voxels, which would be reported as a combined 50% black and 50% white (Figure 5.2 illustrates this schematically).

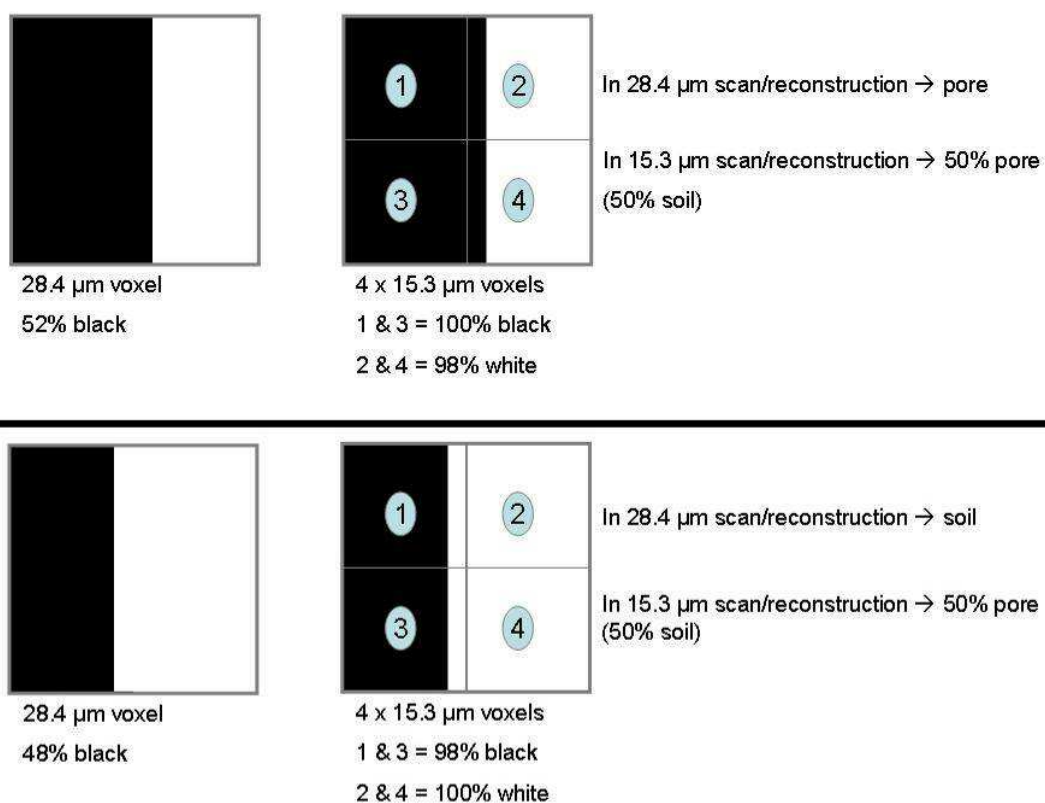


Figure 5.2 Schematic overview of resolution impact on reported porosity in thresholded images. The higher resolution of 15.3 μm gives a more accurate report of porosity than the 28.4 μm report; however, in a complete soil sample, the balance of under- and over-reporting of porosity in a 28.4 μm-scanned dataset could reasonably be accepted as true at the range of resolutions used.

As such, in a given sample, it would be reasonable to expect that where some areas of a core would be reported as pore space, equally other areas would be reported as soil in a sample scanned and reconstructed at a larger resolution. In this study, without going back and reconstructing all 120 samples at the same resolution it is not possible to make definitive quantitative statements about the physical measurements. However, given the above rationalisation of over and under-reporting of pore space versus soil-space, in the case of observed porosity above the given resolution, it is reasonable to assume that the differences reported between the soil systems studied are due to the treatment regimes rather than the resolution.

5.3.1.2 The expected effect of different resolutions on fractal dimension measurements

Fractal dimension looks at porosity at increasing box size (i.e. reported porosity in a box 1 x 1 x 1; in a box 2 x 2 x 2 etc. (power series used in this study)) then SCAMP V1.1 plots the log (box count) against the log of the box scale and the slope of the line determines the fractal dimension. This is illustrated schematically in Figure 3.15 for the box counting method and Figure 3.16 for the determination of fractal dimension.

Samples scanned at higher resolution would have different box scales (r), however, this would be consistently at all box sizes within the image and would not affect the slope of the line, and therefore the fractal dimension reported would not be affected. As such, consideration of fractal dimension in this study is feasible.

5.3.1.3 The expected effect of different resolutions on pore-size distribution measurements

As described in Section 3.8.2 Figure 3.16 this reported measurement starts at the smallest pore size visible to the scanner, i.e. its resolution, therefore this measurement is likely to be affected by the resolution of the data. Whilst disappointing, the overall aims of this study to determine the impact of bacteria on the biophysics of water flow in soil, are not affected by the omission of one set of physical measurements from the analyses at this time.

The aggregates scanned in this study using the synchrotron monochromatic advance photon source beam were all scanned and reconstructed at 5.4 μm . Therefore no consideration of the effects of variability in resolution on segmentation or physical measurements is required.

5.3.2 Core scale soil structure

5.3.2.1 Introduction

Experimental cores packed with Labfield soil were incubated with different bacterial treatments then, following sterilisation, a wet/dry cycle (Cycle A) and oven drying, were subject to μXCT scanning from which 3D volumetric datasets were obtained for the purposes of structural measurements of porosity, pore-size distribution and fractal dimension. Following a second wet/dry cycle (Cycle B) and oven drying the μXCT scanning was repeated and a second set of 3D volumetric datasets was obtained and another set of structural measurements was taken.

5.3.2.2 Investigation of the impact of bacteria on core porosity

Porosity was measured in extracted volumes (10 x 11 x 2.6 mm) from each core using SCAMP v1.1 following segmentation to differentiate solid from pore space. Statistical interactions were observed between treatment type and cycle ($p < 0.001$). Therefore data was split at the cycle level. Once split into cycle A and cycle B, sterilisation method presented no interactive

effects, therefore splitting of the datasets according to sterilisation method was not required (cycle A sterilisation $p = 0.129$ n.s.; cycle B sterilisation $p = 0.152$ n.s.). For Cycle A and Cycle B, mean porosity for each treatment type is shown in Figure 5.3 and the results of the pairwise comparison within each cycle are shown in Table 5.1.

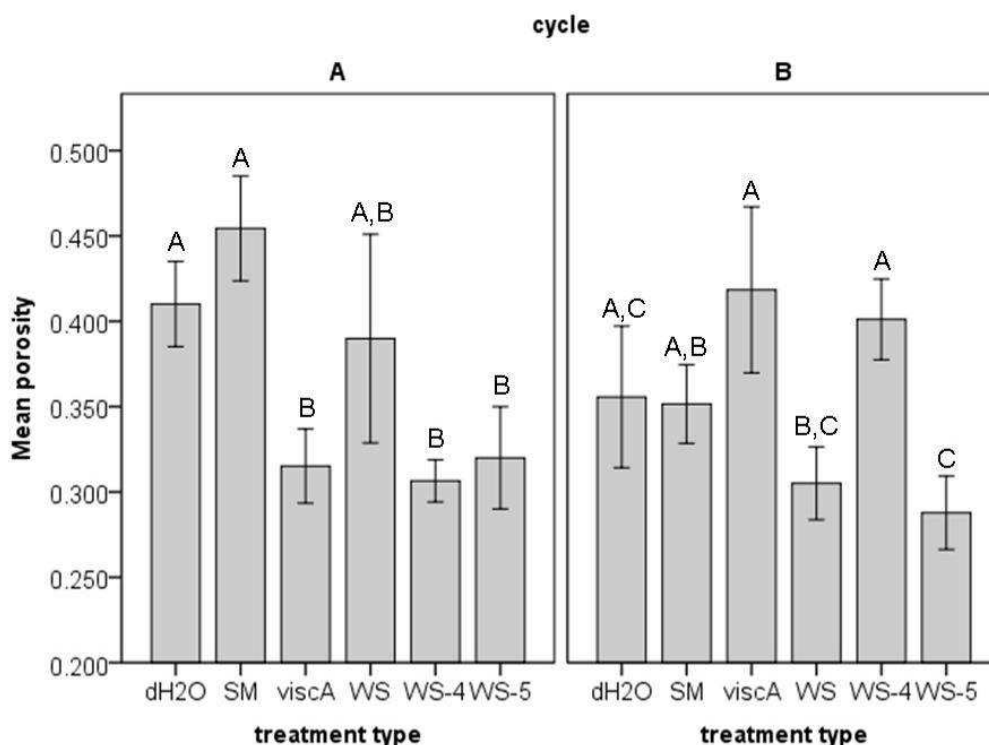


Figure 5.3 Mean porosity of cores under different treatment types. Mean porosity of Labfield soil cores under different treatment types measured using 3D volumetric data generated by μ XCT scanning is shown. Significantly different ($p < 0.05$) treatments are indicated by lettering. No comparison has been made between cycles at this stage and as such no inference is intended between Cycle A and Cycle B. Error bars were calculated as the standard error of the means of each treatment type ($n = 10$).

Table 5.1 Pairwise comparison of the effect of bacterial treatment type on core scale porosity of Labfield soil

		Porosity	
		Cycle A	Cycle B
se treat ment	dH ₂ O vs. SM	0.239	0.927
	SM vs. mutants	<i>see below</i>	<i>see below</i>

SM vs. <i>ViscA</i>	↓ < 0.001	0.184
SM vs. WS	0.319	0.100
SM vs. WS-4	↓ < 0.001	0.104
WS vs. WS-4	0.163	↑ 0.001
SM vs. WS-5	↓ 0.001	↓ 0.027

Bold type indicates statistical significance ($p < 0.05$); ↓ indicates decreased porosity compared with control; ↑ indicates increased porosity compared with control; first term in treatment type column indicates control for comparison.

The mutant strain bacteria have greater impact on the porosity of the cores in Cycle A than in Cycle B, with a decrease observed with *ViscA*, WS-4 and WS-5. Whereas, in both cycles there is no observed impact on porosity by the SM bacteria when compared with the dH₂O control.

5.3.2.3 Investigation of the impact of bacteria on core fractal dimension

Fractal dimension (FD), an indication of soil system pore heterogeneity, was measured in the same extracted volumes (10 x 11 x 2.6 mm) from each core using SCAMP v1.1 following segmentation to differentiate solid from pore space. Statistical interactions were observed between treatment type and cycle ($p < .001$) and therefore, data was split at the cycle level. Once split into cycle A and cycle B, sterilisation method presented no interactive effects in cycle A ($p = 0.145$ n.s). Therefore splitting of this dataset according to sterilisation method was not required. However, in cycle B, statistical interactions were reported between treatment type and sterilisation method ($p = 0.027$) and therefore this dataset was split according to sterilisation method for further investigation. Mean fractal dimension for each treatment

type is shown for Cycle A and in Figure 5.4 and Figure 5.5 and the results of the pairwise comparison within each cycle are shown in Table 5.2.

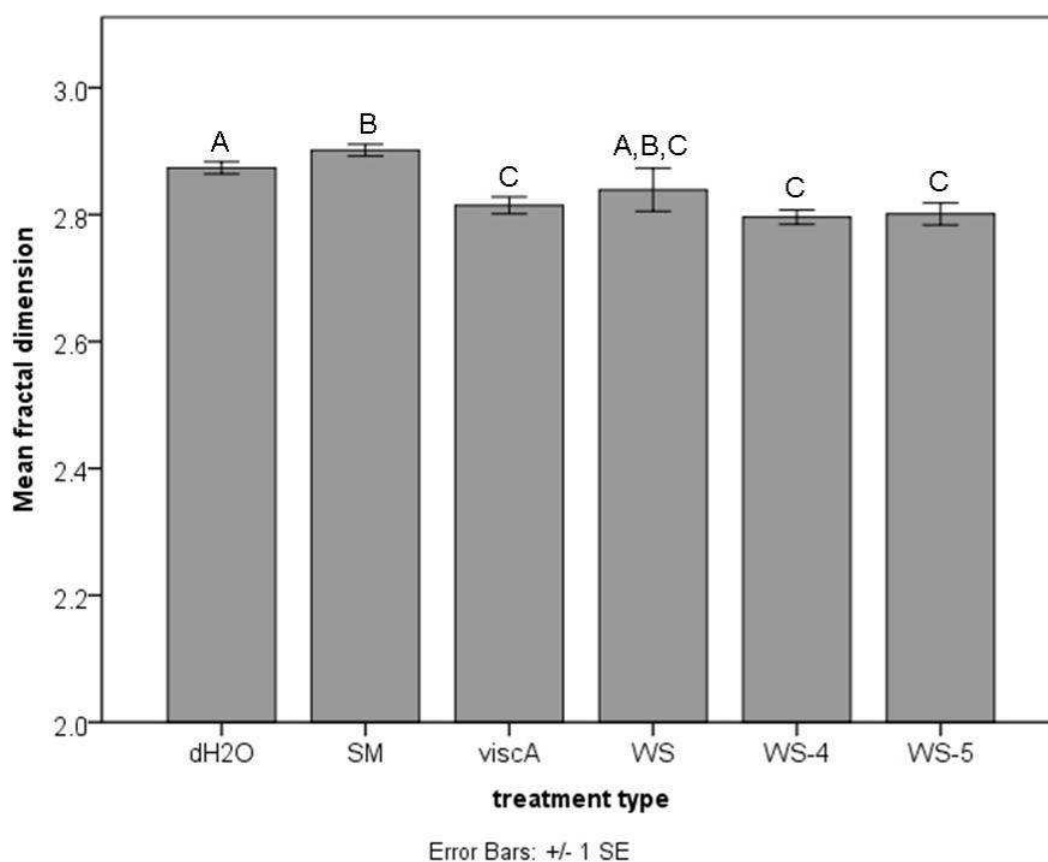


Figure 5.4 Mean fractal dimension of cores under different treatment legacies in cycle A. Mean fractal dimension of Labfield soil cores in Cycle A under different treatment types measured using 3D volumetric data generated by μ XCT scanning is shown. Significantly different ($p < 0.05$) treatments are indicated by lettering. Error bars were calculated as the standard error of the means of each treatment type ($n = 10$).

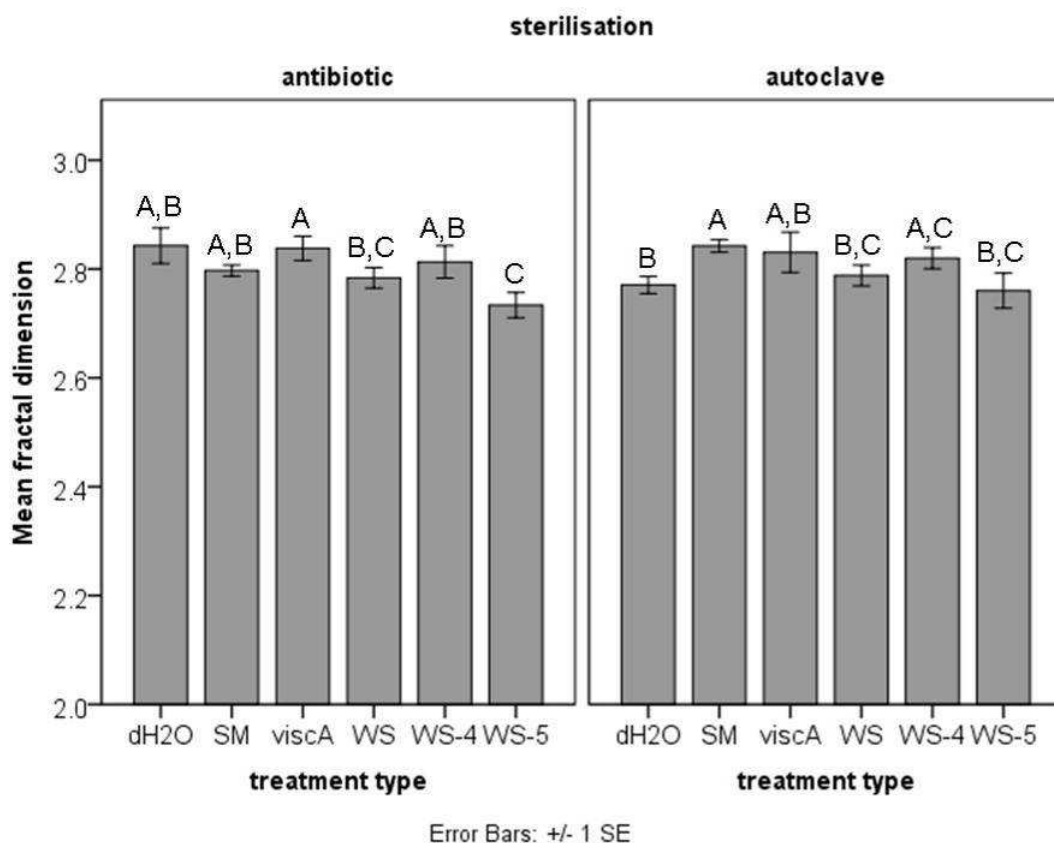


Figure 5.5 Mean fractal dimension of cores under different treatment legacies in cycle B. Mean fractal dimension of Labfield soil cores in Cycle B under different treatment types measured using 3D volumetric data generated by μ XCT scanning is shown. Significantly different ($p < 0.05$) treatments are indicated by lettering. No comparison has been made between sterilisation methods at this stage and as such no inference is intended between antibiotic and autoclave methods. Error bars were calculated as the standard error of the means of each treatment type ($n = 5$).

Table 5.2 Pairwise comparison of the effect of bacterial treatment type on core scale fractal dimension of Labfield soil

Scale fractal dimension of Eabfield soil				
Fractal Dimension				
Cycle A			Cycle B	
sterilisation				
			autoclave	antibiotic
pairwise treatment types	dH ₂ O vs. SM	↑ 0.049	↑ < 0.001	0.133
	SM vs. mutants	<i>see below</i>	<i>see below</i>	<i>see below</i>
	SM vs. <i>ViscA</i>	↓ < 0.001	0.728	0.062
	SM vs. WS	0.061	↓ 0.007	0.482
	SM vs. WS-4	↓ < 0.001	0.259	0.573
	WS vs. WS-4	0.185	0.197	0.353
	SM vs. WS-5	↓ 0.001	↓ 0.007	↓ 0.005

Bold type indicates statistical significance ($p < 0.05$); ↓ indicates decreased porosity compared with control; ↑ indicates increased porosity compared with control; first term in treatment type column indicates control for comparison.

Treatment of the soil system with SM bacteria increased fractal dimension compared with the bacteria-free dH₂O control in Cycle A, and in the autoclaved cores of Cycle B, but not in the cores sterilised by antibiotic treatment. Where a response was observed in the soil systems under the treatment of a mutant strain, the fractal dimension was seen to be decreased. WS-5 treatment consistently decreased fractal dimension in both Cycle A and Cycle B, irrespective of sterilisation method.

5.3.2.4 Summary of observed impact of bacteria on core scale soil structure

The analysis of experimental soil microcosms under different bacterial treatments by μ XCT scanning and 3D volumetric imaging has shown that treatment of soil with the SM control strain has no impact on reported porosity. However, the fractal dimension is increased in Cycle A and in the autoclaved cores in Cycle B. Fractal dimension (FD) in 3D is a value between 2 and 3, 2 being completely homogeneous (even distribution of pores) and 3 being completely heterogeneous (clustered distribution of pores). The addition of SM bacteria to the soil has resulted in a more clustered pore network relative to the bacteria-free dH₂O control soil system. Where an impact is observed in the mutant bacterial systems relative to the SM bacterial-control system, the porosity and fractal dimension are both decreased.

Interestingly, whilst not always significantly different from the bacterial-control SM soil system, the response pattern observed in the *ViscA* and WS-4 soil systems was the same. Porosity compared with the bacterial-control SM system in cycle A went down in both and up in cycle B in both. Fractal dimension for both went down in cycle A and up in cycle B. This suggests that viscosin and cellulose play a similar role in bacterial impact on soil structure and that loss of either from the system leads to a comparable effect.

5.3.3 Aggregate scale soil structure

5.3.3.1 Introduction

Aggregates (2 mm) were destructively sampled from experimental cores packed with Labfield soil that had been incubated with different bacterial treatments and then, following sterilisation, undergone two wet/dry cycles (Cycles A and B), which included oven drying. The aggregates were analysed by monochromatic, synchrotron μ XCT and structural measurements of porosity, fractal dimension, pore-size distribution and pore connectivity were obtained from the 3D volumetric datasets generated.

Due to beamline time constraints at the synchrotron, only the dH₂O and SM controls and the WS-4 treated soil systems were tested at this time. (Beamline Station 13-BM-D at the Advanced Photon Source (Argonne National Laboratory, USA), operated by GeoSoilEnvironCARS (GSECARS) of the University of Chicago). Use of the Advanced Photon Source (APS) beamline for small projects is awarded in 1 day blocks based on research proposals. The data analysis that had been completed up to this point in the study had indicated a significant effect of WS-4 on the soil system and therefore, the WS-4 cores were selected for synchrotron investigation. Additionally, it was hypothesised that interference in the expression of cellulose in the soil would have been most interesting from a structural point of view due to the ability of cellulose to bind the aggregates when present (Or and Friedman, 2002).

Variances in final numbers of aggregates for each soil treatment were unavoidable due to limited access to the synchrotron facility, and the analysis

of the datasets being undertaken after return to the United Kingdom. Some of the aggregates were found not to contain sufficient REV due to the presence of deeply penetrating stones. As such, the analyses were able to be carried out on 15 dH₂O, 11 SM, and 14 WS-4 aggregates. This meant that when the sterilisation split was required during statistical analysis, the final numbers for each treatment type were 6 dH₂O antibiotic sterilised, 9 dH₂O autoclaved, 5 SM antibiotic sterilised, 6 SM autoclaved, 8 WS-4 antibiotic sterilised, and 6 WS-4 autoclaved aggregates. Furthermore, extreme outliers in each analysis were identified and removed in accordance with normal statistical analyses practices. In order to simplify presentation of the data, the average number of samples is reported as n. True n has been used accurately in the statistical analysis package, and as such comparisons are a true representation of statistical significance.

5.3.3.2 Investigation of the impact of bacteria on aggregate porosity

Porosity was measured in extracted volumes (0.831 x 0.831 x 0.831 mm) from each aggregate using SCAMP V1.1 following segmentation to differentiate solid from pore space. No statistical interactions were observed between treatment type and sterilisation method ($p = 0.667$ n.s.) and therefore, the dataset was analysed as a whole. The test of model effects showed no significant difference between treatment type levels ($p = 0.177$ n.s.) and this was confirmed by pairwise comparisons as illustrated in Figure 5.6 below.

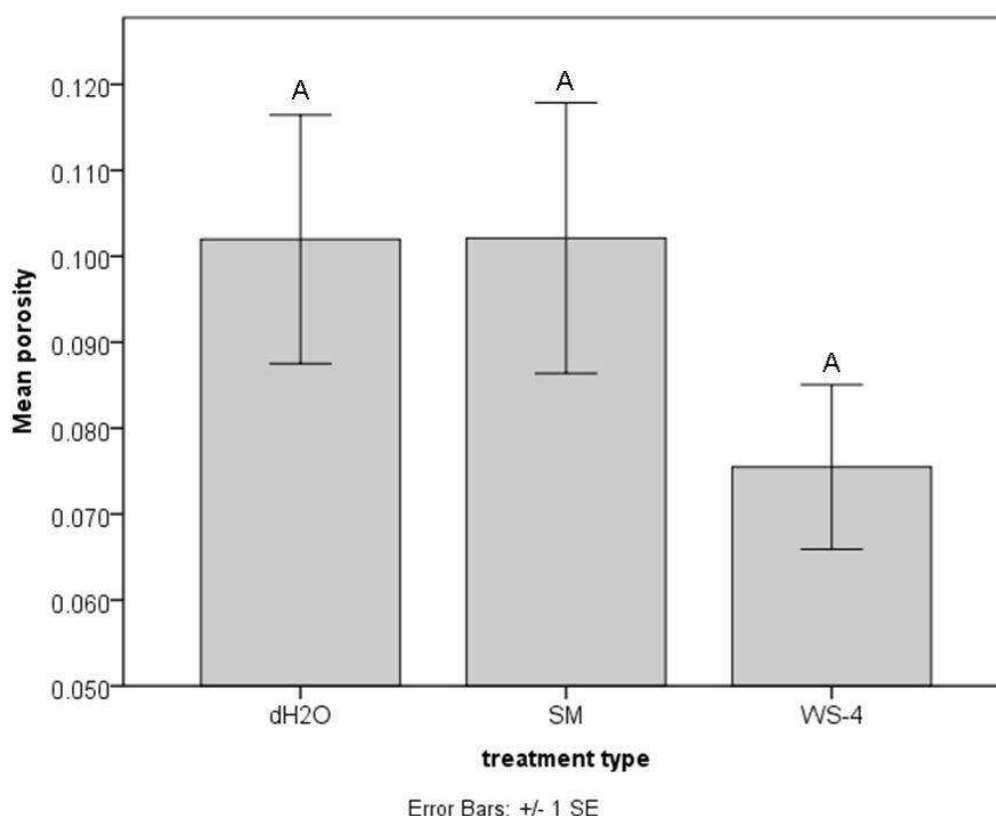


Figure 5.6 Mean porosity of aggregates under different treatment legacies. Mean porosity of 2 mm aggregates from Labfield soils under different treatment types measured using 3D volumetric data generated by synchrotron μ XCT scanning is shown. Significantly different ($p < 0.05$) treatments are indicated by lettering. Error bars were calculated as the standard error of the means of each treatment type ($n = 13$).

No difference was observed between the bacteria-free dH₂O control and SM soil systems ($p = 0.987$ n.s.), nor between the SM bacterial control and WS-4 soil systems ($p = 0.146$ n.s.). It is interesting to note that the porosity measured on the aggregate scale is approximately a third to a fifth of that measured on the core scale (dH₂O mean core porosity was 0.355 and mean aggregate porosity was 0.101; SM mean core porosity was 0.351 and mean aggregate porosity was 0.101; WS-4 mean core porosity was 0.401 and mean aggregate porosity was 0.075).

5.3.3.3 Investigation of the impact of bacteria on aggregate fractal dimension

The fractal dimension was measured in extracted volumes (0.831 x 0.831 x 0.831 mm) from each aggregate using SCAMP V1.1 following segmentation to differentiate solid from pore space. No statistical interactions were observed between treatment type and sterilisation method ($p = 0.763$ n.s.) and therefore the dataset was analysed as a whole. The test of model effects showed no significant difference between treatment type levels ($p = 0.071$ n.s.). However, this was not confirmed by pairwise comparisons as illustrated in Figure 5.7 below.

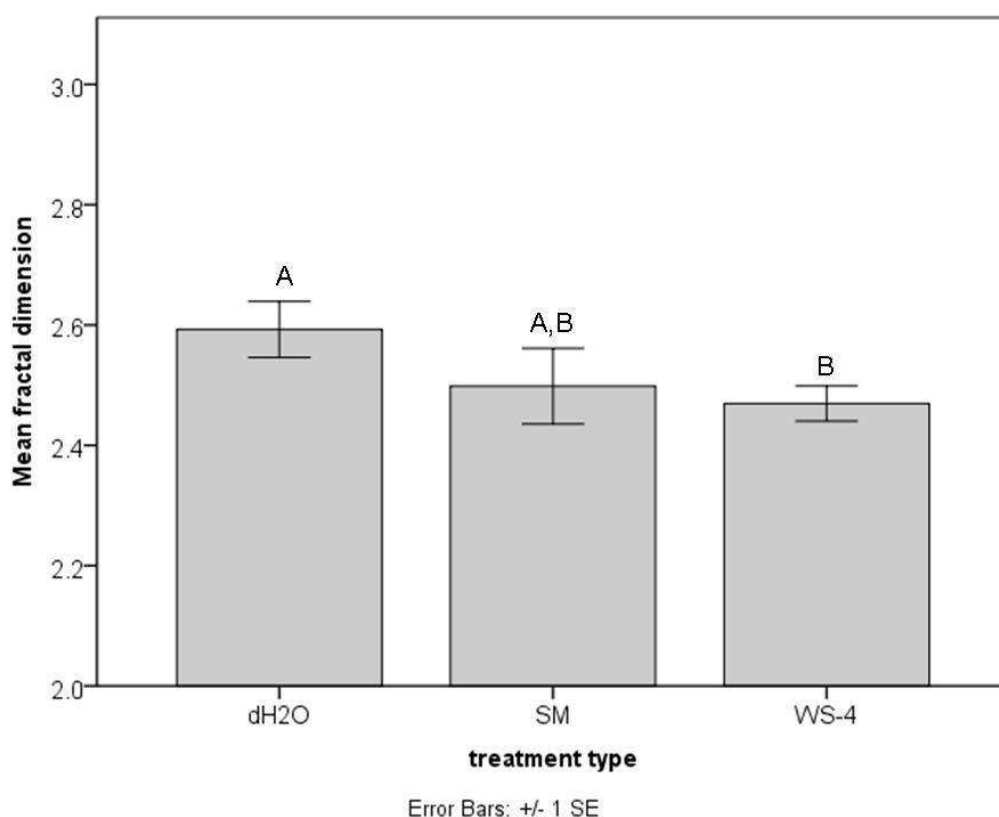


Figure 5.7 Mean fractal dimension of aggregates under different treatment legacies. Mean fractal dimension of 2 mm aggregates from Labfield soils under different treatment types measured using 3D volumetric data generated by synchrotron μ XCT scanning is shown. Significantly different ($p < 0.05$) treatments are indicated by lettering. Error bars were calculated as the standard error of the means of each treatment type ($n = 13$).

No difference was observed in the fractal dimension between the bacteria-free dH₂O control and SM systems ($p = 0.210$ n.s.) and there was also no difference between the SM control and WS-4 soil systems ($p = 0.727$ n.s.). In this study, the comparisons are between the bacteria-free dH₂O control and SM systems, and between the SM bacterial control and mutant bacteria systems, in this instance the WS-4. Therefore, the discrepancy in the statistical significance reports between the whole data analysis and the pairwise analysis is not of concern at this time and was cross-checked using individual sample t-tests to confirm the pairwise comparison findings were

correct for the subjects of analysis in this study (data not shown). As with the decrease in observed total porosity between cores and aggregate measurements, fractal dimensions would appear to be lower in the aggregates (FD \approx 2.5) than in the cores (FD \approx 2.8). This could suggest that aggregates have a more homogeneous distribution of pore space than the cores. Direct comparison between the fractal dimension of the treatment systems in the core and aggregate scale for fractal dimension is not possible. However, as Cycle B for the core scale samples was split according to sterilisation method whereas this was unnecessary in the aggregate samples.

5.3.3.4 Investigation of the impact of bacteria on aggregate pore-size distribution

The issue presented by the soil core data having been scanned at different resolutions was not a factor in the analyses of the aggregates, since all aggregates were scanned and reconstructed at the same resolution (5.54 μm). Therefore pore size distribution can be considered as a reliable measure of physical structure in this section of the study. Pore size distribution, reported in this study in terms of maximum and mean pore sizes, and also distribution of porosity across different pore size classes, in particular the smallest pore size class, was measured in extracted volumes (0.831 x 0.831 x 0.831 mm) from each aggregate using SCAMP v1.1 following segmentation to differentiate solid from pore space. Figure 5.8

illustrates the observed porosity across different pore size classes and the relationship between maximum and mean pore size.

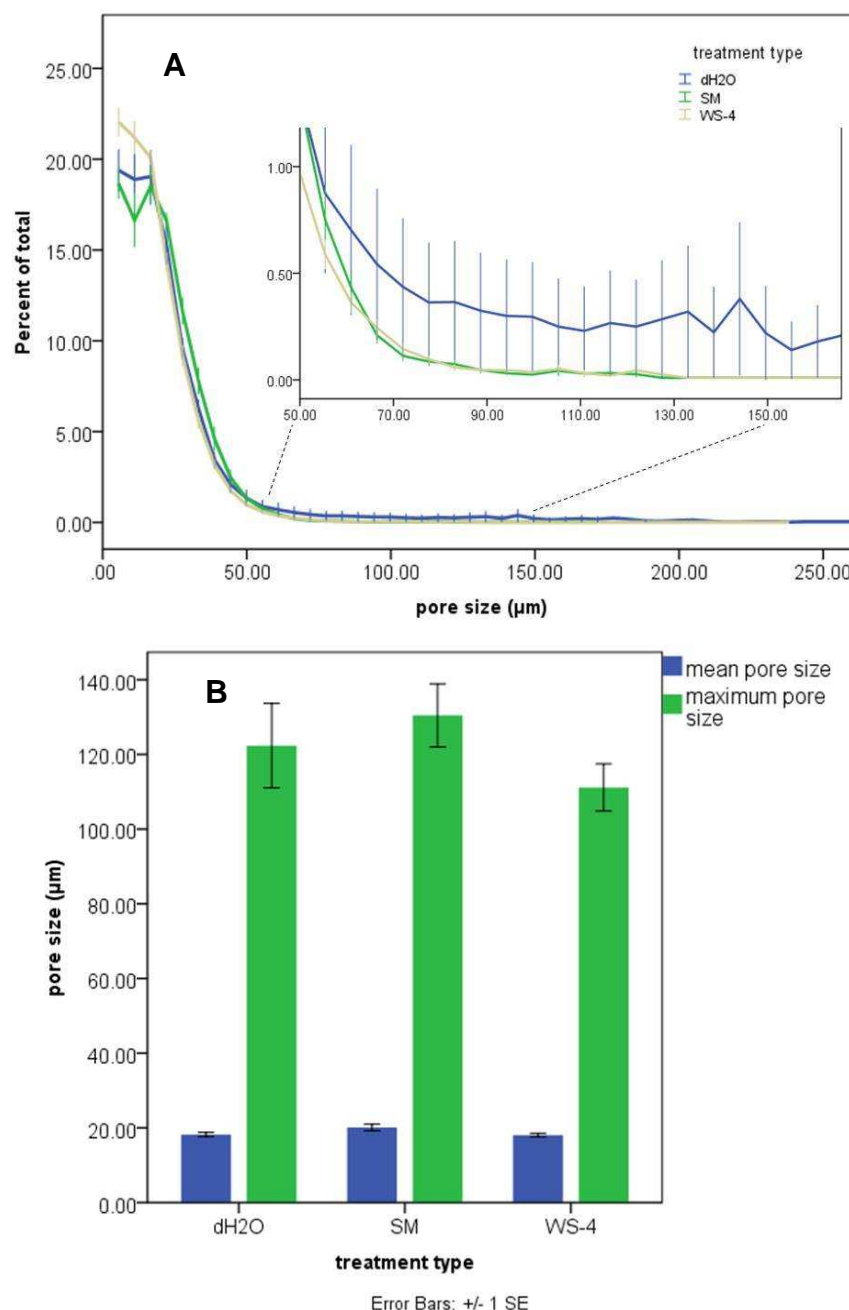


Figure 5.8 Overview of observed porosity across different pore size classes and relationship between maximum and mean pore sizes in aggregates under different treatment legacies. The pore-size distribution curve (A) for 2 mm Labfield aggregates from Labfield soils under different treatment types measure using 3D volumetric data generated by synchrotron μ XCT scanning is shown along with the maximum and mean pore size class relationship (B). Error bars were calculated as the standard error of the means of each treatment type ($n = 13$).

For maximum pore size, no statistical interactions were observed between treatment type and sterilisation method ($p = 0.397$ n.s.) and therefore the dataset was analysed as a whole. The test of model effects showed no significant difference between treatment type levels ($p = 0.181$ n.s.) and this was confirmed by pairwise comparisons and is illustrated in Figure 5.9 below.

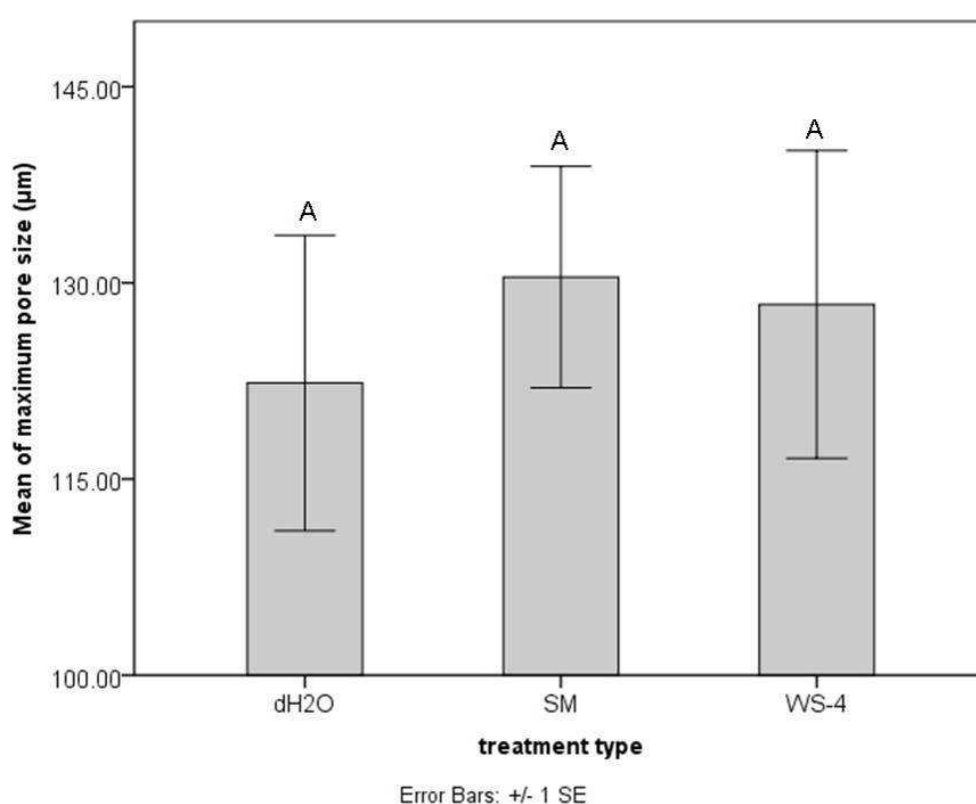


Figure 5.9 Maximum pore size of aggregates from Labfield soils under different treatment types. Pore size distribution was measured using 3D volumetric data generated by synchrotron μ XCT scanning. Significantly different ($p < 0.05$) treatments are indicated by lettering. Error bars were calculated as the standard error of the means of each treatment type ($n = 13$).

For mean pore size, statistical interaction between treatment type and sterilisation method was observed ($p = 0.004$) and so data was split according to sterilisation method. Antibiotic-sterilised samples demonstrated

no statistical difference between treatment types ($p = 0.924$ n.s.). However, autoclaved samples indicated a statistical difference between the treatment types ($p < 0.001$). Results for mean pore size are illustrated in Figure 5.10 below, and the pairwise comparisons of treatment types are highlighted in Table 5.3.

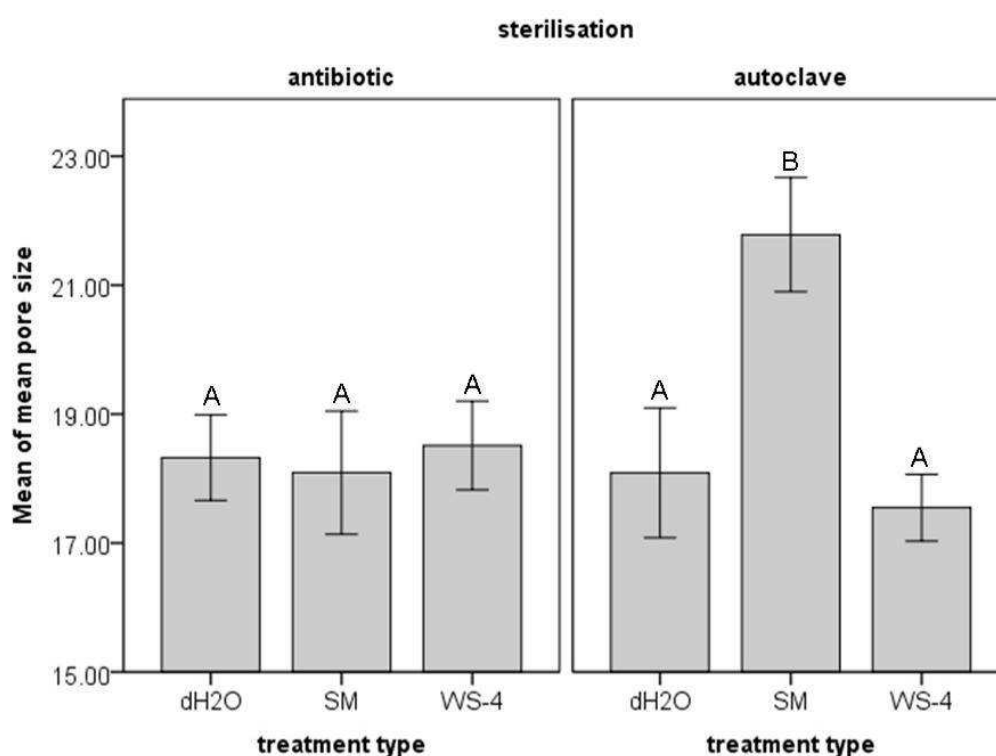


Figure 5.10 Reported mean pore size of aggregates from Labfield soils under different treatment types. Pore size distribution was measured using 3D volumetric data generated by synchrotron μ XCT scanning. No comparison has been made between sterilisation methods at this stage and as such no inference is intended between antibiotic and autoclave methods. Error bars were calculated as the standard error of the means of each treatment type ($n = 7$).

Table 5.3 Pairwise comparison of the effect of bacterial treatment type on aggregate mean pore size in Labfield soil.

		Mean pore size	
		sterilisation method	
		autoclave	antibiotic
pairwise treatment types	dH ₂ O vs. SM	↑ 0.003	0.824
	SM vs. WS-4	↓ < 0.001	0.693

Bold type indicates statistical significance ($p < 0.05$); ↓ indicates decreased mean pore size compared with control; ↑ indicates increased mean pore size compared with control; first term in treatment type column indicates control for comparison.

Mean pore size is increased in the SM bacterial aggregates compared with the dH₂O control soil and decreased in the WS-4 aggregates compared with the SM control soil, but only in the samples that were sterilized by autoclaving.

The overall picture of the distribution of observed porosity can be summarised by looking at the mean values for total porosity, proportion of pores in the smallest size class (5.54 μm) and the maximum pore size class for each treatment type. Mean total porosity and maximum pore size class have been presented in Figure 5.6 and Figure 5.9 above, the proportion of pores in the smallest size class is presented in Figure 5.11 below.

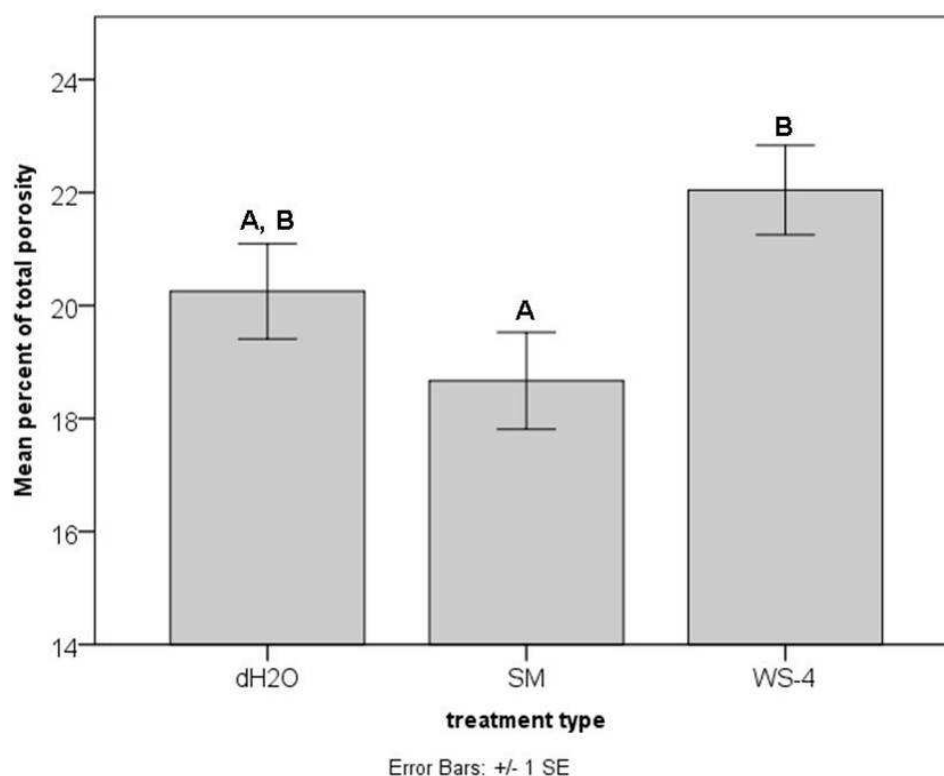


Figure 5.11 Mean percentage of total observed porosity present in the smallest pore class (5.54 μm) of aggregates from Labfield soils under different treatment types. Pore size distribution was measured using 3D volumetric data generated by synchrotron μXCT scanning. Significantly different ($p < 0.05$) treatments are indicated by lettering. Error bars were calculated as the standard error of the means of each treatment type ($n = 13$).

The bacteria-free dH₂O control aggregates had a total observed porosity of 10% of which 20.25% was in the smallest pore class size, with no pores greater than 122 μm . The SM bacterial-control aggregates had a total observed porosity of 10% of which 19.71% was in the smallest pore size class, with no pores greater than 130 μm . The WS-4 aggregates had a total observed porosity of 7.5% of which 22% was in the smallest pore class size, with no pores greater than 123 μm .

5.3.3.5 Investigation of the impact of bacteria on aggregate pore connectivity

Pore connectivity was measured in extracted volumes (0.831 x 0.831 x 0.831 mm) from each aggregate using SCAMP V1.1 following segmentation to differentiate solid from pore space. The largest twenty pores are reported for each treatment type and are presented as an overview in Figure 5.12.

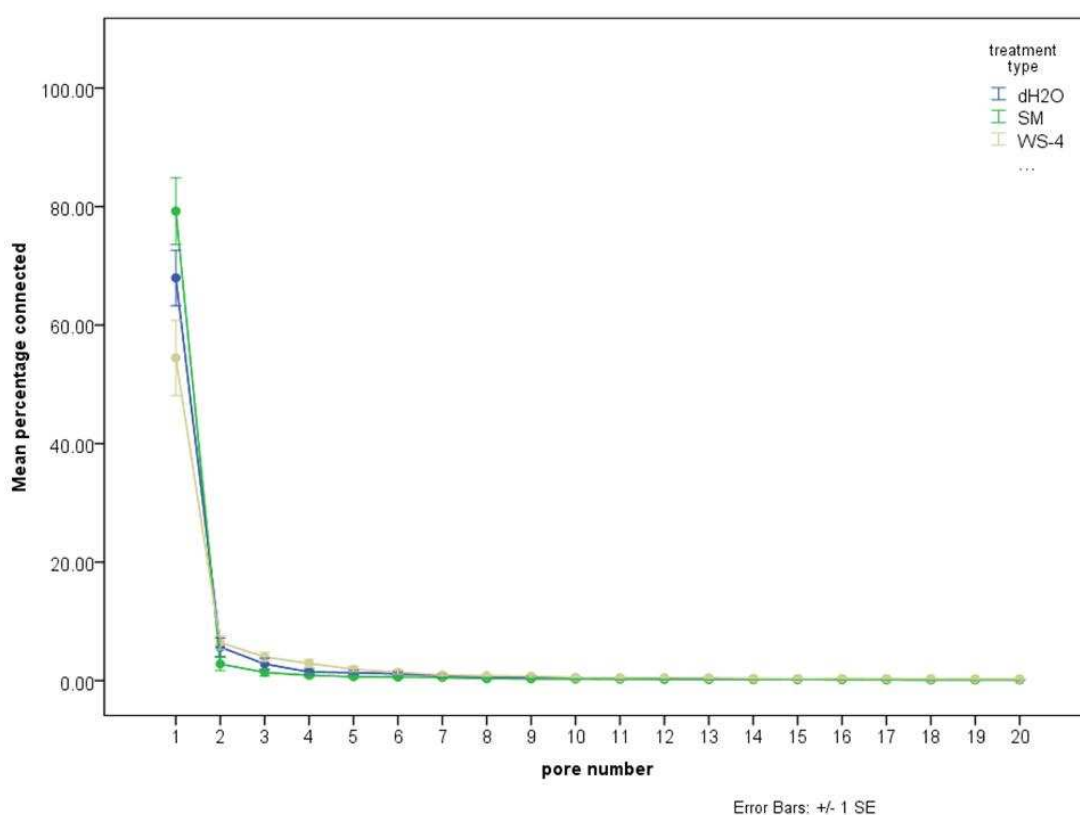


Figure 5.12 Overview of pore connectivity of 20 largest pores in Labfield aggregates under different treatment types measured using 3D volumetric data generated by synchrotron μ XCT scanning. Error bars were calculated as the standard error of the means of each treatment type ($n = 13$).

For individual pore numbers, no statistical interactions were observed between treatment type and sterilisation method in any of the pore number analyses ($p > 0.085$ n.s.) and therefore, within the pore number, datasets

were analysed as a whole. The test of model effects showed significant difference between treatment type levels in all, but pore numbers 2, 6, 7, 10, 11 and 12... Results for pore connectivity are illustrated in Figure 5.13 and the pairwise comparisons of treatment types are highlighted in Table 5.4.

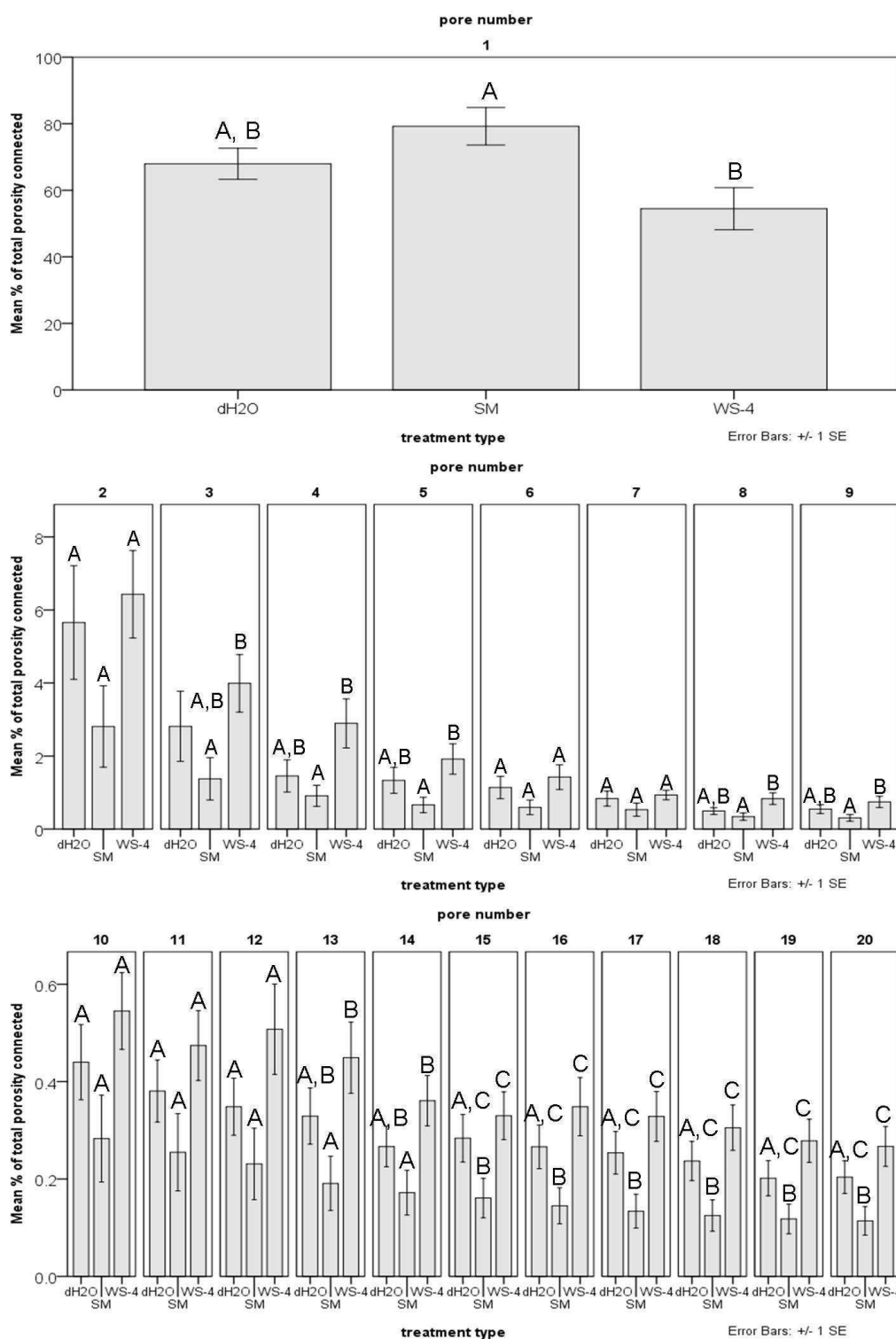


Figure 5.13 Mean pore connectivity in largest 20 pores (top; pore 1, maximum 80% connected; middle pores 2 to 9, maximum 7% connected; bottom: pores 10 to 20, maximum 0.5% connected) of aggregates under different treatment legacies. Pore connectivity was measured using 3D volumetric data generated by synchrotron μ XCT scanning. Significantly different ($p < 0.05$) treatments within pore number are indicated by lettering. No comparison between pore numbers is inferred. Error bars were calculated as the standard error of the means of each treatment type ($n = 13$).

Table 5.4 Pairwise comparisons in 20 largest connected pores of the effect of bacterial treatment type on aggregate scale pore connectivity of Labfield soil

pairwise treatment types				
Mean pore connectivity	pore number	dH ₂ O vs SM		SM vs WS-4
		1	0.081	↓ 0.002
		2	0.116	0.025
		3	0.257	↑ 0.006
		4	0.257	↑ 0.006
		5	0.075	↑ 0.004
		6	0.105	0.029
		7	0.227	0.062
		8	0.202	↑ 0.006
		9	0.092	↑ 0.012
		10	0.156	0.021
		11	0.188	0.031
		12	0.185	0.015
		13	0.064	↑ 0.003
		14	0.096	↑ 0.004
		15	↓ 0.039	↑ 0.005
		16	↓ 0.022	↑ 0.002
		17	↓ 0.018	↑ 0.001
		18	↓ 0.016	↑ 0.001
		19	↓ 0.045	↑ 0.001
		20	↓ 0.024	↑ 0.001

Bold type indicates statistical significance ($p < 0.05$); ↓ indicates decreased pore connectivity compared with control; ↑ indicates increased connectivity compared with control; first term in treatment type column indicates control for comparison. Pores 2, 6, 10, 11, and 12 indicated statistical significance within the SM vs. WS-4 pairwise analysis, but the treatment types as a whole in these pores showed no statistical significance.

In the connected pores where an impact was observed, there is no difference between the bacteria-free dH₂O control and SM aggregates until the 15th largest pore is reached, then consistently lower pore connectivity is observed in the SM aggregates in pores 15 to 20. In the comparison of the SM bacteria-control and WS-4 treatment legacies, with the exception of the largest connected pore (pore 1) a consistent increase in pore connectivity is observed in the WS-4 aggregates throughout the remaining 19 largest pores.

A more comprehensive way of interpreting the pore connectivity is to look at the largest 20 pores as a whole. The proportion of the total observed porosity found in the largest 20 pores was calculated and comparison of the treatment types was carried out. No statistical interactions were observed between treatment type and sterilisation method ($p = 0.321$ n.s.) and therefore the dataset was analysed as a whole. The test of model effects showed significant difference between treatment type levels ($p = 0.044$). Results for pore connectivity are illustrated in Figure 5.14 and the pairwise comparisons of treatment types are highlighted in Table 5.5.

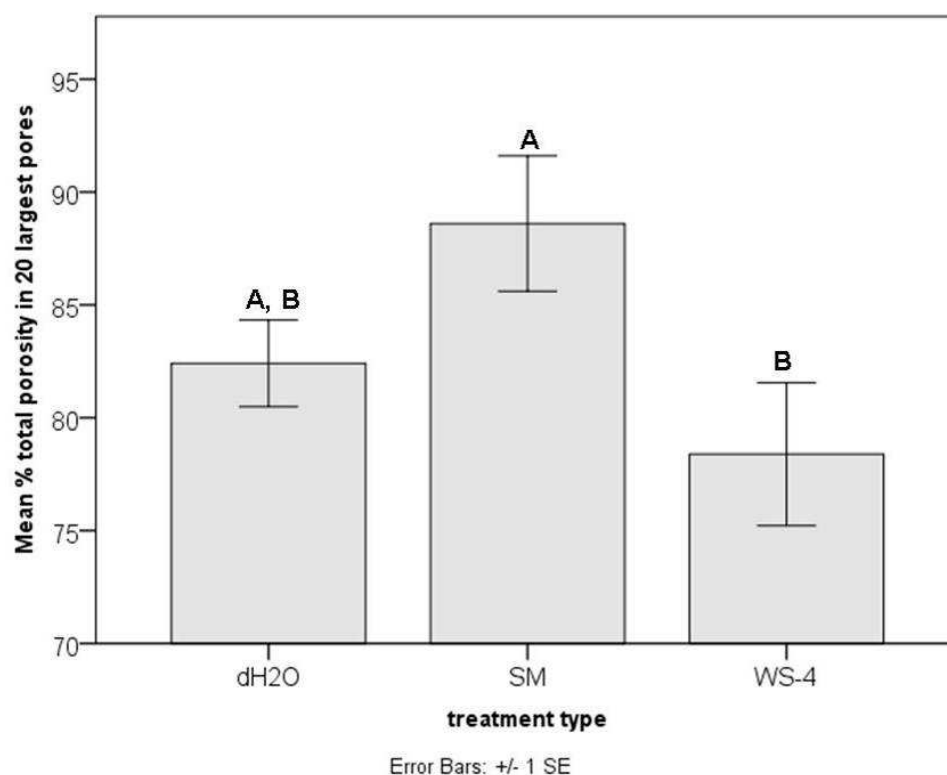


Figure 5.14 Proportion of total observed porosity present in largest 20 connected pores for Labfield aggregates under different treatment types. Mean percentage of total aggregate porosity connected in the 20 largest pores were measured using 3D volumetric data generated by synchrotron μ XCT scanning is shown. Significantly different ($p < 0.05$) treatments are indicated by lettering. Error bars were calculated as the standard error of the means of each treatment type ($n = 13$).

Table 5.5 Pairwise comparison of the effect of bacterial treatment type on aggregate proportion of total porosity in 20 largest connected pores in Labfield soil

Mean % total porosity		
pairwise treatment types	dH ₂ O vs. SM	0.069
	SM vs. WS-4	↓ 0.014

Bold type indicates statistical significance ($p < 0.05$); ↓ indicates decreased mean pore size compared with control; ↑ indicates increased mean pore size compared with control; first term in treatment type column indicates control for comparison.

The connectivity of observed pore space for the three treatment types measured as the proportion of total pore space contained in the largest 20 pores is not significantly different between the bacteria-free dH₂O control

(82.41%) and the SM aggregates ($p = 0.069$, ns), but the 20 largest pores in the WS-4 aggregates comprise 78.38% of the total pore space, which is significantly less than the 88.60% contained in the largest 20 pores of the SM aggregates ($p = 0.014$).

5.3.3.6 Summary of the observed impact of bacteria on aggregate scale soil structure

The presence of bacteria (SM) does not appear to have an impact on the total porosity nor on the pore heterogeneity of the aggregates when compared with the bacteria-free dH₂O control system. Similarly the pore size distribution analysis shows no impact of bacteria on the maximum pore size class, the percentage of total porosity in the smallest pore class, or the reported mean pore size with the exception of the samples that underwent autoclave sterilisation, where the SM bacteria showed a higher mean pore size than the bacteria-free dH₂O control aggregates. The total porosity contained within the largest 20 pores was not affected by the presence of the SM bacteria compared with the bacteria-free dH₂O control. However, more in-depth analysis of the 20 largest pores individually did indicate that at the smaller pore volumes (15th to 20th in size) the percentage of total porosity in these connected pores is less than that in the bacteria-free dH₂O control.

Similarly, the comparison of the SM bacteria control system with the WS-4 bacterial system indicates no impact on total porosity or pore space heterogeneity. Pore size distribution analysis shows no impact of bacteria on the maximum pore size class or the reported mean pore size with the

exception of the samples that underwent autoclave sterilisation, where the SM bacteria showed a higher mean pore size than the WS-4 soil aggregates. In the analysis of the percentage of total porosity in the smallest pore class, WS-4 shows a higher percentage of total porosity than the SM bacterial control aggregates. Interestingly, whilst the in-depth analysis of the 20 largest pores individually indicated that the WS-4 aggregates showed an increased proportion of total porosity in the 2nd to 20th largest pores compared with the SM bacterial control, which fits with the observation that WS-4 aggregates have a higher percentage of total porosity in the smallest pore size class, the overall analysis of the proportion of total porosity in the largest 20 pores showed that WS-4 aggregates in fact had a lower proportion than the SM bacterial control.

5.4 Chapter discussion

5.4.1 Introduction

Tisdall and Oades (1982) stated that the water-stability of aggregates is shown to depend on organic materials. These binding agents have been classified into *transient* (mainly polysaccharides), *temporary* (roots and fungal hyphae) and *persistent* (resistant aromatic compounds associated with polyvalent cations and strongly sorbed polymers).

The compounds of interest in this study are cellulose, lipopolysaccharide and the surfactant viscosin. In terms of binding agents, cellulose and lipopolysaccharide are classed as transient according to the system of Tisdall and Oades (1982) and viscosin is considered an aggregate

destabiliser, as it would be expected to reduce the natural waterproofing of the soil as originally described by Martin *et al.* (1955).

Porosity is a measurement of the void space present in a soil, being occupied by either air or water or both. Elliott and Coleman (1988) described four hierarchical pore categories: (1) macropore, (2) intermacroaggregate (pore space between macroaggregates), (3) intramicroaggregates (pores between microaggregates, but within macroaggregates), which includes (4) intramicroaggregate (pores within microaggregates). These were in association with the aggregate hierarchy concept initially proposed by Tisdall and Oades (1982) in which primary particles ($< 20\ \mu\text{m}$) bind to form microaggregates (20-250 μm), which in turn bind to form macroaggregates ($>250\ \mu\text{m}$). This concept was then modified by Oades (1984) when he postulated that decomposition of roots and hyphae temporarily binding macroaggregates resulted in the formation of microaggregates through the binding of clay particles with mucilage produced during decomposition. Figure 5.15 schematically illustrates both these pore and aggregate hierarchies.

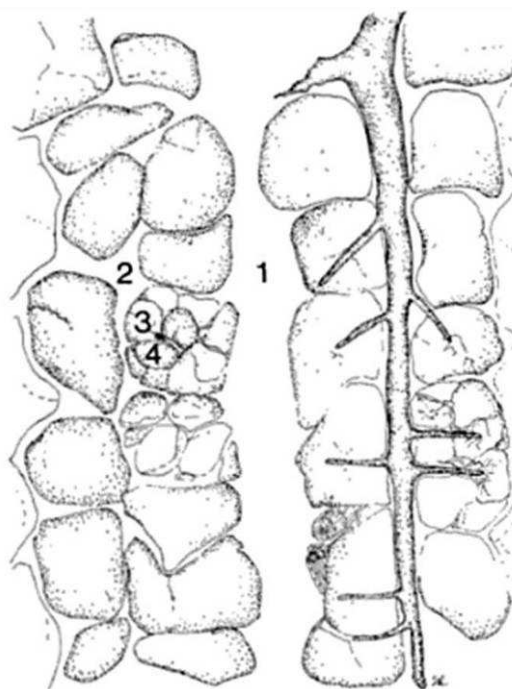


Figure 5.15 Hierarchical categorisation of pores as described by Elliott and Coleman (1988). Vertical cross section of highly structured soil showing macroaggregates ($>250\ \mu\text{m}$) and microaggregates ($20 - 250\ \mu\text{m}$). Pores are categorised into: (1) macropores, (2) intermacroaggregate, (3) intramicroaggregate including (4) intermicroaggregate space. Illustration by S.L. Rose (Figure 3 in Elliott and Coleman (1988) *Let the soil work for us*, p26)

Whilst roots and hyphae are not of concern in this study, the formation and breakdown of macroaggregates and microaggregates will have been mediated by the presence of the model bacteria, with the effect expected to be predominantly visible in the microaggregate structure as categorised by (Elliott and Coleman, 1988), as was evident in $30\text{-}300\ \mu\text{m}$ pores defined as mesopores in the hydrodynamic studies presented in Chapter 4 of this work.

5.4.2 Core scale soil structure

In vitro SM is capable of producing all of the compounds of interest: viscosin in late log phase, cellulose and LPS. Of the mutant strains, *ViscA* is

incapable of viscosin production, WS is a cellulose overproducer, WS-4 is cellulose deficient and WS-5 is LPS deficient. All mutant soil systems in the core analyses, except WS demonstrated a 14-15% decrease in porosity equivalent to an overall 31-33% reduction in the porosity of the soil compared with the SM bacterial control soil system ($p \leq 0.001$) in cycle A. In cycle B, by contrast, only WS-5 affected porosity, in that this soil system demonstrated a 6% decrease equivalent to an overall 18% reduction in the porosity compared with the bacteria control SM soil ($p = 0.027$). Comparison of the cellulose overexpressing and deficient systems (WS and WS-4 respectively) showed no difference in measured porosity in cycle A ($p = 0.163$, n.s.), but a 10 % increase in porosity in the deficient WS-4 system equivalent to an overall increase of 31% ($p = 0.001$) compared with the WS cellulose overexpressing system. No difference in porosity was observed between the bacteria-free dH₂O control and SM bacterial-control soil system, indicating that addition of the complete bacteria has no observable effect on porosity of the soil cores.

The bulk volume of the soil cores in these experiments remained the same throughout the study. Therefore, any change in the value of the porosity is attributable to the rearrangement of the solid volume in the samples. Both the shape and the arrangement of soil particles help determine porosity and since all 60 replicate cores were prepared in the same manner prior to bacterial treatment and all went through the same WD cycle processing prior to scanning, any change in porosity following treatment is attributable to the treatment type. Porosity can be expected to decrease in a soil system following WD cycles due to the loss of large pores

and aggregates when a soil is wetted rapidly, resulting in a reduction of hydraulic conductivity, which is the ease with which water can move through soil spaces and fractures (Grant and Dexter, 1989). When a soil is wetted the aggregates swell differentially and the attractive forces between the primary particles ($< 20 \mu\text{m}$), microaggregates ($20 - 250 \mu\text{m}$) and macroaggregates ($>250 \mu\text{m}$) become interrupted by the presence of the water (particle categorisation after Tisdall and Oades (1982))^{viii}. The result would be the shearing of larger aggregates into their smaller constituent parts, called slaking, thereby increasing the number of smaller grains which would fill the void spaces between the larger aggregates and decrease the overall visible porosity in the core volume. This is illustrated schematically in Figure 5.16.

^{viii} In order to maintain continuity with the pore sizes described at the relevant drainage points in the hydrodynamic experiments in this study, primary particles will hereafter be considered microaggregates ($<30 \mu\text{m}$), the term mesoaggregates will be introduced to refer to particles $30\text{-}300\mu\text{m}$, and macroaggregates will refer to particles $>300 \mu\text{m}$ in size.

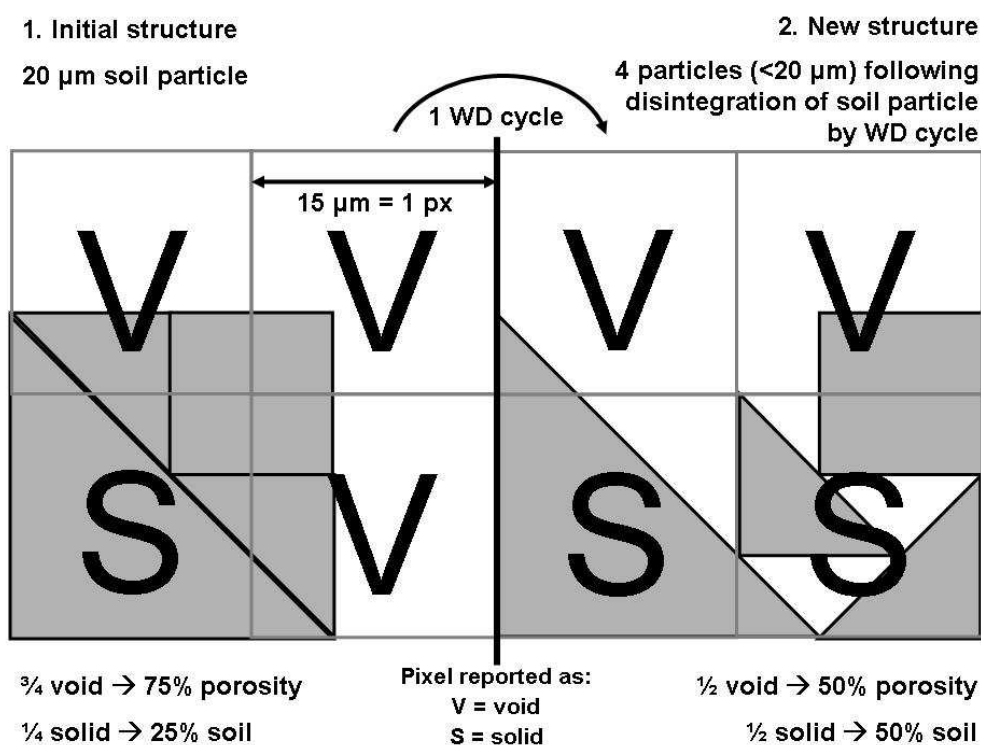


Figure 5.16 Schematic 2D representation of change in porosity due to disintegration of soil particles following a wet/dry (WD) cycle. On the left (1) a 20 μm soil particle occupies one 15 μm pixel entirely, which, on segmentation of the image will be reported as solid (S), the remainder of the particle occupies $\frac{1}{3}$ each of two further pixels, and $\frac{1}{9}$ of the 4th pixel. These three pixels will be reported as void (V) upon segmentation. Thus, the whole volume of 4 pixels will have a porosity of 75%. On the right (2), the 20 μm particle has been swollen upon wetting and disintegrated upon drying leaving 4 new particles each $< 20 \mu\text{m}$. Due to the configuration of the smaller particles within the pixels, reported porosity has been decreased to 50% as measured by image analysis following segmentation.

Each pixel in Figure 5.16 is 15 μm and therefore, the whole area of 4 pixels is 900 μm^2 . The 20 μm particle (with an area of 400 μm^2) and therefore occupies $\frac{4}{9}$ of the whole area, meaning that the true porosity value is $(1 - \frac{4}{9})$ 55.5%. Upon disintegration, the sum of the smaller particles is still going to occupy $\frac{4}{9}$ of the 4 pixel volume, so again true porosity is 55.5%.

The illustration of reported porosities of 75% and 50% detailed above versus the true porosity of 55.5% serves two purposes: (1) to raise awareness of the issue of resolution of imaging technology, which will be

discussed later in this work, and, of importance to this chapter in the context of this study 2) to demonstrate that differences in porosity reported in these results are due to physical rearrangement of the particles in the soil cores, and any observed difference in porosity, when compared against the control system that has also undergone the same WD cycle is due to restructuring of the soil in the presence or absence of the bacterial compounds of interest in this work.

The presence of microbial activity has been shown to stabilize soil aggregates in the rhizosphere by generating adhesive forces (Czarnes *et al.*, 2000), effectively binding soil particles together during drying. All of the soil systems underwent the same number of WD cycles and therefore any decrease in porosity solely due to the WD cycles would be expected across all treatment types, resulting in no observed change in porosity, which again enforces the view that any restructuring is the result of bacterial presence.

Soil aggregates are bound by the presence of exopolymeric substances (EPS) (Chenu and Cosentino, 2011) consisting of primarily polysaccharides and various amounts of proteins, lipids etc. Looking at each of the compounds of interest in terms of their individual impact on the solid phase of the soil matrix, the polysaccharide of interest in this study is cellulose, which would provide a glue-like mesh embedded with soil aggregates enhancing soil stability. The viscosin produced, an amphiphilic surfactant, would also be expected to bind the soil aggregates together through the polar/non-polar moieties attracting mineral grains to each other. LPS, another amphiphilic compound would also serve to maintain attractive forces between soil grains, thereby stabilising the aggregates. During the

course of a wet-dry cycle however, the cellulose mesh would swell along with the aggregates while maintaining the conformation of the grains in the volume of soil. On the contrary, the amphiphilic nature of the viscosin and LPS means that once the critical moisture level was reached, these moieties would invert on the surface of the soil grains and, while their presence may bind individual (macro-)aggregates so as to decrease disintegration into smaller grains (mesoaggregates and primary particles), it would not prevent restructuring of the macroaggregates within the soil volume. Figure 5.17 illustrates the individual component-soil interaction behaviours schematically.

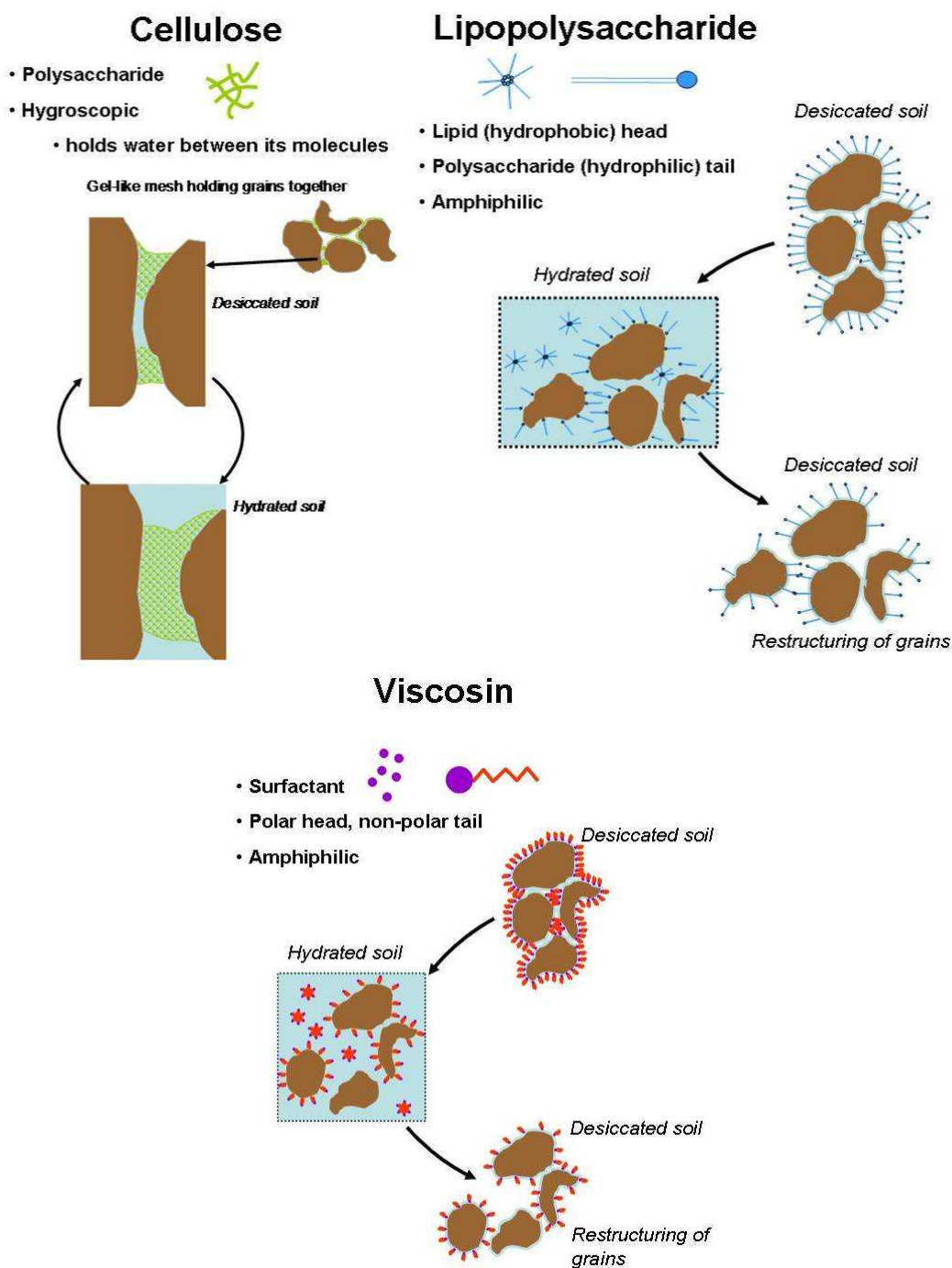


Figure 5.17 Component-soil grain interactions for cellulose, lipopolysaccharide and viscosin. The gel-like mesh provided by cellulose would provide support for the aggregates during hydrated and desiccated stages leading to a physically stable environment. Both LPS and viscosin would provide interaggregate binding during periods of desiccation, but on hydration of the environment, inversion of the amphiphilic moieties would allow movement of grains and restructuring of the soil.

The soil cores were inoculated at -0.2 kPa and incubated for 2 weeks, during which time the bacteria would have been producing the exopolymeric substances particular to the strain. Following sterilisation, the cores were then rehydrated to near saturation (0 kPa) and then slowly drained to -80 kPa, the mesopore (~30 μm) drainage point. If present in the soil system, cellulose would provide cohesion between aggregates, allowing inter- and intra-aggregate swelling in the hydrated phase, preventing slaking within aggregates upon desiccation and maintenance of the physical structure of the soil. Viscosin and lipopolysaccharide, if present, would provide a similar binding of aggregates. However, due to the reorientation of the EC moieties upon rehydration, whilst the intra-aggregate structure would be likely to be maintained, interaggregate bonds would most likely not be maintained and therefore, restructuring of the aggregates within the soil volume could be expected, most likely as a movement of smaller aggregates into voids between larger aggregates. This would then most probably lead to a reduction in porosity following desiccation in viscosin and LPS positive soil cores. However, looking at the overall picture of porosity in cycle A this would seem not to be the case. SM soil showed no difference in porosity compared with the bacteria-free dH_2O control soil. WS soil showed no difference in porosity compared with the SM bacteria control soil. The soil systems deficient in an EC component all had lower porosity than the SM bacteria control soil. It would therefore appear that whilst the presence of all of the EC components in the soil confers no increased or decreased porosity, the absence of any one of the components in a bacterial system results in a decreased porosity in cycle A.

During rehydration of the cores in cycle A, aside from the physical restructuring of the aggregates, the EC components will have undergone changes in terms of their spatial distribution within the pore network. Where narrowing of the pores occurs (pore necks) there is the possibility of biomass accumulation (bioclogging) (Thullner and Baveye, 2008; Morales *et al.*, 2010), as has been discussed in the hydrodynamics chapter (4). The implications of this in terms of the soil structure are that where water flow is impeded by bioclogging, there is the possibility that the negative pressure head being applied to the soil volume pulling on the gel-like mesh of EC components could cause internal pressure on the pore necks, opening necks up and allowing the smaller grain particles to move into connected areas of the pore network. This could lead to decreased reported porosity as voids become interspersed with slaked grains. Additionally, micelles of viscosin or LPS could potentially be removed from the system altogether with water egress. Alternatively, in terms of water ingress during the rehydration of the cores in cycle B, bioclogged networks would be less easily rehydrated resulting in some areas of the soil volume perhaps not reaching the critical moisture point at which the inversion of the amphiphilic viscosin and LPS occurs. Pressure from adjacent, but not clogged pores could physically alter the unsaturated regions resulting in altered porosity and structure. In the analysis of porosity of the soil cores following cycle B, only the WS-5 system showed a significant difference in terms of measured porosity compared with the bacterial-control SM soil. Perhaps more interesting though is that the other mutant systems, WS, *ViscA*, and WS-4 have no difference in porosity compared with the bacteria control. It would appear that a greater change

occurred in the SM system, albeit no different to the change observed in the bacteria-free dH₂O control soil in cycle B. However, the change observed in the bacteria-control soil following cycle B seems to echo the decrease in porosity of the mutant systems observed in cycle A. It is known that a WD cycle decreases porosity (Chenu and Cosentino, 2011) and results indicate that the presence of bacteria capable of complete EC component production confers no structural stabilisation in terms of overall porosity. However, with the exception of the LPS, the absence of one of the EC components no longer affects porosity of the soil volume compared with the bacterial-control system. Perhaps being a key component of integrity of the bacterial cell membrane, the LPS-deficient WS-5 effects on the soil were such that the aggregates were less well stabilised, thus allowing further disruption to the aggregates upon rehydration and subsequent drainage in cycle B. Further WD cycles would be required to see if porosity also reached a steady state in the WS-5 system.

Fractals are, by definition, objects that have a complex, irregular geometry that is apparent over many scales of measurement (Young *et al.*, 2001). Fractal analysis is a widely used method of characterising the heterogeneity and complexity of the soil pore characteristics (Gibson *et al.*, 2006; Papadopoulos *et al.*, 2008; Luo and Lin, 2009; Papadopoulos *et al.*, 2009; Tarquis *et al.*, 2009; Kumar *et al.*, 2010; Kravchenko *et al.*, 2011). All soil cores in this study reported an FD value >2.7, illustrating the heterogeneity of the soil cores under all treatment types. In cycle A, treatment of the soil with the wild-type bacteria (SM) capable of producing all of the EC showed a significant increase in FD compared with that of the

bacteria-free dH₂O soil system, indicating greater heterogeneity of the soil pore network. This observation adds important information to the finding that, whilst the porosity of these samples was not significantly different, the physical arrangement of that same porosity has been affected by the presence of the bacteria.

The mutant bacteria-soil systems, with the exception of WS, showed less heterogeneity compared with the bacteria-control SM soil system. The *ViscA*-soil system showed a 9% decrease (equivalent to a 3% reduction) in the fractal dimension of the soil. The WS-4 soil-system showed an 11% decrease (4% reduction) in fractal dimension, and the WS-5-soil system showed a 10% decrease (3% reduction) in the fractal dimension of the soil ($p < 0.001$). The WS-soil system showed no significant difference in fractal dimension and comparison of the WS and WS-4 models for cellulose-overexpressing and deficient-soil systems showed no significant difference in fractal dimension.

Following antibiotic sterilisation, the bacteria-free dH₂O soil system in cycle B reported an FD which was found not to be significantly different from the FD reported by the system treated with SM. Treatment of the soil system with *ViscA* resulted in no significant change in fractal dimension, compared with the complete bacteria system, as did treatment of with WS or WS-4. Treatment of the soil system with WS-5 resulted in a decrease of 6% in FD from the SM-treated system, an overall reduction of 2% in fractal dimension of the soil indicating less heterogeneity in the absence of LPS.

Following autoclave sterilisation, the SM soil showed a 7% greater FD than the bacteria-free dH₂O control soil giving an overall increase of 3% in

fractal dimension of the soil indicating that, as in cycle A, the bacteria have increased heterogeneity of the pore network. Treatment of the soil with *ViscA* had no observed effect on fractal dimension of soil compared with the bacterial-control and neither did treatment with WS-4. However, the WS and WS-5 system showed a 5% and 8% decrease respectively (both $p = 0.007$), an overall reduction of 2% and 3% in fractal dimension respectively, indicating that cellulose and LPS have an impact on the heterogeneity of the soil pore network. There was no significant difference observed in fractal dimension between WS and WS-4 treated systems ($p = 0.197$ n.s.).

As can be observed in the illustration of the box-counting method in Figure 3.15, samples can have the same porosity value but have completely different distribution of the pores within the volume. Thus, the measurement of the homo- and heterogeneity of the pore network can add valuable information in determining the impact of a treatment type on the structure of the soil. Where the bacteria-free dH₂O control soil and SM soils showed no difference in porosity suggesting no impact of the combined presence of cellulose, viscosin and LPS, greater heterogeneity observed in the measurement of fractal dimension under the influence of the same bacterial legacy, suggests that aggregate binding has indeed been affected most likely by pulling some aggregates together and enlarging the pores networks along existing cracks and decreasing the pore sizes in other areas where the bacteria were not present. This supports the findings of others that describe disparate micro-niches within the soil, rather than an even distribution of bacteria throughout the soil (Nunan *et al.*, 2002; Nunan *et al.*, 2006; Or *et al.*, 2007; Young *et al.*, 2008).

When discussing the impact of the amphiphilic EC components (viscosin and LPS), on the porosity of the soil in cycle A, the observation was that whilst there had been maintenance of the intra-aggregate structure, the interaggregate bonds would most likely not be maintained therefore restructuring of the aggregates within the soil volume could be expected, most likely a movement of smaller aggregates into voids between larger aggregates. In terms of fractal dimension this would be observed as a movement towards homogeneity. In the presence of all three components, such as in the SM bacterial-control system, the cellulose would be expected to be driving the soil structure towards heterogeneity whilst the viscosin and LPS, following a WD cycle would be expected to be driving the soil towards homogeneity. It is known that cellulose is not easily moveable in the soil pore network due to its binding capacity and development of mesh-like structure around the soil grains and therefore, once exuded from the bacteria in the disparate microniches, the cellulose would be expected to remain in the area in which it has been produced. On the other hand, during rehydration of the soil volume, the amphiphilic viscosin and LPS can form micelles in the water and become free-floating in the pore network. Movement of these moieties within the pores could lead to physical rearrangement of soil particles in areas out with the location of the original bacterial activity. It is therefore possible that whilst the cellulose has contributed to greater heterogeneity overall in the soil, the viscosin and LPS have resulted in pockets of increased homogeneity in other areas of the soil volume. These pockets of localised homogeneity actually contribute to the overall heterogeneity of the soil volume, since soil pore heterogeneity is by

definition clumped, unordered distribution of pores. This overall effect is demonstrated by the increase in FD observed in the SM bacterial-control soil. Removal of the amphiphilic viscosin or LPS from the soil system in cycle A lead to a decrease in fractal dimension, which further supports the assertion these water-mobile moieties have been relocated away from the site of bacterial activity and the cellulose. This would seem to suggest that the cellulose actually plays the role of maintaining the soil structure and it is the other EC components that can implement restructuring and redistribution of the soil aggregates. Therefore, removal of cellulose from the soil system should result in the ability of the other components to implement a more homogeneous distribution of the porosity through redistribution of the aggregates. This was observed in the cellulose-deficient WS-4 system. Similarly, the presence of cellulose will maintain the structure of the soil in the environs of the bacterial niches, whilst the production of only one of the other EC components could lead to restructuring in the pores closest to the areas of cellulose binding rather than the farther reaching ability of higher concentrations of the amphiphilic compounds. This localised restructuring towards homogeneity, combined with the natural slaking of aggregates during a WD cycle in other areas of the soil not bound by bacterial cellulose, adding to the more uniform redistribution of pores would lead to an overall decrease in FD, as was observed in the *ViscA* and WS-5 soil cores in cycle A. Increased production of cellulose would be expected to lead to greater binding of the aggregates around the areas of bacterial growth and further afield than that expected in the SM bacterial-control system. This could reduce the ability of the viscosin or LPS to become mobile in the pore water

either through entrapment in the mesh, or bioclogging preventing water movement through pores, due to the greater volume of cellulose in the pore network. This would be expected to lead to simple maintenance of soil structure and therefore, no change in heterogeneity as measured by fractal dimension compared with the SM bacterial-control soil system. This was observed in the WS cellulose-overexpressing model system.

Turning the focus to cycle B of the experimental system, and as presented in the discussion of porosity, during cycle A the EC components will have undergone changes in terms of their spatial distribution within the pore network, micelles of viscosin or LPS could potentially be removed from the system altogether with water egress and bioclogging may lead to opening of pore necks under internal pressure and prevention of movement of the LPS and viscosin in the pore network. As such, the effects of the viscosin and LPS in the systems would be expected to be reduced, leading to less redistribution of the soil matrix towards a homogeneous structure and additionally, opening of pore necks could lead to a more heterogeneous distribution pattern being observed as $N(r)$ would decrease with decreasing distribution of void networks. Each of these effects would lead to restructuring towards greater heterogeneity in cellulose-containing systems and towards homogeneity in bioclogged systems containing LPS and viscosin. All of the soil systems in the study remained classified as heterogeneous in cycle B (all $FD > 2.7$), the trend from cycle A to B is that the bacteria-free control dH_2O , and cellulose and viscosin-containing systems (bacterial control SM, WS and WS-5) have decreased in heterogeneity, whereas the viscosin or cellulose deficient systems (*ViscA*

and WS-4) have increased in heterogeneity. Again it would seem that the presence of cellulose, viscosin and LPS together, playing opposite roles in the restructuring of the soil leads to no observed difference in overall physical measurements. The removal of any of these components individually brings about a significant response in cycle A for all deficient-model systems by way of an increase in porosity and heterogeneity for cellulose- and viscosin-deficient systems and a concurrent decrease in porosity and heterogeneity for the LPS-deficient system. Cycle B, whilst displaying a similar trend to cycle A, showed no significant difference in the cellulose- and viscosin-deficient systems for porosity or heterogeneity, but the LPS-deficient system maintained a significantly lower porosity and heterogeneity. This observation again points to a different behaviour and role for LPS in the structural organisation of soil or the possibility that the cell membranes of the WS-5 were easily disrupted causing earlier release of cell components and debris and less production of cellulose and viscosin into the soil system. Perhaps, rather than as suggested following the discussion from the point of view of just the porosity results, the LPS-deficient WS-5 system is effectively a WD cycle ahead of the other systems in terms of restructuring and further WD cycles would be required to establish the point at which steady state of structural properties is evident in the other model soil systems.

5.4.3 Aggregate scale soil structure

The measurements carried out on the destructively sampled 2 mm aggregates from the bacteria-free dH₂O control, SM bacterial-control and WS-4 cellulose deficient systems at the end of cycle B, were porosity, fractal dimension, pore size distribution and pore connectivity. Given the pattern of response observed for porosity and fractal dimension in the core samples where in the cycle B measurements the cellulose deficient soil system demonstrated greater porosity and heterogeneity, whilst no significant difference was observed between either the bacteria-free control dH₂O and SM systems, or the SM bacterial-control and WS-4 systems at both core and aggregate level, the aggregate patterns of porosity and heterogeneity were in opposition to those observed at the core level. This could suggest variability in the effects of the EC components at macro- and microaggregate levels. However, in the absence of statistical significance in this dataset, further investigation into possibly more aggregates and perhaps better image analysis given the advancement of the field would be of interest.

Additionally, the observation that aggregate porosity measurements were consistently approximately a third of the core porosity measurements led to the consideration that these sieved aggregates are largely composed of stones (<2 mm) rather than predominantly primary particles and microaggregates of soil. For purposes of true scaling investigations between macroaggregates and core scale soil volumes, it would perhaps be prudent to sieve the soil much smaller than 2 mm to eliminate stony interference and then through cultivation allow formation of macroaggregates and take core and aggregate samples from these cultivated systems.

For pore size distribution, the maximum pore size and mean pore size in aggregates was increased under SM bacterial legacy compared with the dH₂O control soil, and decreased in aggregates under WS-4 bacterial legacy compared with the SM control soil in cores that were sterilised by autoclaving. The greater the mean pore size reported by the pore size distribution measurement, the larger the number of larger pores in the soil sample. Smallest pore size class (5.54 µm) contained approximately 1/5th of the total observed porosity in all treatment types, with only the SM and WS-4 treatments showing any significant difference.

Since the dH₂O bacteria free control and WS-4 systems are cellulose deficient and as such would not be expected to have the mesh-like stabilising structure that would be present in the SM soil system, this observation concurs with the view that cellulose affects distribution of pores in the soil volume by binding particles more tightly and in doing so creates larger pores between the soil particles. The reason for this phenomenon only being observed in the autoclaved samples requires further investigation. However, this observation at the aggregate scale agrees with the view that impact of cellulose and other EC materials is predominantly at the microscale rather than the macroscale (Chenu, 1989; Chenu, 1993; Dorioz *et al.*, 1993; Tisdall, 1994; Six *et al.*, 2004; Chenu and Cosentino, 2011).

Porosity, fractal dimension and pore size distribution are important measurements when trying to understand soil structure and, in this study, the impact of bacteria on that soil structure. Taking this knowledge further towards understanding the impact of bacteria on the functionality of the pore network which controls and modulates water flow, and in turn the movement

of solutes, nutrients, microbes and gases through the soil profile, requires and understanding of the connectedness of the pores in the soil matrix. The connectivity of observed porosity for the aggregates samples has been reported as the proportion of total pore space contained in the largest 20 pores.

5.4.4 This research in context

As excellently reviewed by Chenu and Cosentino (2011), the impact of exopolymeric substances (EPS) on the stability of soil and soil aggregate formation has been the subject of many studies either looking at stimulation of the soil microflora via the introduction of metabolic substrates to the soil, introduction of microorganisms into sterile soil or soil models or selective inhibition of specific classes of microorganisms and comparison with untreated soil systems (Chenu (1989), Chenu and Guerif (1991), Tisdall (1994), Dorioz *et al.* (1993), Tisdall (1991), Tisdall *et al.* (1997), Puget (1999), Czarnes *et al.* (2000), Bossuyt *et al.* (2001), Six *et al.* (2004)). These studies look at the structure of soil empirically through hydrodynamic experiments, rather than quantitatively measuring the physical properties of the soil such as total porosity, pore size distribution or pore connectivity. Other studies simply look at aggregate formation and stability through the wet sieving method in which the soil submerged in water is sequentially sieved through meshes of decreasing size to fractionate the aggregates according to sieve size (De Gryze *et al.*, 2005). Of the studies that do measure the effects of EC components on the *in situ* structural indicators

quantitatively, the approach has generally been in 2D rather than 3D (Preston *et al.*, 1999; 2001). These studies are discussed in detail in **Chapter 6**, which looks at the impact of bacteria on the cracking patterns of soil. Studies that do look at the 3D structural changes of soil, such as those by De Gryze (2006), Papadopoulos (2008; 2009), Kravchenko (2011), and Tarquis (2009) are looking at the effects of organic matter (OM) concentrations or different tillage regimens. Similarly, whilst studies into the geometry of soil space architecture have gathered considerable momentum over the last 15 years (Vogel and Roth, 1998; Peat *et al.*, 2000; Young *et al.*, 2001; Johnson *et al.*, 2003; Feeney *et al.*, 2006b), focus has been on comparison of empirical measurements of structure through hydrodynamic analyses, effects of OM and tillage, or effect of addition of sewage sludge and biocides on aggregates (<3 mm) (Nunan *et al.*, 2006).

As far as this author is aware, the investigation of the effect of bacterial EC constituents on soil structure ascertained by *in situ* quantitative structural measurements in this study is novel.

5.4.5 Summary statement

The presence of bacteria in the soil capable of producing all three EC components of interest, cellulose, LPS and viscosin, does not affect observed porosity. However, they did cause an increase in fractal dimension indicating a more heterogeneous clumped and aggregated distribution of pores than in the bacteria-free control system. The use of mutants with individual deficiencies in key EC compounds resulted in lower porosity and

fractal dimension, indicating a physical rearrangement of aggregates and resulting in a more homogeneous distribution of pores. These observations agree with the hypothesis that viscosin, cellulose and LPS contribute to stabilisation of aggregates and that any loss of these compounds from the soil system will result in slaking and creation of greater numbers of smaller soil particles.

These measurements were made based on observed porosity $>15.3\ \mu\text{m}$, which in the context of this study mostly represents the meso- ($30\text{--}300\ \mu\text{m}$) to macropore ($>300\ \mu\text{m}$) range. In the synchrotron analysis ($5.54\ \mu\text{m}$ resolution) of $2\ \text{mm}$ aggregates, bacteria capable of producing all three key compounds of interest had no effect on porosity or fractal dimension compared with bacteria-free aggregates.

Similarly, no difference in porosity or fractal dimension was observed in the cellulose deficient aggregates compared with the bacterial control. The maximum pore size observed was unaffected by the presence of either bacterial treatment, and only the control bacteria treatment increased mean pore size, and only in the autoclaved sample group. Loss of cellulose from the aggregates resulted in a greater percentage of total porosity present in the smallest pore size class ($5.54\ \mu\text{m}$). However, this greater percentage of small pores is less well connected than in the bacteria control aggregates. Presence of the control bacteria did not affect pore connectivity compared with the bacteria-free control. Interestingly, individual evaluation of the largest 20 pores presents differences in the observed connected porosity between the test and control aggregates. In the aggregate studies, no pores

larger than 130 μm were observed, placing these findings in the micro- (<30 μm) to mesopore (30 - 200 μm) scale.

Bacteria have been shown to impact the physical structure of soil at the meso- and macropore level (>30 μm), and less so at the micropore level (<30 μm). Further investigation of these key components in the stabilisation of aggregates, physical restructuring of pores spaces and rearrangement of grains and particles in order to further understand the roles of the bacteria and their legacy is required.

5.5 Future work

There has been great debate in the field of image analysis focussed particularly around the subjects of thresholding algorithms and methodologies (Tarquis *et al.*, 2009; Baveye *et al.*, 2010) and these areas of concern are certainly important as the field moves forward and there is the need for parity amongst studies. However, in this work, the focus was on the differences between the bacteria-free and bacteria-treated soils. All thresholding, image processing and analyses were carried out by the same person and therefore, much of the possible variability in the analyses has been negated. One aspect of the CT data production that does warrant revisiting is the fact that not all samples in the SIMBIOS CT facility study were scanned and reconstructed at the same resolution. As addressed in the results section, the observations made in this study are relative quantifications of physical structure and as such differences between the different treatments are accepted, however for definitive quantitative

measurements reconstruction of all samples at the same resolution would be preferred. Future investigations of soil structure should be scanned at the same resolution or at the very least reconstructed at the same resolution to avoid this pitfall again.

Where the aggregate studies were limited by the availability of access to the beamline at the Argonne National Laboratories' Synchrotron facility, it would be interesting to revisit the samples in this study, analysing the three other treatments and then comparing results at the two different scales - micro- to mesopore, and meso- to macropore. Additional proposals to the triennial call for access requests, and ideally synchrotron-specific funding would facilitate this additional study.

As with the data for the hydrodynamic analyses in **Chapter 4** the data in this part of the study has, for the most part, only been presented and interpreted in this thesis using comparisons of the bacteria-free dH₂O treated and wild-type SM treated soil systems, and of the wild-type treated and mutant treated soil systems. However, the statistical analyses were designed so that pairwise comparisons were made between every permutation of the experimental design and whilst outwith the scope of this thesis, the data is available for future interpretation looking at the level of response of each of the bacterial strains against the dH₂O control soil and also against each other. A question that would be worth asking would be: Does the removal of any of the key legacy compounds negate the presence of the bacteria in terms of their effect on the structural organisation of the soil? This too would serve to inform bioremediation and bioaugmentation processes at the field scale.

The observations in this Chapter have looked at the impact of bacteria on the micro-, meso-, and macrostructure of the soil in terms of porosity, heterogeneity, pore size distribution and pore connectivity. Whilst upscaling to the millimetre and centimetre scale in 3D would have been the ideal scenario and indeed could prove to be a very interesting project for further work, a simple and less time-onerous method of investigating the impact of these bacteria on the biophysics of the soil is to use 2D analysis in the form of cracking plates as has been carried out for over 3 decades (Guidi *et al.*, 1978; Preston *et al.*, 2001; Baer *et al.*, 2009). By having a view of the impact of bacteria on soil structure through the scales a more comprehensive understanding of the effects of the compounds of interest can be built up and the possibility of extrapolation to larger scales can be investigated. Chapter 6 investigates the structural properties of the soil systems using cracking plate photography and image analysis.

Acknowledgement:

Portions of this work were performed at GeoSoilEnviroCARS (Sector 13), Advanced Photon Source (APS), Argonne National Laboratory. GeoSoilEnviroCARS is supported by the National Science Foundation - Earth Sciences (EAR-1128799) and Department of Energy - Geosciences (DE-FG02-94ER14466). Use of the Advanced Photon Source was supported by the U. S. Department of Energy, Office of Science, Office of Basic Energy Sciences, under Contract No. DE-AC02-06CH11357.

CHAPTER 6

6 Study on the effects of *Pseudomonas fluorescens* SBW25 and selected mutants on cracking structure in two sandy loam soils**6.1 Introduction**

Conditions for water flow, which governs the movement of solutes, nutrients, microbes and gases through the soil profile are not stationary material properties (Vogel *et al.*, 2005b). Even without physical or chemical interference, such as tillage or addition of manure or fertilisers, the natural wetting of soil through rain- and snowfall elicits pore structure changes due to the swell-shrink dynamics of the soil. As soil dries, cracks are formed having a significant impact on the soil processes of gas and water flow, and providing passageways for root development and microbial processes (Preston *et al.*, 2001). Shrinkage cracks in the soil are pores formed at the surface during drying and should not be confused with total porosity in soil (Velde, 1999).

Previous 2D cracking studies have demonstrated increasing soil aggregation upon addition of polysaccharides, or addition of microbial populations capable of polysaccharide production to the soil (Dhoot *et al.*, 1974; Preston *et al.*, 1999; Preston *et al.*, 2001) and studies into the different cracking behaviours of different soil types are well documented (Vogel and Kretzschmar, 1996; Velde, 1999; Ringrose-Voase *et al.*, 2000; Velde, 2001; Peng *et al.*, 2006; Li and Zhang, 2011). The study of 2D crack patterns in soil has recently become a numerical pursuit (Guidi *et al.*, 1978; Horgan and Young, 2000; Vogel *et al.*, 2005; Baer *et al.*, 2009) in order to develop a viable model for understanding soil fragmentation by drying.

Studies of the geometry of cracks in soil and muds usually take one of two approaches, the linear approach in which the crack patterns are skeletonised to be represented by constant-width intersecting lines, and the area approach in which the entire crack pattern is observed taking into account the width of cracks and their distribution. For consistency with the structural analyses in Chapter 5, the area approach was undertaken, and measurements of crack density (porosity), heterogeneity (fractal dimension analysis), and crack connectivity (pore connectivity) were taken. Pore size distribution equivalent analysis of crack distribution was not computationally possible at the time of data acquisition.

6.2 Chapter aims and research objectives

The aim of this research chapter is to ascertain the impact of bacteria and bacterial activity on the structure of soil as evidenced by their effects upon soil cracking. In this work, the term bacterial legacy is used to refer to all aspects of bacterial activity. Bacterial legacy consists of (i) exudate compounds produced by the bacteria and released into the immediate environment, (ii) cell debris released when bacteria die and (iii) the footprint left behind when a bacterium attaches to and detaches from a surface.

In order to determine if differences in the structural properties of the soil can be attributed to bacterial activity, poured plates of homogeneous soil slurries of two types of soil, Labfield and Bullionfield, that had been treated with different strains of *Pseudomonas fluorescens* SBW25 were dried and photographed. Physical measurements were taken from the processed images.

Research objectives:

1. Characterisation of the impact of the different bacterial legacies on the density of cracks in slurried soil upon drying.
2. Characterisation of the impact of the different bacterial legacies on the heterogeneity of cracks in slurried soil upon drying.
3. Characterisation of the impact of the different bacterial legacies on the connectivity of cracks in slurried soil upon drying.
4. Characterisation of the impact of soil type on the same properties in the presence of different bacterial legacies.

6.3 Results

In an experiment separate from, but related to, the soil core experiments presented in Chapters 4 and 5, soil from Labfield and Bullionfield experimental sites were inoculated with bacterial treatments, incubated for 2 weeks and then slurried by suspension and homogenisation in distilled water. Petri dishes (8.6 cm \varnothing) were used to create seven replicate plates of each treatment type. The slurried soils were carefully poured into the petri dishes and subjected to air-drying in a temperature controlled laboratory. Individual plates were photographed to obtain 2D greyscale images, which were then subject to binarisation, image processing and physical measurements to obtain data for crack density, heterogeneity and connectivity. Figure 6.1 illustrates the experiment process schematically for reference alongside the experimental design for Chapters 4 and 5.

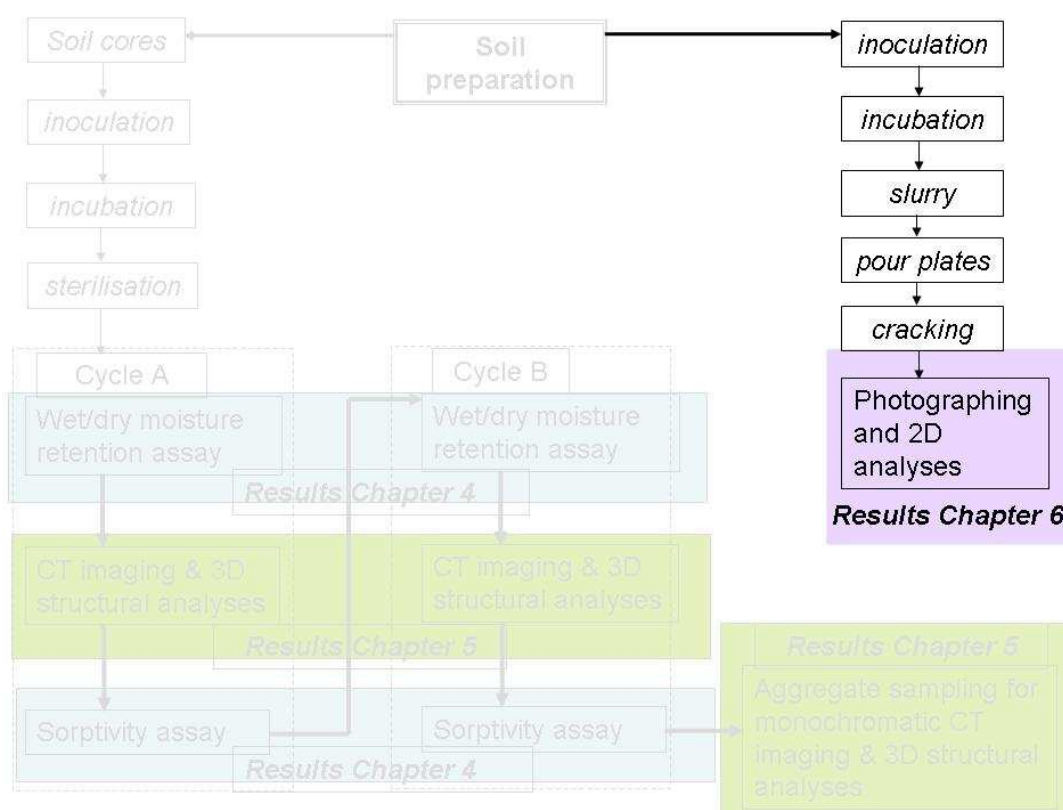


Figure 6.1 Schematic of experimental design highlighting 2D analysis

6.3.1 Soil cracking structure

6.3.1.1 Introduction

Air-dried slurries of Labfield and Bullionfield soils, equivalent to 25 g oven-dried soil per replicate petri dish plate, that had been treated with 5 strains of bacteria and bacteria-free dH₂O control were photographed and subjected to ImageJ processing (Rasband, W.S., ImageJ, U. S. National Institutes of Health, Bethesda, Maryland, USA, <http://rsb.info.nih.gov/ij/>, 1997-2007; version 1.39q) and subsequent SCAMP v1.1 analysis (SIMBIOS CT image Analysis and Manipulation Plug-in) to measure porosity (crack density), pore (crack) connectivity and fractal dimension (homogeneity of crack distribution). The porosity measurement provides a value for crack density

and pore connectivity determination provides a measure of crack connectivity. Fractal dimension determination provides a measure of the heterogeneity of crack distribution, in the experimental plates. Figure 6.2 illustrates typical cracking patterns generated under different treatments on the two soil types.

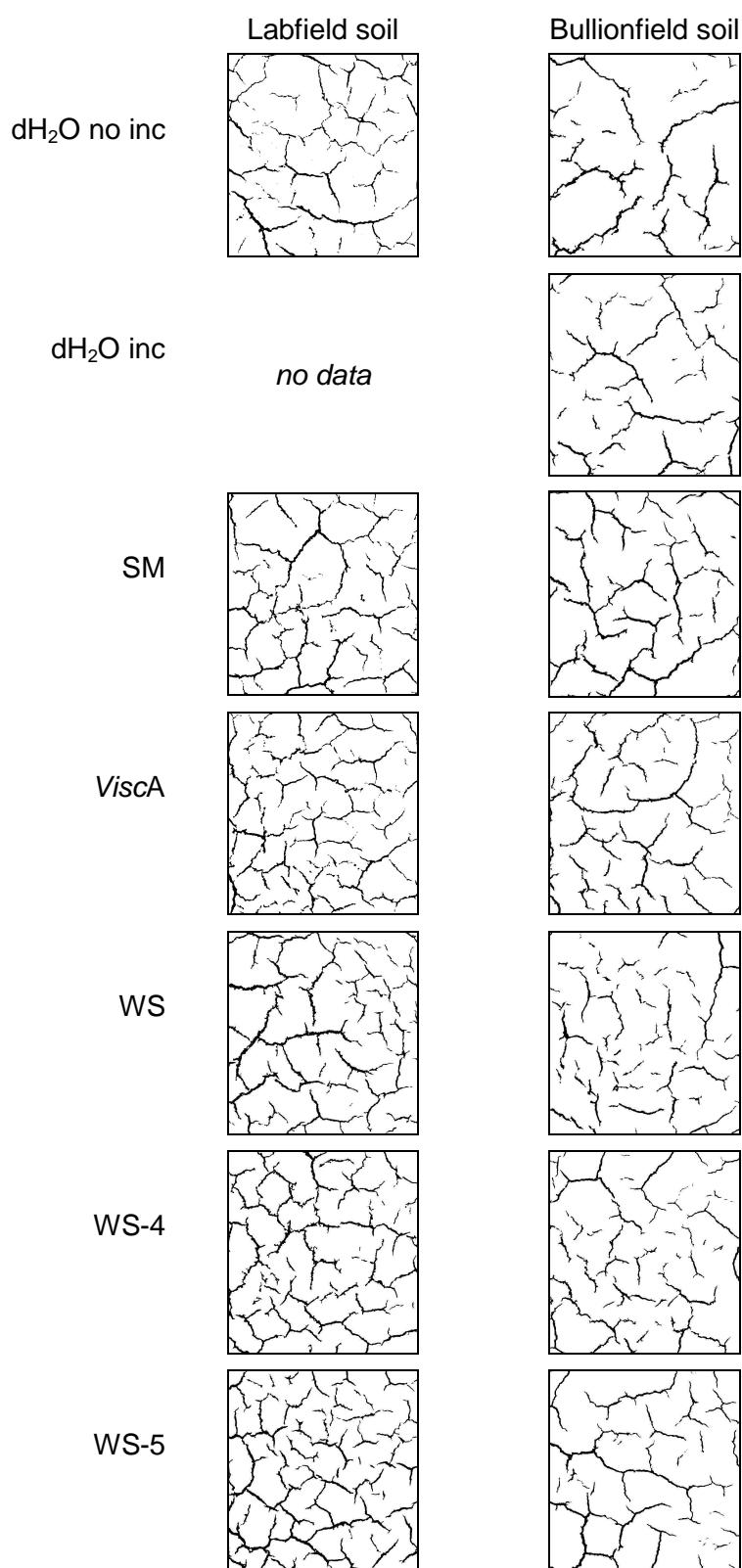


Figure 6.2 Typical cracking patterns for Labfield and Bullionfield soils under different treatment types. dH₂O no inc = unincubated control soil, dH₂O inc = incubated control soil. No data is available for Labfield-dH₂O inc as the slurry bag burst during the homogenisation process.

6.3.1.2 Investigation of the impact of bacteria on crack density

In order to assess the impact of bacteria on the formation of cracks in air-dried, slurried soil, porosity measurements were taken on binarised 2D photographic images of the treated soil plates (pore pixels = black, soil pixels = white). Tests of model effects indicated necessary splitting of the data by soil type or by treatment type ($p < 0.001$). In the first instance, the analysis was split by soil type to assess the impact of bacterial treatment on the soil with respect to treatment controls. Mean crack density for each treatment type is shown in Figure 6.3 and the results of the pairwise comparison of treatment types in each soil type are shown in Table 6.1.

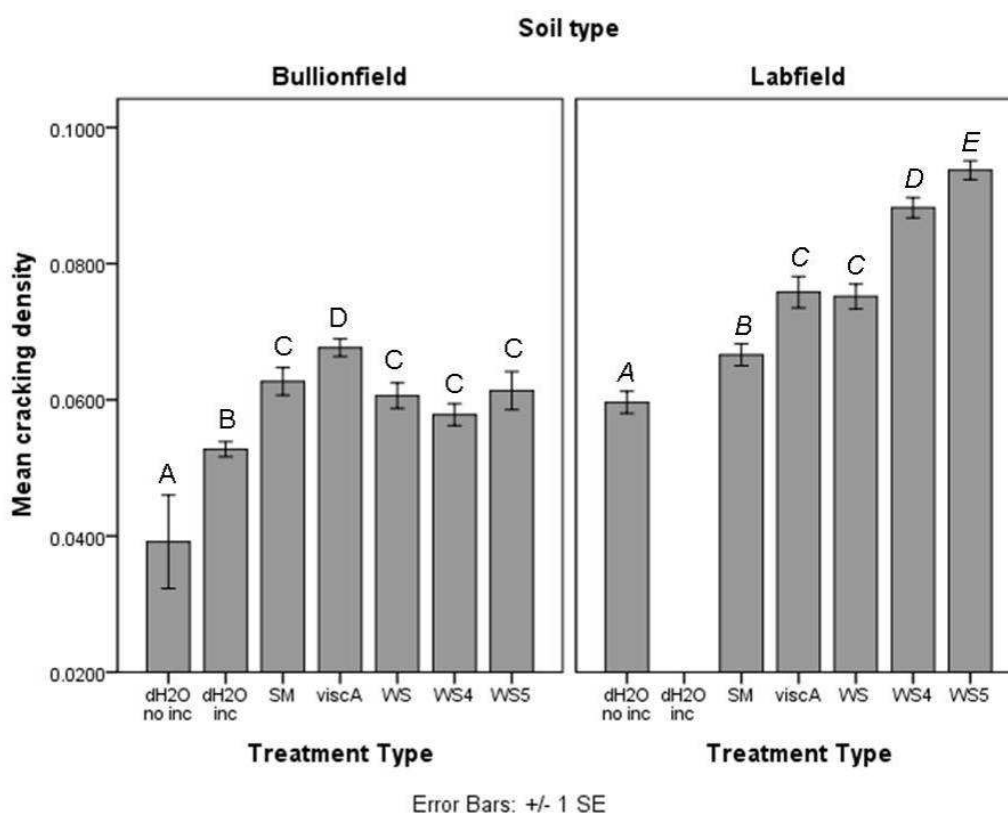


Figure 6.3 Comparison of different bacterial treatments on the crack density of two sandy loam soils. Mean crack density is shown for experimental cracking plates of two different soil types under different bacterial treatments. Statistical differences between the measured crack density for the treatment types within each soil type are shown ($p < 0.05$). No analysis between soil types is shown in this figure. ABCD refer to Bullionfield soil only; *ABCDE* refer to Labfield soil only. No data is available for Labfield dH₂O incubated (dH₂O inc) treatment. dH₂O no inc = not incubated soil control. Error bars were calculated as the standard error of the means of each treatment type ($n = 7$).

Table 6.1 Pairwise comparison of the effect of bacterial treatment type on crack density for Bullionfield and Labfield soils

		Crack density	
		Bullionfield	Labfield
pairwise treatment types	dH ₂ O no inc vs. dH ₂ O inc	↑ 0.020	<i>no data</i>
	dH ₂ O inc vs. SM	↑ < 0.001	<i>no data</i>
	SM vs. mutants	<i>see below</i>	<i>see below</i>
	SM vs. <i>ViscA</i>	↑ 0.040	↑ 0.002
	SM vs. WS	0.506	↑ < 0.001
	SM vs. WS-4	0.127	↑ < 0.001
	WS vs. WS-4	0.121	↑ < 0.001
	SM vs. WS-5	0.625	↑ < 0.001

Bold type indicates statistical significance ($p < 0.05$); ↓ indicates decreased crack density compared with control; ↑ indicates increased crack density compared with control; first term in treatment type column indicates control for comparison

In the Bullionfield soil, incubation alone was observed to lead to higher crack density and treatment with the bacteria (SM) demonstrated higher again crack density. Only the *ViscA* mutant bacteria treatment demonstrated a significantly different (higher) crack density than the SM bacterial control plates. In the Labfield analysis there is no data for the dH₂O incubated plates as the bag burst in the stomacher following the 2 week incubation. All of the mutant strains showed higher crack density compared with the SM bacterial control, and the cellulose-deficient WS-4 treated soil showed higher crack density than the cellulose overexpressing WS treated soil.

Following this, the analysis was split by treatment type to assess the effect of soil composition on the impact of bacterial treatment on the soil. Mean crack density for each treatment type is shown in Figure 6.4 and the results of the pairwise comparison of soil types within each treatment type are shown in Table 6.2.

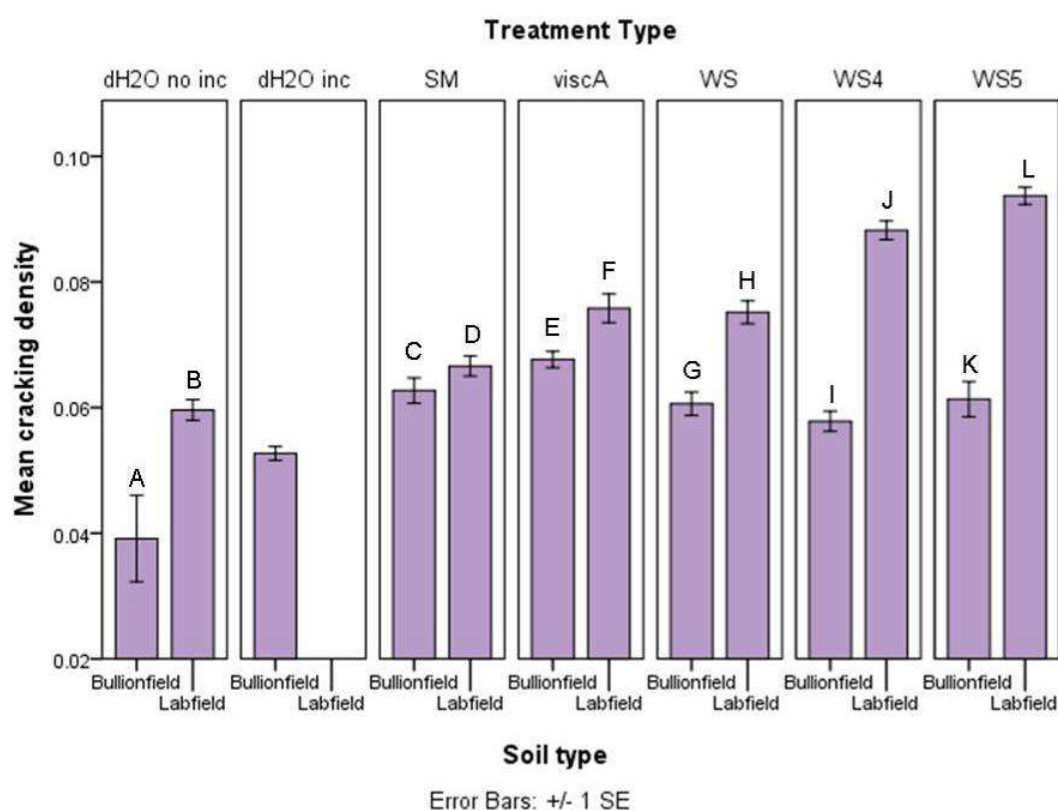


Figure 6.4 Comparison of crack density in two sandy loam soils with different bacterial legacies. Mean crack density is shown for experimental cracking plates of two different soil types under different bacterial treatments. Statistical differences between the measured crack density for the soil types within each treatment type are shown ($p < 0.05$). No analysis between treatment types is shown in this figure. AB, CD, EF, GH, IJ and KL refer to statistically significant difference in disparate analyses. No data is available for Labfield dH₂O incubated (dH₂O inc) treatment. dH₂O no inc = unincubated soil control. Error bars were calculated as the standard error of the means of each treatment type ($n = 7$).

Table 6.2 Pairwise comparison of the effect of soil type on the crack density of soils under different bacterial treatments

pairwise soil type		
Bullionfield vs. Labfield		
Crack density	dH₂O no inc	↑ < 0.001
	dH₂O inc	<i>no data</i>
	SM	↑ 0.010
	ViscA	↑ 0.002
	WS	↑ < 0.001
	WS-4	↑ < 0.001
	WS-5	↑ < 0.001
Bold type indicates statistical significance ($p < 0.05$); ↓ indicates decreased crack density compared with Bullionfield; ↑ indicates increased crack density compared with Bullionfield		

Labfield soil demonstrated a consistently higher crack density than Bullionfield soil under all treatment types.

6.3.1.3 Investigation of the impact of bacteria on crack heterogeneity

In order to assess the impact of bacteria on the distribution of cracks in air-dried, slurried soil, fractal dimension measurements were taken on 2D photographic images of the treated soil plates. Tests of model effects indicated necessary splitting of the data by soil type or by treatment type ($p < 0.001$). In the first instance, the analysis was split by soil type to assess the impact of bacterial treatment on the soil with respect to treatment controls. Mean crack heterogeneity for each treatment type is shown in Figure 6.5 and the results of the pairwise comparison of treatment types in each soil type are shown in Table 6.3.

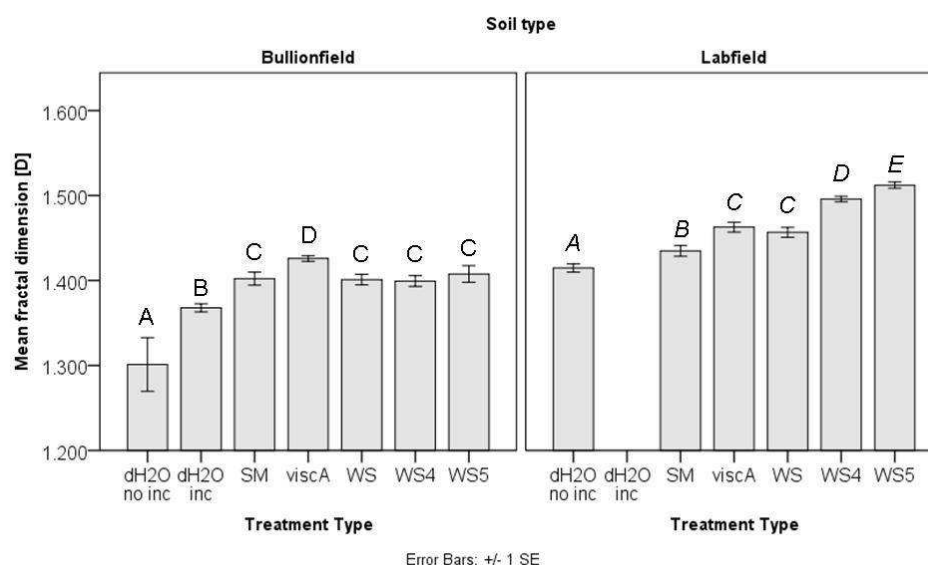


Figure 6.5 Comparison of different bacterial treatments on the fractal dimension of cracking patterns in two sandy loam soils. Mean fractal dimension is shown for experimental cracking plates under different bacterial treatments. Statistical differences between the fractal dimensions for the treatment types within each soil type are shown ($p < 0.05$). No analysis between soil types is shown in this figure. ABCD refer to Bullionfield soil only. ABCDE refer to Labfield soil only. No data is available for Labfield dH₂O incubated (dH₂O inc) treatment. dH₂O no inc = not incubated soil control. Error bars were calculated as the standard error of the means of each treatment type ($n = 7$).

Table 6.3 Pairwise comparison of the effect of bacterial treatment type on crack heterogeneity for Bullionfield and Labfield soils

		Crack heterogeneity	
		Bullionfield	Labfield
pairwise treatment types	dH ₂ O no inc vs. dH ₂ O inc	↑ 0.013	<i>no data</i>
	dH ₂ O inc vs. SM	↑ < 0.001	<i>no data</i>
	SM vs. mutants	<i>see below</i>	<i>see below</i>
	SM vs. <i>ViscA</i>	↑ 0.002	↑ < 0.001
	SM vs. WS	0.924	↑ < 0.001
	SM vs. WS-4	0.815	↑ < 0.001
	WS vs. WS-4	0.809	↑ < 0.001
	SM vs. WS-5	0.584	↑ < 0.001

Bold type indicates statistical significance ($p < 0.05$); ↓ indicates decreased crack heterogeneity compared with control; ↑ indicates increased crack heterogeneity compared with control; first term in treatment type column indicates control for comparison

Although the fractal dimensions of the crack patterns is predominantly in the homogeneous range, the results are presented as heterogeneity as the control groups demonstrate lower fractal dimension (lower heterogeneity) than the test subjects, therefore the observation is that the test subjects have increased heterogeneity where statistical significance is observed.

As with the crack density observations, in the Bullionfield soil, incubation alone was observed to lead to higher crack heterogeneity and treatment with the bacteria (SM) demonstrated higher again crack heterogeneity. Only the *ViscA* mutant bacteria treatment demonstrated significantly different (higher) crack heterogeneity than the SM bacterial control plates. In the Labfield analysis there is no data for the dH₂O incubated plates as the bag burst in the stomacher following the 2 week incubation. All of the mutant strains showed higher crack heterogeneity

compared with the SM bacterial control, and the cellulose-deficient WS-4 treated soil showed higher crack heterogeneity than the cellulose overexpressing WS treated soil.

Following this, the analysis was split by treatment type to assess the effect of soil composition on the impact of bacterial treatment on the soil. Mean crack heterogeneity for each treatment type is shown in Figure 6.6 and the results of the pairwise comparison of soil types within each treatment type are shown in Table 6.4.

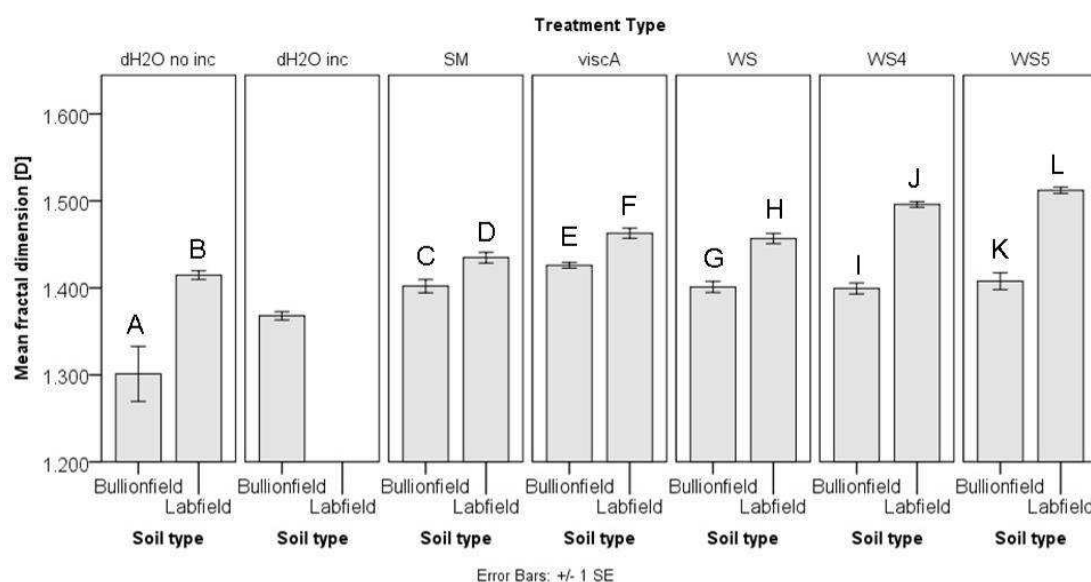


Figure 6.6 Comparison of the fractal dimension of cracks in two sandy loam soils with different bacterial legacies. Mean fractal dimension is shown for experimental cracking plates of two different soil types under different bacterial treatments. Statistical differences between the measured fractal dimensions for the soil types within each treatment type are shown ($p < 0.05$). No analysis between treatment types is shown in this figure. AB, CD, EF, GH, IJ and KL refer to statistically significant difference in disparate analyses. No data is available for Labfield dH₂O incubated (dH₂O inc) treatment. dH₂O no inc = unincubated soil control. Error bars were calculated as the standard error of the means of each treatment type ($n = 7$).

Table 6.4 Pairwise comparison of the effect of soil type on the heterogeneity of soils under different bacterial treatments

pairwise soil type		
Bullionfield vs. Labfield		
Crack Heterogeneity	dH₂O no inc	↑ < 0.001
	dH₂O inc	<i>no data</i>
	SM	↑ < 0.001
	ViscA	↑ < 0.001
	WS	↑ < 0.001
	WS-4	↑ < 0.001
	WS-5	↑ < 0.001

Bold type indicates statistical significance ($p < 0.05$); ↓ indicates decreased crack heterogeneity compared with Bullionfield; ↑ indicates increased crack heterogeneity compared with Bullionfield.

Again, as with the observations with the crack density, Labfield soil consistently demonstrated higher fractal dimension, greater heterogeneity, than the Bullionfield soil.

6.3.1.4 Investigation of the impact of bacteria on crack connectivity

In order to assess the impact of bacteria on the distribution of cracks in air-dried, slurried soil, crack connectivity measurements were taken on 2D photographic images of the treated soil plates. The total percentage of reported crack density observed in the largest 20 cracks is presented. Tests of model effects indicated necessary splitting of the data by soil type or by treatment type ($p < 0.001$). In the first instance, the analysis was split by soil type to assess the impact of bacterial treatment on the soil with respect to treatment controls. Mean total percentage connectivity for each treatment

type is shown in Figure 6.7 and the results of the pairwise comparison of treatment types in each soil type are shown in Table 6.5.

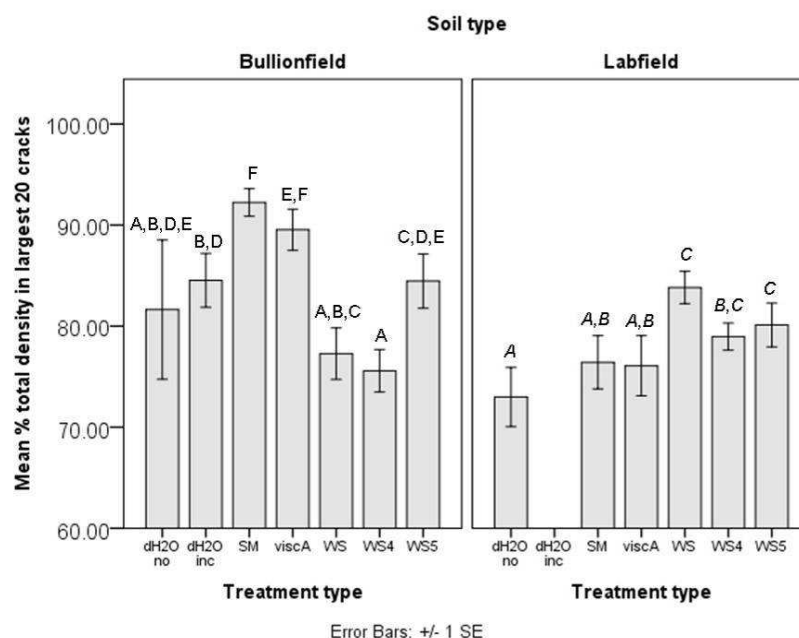


Figure 6.7 Comparison of different bacterial treatments on the connectivity of cracking in two sandy loam soils. Mean percentage of total crack density in the largest 20 cracks is shown for experimental cracking plates under different bacterial treatments. Statistical differences between the connectivity for the treatment types within each soil type are shown ($p < 0.05$). No analysis between soil types is shown in this figure. ABCDEF refer to Bullionfield soil only. ABC refer to Labfield soil only. No data is available for Labfield dH₂O incubated (dH₂O inc) treatment. dH₂O no inc = not incubated soil control. Error bars were calculated as the standard error of the means of each treatment type ($n = 7$).

Table 6.5 Pairwise comparison of the effect of bacterial treatment type on crack connectivity for Bullionfield and Labfield soils

		Crack connectivity	
		Bullionfield	Labfield
pairwise treatment types	dH ₂ O no inc vs. dH ₂ O inc	0.674	<i>no data</i>
	dH ₂ O inc vs. SM	↑ 0.030	<i>no data</i>
	SM vs. mutants	<i>see below</i>	<i>see below</i>
	SM vs. <i>ViscA</i>	0.301	0.928
	SM vs. WS	↓ < 0.001	↑ 0.022
	SM vs. WS-4	↓ < 0.001	0.363
	WS vs. WS-4	0.576	0.062
	SM vs. WS-5	↓ 0.002	↑ 0.013

Bold type indicates statistical significance ($p < 0.05$); ↓ indicates decreased connectivity compared with control; ↑ indicates increased connectivity compared with control; first term in treatment type column indicates control for comparison

Analysis of crack connectivity demonstrated much more variation in response compared with the crack density and heterogeneity analyses. In Bullionfield soil, no difference in connectivity was observed between the unincubated and incubated bacteria-free dH₂O control plates. SM soil showed greater connectivity than the dH₂O incubated control and whilst *ViscA* had no difference in connectivity compared with the SM control plates, the cracks in WS, WS-4 and WS-5 treated plates were less well connected than the SM control plates. In the Labfield soil, only the WS and WS-5 treated plates showed significantly different (increased) crack connectivity than the SM control plate.

Subsequently, the analysis was split by treatment type to assess the effect of soil composition on the impact of bacterial treatment on the soil. Mean crack heterogeneity for each treatment type is shown in Figure 6.8 and

the results of the pairwise comparison of soil types within each treatment type are shown in Table 6.6.

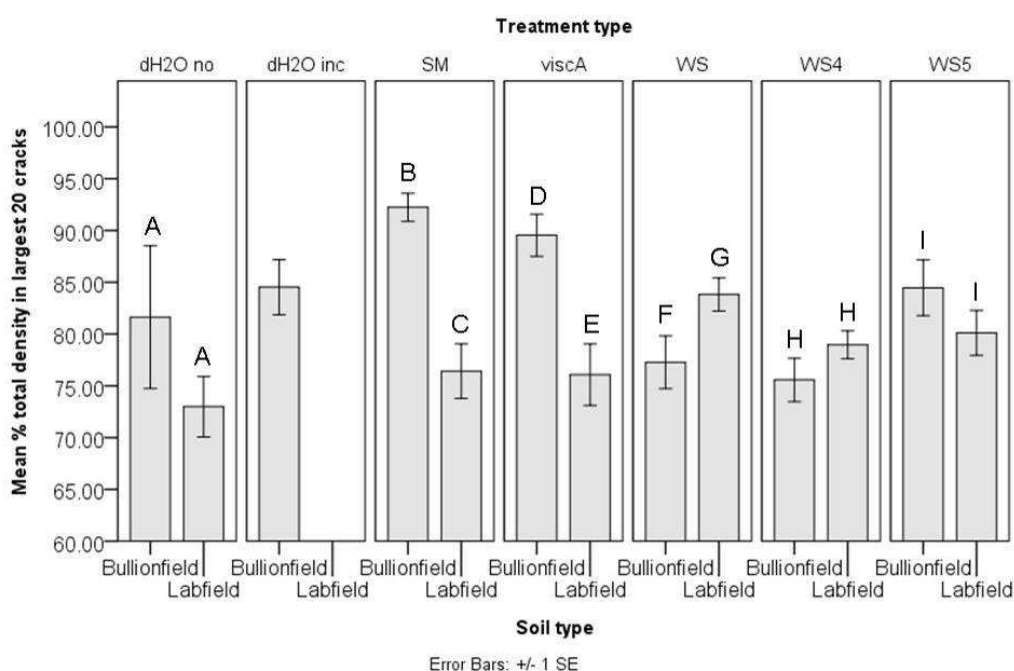


Figure 6.8 Comparison of the connectivity of cracks in two sandy loam soils with different bacterial legacies. Mean percentage of total crack density in the largest 20 cracks is shown for experimental cracking plates of two different soil types under different bacterial treatments. Statistical differences between the measured connectivity of the soil types within each treatment type are shown ($p < 0.05$). No analysis between treatment types is shown in this figure. A, BC, DE, FG, H and I refer to statistically significant difference in disparate analyses. No data is available for Labfield dH₂O incubated (dH₂O inc) treatment. dH₂O no inc = unincubated soil control. Error bars were calculated as the standard error of the means of each treatment type ($n = 7$).

Table 6.6 Pairwise comparison of the effect of soil type on the connectivity of soils under different bacterial treatments

pairwise soil type		
Bullionfield vs. Labfield		
Connectivity	dH ₂ O no inc	0.093
	dH ₂ O inc	<i>no data</i>
	SM	↓ < 0.001
	ViscA	↓ < 0.001
	WS	↑ < 0.001
	WS-4	0.136
	WS-5	0.051

Bold type indicates statistical significance ($p < 0.05$); ↓ indicates decreased crack connectivity compared with Bullionfield; ↑ indicates increased crack connectivity compared with Bullionfield.

Differences between the crack connectivity of the two soil types were only observed in the SM, *ViscA* (both less well connected in the Labfield soil) (better connected in the Labfield soil) and WS treated plates.

6.3.1.5 Summary of the impact of bacteria on soil cracking structure

The analysis of dried slurries of two different soil types under different treatment regimes has shown that both soil type and treatment type have an effect on the resulting cracking structure. The incubation process alone of the soil caused an increase in crack density and heterogeneity in Bullionfield soil and, in comparison to the bacteria-free control soil, addition of bacteria capable of producing cellulose, LPS and viscosin caused an increase in crack density and heterogeneity (data for Labfield soil was not available). In comparison with the bacterial control soil and with the exception of the soil treated with the surfactant deficient mutant, Bullionfield soil crack density and heterogeneity were not affected by the presence of the mutant bacteria. On the other hand, density and heterogeneity of cracks in Labfield soil were increased by all of the mutant bacteria treatments. Where bacteria capable of producing LPS, cellulose and viscosin increased crack connectivity, component-deficient mutant bacteria decreased crack connectivity in Bullionfield soil. In the Labfield soil, only the cellulose-overexpressing and LPS deficient mutants affected crack connectivity.

In the comparison of the two soil types, the Labfield soil consistently demonstrated higher crack density and heterogeneity than the Bullionfield soil. Crack connectivity was not affected by soil type in the bacteria-free unincubated, cellulose-deficient and LPS deficient treatment types. However, Labfield soil was less well connected in the presence of the bacterial control and surfactant deficient treatment type and better connected in the presence of the cellulose overexpressing treatment type. A summary overview of responses for cracking structure in the presence of bacteria is presented in Table 6.7.

Table 6.7 Summary overview of changes in soil crack structure in the presence of different bacterial treatment types.

Bacterial treatment type	Crack property	Soil type	
		Bullionfield	Labfield
SM	density	↑	<i>no data available</i>
	heterogeneity	↑	
	connectivity	↑	
ViscA	density	↑	↑
	heterogeneity	↑	↑
	connectivity	-	-
WS	density	-	↑
	heterogeneity	-	↑
	connectivity	↓	↑
WS-4	density	-	↑
	heterogeneity	-	↑
	connectivity	↓	-
WS-5	density	-	↑
	heterogeneity	-	↑
	connectivity	↓	↑

↓ indicates a decrease in the measured property; ↑ indicates an increase in the measured property; - indicates no change in the measured property. SM is compared against the bacteria-free dH₂O inc control. The mutants are compared

against the bacteria-control SM.

6.4 Chapter discussion

6.4.1 Introduction

Two types of sandy loam soil, Labfield and Bullionfield from experimental sites at The James Hutton Institute (Invergowrie, Scotland, UK) were sieved, incubated, slurried and poured into replicate petri-dish plates to test the impact of bacterial treatment on the structure of surface cracking in air-dried soils. The bacteria-free dH₂O controls were distilled water treatments, one set underwent the same conditions as the bacterial treatments and a second set were left unincubated to provide information about the effect of the incubation process on crack structure formation. Seven replicates per treatment per soil type were photographed and the images processed and analysed for crack density, fractal dimension and connectivity, comparing treatment types within soil types and also soil types within treatment types for differences.

Laboratory studies of surface cracking properties often give different results to those observed in the field (Velde, 1999). Whilst laboratory preparation procedures may eradicate some of the variables experienced in nature, in this study the focus was on the individual effects of key EC components on the structure of soil cracking and therefore effacing additional variables is desirable. In the laboratory it is possible to control lighting conditions so as to evenly photograph the cracking patterns without introduction of shadows. However, in the field, changing light and surface

irregularities can create challenges to subsequent image processing that relies on differentiating soil and pore space by way of binarisation of greyscale images to black and white. As such, it is pertinent to ascertain the best situation for the experimental question at hand. The requirement of this study was that the only variable should be the soil type or the treatment type and this was achieved.

Crack density is a measure of the porous proportion of the soil surface in relation to the whole soil volume. The distribution of the cracks (heterogeneity) is determined using the box-counting fractal dimension, which is obtained as the slope of the log-transformed equation for fractal dimension (as illustrated in Figure 3.15, Section 5.3.1.2). Crack connectivity provides additional information about how well connected the cracks are in the soil volume.

6.4.2 Discussion

In vitro SM is capable of producing all of the compounds of interest, viscosin in late exponential (logarithmic) phase, cellulose and LPS. Of the mutant strains, *ViscA* is incapable of viscosin production, WS is a cellulose overproducer, WS-4 is cellulose deficient, and WS-5 is LPS deficient.

The behaviours of the extracellular (EC) components produced by the bacteria would be expected to have the same effects on crack formation as they do on porosity in the 3D structure. However, it is important to remember that cracks are surface connected structures and therefore, do not represent the totality of the porosity in the soil volume. In terms of binding agents, cellulose and lipopolysaccharide are classed as transient according to the system of Tisdall and Oades (1982) and viscosin is considered an aggregate

destabiliser, as it would be expected to reduce the natural waterproofing of the soil as originally described by Martin *et al.* (1955). The addition of carbohydrate substrates or polysaccharides, in particular cellulose, to soil has long been shown to increase soil aggregation (Dhoot *et al.*, 1974), whilst the addition of specific polysaccharides has been shown to increase the connectivity of cracks and increase the irregularity of their distribution (Preston *et al.*, 2001). Figure 6.9 illustrates the cracking patterns observed by Preston *et al.* (2001) and the measured crack heterogeneity.

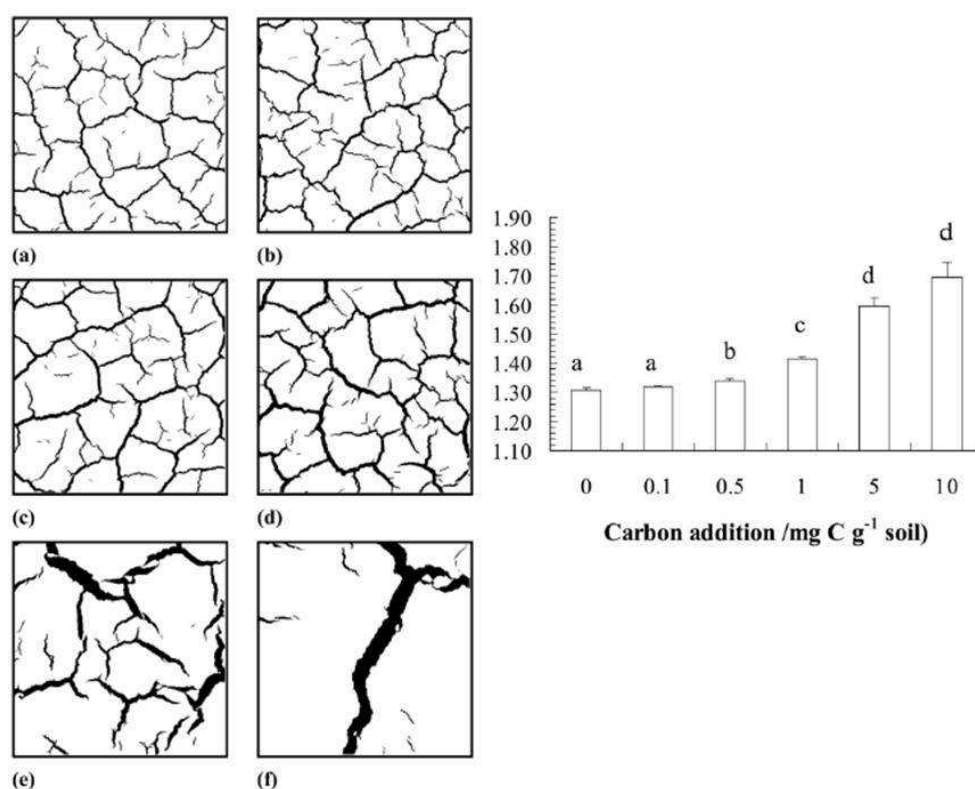


Figure 6.9 Typical cracking patterns generated under different carbon additions: (a) 0 control, (b) 0.1, (c) 0.5, (d) 1.0, (e) 5.0 and (f) 10 mg C g⁻¹ soil, and the accompanying graph of crack heterogeneity (+1 SEM is indicated). Different letters denote significant differences ($p < 0.05$). From Fig.1 and Fig.2 Preston *et al.* (2001).

The overall observations from this cracking structure study were that the presence of any of the control or mutant bacteria in the soil increased

crack density and heterogeneity in Labfield soil, but only in the bacteria control and surfactant deficient treatments in the Bullionfield soil. Cracking connectivity was largely unaffected in the Labfield soil, but increased in the bacteria control soil, and decreased in the bacteria mutant soils. Looking at the increased aggregation, connectivity and homogeneity of cracks described above for the addition of polysaccharides or cellulose to soil, the observations in this study are in agreement in terms of the crack density measurements, but not in terms of the connectivity or heterogeneity measurements, thus indicating a role for the other EC components viscosin and LPS in affecting soil structure. The presence of cellulose, viscosin and LPS, such as in the SM soil plates, has increased connectivity in the Bullionfield soil (no comparative data is available for the Labfield soil), but the WS soil plates (representative of cellulose overexpression) shows an increased connectivity in the Labfield soil, but a decreased connectivity in the Bullionfield soil. This same conflicting observation is seen in the cellulose deficient WS-4 and LPS deficient WS-5 soils. It is apparent that the soil type and its composition must be taken into account. Labfield is a Macmerry series Eutric cambisol (organic matter, 6.3%; sand, 59%; silt, 34%; clay, 7%) (Hallett and Young, 1999), and Bullionfield is a Carpow series Eutric cambisol (organic matter, 2.6%; sand, 71%; silt, 19%; clay, 10%; pH 6.2) (Harris *et al.*, 2002a). Organic matter (OM) is important in aggregate binding and stabilisation and also is the primary source of metabolic substrates for microbes in the soil. This would be particularly true in the laboratory manipulated soil, as other decomposing matter would have been removed by the preparation process. As the introduced bacteria grow and reproduce,

levels of available organic matter would be expected to decrease, thereby destabilising the soil and leading to greater breakdown of the aggregated structure and greater observed porosity (cracks). This phenomenon was observed in all of the Labfield plates, but only in the bacteria control and surfactant deficient Bullionfield plates. Labfield has 2.5 times the amount of OM of Bullionfield which could account for the consistent increase in crack density seen in Labfield soil. With higher levels of OM for metabolism by the bacteria, a greater bacterial presence would be expected in the Labfield soil, which was also observed by Preston *et al.* (2001). In Bullionfield soil, the cracks were more regularly distributed over the surface indicating greater stability in the aggregation of soil particles. Sand and clay proportions are higher in Bullionfield soil than in Labfield soil, and silt proportion is much higher in Labfield than in Bullionfield soil, which would undoubtedly influence the binding properties of the soil even prior to bacterial amendment. These effects were observed in the unincubated bacteria-free control plates which showed higher crack density and heterogeneity in the Labfield soil compared with the Bullionfield soil, but lower connectivity of cracks in the Labfield soil. What these observations show is that when considering the impact of bacteria and their legacy on the physical structure of soil, it is imperative that the soil type is taken into account. A greater understanding of the chemical bonding between different soil type grains and the EC components of bacteria and the bacteria themselves is crucial to predicting the influence of bacteria on soil aggregation and stabilisation.

These preliminary investigations into the effect of bacteria on cracking of soil upon drying were limited in replicate number due to time constraints. All of the replicate plates in this part of the study were poured from one inoculation of each treatment type. For conclusive determination of the effects of the treatments on the soil, replicate treatments should also be undertaken.

6.5 Future work

These investigations using the same bacterial treatments on different soil types have raised interesting questions about the effects of soil type on the impact of the bacteria on the physical properties. In order to elucidate the interactions of the different soil components with the bacteria, the use of a single soil type and a single bacteria type could serve as a control. Then by amending percentages of soil components in that soil and observing the changes in physical properties due to these differences would allow a better understanding of the interactions between soil components and the bacteria. This could then be repeated for each bacterial mutant in order to elucidate the individual bacterial legacy components' roles in soil aggregation and stabilisation. Additionally quantification of bacterial populations in the soils at given times would be useful in predicting the relative concentration of bacterial components in the soil would add further information to the understanding of what is happening in the soil in the presence of these bacteria.

7 Discussion and conclusions

The aims of this study were to examine the impact that bacteria have on soil. Using soil inoculated with different strains of *Pseudomonas fluorescens* SBW25 with particular properties in the production of specific materials (cellulose, LPS and viscosin) moisture release curves and sorptivity analyses were used to determine changes in water retention and flow. 3D X-ray computed tomography (XCT) and 2D surface-crack pattern analysis were used to elucidate changes in the physical properties of the pore networks. The hypothesis was that bacteria and bacterial legacies affect the biophysics of water retention and flow in soil. These observed changes would hence, be due to the presence of the bacteria and their extra-cellular components in the pore networks affecting the polarity of the solid phase and physically interfering with water flow by blocking narrow pore passages. Their chemical properties would also affect aggregate stability and result in the structural rearrangement of the soil matrix. Chapter 4 investigated the wetting and drainage behaviour of the soil through hydrodynamic analysis. Chapter 5 investigated the structure of soil after wetting - drying cycles and in Chapter 6 the fragmentation of the soil surface upon drying was investigated.

7.1 The behaviour of bacteria in soil

In this work bacteria have been shown to reduce the wettability of soil leading to a reduction in water content at saturation. Upon drainage, soil containing bacteria retains water to greater effect than bacteria-free soil. The

absence of the key extra-cellular components cellulose, lipopolysaccharide and the surfactant viscosin in the soil system results in destabilisation of the soil aggregate structure and decreased pore connectivity. A less well connected pore space creates a greater number of distinct, protective microenvironments within a soil volume. In an unsaturated porous medium these microenvironments are connected only by thin films of water, which not only restrict or prevent motility of microorganisms, but also limit solute diffusive fluxes. What this implies is that competitive Darwinian survival-of-the-fittest rules do not necessarily apply in these microenvironments and that this contributes to the huge diversity of microbial life in the vadose zone (Long and Or, 2005; Dechesne *et al.*, 2008; Carson *et al.*, 2010).

This study showed that the different strains of bacteria will differentially influence their environment to restructure the aggregate organisation through destabilisation, thus affecting water availability in the microenvironments. Carson *et al.* (2010) showed that low pore connectivity created by low water potential and therefore low water content resulted in greater bacterial diversity in soil. Having used decreasing water potential in a hanging column setup to create low pore connectivity, their pore connectivity is demonstrative of water-connected porosity (wet >306 μm , to dry >51 μm). Competitiveness of species in the wetter, water-connected pores of the Carson *et al.* (2010) setup meant that diversity was decreased in these areas. There was no species or strain competitiveness in the study in this thesis as each replicate soil sample was inoculated with a separate strain. Nor were there any textural differences in the soil samples between replicates. Therefore changes in soil physical properties in terms of structure

and hydrodynamic responses were attributable only to the bacteria. Additionally, pore connectivity in this study was physically measured in pores of $>5.4\ \mu\text{m}$ (aggregate scale) in dry soil and therefore water-connection of pores was not under investigation. Nevertheless, both studies, from micro- to macroscale and using different methodologies to determine physical parameters, show that poorly connected soils creating spatially isolated microenvironments within the soil are conducive to bacterial diversity and survival. In this study, the presence of bacteria destabilised the aggregates creating a greater proportion of smaller grains and decreased water content. This raises the question: Are bacteria architects of their own environment?

This study incubated sterilised soil with a bacterial strain for two weeks at one moisture content level. Carson *et al.* (2010) incubated unsterilised soil for 1 week at a range of water contents within a 55 cm column. Greater bacterial diversity was observed in the drier, less well connected pores and therefore, there would be greater amounts of extracellular components expected in these spatially distinct pores. Drawing on the observations from the study in this thesis, the aggregates in the Carson *et al.* (2010) experiment would be expected to be stabilised by the presence of bacteria capable of production of the full complement of extracellular components (albeit not all bacteria produce surfactants). This appears to be consistent with the observations by scanning electron microscopy SEM (Figure 7.1), where there is no change to the textural structure of the individual column setups following incubation. In this thesis, the destabilisation of the aggregates by the mutant bacterial strains is proposed to have occurred during the wet-dry cycles following incubation,

and in fact, the restructuring would be comparable to the quartz only soil representing the 'before destabilisation' and the silt+clay soil representing the 'after destabilisation' structures.

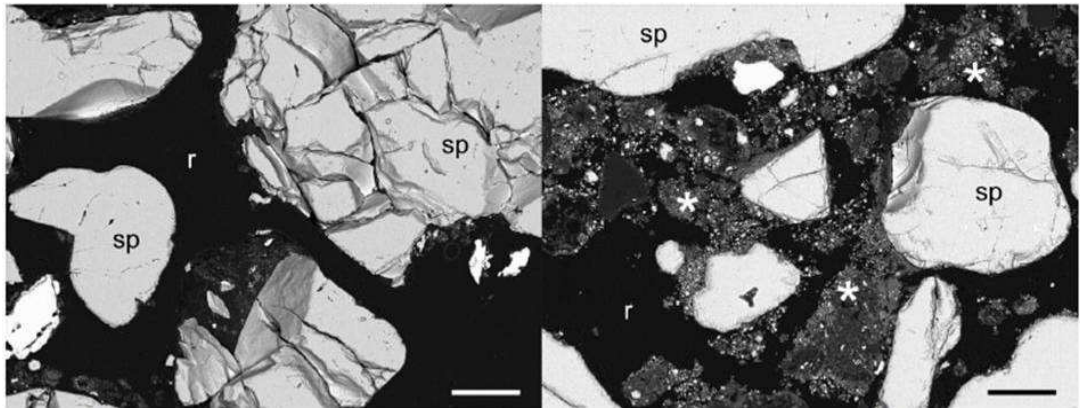


Figure 7.1 Back-scattered scanning electron micrographs of particle and pore size in sand (left) and silt+clay (right). Large sand-sized quartz particles (sp) are visible in both environments, while smaller ground quartz particles (*) are only present in the resin (r)-infiltrated pore space in the silt+clay environment. Scale bars = 100 μm . These images would be the expected before and after destabilisation (left and right respectively) observations following a wet-dry cycle of soil incubated with the mutant bacterial strains. Image from Carson *et al.* (2010).

Even though the bacterial strains in this study had no competition for substrates, and in the short incubation time of these experiments their actions may suggest that bacteria with a competitive disadvantage act to create non-competitive spatially isolated microenvironments, which in an unsaturated medium creates conditions conducive to low diffusive fluxes, the bacteria are promoting coexistence. Feeney *et al.* (2006b) showed that with fungi the structural properties of the soil as assessed by synchrotron-XCT were changed within 7 days of introduction to the soil in planted cores. The assertion that bacteria can also influence soil structure in such short time periods warrants further investigation.

Of course in the environment, bacteria do not exist as disparate communities of single species, but rather as consortia in surface attached biofilms (Costerton *et al.*, 1995; Davey and O'Toole G, 2000; Li *et al.*, 2009) with the EC components, in particular the exopolysaccharides providing the structural framework. The bacteria in these diverse communities undertake different roles, for example in the production and degradation of organic matter, nitrogen and sulphur cycling, biodegradation of environmental pollutants etc. (Davey and O'Toole G, 2000). The next step in understanding the interactions of the bacteria in soil would be to introduce more than one species or perhaps initially start with two strains of the same species with different extracellular component production capabilities to study the effects of having, for example two bacteria capable of cellulose and LPS production, but only one able to produce viscosin. Experiments of this nature could be undertaken with a view to establishing the amounts and types of extracellular components required to affect structure, aggregate stability and hydrodynamic responses. In further investigations it would be of great advantage to be able to visually localise the bacteria within the soil structure, and quantify relative bacterial populations to the measured responses in hydrodynamics and changes in soil structural properties, and as technologies advance this will become a significant tool in developing and understanding of how bacteria behave in soil and how they influence their environment. Already the use of XCT in conjunction with biological and biochemical analyses of soil has been assessed by Bouckaert *et al.* (2012) and “*may very well open up a huge potential in evaluating the role of the soil pore network in regulating soil biological processes.*”

Young and Ritz (2000) state that *“it is not merely the basic spatial architecture of pore networks that modulates biological activity in soils, but the interaction between pores and water. Water films act essentially as valves restricting the flow of oxygen, and other gases, through the pore network with great consequences for biological activity”*. These water films would be most noticeable and effective at the micropore level in which more than 80% of bacteria found in soils under different fertilisation treatments were located (Ranjard and Richaume, 2001; Sessitsch *et al.*, 2001). This is in agreement with the observation in this study that bacterial activity influenced the hydrodynamics of the smaller mesopores (<30 μm) and to a lesser extent in the macropores (30 - 300 μm). In addition to the statement that the interaction between water and pores affects microbial activity (Young and Ritz, 2000) the observation from this study is that the interaction between microbes and pores affects local water activity in the soil. The production of EC components by bacteria and the presence of bacteria themselves have been shown to increase water repellency of soil at the mesopore level. Again, is this the bacteria engineering their environment so as to maintain a drier habitat more suited to gaseous exchange required for aerobic activity?

Whilst bacterial colonisation appears to be localised to the meso- and micropores in soil, this study and others (Dhoot *et al.*, 1974; Preston *et al.*, 1999; Preston *et al.*, 2001) have shown the effects of bacterial presence to be felt at the scale of crack formation. Cracks in soil form the boundaries between the major flow paths of water and chemicals, and the subsurface inter- and intra-aggregate pore networks (Hallett and Newson, 2005). The

cracking of soil is a temporal phenomenon observed during dry periods. The behaviour of water flow and solute transport is greatly affected by these large cracks in the soil structure (Vogel *et al.*, 2005a; Vogel *et al.*, 2005b). In their studies of the addition of substrates to the soil to influence microbial activity Preston *et al.* (1999; 2001) showed that microbial activity affects the genesis of cracks in soil. The application of substrates to the soil and the control of the balance of available substrates have been shown to control microbial exopolysaccharide production (Auer and Seviour, 1990; Roberson *et al.*, 1991; Roberson *et al.*, 1995). Applying these strategies to the investigation of soil structure at the smaller scales using XCT and synchrotron-XCT could help elucidate further the effects of bacteria and the bacterial legacy materials on the structure and hydrodynamics of soil.

In both cracking analysis and 3D structural analysis one of the difficulties encountered when comparing the results of previous studies using fractal dimension in their interpretation of soil structure with this study was the apparent discrepancy in the use of the terms 'homogeneous' and 'heterogeneous'. Using the fractal equation ($D = \log N / \log r$) at each box size (r), where N is the number of boxes of size r containing pore space and taking an average of D , some studies refer to a higher fractal number indicating a greater homogeneity of pore distribution and a lower fractal number indicating a greater heterogeneity (Crawford and Matsui, 1996; Preston *et al.*, 1999; Velde, 1999). This study, like that of Kravchenko (2011), uses the slope of the log-transformed equation, $N(r) \propto r^{-D}$ where $N(r)$ is the number of boxes of size r containing pore space, r is the box size and D is the fractal dimension. By plotting the $\log N(r)$ against $\log r$, the slope of

the log-log plot reveals the fractal dimension of the volume under investigation, D . Another discrepancy is in the box-counting method itself. Whilst some studies start with the smallest box size (r) at the resolution of the image, and increase this box to $2r$, $3r$ $4r$ etc., many texts start with the largest box that encompasses the entire image and then magnify the image within the box increasing the number of boxes required to cover the image. This introduces the need to divide the box size into 1 , and then plot the negative log-log to arrive at a positive value for D .

Figure 7.2 illustrates the straightforward equation method and the slope of the log-log plot of the calculation method on the image magnification method on the same simulated image set.

method of analysis or a clearer presentation of the terminology used in each study is suggested to avoid misinterpretation by readers. An alternative approach may be the use of the term “fractal dimension”, with the understanding that a lower FD number corresponds to an irregular or clustered distribution of pore space and a higher FD number corresponds to a regular or even distribution of pore space.

7.2 The applicability of laboratory investigations to the field

In this study, one type of soil texture was sterilised and sieved and used to create replicate repacked cores and homogenised slurries. In the United Kingdom there are 12 different recognised soil textures. Soil is not made up of same-sized aggregates, neatly packed at equal bulk densities. It contains plants, fungi and over 5000 microbial genotypes per gram of soil (Torsvik and Ovreas, 2002). The reasons for focussing on such a narrow view of the soil have been discussed in previous chapters. It is only by focussing upon one soil type, arranged uniformly and sterilised so as to remove unidentified and uncontrolled organisms from the experimental system, that the first steps in understanding actions of bacteria and the functions of the different components of the bacterial legacy can be taken. Similarly, the question may be asked: How relevant is looking at laboratory microcosms at a 2 mm aggregate or a 5 cm³ core scale to *in vivo* and *in situ* soil? It is actually probably more important to look at the microscale, since the field scale is an averaged view of the interactions between biology, chemistry and physics of the environment. Looking at the “*real world*” scale is all very well, however bigger is not always better. To look at the planet as a whole would give

average information about all the seas, lakes and waterways and all the land masses, deserts, mountains, rainforests, ice-plains etc. Much like larger pores are separated from each other in the soil connected by tortuous and more narrow pore networks. We know that the “pockets” created by land masses separate seas from lakes and that the rivers, streams and estuaries provide connections between these areas of water. Similarly environmental history has shaped the placement of these land masses and waterways through earthquakes, movement of tectonic plates, ice ages, volcanic eruptions. Man has moulded the land to suit his own purposes throughout the ages too through the destruction of rainforests, construction of cities, and reclamation of land from the sea. Each of these events and processes has both immediate and long-term, and often irreversible effects on its proximal surroundings. Whilst ploughing of land will disturb the larger soil structure, the smaller aggregate structure will not necessarily be affected immediately. However, as water flow is changed by gross-structure rearrangement and larger structure stability is affected by for example planting or construction, the effects will eventually be translated to or cause an effect in the smaller aggregates. Different areas will be affected in different ways depending on what is already happening at the smaller scale. This picture is similarly applicable to the actual soil layer itself in that to suppose that average information over the field scale without understanding the microscale is counterintuitive and most likely counterproductive in the long-term. For example, large scale amelioration of land based upon the analysis of the average of samples of a field may not be the most effective or cost effective path. This phenomenon is known as volume averaging and results in loss of

key information. Heterogeneous distribution of soil components have been demonstrated for example with element maps of soil using microfocus synchrotron X-ray fluorescence (μ -SXRF) (Strawn and Baker, 2008) (Figure 7.3).

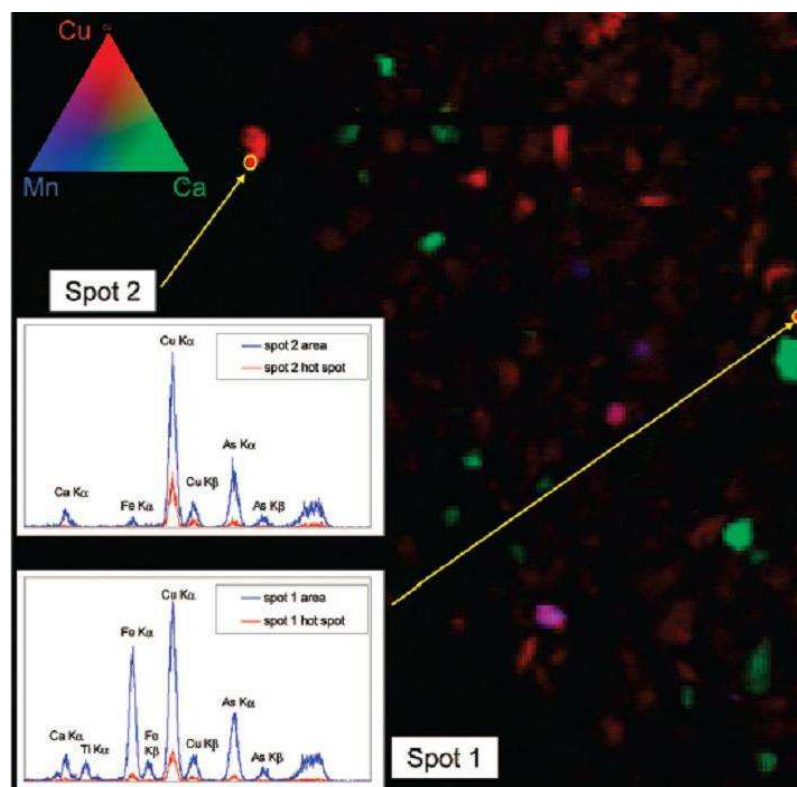


Figure 7.3 Elemental map of soil thin section showing heterogeneity of distribution of copper (Cu = red), manganese (Mn = blue) and calcium (Ca = green). Hotspots of copper have been analysed by μ -SXRF and the multichannel analyser (MCA) spectra are shown in the inset graphs. In each inset graph, the blue curve shows the summed MCA spectra of the high-Cu region and the red curve shows the individual MCA spectrum of the highest-Cu pixel in the region. Pixel size is 5 μ m. The total map area is 0.870 \times 0.875 mm. Image from Strawn and Baker (2008).

This phenomenon is also discussed by Baveye (2010) in reference to a similar study by Jacobson *et al.* (2007) where sharp differences in the accumulation of these trace elements have been observed over minute distances (nanometers). What this tells us is that it is vitally important to

understand the microscale and from there build the picture of the field scale and so on.

7.3 Future work

The impact of bacteria and the bacterial legacy on the 3D structure and hydrodynamics of soil has been investigated at the macro-, meso- and microscale. In addition, analysis of the effect of bacteria and their associated metabolic products on the formation of cracks in the soil surface was undertaken. This has lead to hypotheses about the actions of individual components of extracellular substances, cellulose, lipopolysaccharide and viscosin, on soil aggregate stability and in the pore networks. Visualisation of the spatial location of the bacteria and of the exopolymeric substances in the soil structure would prove where in the soil these effects are occurring. Quantification of extracellular substances and bacteria in relation to the effects on structure and hydrodynamics could serve to inform bioremediation and bioaugmentation procedures. This overall picture of biology, chemistry and physics of the soil requires the input of a wide range of traditional laboratory scientists and additionally computer and mathematical scientists to improve the processing of data generated by increasingly computationally sophisticated equipment.

Additionally, quantification of the biomass of the bacteria in the soil following inoculation would add further detail as to the level of hydrodynamic response and effect on soil physical structure in relation to the growth rate and survival of the different bacterial strains in the soil.

The data generated during this project has provided a solid framework for the comparison of structural properties such as porosity, pore size distribution, and hydrodynamic measurements such as drainage profiles and sorptivity between the measured values reported in this thesis and the deduced values as can be determined using the various soil property equations. Future data processing would allow direct comparison of these measured and derived values.

Detailed analysis of the drainage profiles with respect to traditional fitted curves, is also possible since the whole WRC dataset was measured but not analysed in this work.

Similarly, further comparison of the effect of mutants on soil with respect to each other, and in direct comparison to bacteria-free soil is possible as the statistical analyses carried out throughout this work presents all paired comparisons, adding to the comparisons made in this thesis.

7.3.1 Adding the 4th dimension, the time scale

This study, in particular the 3D structural analyses and the hydrodynamic analyses had an element of the 4th dimension in it in terms of investigating soil properties after 1 and 2 wet-dry cycles. This provides a temporal aspect to this research. However, both sets of structural measurements were taken in the dry phase. It would be interesting to investigate the 3D structure of the soil during the drying phase of the wet-dry cycle using X-ray detectable tracer dyes to map preferential flow through the soil structure. This would

also provide repellency information about the soil as empty pore structures in a wetted sample would indicate areas of higher hydrophobicity. As the technology of XCT advances along with computational power, faster scans at higher resolutions becomes possible and provides the possibility of performing temporal investigations of structural changes and concurrent water flow experimentation.

7.4 Conclusions

The original hypothesis of this work was that the presence of bacteria and bacterial legacy materials affects the biophysics of water retention and flow in soil. These changes would be due to the presence of the bacteria and their extracellular components in the pore networks affecting the polarity of the solid phase and physically interfering with water flow by blocking narrow pore passages. Their chemical properties would also affect aggregate stability and result in the structural rearrangement of the soil matrix.

Bacteria have been shown to increase water repellency of soil, decrease the total water content at saturation and increase the water retaining ability of the soil as it drains. Structurally, decreased pore connectivity and destabilisation of aggregates have been observed in soil systems treated with bacteria deficient in the production of a key extracellular component, cellulose, LPS or viscosin.

This study has provided clear evidence of the ability of bacteria and their extracellular components to impact upon (i) the hydrodynamics of water retention and flow in soil and (ii) the structural organisation, aggregation and

stabilisation of soil. The multifaceted nature of soil and its many varying compositions, as well as the complexity of bacterial behaviour and indeed their own multifaceted properties, have served to highlight just how much is unknown about the interactions of bacteria and soil. A back-to-basics approach in terms of chemical bonding and polar interactions is required in order to truly understand how soil, water and bacteria interact with themselves and each other, not to mention the many other constituents of soil in nature. By combining information on these elements through the use of synchrotron-based technologies including tomography and chemical mapping, and by using advanced methods in μ CT to elucidate multiphase spatial distribution, the microscale of soil will start to yield the much needed information of its complex nature.

REFERENCES

- Abu-Zreig, M., Rudra, R. P. and Dickinson, W. T., 2003. Effect of application of surfactants on hydraulic properties of soils. *Biosystems Engineering*. 84(3): pp.363-372.
- Adav, S. S., Lin, J. C.-T., Yang, Z., Whiteley, C. G., Lee, D.-J., Peng, X.-F. and Zhang, Z.-P., 2010. Stereological assessment of extracellular polymeric substances, exo-enzymes, and specific bacterial strains in bioaggregates using fluorescence experiments. *Biotechnology Advances*. 28(2): pp.255-280.
- Al-Raoush, R. I. and Willson, C. S., 2005. Extraction of physically realistic pore network properties from three-dimensional synchrotron X-ray microtomography images of unconsolidated porous media systems. *Journal of Hydrology*. 300(1-4): pp.44-64.
- Allred, B. and Brown, G. O., 1994. Surfactant induced reduction in soil hydraulic conductivity. *Ground Water Monitorin and Remedication*. 14(2): pp.174-184.
- Allton, K., 2012. *Planet Under Pressure 2012*. British Soil Science Society.
- Amos, M., 2010. Advanced industrial X-ray computed tomography for defect detection and characterisation of composite structures. PhD thesis. (Faculty of Engineering and Physical Sciences). The University of Manchester.
- Anderson, S. H., Peyton, R. L. and Gantzer, C. J., 1990. Evaluation of constructed and natural soil macropores using X-ray computed tomography. *Geoderma*. 46(1-3): pp.13-29.
- Auer, D. P. F. and Seviour, R. J., 1990. Influence of Varying Nitrogen-Sources on Polysaccharide Production by *Aureobasidium-Pullulans* in Batch Culture. *Applied Microbiology and Biotechnology*. 32(6): pp.637-644.
- Baer, J. U., Kent, T. F. and Anderson, S. H., 2009. Image analysis and fractal geometry to characterize soil desiccation cracks. *Geoderma*. 154(1-2): pp.153-163.
- Bantinaki, E., Kassen, R., Knight, C. G., Robinson, Z., Spiers, A. J. and Rainey, P. B., 2007. Adaptive Divergence in Experimental Populations of *Pseudomonas fluorescens*. III. Mutational Origins of Wrinkly Spreader Diversity. *Genetics*. 176(1): pp.441-453.
- Bauters, T. W. J., Steenhuis, T. S., DiCarlo, D. A., Nieber, J. L., Dekker, L. W., Ritsema, C. J., Parlange, J. Y. and Haverkamp, R., 2000. Physics of water repellent soils. *Journal of Hydrology*. 231-232 pp.233-243.

Baveye, P., 2010. Comment on "The role of scaling laws in upscaling" by B.D. Wood. *Advances in Water Resources*. 33(1): pp.123-124.

Baveye, P. C., Laba, M., Otten, W., Bouckaert, L., Dello Sterpaio, P., Goswami, R. R., Grinev, D., Houston, A., Hu, Y., Liu, J., Mooney, S., Pajor, R., Sleutel, S., Tarquis, A., Wang, W., Wei, Q. and Sezgin, M., 2010. Observer-dependent variability of the thresholding step in the quantitative analysis of soil images and X-ray microtomography data. *Geoderma*. 157(1-2): pp.51-63.

Beech, I., Hanjagsit, L., Kalaji, M., Neal, A. L. and Zinkevich, V., 1999. Chemical and structural characterization of exopolymers produced by *Pseudomonas* sp. NCIMB 2021 in continuous culture. *Microbiology*. 145(6): pp.1491-1497.

Berns, A. E., Philipp, H., Narres, H. D., Burauel, P., Vereecken, H. and Tappe, W., 2008. Effect of gamma-sterilization and autoclaving on soil organic matter structure as studied by solid state NMR, UV and fluorescence spectroscopy. *European Journal of Soil Science*. 59(3): pp.540-550.

Bielecki, S., Krystynowicz, A., Turkiewicz, M. and Kalinowska, H., 2002. Bacterial Cellulose. In: Vandamme, E., De Baets, S. and Steinbuchel, A., eds. *Biopolymers: Polysaccharides I - Polysaccharides from Prokaryotes v.5*. Weinheim ; Chichester: Wiley-VCH, pp. 37-85.

Bird, M. I., Ascough, P. L., Young, I. M., Wood, C. V. and Scott, A. C., 2008. X-ray microtomographic imaging of charcoal. *Journal of Archaeological Science*. 35(10): pp.2698-2706.

Bond, K. B. and Harris, J. R., 1964. The influence of the microflora on physical properties of soils 1. Effects associated with filamentous algae and fungi. *Australian Journal of Soil Research*. 2 pp.111-122.

Bossuyt, H., Denef, K., Six, J., Frey, S. D., Merckx, R. and Paustian, K., 2001. Influence of microbial populations and residue quality on aggregate stability. *Applied Soil Ecology*. 16(3): pp.195-208.

Bouckaert, L., Van Loo, D., Ameloot, N., Buchan, D., Van Hoorebeke, L. and Sleutel, S., 2012. Compatibility of X-ray micro-Computed Tomography with soil biological experiments. *Soil Biology and Biochemistry*.(article in press).

Braun, P. G., Hildebrand, P. D., Ells, T. C. and Kobayashi, D. Y., 2001. Evidence and characterization of a gene cluster required for the production of viscosin, a lipopeptide biosurfactant, by a strain of *Pseudomonas fluorescens*. *Can J Microbiol*. 47(4): pp.294-301.

Bronick, 2005. Soil structure and management: a review. *Geoderma*. 124 pp.3-22.

Carson, J. K., Gonzalez-Quinones, V., Murphy, D. V., Hinz, C., Shaw, J. A. and Gleeson, D. B., 2010. Low pore connectivity increases bacterial diversity in soil. *Applied and Environmental Microbiology*. 76(12): pp.3936-3942.

Chaplin, M. 2012. *Hydrocolloids: Cellulose*. London South Bank University. [Online] Available from: <http://www.lsbu.ac.uk/water/hycel.html>.

Chen, G. and Zhu, H., 2004. Impact of lipopolysaccharide coating on clay particle wettability. *Colloids and Surfaces B: Biointerfaces*. 35(2): pp.143-147.

Chenu, C., 1989. Influence of a fungal polysaccharide, scleroglucan, on clay microstructures. *Soil Biology and Biochemistry*. 21(2): pp.299-305.

Chenu, C., 1993. Clay- or sand-polysaccharide associations as models for the interface between micro-organisms and soil: water related properties and microstructure. *Geoderma*. 56(1-4): pp.143-156.

Chenu, C. and Cosentino, D., 2011. Microbial regulation of soil structure dynamics. In: Ritz, K. and Young, I. M. eds. *The Architecture and Biology of Soils: Life in Inner Space*, Wallingford, Oxfordshire: CAB International, 2011.

Chenu, C. and Guerif, J., 1991. Mechanical strength of clay minerals as influenced by an adsorbed polysaccharide. *Soil Science Society of America Journal*. 55 pp.1076-1080.

Colman, B. P., Fierer, N. and Schimel, J. P., 2007. Abiotic nitrate incorporation in soil: is it real? *Biogeochemistry*. 84(2): pp.161-169.

Costerton, J. W., Lewandowski, Z., Caldwell, D. E., Korber, D. R. and Lappin-Scott, H. M., 1995. Microbial biofilms. *Annu Rev Microbiol*. 49 pp.711-745.

Crawford, J. W., Harris, J. A., Ritz, K. and Young, I. M., 2005. Towards an evolutionary ecology of life in soil. *Trends in Ecology & Evolution*. 20(2): pp.81-87.

Crawford, J. W. and Matsui, N., 1996. Heterogeneity of the pore and solid volume of soil: distinguishing a fractal space from its non-fractal complement. *Geoderma*. 73(3-4): pp.183-195.

Crawford, J. W., Matsui, N. and Young, I. M., 1995. The relation between the moisture-release curve and the structure of soil. *European Journal of Soil Science*. 46(3): pp.369-375.

Czarnes, S., Hallett, P. D., Bengough, A. G. and Young, I. M., 2000. Root- and microbial-derived mucilages affect soil structure and water transport. *European Journal of Soil Science*. 51(3): pp.435-443.

Dathe, A. and Thullner, M., 2005. The relationship between fractal properties of solid matrix and pore space in porous media. *Geoderma*. 129 pp.279-290.

Davey, M. E. and O'Toole G, A., 2000. Microbial biofilms: from ecology to molecular genetics. *Microbiol Mol Biol Rev*. 64(4): pp.847-867.

de Bruijn, I., de Kock, M. J. D., Yang, M., de Waard, P., van Beek, T. A. and Raaijmakers, J. M., 2007. Genome-based discovery, structure prediction and functional analysis of cyclic lipopeptide antibiotics in *Pseudomonas* species. *Molecular Microbiology*. 63 pp.417-428.

De Gryze, S., Jassogne, L., Six, J., Bossuyt, H., Wevers, M. and Merckx, R., 2006. Pore structure changes during decomposition of fresh residue: X-ray tomography analyses. *Geoderma*. 134(1-2): pp.82-96.

De Gryze, S., Six, J., Brits, C. and Merckx, R., 2005. A quantification of short-term macroaggregate dynamics: influences of wheat residue input and texture. *Soil Biology and Biochemistry*. 37(1): pp.55-66.

DeBano, L. F., 2000. Water repellency in soils. *Journal of Hydrology*. 231-232 pp.4-32.

Dechesne, A., Or, D. and Smets, B. F., 2008. Limited diffusive fluxes of substrate facilitate coexistence of two competing bacterial strains. *FEMS Microbiology Ecology*. 64 pp.1-8.

Desai, J. D. and Banat, I. M., 1997. Microbial production of surfactants and their commercial potential. *Microbiol. Mol. Biol. Rev*. 61(1): pp.47-64.

Dhoot, J. S., Singh, N. T. and Brar, S. S., 1974. Polysaccharides in relation to soil aggregation under aerobic and anaerobic Conditions. *Journal of the Indian Society of Soil Science*. 22(3): pp.217-219.

Doerr, S. H., Llewellyn, T. C., Douglas, P., Morley, C. P., Haskins, C., Johnsey, L., Ritsema, C. J., Stagnitti, F. and Ferreira, A. J. D., 2002. Investigation of compounds causing water repellency in the rhizosphere of sandy soils from a wide range of locations. In: *17th WCSS, Thailand*.

Doerr, S. H., Shakesby, R. A. and Walsh, R. P., 2000. Soil water repellency: its causes, characteristics and hydro-geomorphological significance. *Earth Science Reviews*. 51(1-4): pp.33-65.

Donlan, R. M., 2002. Biofilms: microbial life on surfaces. *Emerging Infections Diseases*. 8(9): pp.881-890.

Dorioz, J. M., Robert, M. and Chenu, C., 1993. The role of roots, fungi and bacteria on clay particle organization. An experimental approach. *Geoderma*. 56(1-4): pp.179-194.

Elliott, E. T. and Coleman, D. C., 1988. Let the soil work for us. In: *Ecological implications of contemporary agriculture, Wageningen, 7-12 September, 1986*. Munksgaard International Booksellers and Publishers, pp.23-32.

Eng, R. H. K., Smith, S. M., Fan-Havard, P. and Ogbara, T., 1993. Effect of antibiotics on endotoxin release from gram-negative bacteria. *Diagnostic Microbiology and Infectious Disease*. 16(3): pp.185-189.

Falconer, K., 2003. *Fractal geometry*. New York: Wiley

Fechtner, J., Koza, A., Sterpaio, P. D., Hapca, S. M. and Spiers, A. J., 2011. Surfactants expressed by soil pseudomonads alter local soil-water distribution, suggesting a hydrological role for these compounds. *FEMS Microbiology Ecology*.

Feeney, D. S., Bengough, A. G., Hallett, P. D., Rodger, S., White, N. and Young, I. M., 2006a. Assessing the impact of biological exudates associated with soil water repellency. *Soil Management for Sustainability*, Vol 38. 2006a, pp.475-483.

Feeney, D. S., Crawford, J. W., Daniell, T., Hallett, P. D., Nunan, N., Ritz, K., Rivers, M. and Young, I. M., 2006b. Three-dimensional microorganization of the soil-root-microbe system. *Microbial Ecology*. 52(1): pp.151-158.

Feeney, D. S., Hallett, P. D., Rodger, S., Bengough, A. G., White, N. A. and Young, I. M., 2006c. Impact of fungal and bacterial biocides on microbial induced water repellency in arable soil. *Geoderma*. 135 pp.72-80.

Festucci-Buselli, R. A., Otoni, W. C. and Joshi, C. P., 2007. Structure, organization, and functions of cellulose synthase complexes in higher plants. *Braz. J. Plant Physiol.* 19(1): pp.1-13.

Fredlund, D. G. and Xing, A., 1994. Equations for the soil water characteristic curve. *Canadian Geotechnical Journal*. 31 pp.521-532.

Gal, M., Preston, G. M., Massey, R. C., Spiers, A. J. and Rainey, P. B., 2003. Genes encoding a cellulosic polymer contribute toward the ecological success of *Pseudomonas fluorescens* SBW25 on plant surfaces. *Mol Ecol*. 12(11): pp.3109-3121.

Gibson, J. R., Lin, H. and Bruns, M. A., 2006. A comparison of fractal analytical methods on 2- and 3-dimensional computed tomographic scans of soil aggregates. *Geoderma*. 134 pp.335-348.

Gomez-Suarez, C., Pasma, J., van der Borden, A. J., Wingender, J., Flemming, H.-C., Busscher, H. J. and van der Mei, H. C., 2002. Influence of extracellular polymeric substances on deposition and redeposition of *Pseudomonas aeruginosa* to surfaces. *Microbiology*. 148(4): pp.1161-1169.

Gram, C., 1884. The differential staining of Schizomycetes in tissue sections and in dried preparations. *Fortschritte der Medicin*. 2 pp.185-189.

Grant, C. and Dexter, A., 1989. Generation of microcracks in molded soils by rapid wetting. *Australian Journal of Soil Research*. 27 pp.169-182.

Guidi, G., Pagliai, M. and Petruzzelli, G., 1978. Quantitative size evaluation of cracks and clods in artificially dried soil samples. *Geoderma*. 20(2): pp.105-113.

Haines, W. B., 1930. Studies in the physical properties of soil - V: The hysteresis effect in capillary properties and the modes of water distribution associated therewith. *Journal of Agricultural Science*. 20 pp.97-116.

Hallett, P., 2007. An introduction to soil water repellency. In: *Proceedings of the 8th International Symposium on Adjuvants for Agrochemicals, Columbus, Ohio, USA*: International Society for Agrochemical Adjuvants (ISAA)

Hallett, P. and Newson, T. A., 2005. Describing soil crack formation using elastic-plastic fracture mechanics. *European Journal of Soil Science*. 56 pp.31-38.

Hallett, P. D., Gordon, D. C. and Bengough, A. G., 2003. Plant influence on rhizosphere hydraulic properties: direct measurements using a miniaturized infiltrometer. *New Phytologist*. 157(3): pp.597-603.

Hallett, P. D., Nunan, N., Douglas, J. T. and Young, I. M., 2004. Millimeter-Scale Spatial Variability in Soil Water Sorptivity: Scale, Surface Elevation, and Subcritical Repellency Effects. *Soil Sci Soc Am J*. 68(2): pp.352-358.

Hallett, P. D. and Young, I. M., 1999. Changes to water repellence of soil aggregates caused by substrate-induced microbial activity. *European Journal of Soil Science*. 50(1): pp.35-40.

Harris, K., Crabb, D., Young, I. M., Weaver, H., Gilligan, C. A., Otten, W. and Ritz, K., 2002a. In situ visualisation of fungi in soil thin sections: problems with crystallisation of the fluorochrome FB 28 (Calcofluor M2R) and improved staining by SCRI Renaissance 2200. *Mycological Research*. 106 pp.293-297.

Harris, K., Crabb, D., Young, I. M., Weaver, H., Gilligan, C. A., Otten, W. and Ritz, K., 2002b. In situ visualization of fungi in soil thin sections: problems with crystallisation of the fluorochrome FB 28 (Calcofluor M2R) and improved staining by SCRI Renaissance 2200. *Mycological Research*. 106(3): pp.293-297.

Harris, K., Young, I. M., Gilligan, C. A., Otten, W. and Ritz, K., 2003. Effect of bulk density on the spatial organisation of the fungus *Rhizoctonia solani* in soil. *FEMS Microbiology Ecology*. 44(1): pp.45-56.

Healy, M. G., Devine, C. M. and Murphy, R., 1996. Microbial production of biosurfactants. *Resources, Conservation and Recycling*. 18(1-4): pp.41-57.

Hillel, D., 1998. *Environmental Soil Physics*. London: Academic Press

Horgan, G. W. and Young, I. M., 2000. An empirical stochastic model for the geometry of two-dimensional crack growth in soil (with Discussion). *Geoderma*. 96(4): pp.263-276.

Horii, T., Kimura, T., Nadai, M. and Kobayashi, M., 2000. Lincomycin-induced endotoxin release in Escherichia coli sepsis: evidence for release in vitro and in vivo. *International Journal of Infectious Diseases*. 4(3): pp.118-122.

Horii, T., Kobayashi, M., Nadai, M., Ichiyama, S. and Ohta, M., 1998. Carbapenem-induced endotoxin release in Gram-negative bacterial sepsis rat models. *FEMS Immunology and Medical Microbiology*. 21(4): pp.297-302.

Horn, R. and Baumgartl, T., 2002. Dynamic properties of soils. In: Warrick, A. W. ed. *Soil physics companion*, Boca Raton, FL: CRC Press, 2002, p389.

Iassonov, P., Gebrenegus, T. and Tuller, M., 2009. Segmentation of X-ray computed tomography images of porous materials: A crucial step for characterization and quantitative analysis of pore structures. *Water Resources Research*. 45 p.W09415.

Jacobson, A. R., Dousset, S., Andreux, F. and Baveye, P. C., 2007. Electron microprobe and synchrotron X-ray fluorescence mapping of the heterogeneous distribution of copper in high-copper vineyard soils. *Environmental Science & Technology*. 41(18): pp.6350-6356.

Janssen, P., 2006. Identifying the dominant soil bacterial taxa in libraries of 16S rRNA and 16SrRNA genes. *Applied and Environmental Microbiology*. 72(3): pp.1719-1728.

Johnson, A., Roy, I. M., Matthews, G. P. and Patel, D., 2003. An improved simulation of void structure, water retention and hydraulic conductivity in soil with the Pore-Cor three-dimensional network. *European Journal of Soil Science*. 54(3): pp.477-489.

Jonas, R. and Farah, L. F., 1998. Production and application of microbial cellulose. *Polymer Degradation and Stability*. 59(1-3): pp.101-106.

Kilfeather, A. A. and van der Meer, J. J. M., 2008. Pore size, shape and connectivity in tills and their relationship to deformation processes. *Quaternary Science Reviews*. 27(3-4): pp.250-266.

King, E. O., Ward, M. K. and Raney, D. E., 1954. 2 Simple Media for the Demonstration of Pyocyanin and Fluorescin. *Journal of Laboratory and Clinical Medicine*. 44(2): pp.301-307.

Koza, A., Hallett, P. D., Moon, C. D. and Spiers, A. J., 2009. Characterization of a novel air-liquid interface biofilm of *Pseudomonas fluorescens* SBW25. *Microbiology-Sgm*. 155 pp.1397-1406.

Kravchenko, A. N., Wang, A. N. W., Smucker, A. J. M. and Rivers, M. L., 2011. Long-term differences in tillage and land use affect intra-aggregate pore heterogeneity. *Soil Science Society of America Journal*. 75 pp.1658-1666.

Kumar, S., Anderson, S. H., Udawatta, R. P. and Gantzer, C. J., 2010. CT-measured macropores as affected by agroforestry and grass buffers for grazed pasture systems. *Agroforestry Systems*. 79(1): pp.59-65.

Lal, R., 1991. Soil Structure and Sustainability. *Journal of Sustainable Agriculture*. 1(4): pp.67-92.

Laycock, M. V., Hildebrand, P., Thobault, J. A., Walter, J. A. and Wright, J. L. C., 1991. Viscosin, a potent peptidolipid biosurfactant and phytopathogenic mediator produced by a pectolytic strain of *Pseudomonas fluorescens*. *J. Agric. Food Chem*. 39 pp.483-489.

Leeds-Harrison, P. B., Youngs, E. G. and Uddin, B., 1994. A device for determining the sorptivity of soil aggregates. *European Journal of Soil Science*. 45 pp.269-272.

Li, B.-L., 2000. Fractal geometry applications in description and analysis of patch patterns and patch dynamics. *Ecological Modelling*. 132 pp.33-50.

Li, D. C., Velde, B. and Zhang, T. L., 2004. Observations of pores and aggregates during aggregation in some clay-rich agricultural soils as seen in 2D image analysis. *Geoderma*. 118(3-4): pp.191-207.

Li, J. H. and Zhang, L. M., 2011. Study of desiccation crack initiation and development at ground surface. *Engineering Geology*. 123(4): pp.347-358.

Li, M.-Y., Zhang, J.-H., Lu, P., Xu, J.-L. and Li, S.-P., 2009. Evaluation of biological characteristics of bacteria contributing to biofilm formation. *Pedosphere*. 19(5): pp.554-561.

Liang, K. Y. and Zeger, S. L., 1986. Longitudinal Data-Analysis Using Generalized Linear-Models. *Biometrika*. 73(1): pp.13-22.

Long, T. and Or, D., 2005. Aquatic habitats and diffusion constraints affecting microbial coexistence in unsaturated porous media. *Water Resources Research*. 41(W08409): p.10.

Luo, L. and Lin, H., 2009. Lacunarity and Fractal Analyses of Soil Macropores and Preferential Transport Using Micro-X-Ray Computed Tomography. *Vadose Zone Journal*. 8(1): pp.233-241.

Mack, D., Fischer, W., Krokotsch, A., Leopold, K., Hartmann, R., Egge, H. and Laufs, R., 1996. The intercellular adhesin involved in biofilm accumulation of *Staphylococcus epidermis* is a linear β -1,6-linked glucosaminoglycan: purification and structural analysis. *J. Bacteriol.* 178(175-183).

Magalhaes, P. O., Lopes, A. M., Mazzola, P. G., Rangel-Yagui, C., Penna, T. C. V. and Pessoa, A., 2007. Methods of endotoxin removal from biological preparations: a review. *Journal of Pharmacy and Pharmaceutical Sciences*. 10(3): pp.388-404.

Makin, S. A. and Beveridge, T. J., 1996. The influence of A-band and B-band lipopolysaccharide on the surface characteristics and adhesion of *Pseudomonas aeruginosa* to surfaces. *Microbiology*. 142(2): pp.299-307.

Marshall, T. J. and Holmes, J. W., 1979. *Soil Physics*. Cambridge: Cambridge University Press

Martin, J. P., Martin, W. P., Page, J. B., Raney, W. A. and De Ment, J. D., 1955. Soil Aggregation. In: Norman, A. G. ed. *Advances in Agronomy*, Vol 7. New York: Academic Press Inc., 1955, pp.2-35.

McNamara, N. P., Black, H. I. J., Beresford, N. A. and Parekh, N. R., 2003. Effects of acute gamma irradiation on chemical, physical and biological properties of soils. *Applied Soil Ecology*. 24(2): pp.117-132.

Mele, G., Basile, A., Leone, A., Moreau, E., Terribile, F. and Velde, B., 1999. The study of soil structure by coupling serial sections and 3D image analysis: 1999. In: *International Workshop of the European-Society-of-Agricultural-Engineers Field of Interest on Soil and Water, Leuven, Belgium, Nov 24-26, 1999*. Wageningen (Netherlands): Wageningen Pers pp.142-152.

Messing, I. and Jarvis, N. J., 1995. A comparison of near-saturated hydraulic properties measured in small cores and large monoliths in a clay soil. *Soil Technology*. 7(4): pp.291-302.

Morales, V. L., Parlange, J. Y. and Steenhuis, T. S., 2010. Are preferential flow paths perpetuated by microbial activity in the soil matrix? A review. *Journal of Hydrology*. 393(1-2): pp.29-36.

Morel-Seytoux, H. J. and Nimmo, J. R., 1999. Soil water retention and maximum capillary drive from saturation to oven dryness. *Water Resour. Res.* 35(7): pp.2031-2041.

Neu, T. R., 1996. Significance of bacterial surface-active compounds in interaction of bacteria with interfaces. *Microbiol. Rev.* 60(1): pp.151-166.

Neu, T. R., Hartner, T. and Poralla, K., 1990. Surface-Active Properties of Viscosin - a Peptidolipid Antibiotic. *Applied Microbiology and Biotechnology*. 32(5): pp.518-520.

Nimmo, J. R., 2004. Porosity and pore size distribution. In: Hillel, D. ed. *Encyclopedia of soils in the environment*, Vol 3. London: Elsevier, 2004, pp.295-303.

Nishiyama, Y., Langan, P. and Chanzy, H., 2002. Crystal structure and hydrogen-bonding system in cellulose I β from synchrotron X-ray and neutron fiber diffraction. *J. Am. Chem. Soc.* 124 pp.9074-9082.

Nishiyama, Y., Sugiyama, J., Chanzy, H. and Langan, P., 2003. Crystal structure and hydrogen bonding system in cellulose I alpha from synchrotron X-ray and neutron fiber diffraction. *J. Am. Chem. Soc.* 125 pp.14300-14306.

Nunan, N., Ritz, K., Crabb, D., Harris, K., Wu, K., Crawford, J. W. and Young, I. M., 2001. Quantification of the in situ distribution of soil bacteria by large-scale imaging of thin sections of undisturbed soil. *FEMS Microbiology Ecology*. 37(1): pp.67-77.

Nunan, N., Ritz, K., Rivers, M., Feeney, D. S. and Young, I. M., 2006. Investigating microbial micro-habitat structure using X-ray computed tomography. *Geoderma*. 133 pp.398-407.

Nunan, N., Wu, K., Young, I. M., Crawford, J. W. and Ritz, K., 2002. *In situ* spatial patterns of soil bacterial populations, mapped at multiple scales, in an arable soil. *Microb Ecol.* 44(4): pp.296-305.

Nunan, N., Wu, K., Young, I. M., Crawford, J. W. and Ritz, K., 2003. Spatial distribution of bacterial communities and their relationships with the micro-architecture of soil. *FEMS Microbiology Ecology*. 44(2): pp.203-215.

O'Donnell, A. G., Young, I. M., Rushton, S. P., Shirley, M. D. and Crawford, J. W., 2007. Visualization, modelling and prediction in soil microbiology. *Nature Reviews Microbiology*. 5(9): pp.689-699.

Oades, J. M., 1984. Soil organic matter and structural stability: mechanisms and implications for management. *Plant and Soil*. 76 pp.319-337.

Oades, J. M., 1993. The role of biology in the formation, stabilization and degradation of soil structure. *Geoderma*. 56 pp.377-400.

Or, D. and Friedman, S., 2002. Physical processes affecting microbial habitats and activity in unsaturated porous media. In: *17th World Congress of Soil Science*.

Or, D., Smets, B. F., Wraith, J. M., Dechesne, A. and Friedman, S. P., 2007. Physical constraints affecting bacterial habitats and activity in unsaturated porous media: a review. *Advances in Water Resources*. 30(6-7): pp.1505-1527.

Or, D. and Tuller, M., 1999. Liquid retention and interfacial area in variably saturated porous media: Upscaling from single-pore to sample-scale model. *Water Resour. Res.* 35(12): pp.3591-3605.

Pajor, R., Falconer, R., Hapca, S. and Otten, W., 2010. Modelling and quantifying the effect of heterogeneity in soil physical conditions on fungal growth. *Biogeosciences*. 7(11): pp.3731-3740.

Papadopoulos, A., Bird, N. R. A., Mooney, S. J. and Whitmore, A. P., 2008. Fractal analysis of pore roughness in images of soil using the slit island method. *Vadose Zone Journal*. 7(2): pp.456-460.

Papadopoulos, A., Whitmore, A. P., White, R. P., Mooney, S. J. and Bird, N. R. A., 2009. Combining Spatial Resolutions in the Multiscale Analysis of Soil Pore-Size Distributions. *Vadose Zone Journal*. 8(1): pp.227-232.

Peat, D. M. W., Matthews, G. P., Worsfold, P. J. and Jarvis, S. C., 2000. Simulation of water retention and hydraulic conductivity in soil using a three-dimensional network. 51(1): pp.65-79.

Peng, X., Hallett, P. D., Zhang, B. and Horn, R., 2011. Physical response of rigid and non-rigid soils to analogues of biological exudates. *European Journal of Soil Science*. 62(5): pp.676-684.

Perret, J., Prasher, S. O., Kantzas, A. and Langford, C., 1999. Three-dimensional quantification of macropore networks in undisturbed soil cores. *Soil Science Society of America Journal*. 63(6): pp.1530-1543.

Philip, J. R., 1957. The theory of infiltration: 4. Sorptivity and algebraic infiltration equations. *Soil Science*. 84 pp.257-264.

Piccolo, A. and Mbagwu, J. S., 1989. Effects of humic substances and surfactants on the stability of soil aggregates. *Soil Science*. 147(1): pp.47-54.

Pierret, A., Capowiez, Y., Belzunces, L. and Moran, C. J., 2002. 3D reconstruction and quantification of macropores using X-ray computed tomography and image analysis. *Geoderma*. 106(3-4): pp.247-271.

Pires, L. F., Borges, J. A. R., Bacchi, O. O. S. and Reichardt, K., 2010. Twenty-five years of computed tomography in soil physics: A literature review of the Brazilian contribution. *Soil and Tillage Research*. 110(2): pp.197-210.

Preston, G., Spiers, A., Zhang, X. X., Jackson, R., Gal, M., Knight, C., Gehrig, S., Malone, J., Moon, C., Godfrey, S., Robinson, Z., Bertrand, N., Field, D. and Rainey, P., 2003. *Pseudomonas* in the underworld: The secret life of *Pseudomonas fluorescens* SBW25. *Pseudomonas Syringae and Related Pathogens: Biology and Genetics*, 2003, pp.347-353.

Preston, S., Griffiths, B. S. and Young, I. M., 1999. Links between substrate additions, native microbes, and the structural complexity and stability of soils. *Soil Biology and Biochemistry*. 31(11): pp.1541-1547.

Preston, S., Wirth, S., Ritz, K., Griffiths, B. S. and Young, I. M., 2001. The role played by microorganisms in the biogenesis of soil cracks: importance of substrate quantity and quality. *Soil Biology and Biochemistry*. 33(12-13): pp.1851-1858.

Puget, P., Angers, D. A. and Chenu, C., 1999. Nature of carbohydrates associated with water-stable aggregates of two cultivated soils. *Soil Biology and Biochemistry*. 31(1): pp.55-63.

Pupo, E. and Hardy, E., 2009. Complexity and solutions to the isolation problem of Gram negative lipopolysaccharides' bacteria molecular species. *Biotechnologia Aplicada*. 26 pp.9-15.

Rainey, P. B. and Bailey, M. J., 1996. Physical and genetic map of the *Pseudomonas fluorescens* SBW25 chromosome. *Molecular Microbiology*. 19(3): pp.521-533.

Rainey, P. B., Spiers, A. J. and Bantinaki, E. 2003. *Production of a cellulose-like polysaccharide by Pseudomonas fluorescens*. Europe, Innovation.EP1301603.

Ranjard, L. and Richaume, A. S., 2001. Quantitative and qualitative microscale distribution of bacteria in soil. *Research in Microbiology*. 152(8): pp.707-716.

Rao, P., He, M., Yang, X., SZhang, Y., Sun, S. and Wang, J., 2006. Effect of an anionic surfactant on hydraulic conductivity of sodium- and calcium saturated soils. *Pedosphere*. 16(5): pp.673-680.

Razavi Darbar, S. and Lakzian, A., 2007. Evaluation of chemical and biological consequences of soil sterilization methods. *Caspian J. Env. Sci*. 5(2): pp.87-91.

Remminghorst, U. and Rehm, B. H. A., 2009. Microbial production of alginate: biosynthesis and applications. In: Rehm, B. H. A. ed. *Microbial production of biopolymers and polymer precursors: applications and perspectives*, Norfolk, UK: Caister Academic Press, 2009.

Ritsema, C. J., Nieber, J. L., Dekker, L. W. and Steenhuis, T. S., 1998. Stable or unstable wetting fronts in water repellent soils - effect of antecedent soil moisture content. *Soil and Tillage Research*. 47(1-2): pp.111-123.

Roberson, E. B., Sarig, S. and Firestone, M. K., 1991. Cover crop managements of polysaccharide-mediated aggregation in and orchard soil. *Soil Science Society of America Journal*. 55 pp.734-739.

Roberson, E. B., Sarig, S., Shennan, C. and Firestone, M. K., 1995. Nutritional Management of Microbial Polysaccharide Production and Aggregation in an Agricultural Soil. *Soil Science Society of America Journal*. 59(6): pp.1587-1594.

Ross, P., Mayer, R. and Benziman, M., 1991. Cellulose Biosynthesis and Function in Bacteria. *Microbiological Reviews*. 55(1): pp.35-58.

Ruamps, L. S., Nunan, N. and Chenu, C., 2011. Microbial biogeography at the soil pore scale. *Soil Biology and Biochemistry*. 43(2): pp.280-286.

Saini, H. S., Barragan-Huerta, B. E., Lebron-Paler, A., Pemberton, J. E., Vazquez, R. R., Burns, A. M., Marron, M. T., Seliga, C. J., Gunatilaka, A. A. L. and Maier, R. M., 2008. Efficient purification of the biosurfactant viscosin from *Pseudomonas libanensis* strain M9-3 and its physicochemical and biological properties. *Journal of Natural Products*. 71(6): pp.1011-1015.

San José Martínez, F., Martínn, M. A., Caniego, F. J., Tuller, M., Guber, A., Pachepsky, Y. and García-Gutiérrez, C., 2010. Multifractal analysis of discretized X-ray CT images for the characterization of soil macropore structures. *Geoderma*. 156(1-2): pp.32-42.

Schjønning, P., Thomsen, I. K., Møberg, J. P., de Jonge, H., Kristensen, K. and Christensen, B. T., 1999. Turnover of organic matter in differently textured soils: I. Physical characteristics of structurally disturbed and intact soils. *Geoderma*. 89(3-4): pp.177-198.

Schloss, P. D. and Handelsman, J., 2006. Toward a census of bacteria in soil. *PLoS Comput Biol*. 2(7): p.e92.

Sessitsch, A., Weilharter, A., Gerzabek, M. H., Kirchmann, H. and Kandeler, E., 2001. Microbial population structures in soil particle size fractions of a long-term fertilizer field experiment. *Applied and Environmental Microbiology*. 67(9): pp.4215-4224.

Silby, M. W., Cerdeno-Tarraga, A. M., Vernikos, G. S., Giddens, S. R., Jackson, R. W., Preston, G. M., Zhang, X.-X., Moon, C. D., Gehrig, S. M., Godfrey, S. A. C., Knight, C. G., Malone, J. G., Robinson, Z., Spiers, A. J., Harris, S., Challis, G. L., Yaxley, A. M., Harris, D., Seeger, K., Murphy, L., Rutter, S., Squares, R., Quail, M. A., Saunders, E., Mavromatis, K., Brettin, T. S., Bentley, S. D., Hothersall, J., Stephens, E., Thomas, C. M., Parkhill, J.,

Levy, S. B., Rainey, P. B. and Thomson, N. R., 2009. Genomic and genetic analyses of diversity and plant interactions of *Pseudomonas fluorescens*. *Genome Biology*. 10(5).

Six, J., Bossuyt, H., Degryze, S. and Denef, K., 2004. A history of research on the link between (micro)aggregates, soil biota, and soil organic matter dynamics. *Soil and Tillage Research*. 79(1): pp.7-31.

Sleutel, S., Cnudde, V., Masschaele, B., Vlassenbroek, J., Dierick, M., Van Hoorebeke, L., Jacobs, P. and De Neve, S., 2008. Comparison of different nano- and micro-focus X-ray computed tomography set-ups for the visualization of the soil microstructure and soil organic matter. *Computers & Geosciences*. 34(8): pp.931-938.

Smith, S. W., 1997. Special imaging techniques. *The Scientist and Engineer's Guide to Digital Signal Processing*: California Technical Publishing, 1997.

Spain, A. M., Krumholz, L. R. and Elshahed, M. S., 2009. Abundance, composition, diversity and novelty of soil Proteobacteria. *ISME Journal*. 3 pp.992-1000.

Spiers, A. J., 2007. Wrinkly-Spreader Fitness in the Two-Dimensional Agar Plate Microcosm: Maladaptation, Compensation and Ecological Success. *Plos One*. 2(8).

Spiers, A. J., Bohannon, J., Gehrig, S. M. and Rainey, P. B., 2003. Biofilm formation at the air-liquid interface by the *Pseudomonas fluorescens* SBW25 wrinkly spreader requires an acetylated form of cellulose. *Mol Microbiol*. 50(1): pp.15-27.

Spiers, A. J., Kahn, S. G., Bohannon, J., Travisano, M. and Rainey, P. B., 2002. Adaptive Divergence in Experimental Populations of *Pseudomonas fluorescens*. I. Genetic and Phenotypic Bases of Wrinkly Spreader Fitness. *Genetics*. 161(1): pp.33-46.

Spiers, A. J. and Rainey, P. B., 2005. The *Pseudomonas fluorescens* SBW25 wrinkly spreader biofilm requires attachment factor, cellulose fibre and LPS interactions to maintain strength and integrity. *Microbiology*. 151(9): pp.2829-2839.

SSSA. 2012. *Soil Science Glossary*. Soil Science Society of America. [Online] Available from: <https://www.soils.org/publications/soils-glossary>. [Accessed 14-02-2012].

Strawn, D. G. and Baker, L. L., 2008. Speciation of Cu in a contaminated agricultural soil measured by XAFS, μ -XAFS, and μ -XRF. *Environmental Science & Technology*. 42(1): pp.37-42.

Sutherland, I. W., 1997. Microbial exopolysaccharides - structural subtleties and their consequences. *Pure Applied Chemistry*. 69 pp.1911-1917.

Sutherland, I. W., 2001. Biofilm exopolysaccharides: a strong and sticky framework. *Microbiology*. 147(1): pp.3-9.

Taina, I. A., Heck, R. J. and Elliot, T. R., 2008. Application of X-ray computed tomography to soil science: A literature review. *Canadian Journal of Soil Science*. 88(1): pp.1-19.

Tarquis, A. M., Heck, R. J., Andina, D., Alvarez, A. and Antón, J. M., 2009. Pore network complexity and thresholding of 3D soil images. *Ecological Complexity*. 6(3): pp.230-239.

Thompson, I. P., Lilley, A. K., Ellis, R. J., Bramwell, P. A. and Bailey, M. J., 1995. Survival, Colonization and Dispersal of Genetically-Modified *Pseudomonas fluorescens* SBW25 in the Phytosphere of Field-Grown Sugar-Beet. *Bio-Technology*. 13(13): pp.1493-1497.

Thullner, M. and Baveye, P., 2008. Computational pore network modeling of the influence of biofilm permeability on bioclogging in porous media. *Biotechnology and Bioengineering*. 99(6): pp.1337-1351.

Tisdall, J. M., 1991. Fungal hyphae and structural stability of soil. *Australian Journal of Soil Research*. 29 pp.729-743.

Tisdall, J. M., 1994. Possible role of soil microorganisms in aggregation in soils. *Plant and Soil*. 159(1): p.115.

Tisdall, J. M. and Oades, J. M., 1982. Organic matter and water-stable aggregates in soils. *Journal of Soil Science*. 33 pp.141-163.

Tisdall, J. M., Smith, S. E. and Rengasamy, P., 1997. Aggregation of soil by fungal hyphae. *Australian Journal of Soil Research*. 35 pp.55-60.

Torsvik, V. and Ovreas, L., 2002. Microbial diversity and function in soil: from genes to ecosystems. *Current Opinion in Microbiology*. 5(3): pp.240-245.

Trevors, J. T., 1996. Sterilization and inhibition of microbial activity in soil. *Journal of Microbiological Methods*. 26(1-2): pp.53-59.

Tsumura, H., Hiyama, E., Kodama, T., Sueda, T. and Yokoyama, T., 2003. Relevance of antimicrobial agent-induced endotoxin release from in vitro cultured *Escherichia coli* and in vivo experimental infection with Gram-negative bacilli. *International Journal of Antimicrobial Agents*. 21(5): pp.463-470.

Ude, S., Arnold, D. L., Moon, C. D., Timms-Wilson, T. and Spiers, A. J., 2006. Biofilm formation and cellulose expression among diverse

environmental *Pseudomonas* isolates. *Environmental Microbiology*. 8(11): pp.1997-2011.

Velde, B., 1999. Structure of surface cracks in soil and muds. *Geoderma*. 93(1-2): pp.101-124.

Velde, B., 2001. Surface cracking and aggregate formation observed in a Rendzina soil, La Touche (Vienne) France. *Geoderma*. 99(3-4): pp.261-276.

Vogel, H. J., Hoffmann, H., Leopold, A. and Roth, K., 2005a. Studies of crack dynamics in clay soil - II. A physically based model for crack formation. *Geoderma*. 125(3-4): pp.213-223.

Vogel, H. J., Hoffmann, H. and Roth, K., 2005b. Studies of crack dynamics in clay soil - I. Experimental methods, results, and morphological quantification. *Geoderma*. 125(3-4): pp.203-211.

Vogel, H. J. and Roth, K., 1998. A new approach for determining effective soil hydraulic functions. *European Journal of Soil Science*. 49(4): pp.547-556.

Vollmer, W., 2012. Bacterial outer membrane evolution via sporulation? *Nature Chem Biol*. 8(1): pp.14-18.

West, A. W., 1986. Improvement of the selective respiratory inhibition technique to measure eukaryote:prokaryote ratios in soils. *Journal of Microbiological Methods*. 5(3-4): pp.125-138.

White, I. and Sully, M. J., 1987. Macroscopic and Microscopic Capillary Length and Time Scales from Field Infiltration. *Water Resources Research*. 23(8): pp.1514-1522.

White, N. A., Hallett, P. D., Feeney, D., Palfreyman, J. W. and Ritz, K., 2000. Changes to water repellence of soil caused by the growth of white-rot fungi: studies using a novel microcosm system. *FEMS Microbiology Letters*. 184(1): pp.73-77.

Whitman, W. B., Coleman, D. C. and Wiebe, W. J., 1998. Prokaryotes: The unseen majority. *PNAS*. 95(12): pp.6578-6583.

Wildenschild, D., Hopmans, J. W., Vaz, C. M. P. and Rivers, M. L., 2001. Using x-ray beams to study flow processes in underground porous media. *Advanced Photon Source Research*. 4 pp.48-50.

Williams, V. and Fletcher, M., 1996. *Pseudomonas fluorescens* adhesion and transport through porous media are affected by lipopolysaccharide composition. *Appl Environ Microbiol*. 62(1): pp.100-104.

Wolf, D. C., Dao, T. H., Scott, H. D. and Lavy, T. L., 1989. Influence of Sterilization Methods on Selected Soil Microbiological, Physical, and Chemical-Properties. *Journal of Environmental Quality*. 18(1): pp.39-44.

Young, I. M. 2010. *Personal Webpage*. Armidale, NSW, Australia. [Online] Available from: <http://www.une.edu.au/staff/iyoung4.php>.

Young, I. M. and Crawford, J. W., 1991. The fractal structure of soil aggregates: its measurement and interpretation. *Journal of Soil Science*. 42(2): pp.187-192.

Young, I. M. and Crawford, J. W., 2001. Protozoan Life in a Fractal World. *Protist*. 152(2): pp.123-126.

Young, I. M., Crawford, J. W., Nunan, N., Otten, W. and Spiers, A., 2008. Microbial distribution in soils: Physics and scaling. In: Sparks, D. L. ed. *Advances in Agronomy*, Vol 100. Burlington: Academic Press, 2008, pp.81-121.

Young, I. M., Crawford, J. W. and Rappoldt, C., 2001. New methods and models for characterising structural heterogeneity of soil. *Soil and Tillage Research*. 61(1-2): pp.33-45.

Young, I. M. and Ritz, K., 2000. Tillage, habitat space and function of soil microbes. *Soil and Tillage Research*. 53(3-4): pp.201-213.

Zeger, S. L. and Liang, K. Y., 1986. Longitudinal Data-Analysis for Discrete and Continuous Outcomes. *Biometrics*. 42(1): pp.121-130.

Ziegler, A., Kastner, C. and Blettner, M., 1998. The generalised estimating equations: An annotated bibliography. *Biometrical Journal*. 40(2): pp.115-139.